

Large scale microwave synthesis of Metal-Organic Frameworks

Ieuan Thomas-Hillman MCHEM

Thesis submitted to the University of Nottingham for the degree of Doctor of Philosophy

November 2020

Large scale microwave synthesis of Metal-Organic Frameworks

Ieuan Thomas-Hillman MCHEM

Thesis submitted to the University of Nottingham for the degree of Doctor of Philosophy

Faculty of Engineering, Department of Chemical and Environmental Engineering

November 2020

Doctoral supervisors: Dr. Andrea Laybourn, Dr. Chris Dodds, Prof. Sam Kingman

“There is no such thing, as an unsolvable problem”

Sergei Pavlovich Korolev

“If you wish to make an apple pie from scratch, you must first invent the universe.”

Carl Sagan

Abstract

This thesis contains a collection of manuscripts and commentary reporting on the microwave synthesis of metal-organic frameworks (MOFs), a broad class of porous materials. The central aim of this scheme of work was to use microwave heating solutions to realise the rapid synthesis of MOF materials. This has the potential to enable large scale production of these materials whilst also elucidating on the consequences of using this alternative heating method and the underlying mechanism by which the materials are synthesised. To that end this thesis contains the following sections, each represented by a manuscript (in appendix) and associated commentary:

Chapter 1 and Appendix 1[1] contain an introduction to Metal-organic frameworks, microwave synthesis of these materials and existing efforts to use microwave heating to achieve large scale MOF synthesis. It also briefly introduces the primary MOF studied in this thesis, MFM-300(Al)

Chapter 2 and Appendix 2[2] contain details of the development of MW synthesis of MFM-300(Al) in a commercial temperature-controlled reactor

Chapter 3 and Appendix 3 detail the use of a bespoke reactor to synthesise MFM-300(Al) with control over microwave power and energy enabling extremely short reaction times and revealing a profound level of control over the morphology of the MOF crystals.

Chapter 4 and Appendix 4 detail a methodology for purifying MFM-300(Al) post-synthesis using mild base, with the aim of obtaining a pristine framework and reclaiming the expensive linker.

Chapter 5 and Appendix 5[3] describe the use of a continuous flow oscillatory baffled microwave reactor to synthesise HKUST-1, whilst also detailing the effects of microwave power and flow rate on the morphology and properties of the yielded crystals. It is shown that the use of such an efficient reactor enables synthesis of highly porous HKUST-1 in as little as 2.2 seconds at the highest flowrate, resulting in the highest MOF production rate reported to date

Chapter 6 contains general summary remarks and highlights avenues for potential further investigation.

Declaration

I declare that no portion of the works presented within the thesis have been submitted in support of an application for another degree or qualification of this or any other institution.

Signed:

Ieuan Thomas-Hillman

The three published manuscripts (in appendices 1 2 & 5) were published by the Royal Society of Chemistry (Appendix 1 & 2) and Elsevier (Appendix 5). Both allow reusing and reproducing the entire published material in an in the PhD Thesis:

Elsevier:[i]

"Theses and dissertations which contain embedded PJAs [Published Journal Article] as part of the formal submission can be posted publicly by the awarding institution with DOI links back to the formal publications on ScienceDirect."

Royal Society of Chemistry:[ii]

"You do not need to request permission to reuse your own figures, diagrams, etc, that were originally published in a Royal Society of Chemistry publication. However, permission should be requested for use of the whole article or chapter except if reusing it in a thesis. If you are including an article or book chapter published by us in your thesis please ensure that your co-authors are aware of this."

i https://www.elsevier.com/about/policies/sharing accessed 20-09-2020

ii https://www.rsc.org/journals-books-databases/journal-authors-reviewers/licences-copyright-permissions/ accessed 20-09-2020

Acknowledgements

Over the course of the last three and a half years of my life I have been indebted both professionally and personally to a great many people, if not for whom this thesis could never have materialised.

Firstly, I must extend the greatest thanks to my three supervisors, Dr. Andrea Laybourn, Dr. Chris Dodds and Prof. Sam Kingman. The three of them took me on, cared for me, aided my research, offered valued council, and have kept me from deviating off course. It has been an experience moving somewhat across fields to engineering, and one I feel I am better for. In my entire time I never once felt like I worked for them, but always as though I worked with them, something I know not all students are lucky enough to feel. It is my sincerest hope that they consider the time they invested in me worthwhile, and when it comes to my time to supervise the next set of students I hope I am guided by the memories of my own time – and of my supervisors.

Next to my friends and respected colleagues Alex, Jose, Gaby, Maria, Ali, Khalid, Muhammed, Becca, Ben, Roads, Sanad, Fatima, Lorena, Juliano, Adam, Batch, Buddy Orla & Emily. Christ there is a lot of them who have been through the group and university and all of them have been wonderous to work with and around. I wish to extend special thanks to Miguel & Yujie, who were there at the very start of my PhD, willing to answer any inane question I had ranging from “what are you doing with that bit of microwave equipment” to “where do we go to submit these monthly reports?” One can read all the books of theory in the world, but there is no substitute for first-hand experience.

To my more direct co-workers Jessy, Claire, Aoife, Max, Tesh & Ricardo, so often helpful in conversation as I vomited forth incoherent mumblings about my crystals, tolerant of my somewhat ego driven rants, assisting with running my reactors on a time schedule that was incomprehensible even by my crazy standards and comforting when I lay underneath my desk exhausted and miserable, simply wishing to end one week feeling as good about it as I had started. Greater companions I could not have wished for – and I love them all dearly, though I am lousy at showing it. They all are on their own journeys and I wish them every success in every endeavour they tackle.

To the technicians, Hannah Beska, Hannah Constantin, Joe Meehan, Gvido Ozolins, Vikki Archibald & Jacob Uguna for aiding in keeping me sane, assistance with equipment, guidance in my dealings with undergraduates and aid with experiments which sadly never materialised into usable data. Thanks go to Mathew Nichols for his assistance in setting up reactors and workstations.

I would like to additionally Sam Murray and Mel Hemsley for their assistance in fabricating replacement parts for the flow reactor, despite me breaking it at least ten times in quick succession. I count it as my biggest failure that the goal of achieving MOF synthesis with this flow reactor and thus their labours are not contained here – but I have no doubt that this will eventually be realised. I would like to thank my overseas co-workers Marcus Lange and Jens Möllmer, I regret that our collaboration was limited to a single paper, at least for the time being.

And thanks go to my friends and loved ones, who have stood beside me throughout this time, occasionally aiding my task of drowning my stresses in unhealthy quantities of Guinness and Heavy Metal. Especially in the last months, while the entire world has gone to hell, my stress and gloom has not deterred them from being there for me, and I hope they always feel they can count on me to be there for them when time comes to return the favour.

List of Publications

Published

I. Thomas-Hillman, A. Laybourn, C. Dodds and S. W. Kingman, Realising the environmental benefits of metal-organic frameworks: recent advances in microwave synthesis: ***J. Mater. Chem. A***, 2018, **6**, 11564–11581.

A. Laybourn, A. M. López-Fernández, I. Thomas-Hillman, J. Katrib, W. Lewis, C. Dodds, A. P. Harvey and S. W. Kingman, Combining continuous flow oscillatory baffled reactors and microwave heating: Process intensification and accelerated synthesis of metal-organic frameworks: ***Chemical Engineering Journal***, 2019, **356**, 170–177.

I. Thomas-Hillman, L. A. Stevens, M. Lange, J. Möllmer, W. Lewis, C. Dodds, S. Kingman and A. Laybourn, Developing a sustainable route to environmentally relevant metal-organic frameworks: ultra-rapid synthesis of MFM-300(Al) using microwave heating: ***Green Chem.***, 2019, **21**, 5039-5045

Drafts

I Thomas-Hillman, Y Zhang, R Caldas, Z Huang, X Zou, C Dodds, S Kingman, A Laybourn. Crystallisation mechanism of a microwave-synthesised metal-organic framework: the long and the short of it.

I Thomas-Hillman, L Stevens, C Dodds, S Kingman, A Laybourn. Basic removal of residual linker from metal organic framework synthesis

Table of Contents

Abstract i

Declaration ii

Acknowledgements iv

List of Publications vi

Table of Contents vii

List of Figures xiii

List of Abbreviations xiv

Chapter 1 – Introduction 1

1.1 – Metal-Organic Frameworks 1

1.2 – Microwave synthesis 1

1.3 – MFM-300 4

Chapter 2 – Transferring the synthesis of MFM-300(Al) from conventional to a microwave heated route 7

2.1 – Aluminium oxyhydroxide: conventionally heated synthesis and excess aluminium trichloride 8

2.2 – Long duration synthesis 9

2.3 – Synthesis of MFM-300 at higher reaction ratios. 12

2.4 – Summary 13

Chapter 3 – Understanding the effect of MW energy delivery using a controllable batch MW reactor 15

Chapter 4 – Purification of MFM-300(Al) 21

Chapter 5 – Continuous flow microwave synthesis of MOFs 24

Chapter 6 – General conclusions and future work 26

6.1 – Conclusions of the attached manuscripts. 26

6.2 – Future work 27

6.2.1. – Flow synthesis of MFM-300(Al) and other frameworks 27

6.2.2. – Morphology & penetration depth. 27

6.2.3. – Synchrotron powder x-ray diffraction experiments, *in-situ* understanding 29

6.2.4. – Summary of future work 29

References 30

Appendices: 35

Appendix 1: Realising the environmental benefits of metal–organic frameworks: recent advances in microwave synthesis 37

Statement of contribution of joint authorship 37

Abstract 37

1. Introduction 38

2. The theory of microwave heating and its application to MOF synthesis 41

3. Microwave synthesis of MOFs: a comparison of time with conventionally heated reactions 44

3.1. Background 44

3.2. Influence of microwave heating on MOF reaction time 45

3.3. Influence of microwave heating on MOF crystal size 47

3.4. Influence of microwave heating on the morphology of MOFs 48

3.5. Influence of microwave heating on the surface area of MOFs 50

3.6. Summary 52

4. Microwave synthesis of new MOFs and MOF-hybrids 53

4.1. Background 53

4.2. Phase-selective synthesis of MOFs 53

4.3. "One pot" synthesis of MOF hybrids 55

4.4. Post-synthetic modification of MOFs 57

4.5. Summary 60

5. Towards industrial scale microwave synthesis of MOFs 60

5.1. Background 60

5.2. Current efforts in scaling-up MOF synthesis using microwave heating 61

5.3. Development of industrial scale microwave reactors; important factors to consider 66

6. Conclusions 68

Conflicts of interest 69

List of abbreviations for linkers and MOFs 69

Acknowledgements 69

References 70

Appendix 2: Developing a sustainable route to environmentally relevant metal–organic frameworks: ultra-rapid synthesis of MFM-300(Al) using microwave heating 83

Statement of contribution of joint authorship 83

Abstract 83

Main text of paper 84

Experimental section 92

Materials and methods 92

Characterisation 92

Conflicts of interest 94

Acknowledgements 94

References 94

Supporting Information 99

References: 99

Appendix 3: Crystallisation mechanism of a microwave-synthesised metal-organic framework: the long and the short of it. 100

Statement of contribution of joint authorship 100

Abstract 100

Introduction 101

Experimental Procedures 104

General experimental notes: 104

Synthesis of MFM-300 in a TC commercial microwave system 104

Synthesis of MFM-300 in a bespoke P/EC single mode cavity 105

Pressure warning: 105

SEM / EDX 106

TEM analysis 106

TGA 107

Powder X-ray diffraction (PXRD) 107

Results and discussion: 107

Detailing the differences between TC and P/EC reactions 107

The effects of reactant ratio and applied microwave power on synthesised MFM-300(Al): Identity & Yield 109

Morphology of yielded MOF particles from different powers and reactant ratios. 116

TEM and electron diffraction 120

Rationalisation of observed morphological control 122

Conclusions 124

Acknowledgements 125

Supplementary Information 126

References 135

Appendix 4: Basic removal of residual linker from metal organic framework synthesis 143

Statement of contribution of joint authorship 143

Abstract 143

Introduction 143

Experimental: 144

Synthesis of MFM-300(Al). 144

Ammonia, NaOH, washing experiments 145

Linker reclamation 146

PXRD 146

TGA 147

Scanning electron microscopy 147

Gas sorption analysis 147

Results and discussion 148

Mass out 148

Crystal surface damage 153

Gas adsorption 154

Conclusions: 156

References 156

Supplementary Information 159

Appendix 5: Combining continuous flow oscillatory baffled reactors and microwave heating: Process intensification and accelerated synthesis of metal-organic frameworks 164

Statement of contribution of joint authorship 164

Abstract 164

Keywords 165

1. Introduction 165

2. Experimental 170

3. Results and discussion 173

3.1. Yield of HKUST-1 176

3.2. Quality of HKUST-1: crystallinity, morphology and porosity 178

4. Conclusions 183

Acknowledgements 183

References 185

Supplementary Information 189

Contents 189

1. Further experimental details and data 189

2. Powder X-ray diffraction data 196

3. Gas sorption isotherms 198

4. Scanning electron microscopy (SEM) images and histogram plots 200

5. Thermogravimetric analysis (TGA) 206

6. References 207

List of Figures

Figure 1: The crystal structure of MFM-300(Al) viewed down the C-axis. Note the "wine rack" topology……..…….[5]

Figure 2: The crystal structure of MFM-303(Al) viewed down the C-axis. Note the more densely packed "wine rack" topology in comparison to MFM-300……[8]

Figure 3: PXRD data of MFM-300(Al) (microwave experiments while developing the synthesis)……...[10]

Figure 4: PXRD data of conventionally heated reactions, using aluminium trichloride and linker in a 2:1 reaction ratio……[11]

Figure 5: LeBail refinement of PXRD data for a 3 day solvothermal reaction (2:1:water ratio of AlCl3:linker …….……[11]

Figure 6: TGA data of conventionally heated reactions ……..….[12]

Figure 7: PXRD data of MFM-300(Al) synthesised in an 8-1 metal:linker ratio, with extra reflections clear in the difference spectrum from a leBail refinement (~9 and 27.5 °2 theta)…….[13]

Figure 8: SEM images of MFM-300(Al) synthesised in the CEM cavity at an 8:1 metal:linker ratio, showing the peculiar sponge/anemone like morphology, along with the stocky cylinders of MFM-300…….…..…[13]

Figure 9: EDX spectrum of MFM-300(Al) synthesised in the P/EC reactor, corresponding to sample P/EC-8 (see Appendix 3 for details)……..…[17]

Figure 10: (Top) SEM micrograph of MFM-300(Al) synthesised in the P/EC reactor and (Bottom) the EDX map of the micrograph for chlorine…….…….[18]

Figure 11: LeBail refinements of PXRD data for an MFM-300(Al) sample.....[19]

Figure 12: SEM of MFM-300(Al) washed with 0.1 M piperazine solution……..[22]

Appendices 1 – 5 contain their own figures which are not listed here.

List of Abbreviations

BDC	terephthalic acid (benzene-1,4-dicarboxylic acid) ¦ used interchangeably for the conjugate base
BTC	trimesic acid (benzene-1,3,5-tetracarboxylic acid) ¦ used interchangeably for the conjugate base
BET	Brunauer–Emmett–Teller
BPTC	biphenyl-3,3’,5,5’-tetracarboxylate
CH	Conventional Heating
ED	Electron Diffraction
EDX	Energy-dispersive X-ray spectroscopy
HKUST-1	Hong Kong University of Science and Technology
H_4BPTC	biphenyl-3,3’,5,5’-tetracarboxylic acid
IR	Infra Red
MFM	Manchester Framework Material (MOF given name)
MOF	Metal-Organic Framework
MW	Microwave
NOTT	Nottingham (MOF given name)
OBR	Oscillatory Baffled Reactor
P/EC	Power & Energy Controlled
PXRD	Powder X-Ray Diffraction
SAPR	Surface Area Production Rate
SEM	Scanning Electron Microscopy
STY	Space Time Yield
T/C	Temperature Controlled
TEM	Transition Electron Microscopy
UiO	University of Oslo (MOF given name)

Chapter 1 – Introduction

1.1 – Metal-Organic Frameworks

Metal-organic frameworks offer great potential in a variety of applications, including gas storage,[4–8] catalysis,[9–13] sensing,[14–16] biomedical applications,[17–19] energy storage[20–22] and specifically of interest here, environmental clean up.[23–26] The permanent porosity, tailorable pore environments and chemical orthogonality of MOFs allow for the realisation of bespoke materials at the atomic level, and the incorporation of theoretically any chemistry into solid material hosts. However, in order for MOFs, or indeed any materials, to be useful they must be produced in sufficient quantities required for their commercial application. The need for large, kilogram to tonne scale synthesis of MOFs can be most easily illustrated in the most basic of applications, gas adsorption, in which large tonnage scale quantities are required to make an impact.

For example, the work presented by Yilmaz et al.[27] depicted the use of a car fuelled by methane using a tank filled with the copper MOF HKUST-1 as an adsorbate to increase the tank capacity. To fill a single 50 litre methane tank in an automobile 4 Kg of MOF is required; 70 million cars were manufactured globally in 2018[28], and so to meet the demands of this industry would require in excess of 280,000 tonnes of MOF per year, with even more required for other internal combustion engine based vehicles and machinery. For many other applications such as catalysis, the necessary production quantities to make an impact on billion tonne plus scale industries are similarly large, with consistent properties of the yielded MOF product also being required. For MOFs to become feasible entrants into these industries their synthesis must be scalable, and as efficient as possible in terms of time, area, energy, environmental burden, and consumption of feedstocks.

1.2 – Microwave synthesis

Microwave heating is a well-documented method of process intensification offering an efficient alternative to conventional heating.[29–32] In the case of MOF synthesis microwave heating has been found to profoundly accelerate the rate at which MOFs crystallise, first down to minutes, and then to seconds. This rapidity is believed to be a consequence of the formation of selective and elevated temperatures around the metal ion, in which the temperature is significantly higher than that of the bulk reaction

mixture, often described simply as a "hotspot". As is detailed in the attached manuscripts a wide range of MOFs have been successfully synthesised in small scale batch processes, and while microwave heating has been used to accelerate the synthesis it has also been shown to consequentially effect other MOF properties (which is further explored below). Thus, the total aim of this project was to realise a microwave heated solution to the large-scale synthesis of a particular MOF and to gain further understanding of how microwave MOF synthesis occurs; the two aspects of course being directly related.

The first published paper in this thesis[1] (see Appendix 1) was a literature review addressing the topic of microwave heated MOF synthesis, entitled "Realising the environmental benefits of metal–organic frameworks: recent advances in microwave synthesis." The text commences with a brief review of the field of MOFs, highlighting the same themes discussed in this commentary of the many possible applications of MOFs and the need to realise a large-scale synthesis method. Following this, the theory of microwave heating and how it specifically applies to the synthesis of MOFs is detailed. The suggested mechanism of MOF formation under microwave heating is the "hotspot" mechanism, in which the area around solvated metal ions is heated preferentially due to their interaction with the electric field, and this drives the synthesis forward at a significantly faster rate compared to conventionally bulk heated synthesis.

The use of microwave heating for MOF synthesis is discussed, beginning by a comparison with conventional heating methods (where reduced reaction times are seen as a universal positive, and with crystal size, morphology and adsorption properties showing some variation). After this the unique characteristics of microwave heating are described by highlighting how it had been applied to a vast library of different frameworks. A summary of some of the more unique achievements of microwave synthesis of MOFs was then described; this includes:

- Phase selectivity – in which multiple different MOF structures exist with the same metal and linker combination, and can be selectively synthesised by choosing the appropriate parameters

- One pot MOF hybrid synthesis – where MOFs can be synthesised in conjunction with other materials, with molecules entrapped or ‘doped’ into their structure, or with multiple metal ion components
- Post synthetic modification of MOFs – in which a synthesised framework is chemically modified, such as augmenting the pore environment of the framework with addition chemical functionality.

The final section of the review centred on developing microwave synthesis beyond the lab scale and towards industrial scale manufacture. This highlighted that the short duration of microwave synthesis makes it perfect for continuous flow reactions where low residence times can facilitate exceptionally large production rates.

The key themes for the review were:

- Rapidity: From days down to a matter of seconds, microwave heating enables exceptionally fast reactions which makes this method of heating ideal for larger scale synthesis, rapid screening of reaction conditions and general ease of use with widely available off the shelf microwave reactors.
- Control: MW heating can facilitate another method of control over the MOF materials that are synthesised, by influencing surface area, crystal morphology, and structural phase.
- Efficiency: A combination of the rapid reactions and targeted heating leads to a great reduction in the energy requirement for synthesis compared to a conventionally heated system.
- A current lack of understanding of the interaction of microwave energy with chemical reactants and structures, and how this information can be used to underpin successful scale up: The review highlighted a reliance on generic microwave reactors (sometimes even based on domestic kitchen equipment) which at best simply offer control over the forward power and the target temperature of the reaction. In such reactors it is not possible to meaningfully describe the environment in which MOF crystallisation is occurring, as the electric field density and power environment is not characterised and constantly varying due to the change in the dielectric properties of the reaction mixture. This limits the ability of workers in the field to fully understand the

effects of microwave heating and subsequently prevents proper realisation of microwave heating as a tool for scale up.

Since the review was published in 2017 there have been further developments in the field. A repeat of the Scopus search conducted for the review paper (Scopus database search for "Metal–Organic Framework" or "Metal Organic Framework" and "Microwave") now returns 526 results, or an increase of 242. Many of these papers are of similar nature to those summarised in the original literature review article, using off the shelf microwave reactors to synthesis MOFs, including further examples of one pot synthesis of hybrids and post synthetic modification.

Additionally, microwave heating has now been used to assist mechanochemical synthesis using ball mills.[33–37] In these cases a Teflon milling pot containing the reactants and a stainless steel ball is placed inside of a microwave oven. The synthesis can be performed using a solvent or solvent free, yielding MOF products in as low a time as 15 minutes. Additionally, this method has been used to prepare a one pot synthesis of graphene oxide/MOF hybrids. Both MOF and hybrids were subsequently used as candidate materials for dye removal from aqueous solutions. In the publications reporting this method the authors mention that stirring (at a constant rate of 200 rpm) was turned on concurrently with the microwave oven; however, no details of the microwave cavity, its power or the materials position within it are provided.

Finally, an additional example of microwave heated continuous flow synthesis has been detailed in recent publications by Vo *et al*.[38,39] Similar to the research conducted previously by Taddei *et al*.[40] a PTFE tube was wound inside of a multimode microwave cavity through which the reaction mixture is fed. The mixture is constantly irradiated to yield MOF. The MOFs synthesised by Vo *et al* were variations of UiO-66 and were used for toluene capture where the authors noted a favourable correlation between adsorption ability and the amount of pendant NH_2 groups in the MOF. A high level of recyclability was also achieved with 95% of the adsorbed toluene being retrievable at room temperature.

1.3 – MFM-300

The MOF chosen as the main focus of this research was $[Al_2(OH)_2(C_{16}O_8H_6)]$ (NOTT-300/MFM-300), first reported in 2012[41]. The structure of MFM-300 features 1 dimensional channels running between walls of linker (biphenyl-3,3',5,5'-

tetracarboxylic acid) connecting the octahedra of the aluminium oxide backbone secondary building unit, forming a "wine rack" topology (Figure 1). It is water stable, shows high selective adsorption of polluting dioxides (CO_2, SO_2 and NO_2, while being nonporous to oxygen and nitrogen), and has been shown to adsorb iodine[42] and ammonia.[43] It has also recently been demonstrated as being stable under long duration (~4 years) exposure to SO_2, NO_2 and NH_3.[44] A disadvantage compared to archetypal MOFs such as MIL-53 or HKUST-1 is the cost and commercial availability of the linker. The conventional synthesis of MFM-300 is a 3-day conventionally heated solvothermal reaction yielding approximately 100 mg;[41] thus, to realise the potential applications of this framework the synthesis needs to be scaled up, and microwave heating (as detailed above) offers a potential solution to this.

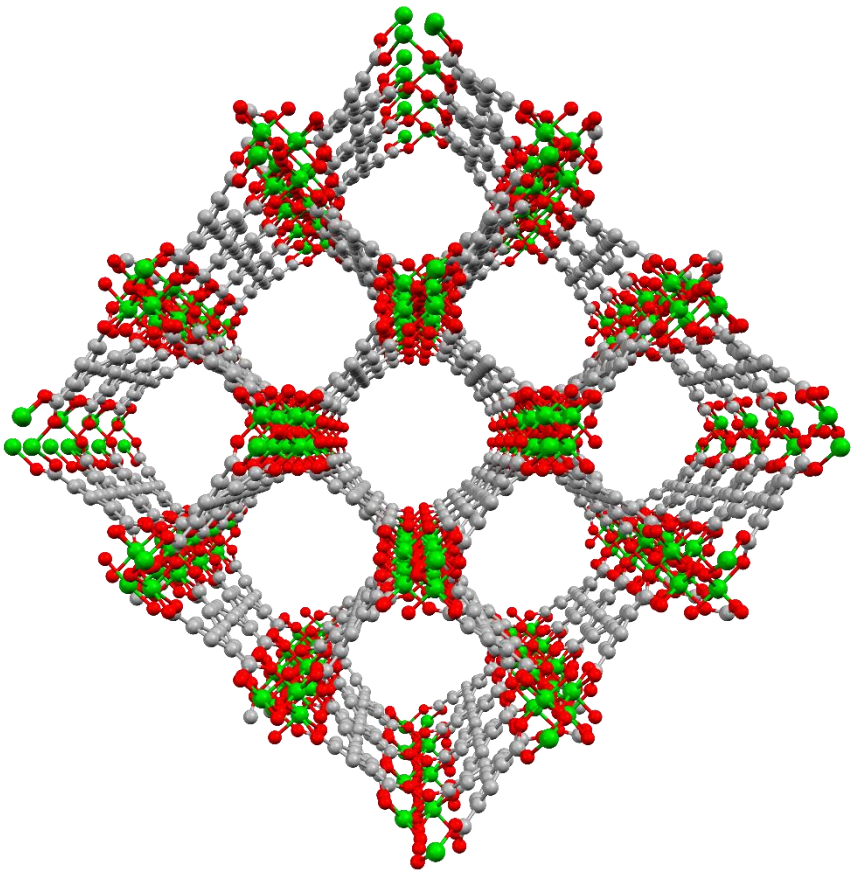


Figure 1: The crystal structure of MFM-300 viewed down the C-axis. Note the "wine rack" topology. Grey = Carbon, Red = Oxygen, Green = Metal cation. Obtained from the CCDC entry NIRPIQ.[45]

To address the synthesis of MFM-300(Al) the following activities were carried out:

i) A microwave synthesis of MFM-300(Al) was developed.

ii) It was investigated whether MFM-300(Al) could be synthesised using a power ramp only methodology, and how incident power affected crystallisation of the MOF.

iii) In anticipation of <100% yields a facile method for purifying the MOF and reclaiming unreacted linker for further synthesis was developed.

iv) Additionally, the gram per minute scale MW synthesis of HKUST-1 was achieved in an oscillatory baffled reactor, with the effect of power and flow rate on MOF morphology investigated.

These activities correspond to the manuscripts contained in Appendices 2 - 5, with commentary in the similarly numbered chapters. Overall, this thesis details the efforts to realise the underpinning science for the large-scale microwave synthesis of two target metal-organic frameworks, and better investigate and characterise the synthetic outcomes when using this heating method for the synthesis of these materials.

Chapter 2 – Transferring the synthesis of MFM-300(Al) from conventional to a microwave heated route

Appendix 2 contains the published manuscript "Developing a sustainable route to environmentally relevant metal–organic frameworks: ultra-rapid synthesis of MFM-300(Al) using microwave heating"[2] which details a new method for the microwave synthesis of MFM-300(Al) and the properties of the yielded framework.

MFM-300(Al) is conventionally synthesised using the method reported by Yang *et al.*[41] from aluminium nitrate, piperazine, and the H_4BPTC linker in water and nitric acid. For synthesising MFM-300 using a microwave route a few challenges had to be overcome. Development of this route began with using aluminium sulfate as per the synthesis of MIL-53(Al) or addition of nitric acid as per the original synthesis parameters of MFM-300(Al),[41] these reactions both led to explosive venting of the reaction mixture. Following this a route using DMF as a solvent was investigated, however, neither conventional nor microwave heating yielded MFM-300, with only broad amorphous powder patterns being collected. A successful microwave route was developed using a novel reaction mixture of aluminium trichloride, linker and water. Attempts to synthesis the MOF from this reaction mixture using conventional heating precipitate aluminium oxyhydroxide and a polymorph MFM-303 (Figure 2); further experimental details relevant to this are discussed in section 2.1.

This work culminated in the published synthesis and the resulting MOF properties. The structure and thermal stability were in line with previously reported MFM-300, however, of note was the increased uptake of the polluting dioxides CO_2, SO_2 and NO_2 relative to literature values[41,46] (details in the manuscript). Interestingly an N_2 uptake at 77 K was also observed, this is in contrast to conventionally synthesised MFM-300(Al) which is non-porous to nitrogen. While such enhancement is important for pollutant capture applications it also points to a fundamental difference between samples prepared conventionally and samples prepared with microwave heating. The extra gas must be stored somewhere within the structure most likely through defects within the crystal. For the targeted polluting dioxides, PXRD studies[41,46,47] have shown that the adsorption is highly structured. Additionally, the crystal morphology was found to be different, a theme which would reoccur later in the research.

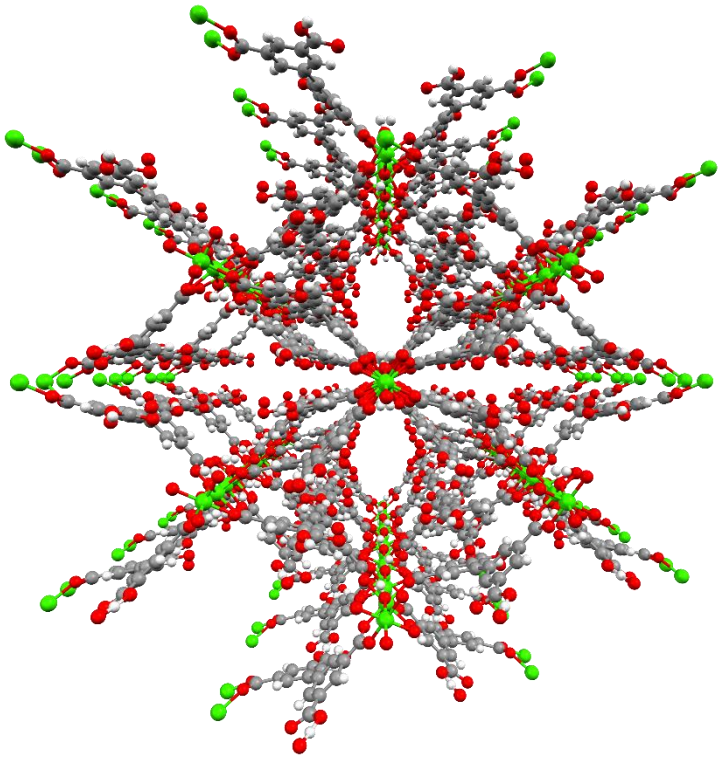


Figure 2: The crystal structure of MFM-303(Al) viewed down the C-axis. Note the more densely packed "wine rack" topology in comparison to MFM-300. Grey = Carbon, Red = Oxygen, Green = Metal cation.[48]

2.1 – Aluminium oxyhydroxide: conventionally heated synthesis and excess aluminium trichloride

As mentioned in section 2.0 the reaction mixture used to synthesis MFM-300(Al) by microwave heating could not be used to prepare the MOF by conventional heating. This was briefly alluded to in the published manuscript when detailing the PXRD results and mentioning conventionally heated reactions:

"No peaks corresponding to γ-Al(O)OH or other MOF phases beyond MFM-300(Al) were observed. Attempts to synthesise MFM-300(Al) using these conditions with conventional heating for 24 to 72 hours (rather than rapidly using microwaves) gave a mixture of MOF phases and γ-Al(O)OH."

γ- Aluminium oxyhydroxide (böhmite, γ-Al(O)OH) is a naturally occurring mineral, and has been reported as a possible side product of the synthesis of other aluminium containing MOFs, e.g. in synthesis of MIL-53 when the synthesis duration was longer than 3 days.[49] Since it is an undesirable synthetic contaminant references to its

synthesis alongside MOFs are limited, however direct synthesis of böhmite has been published[50,51] and bears a great similarity with the synthesis of aluminium MOFs (hydrothermal conditions of aluminium salt solutions). In this work several experimental conditions led to the formation of böhmite as discussed below.

2.2 – Long duration synthesis

When originally working on the MFM-300 synthesis the reaction time was significantly longer than the 10 minutes published. Originally the reaction mixture was maintained at 210°C for 2 hours, which was subsequently shortened to 30 minutes (N.B. these reactions were performed with a 2:1 metal to linker ratio, however with a different batch of linker). PXRD analysis of these experiments exhibited broad extra reflections at ~14.3, 28, 38.2 and 49° 2Θ, in addition to peaks corresponding to MFM-300(Al) (Figure 3). These peaks were not present in PXRD data of shorter syntheses, and formal analysis of these peaks was avoided due to the poor quality of the PXRD data (low relative intensity, few distinctly visible reflections and broad reflections combined with instrument optics would make indexing and space group refinement difficult and unreliable).

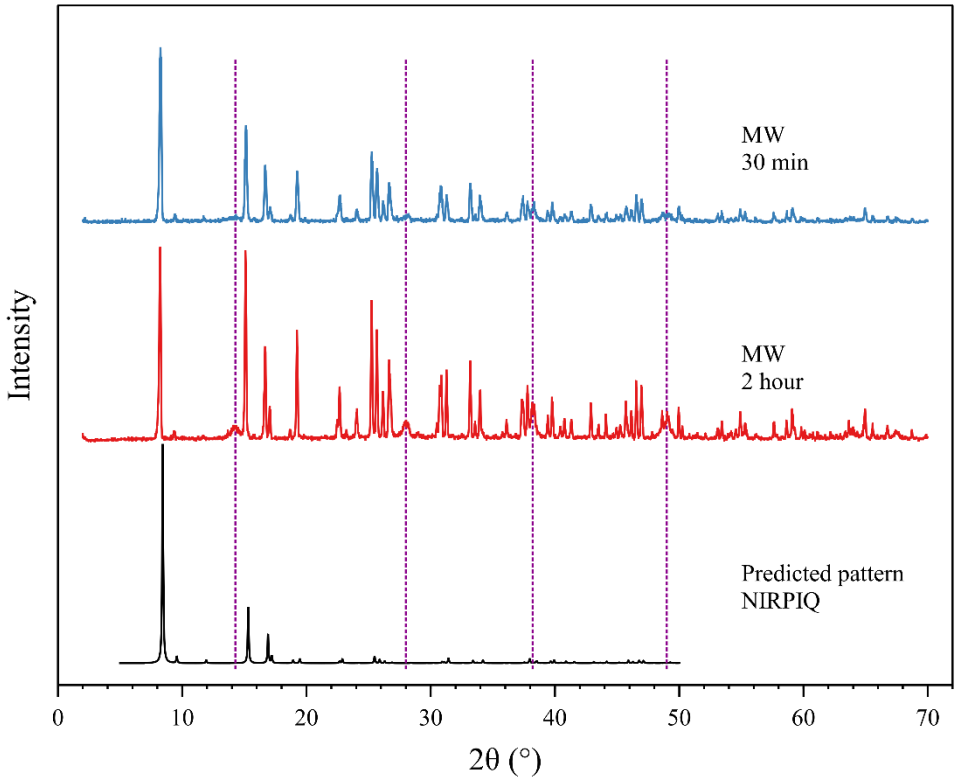


Figure 3 PXRD data of MFM-300 (microwave experiments while developing the synthesis). Reflections in addition to those corresponding to MFM-300 are highlighted with vertical dashed lines.

However when comparison experiments were performed in a conventionally heated solvothermal bomb these reflections grew to be a dominant phase over the course of three days, as shown in Figure 4. A 1 day solvothermal reaction yielded multiple phases, MFM-300 and MFM-303,[48] and these reflections previously identified in the 2 hour microwave reaction (marked in Figure 4 with purple dashed lines). As the synthesis duration increased the relative intensity of the MOF reflections decreased and the highlighted reflections at ~14.3, 28, 38.2 and 49° 2Θ increased in intensity. The increased intensity allowed for easy identification of the reflections as matching the powder pattern for γ-Al(O)OH, and a leBail refinement (Figure 5) was performed to refine the unit cell. (Refined unit cell: Cmcm, a = 2.865542, b = 12.071167, c= 3.680912 || c.f. Cmcm, a = 2.85 b =11.8-12.2, c = 3.69 – 3.78. All cell axis given in Angstrom)[50] TGA thermograms (Figure 6) also showed behaviour concordant with that reported for γ-Al(O)OH. From this evidence, combined with the knowledge of γ-Al(O)OH as a known product of extended MOF synthesis and the similarity of synthetic methodology, the product was identified as böhmite.

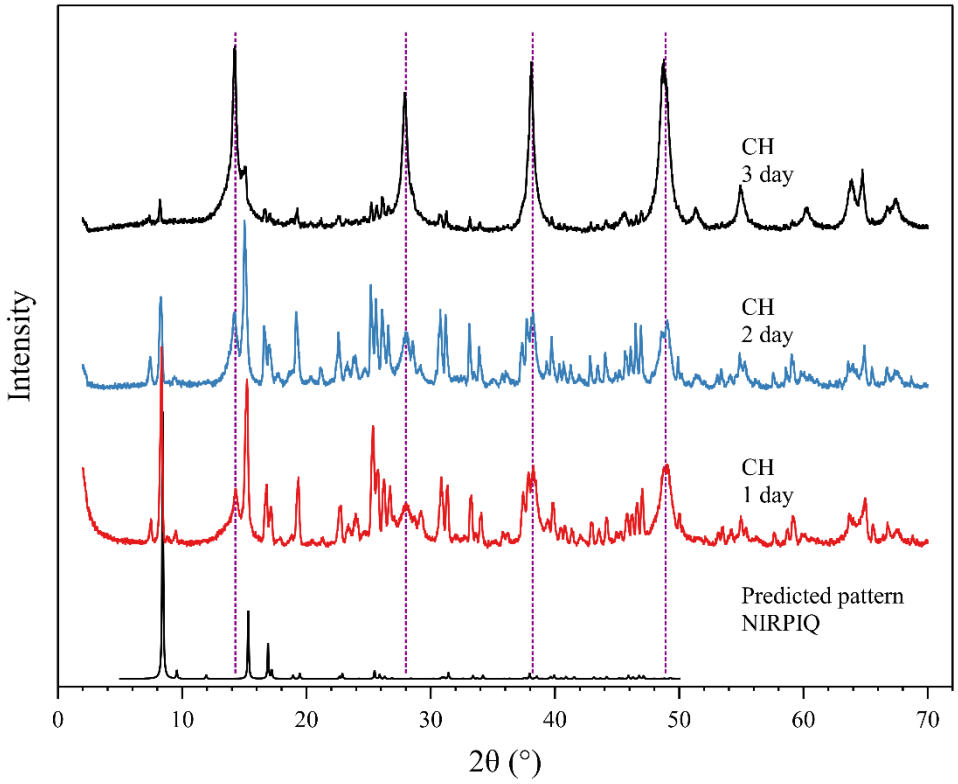


Figure 4 PXRD data of conventionally heated reactions, using aluminium trichloride and linker in a 2:1 reaction ratio. The patterns show reflections corresponding to MOF phases MFM-300 and MFM-303, however as reaction time increases the reflections corresponding to γ-Al(O)OH become dominant (highlighted by purple dotted lines).

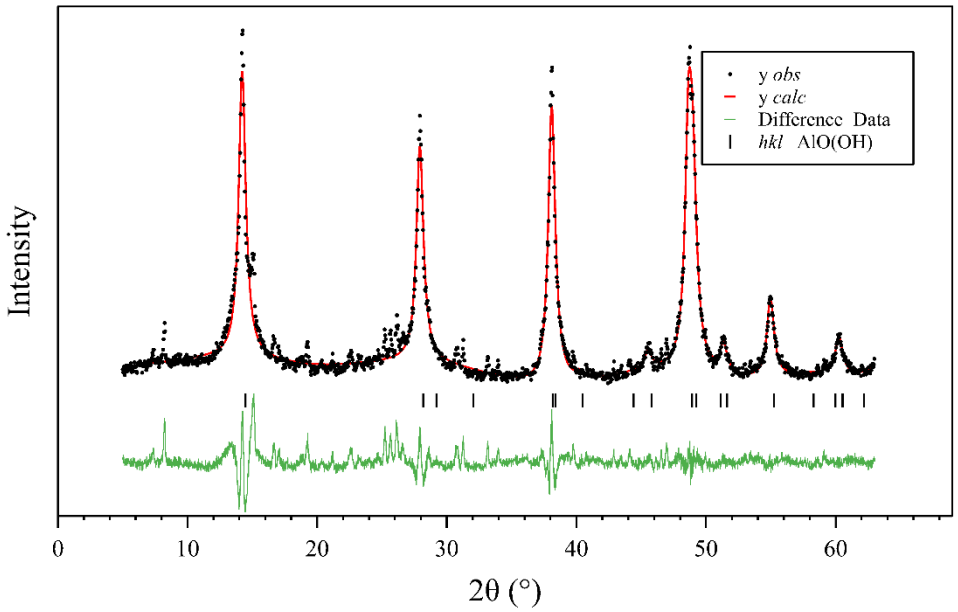


Figure 5 LeBail refinement of PXRD data for a 3 day solvothermal reaction (2:1:water ratio of $AlCl_3$:linker) The refinement is performed to the orthorhombic space group Cmcm, with the corresponding tick marks depicted below. The reflections corresponding to MOF phases are still apparent in the diffraction data, and made clearly visible in the difference plot.

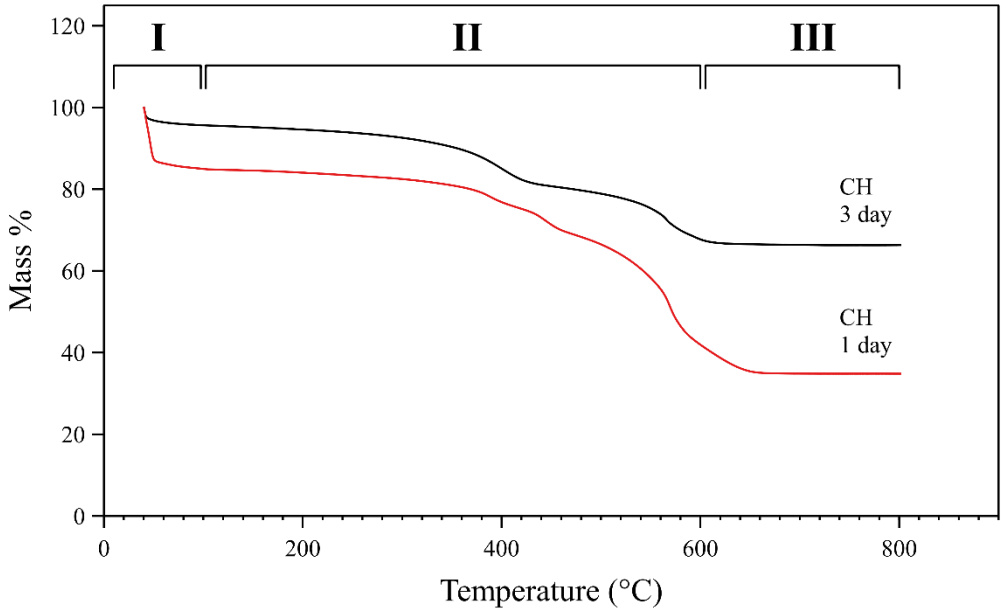


Figure 6 TGA data of conventionally heated reactions. (I) loss of adsorbed water from MFM-300 in the sample, (II) Mass losses due to material decomposition, (III) Final residue of decomposition. Reduced water content (I) is indicative of a large amount of non-porous mass in the sample, and the large left over residue (III) indicates a higher metal content than that of a carbon containing MOF, concordant with PXRD data which indicated large quantities of γ-Al(O)OH.

2.3 – Synthesis of MFM-300 at higher reaction ratios.

When experimenting with the synthesis of MFM-300 in a CEM single mode microwave reactor one of the variables that was adjusted was the ratio between aluminium trichloride and the H_4BPTC linker. One driving force behind this was a desire to consume as close to 100% of the linker in the synthesis. However elevating the ratio of metal to linker beyond 4:1 resulted in problems. PXRD of these samples revealed some peculiar reflections that did not match those of MFM-300, (shown in Figure 7) however, most strikingly when analysed using SEM (Figure 8) large species were immediately apparent. It is believed that these are γ-Al(O)OH.

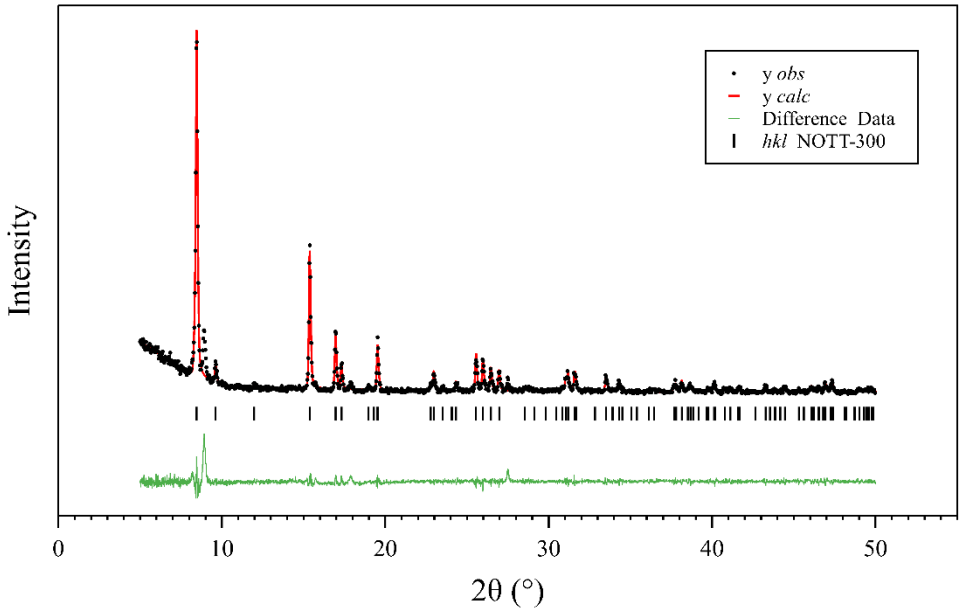


Figure 7 PXRD data of MFM-300(Al) synthesised in an 8-1 metal:linker ratio, with extra reflections clear in the difference spectrum from a leBail refinement (~9 and 27.5 °2 theta). Identification of this phase was not possible as only two peaks are clearly present in the diffraction pattern.

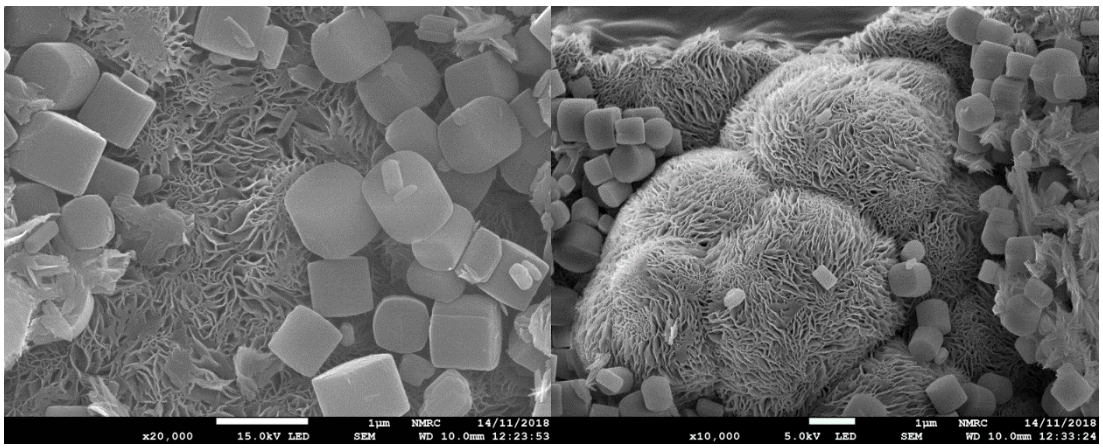


Figure 8 SEM images of MFM-300 synthesised in the CEM cavity at an 8:1 metal:linker ratio, showing the peculiar sponge/anemone like morphology, along with the stocky cylinders of MFM-300. Though there was limited information contained in the PXRD experiment the sponge like morphology is similar to that previously seen in the synthesis of γ-Al(O)OH as reported by Dubey et al.[51]

2.4 – Summary

In this work the successful synthesis of MFM-300(Al) by microwave heating was presented. The next stage was to investigate whether MFM-300 could be synthesised using a ramp only methodology, which would confirm that the MOF was likely self-assembling under the "hotspot" mechanism rather than relying on bulk temperature. The vast majority of microwave MOF synthesis research is conducted in commercially

available reactors in which the actual delivery of microwave energy is controlled by inbuilt software, and the user only inputs a temperature for the reaction to be taken to, and a duration for it to be maintained at. Here it was aimed to translate the synthesis into more controllable microwave reactors where control of energy and power delivery could be used to achieve a greater understanding of the reaction, through characterising the product (morphology and yield) in relation to the power input into the reaction i.e. controlling the power density (volumetric energy deposition) in the heated phase.

Chapter 3 – Understanding the effect of MW energy delivery using a controllable batch MW reactor

Appendix 3 contains the manuscript "*Crystallisation mechanism of a microwave-synthesised metal-organic framework: the long and the short of it*" and supplementary information. A running theme identified in Chapter 1 is an over reliance on generic off the shelf microwave systems for MOF synthesis, and, therefore, a lack of characterisation and understanding of how microwave heating is influencing the reaction. The aim of the work in this chapter is to understand microwave synthesis on a fundamental level and using the developed MFM-300 route as a case study. The work in this chapter and corresponding appendix 3 follows on from previously published work on MIL-53(Al),[52] where synthesis was achieved rapidly, although it was found that for the MFM-300(Al) reaction stirring was required due to the linker sinking to the bottom of the reactor. The reaction mixture was used as described in the previously published paper in appendix 2, with a slight adaption being the inclusion of a second set of experiments using a 2:1 metal to linker reactant ratio in addition to the previously reported 4:1 metal-linker reactant ratio.

The objectives of this work were.

a) To ensure that the power ramp only microwave heating methodology could be applied to the synthesis – this would provide further confirmation of the "hot spot" mechanism of MOF formation
b) To characterise the products and investigate any trends relating incident power into the reaction to the resulting MOF crystals – how did the incident power effect yield, crystallinity, and morphology, were we able to produce polymorphs?
c) To rationalise any effects with regards to the interaction between incident microwave radiation.

With these in mind a scheme of reactions at different power levels were carried out; altering the power level while keeping the energy constant allowed for realisation of how MOF crystallisation was affected by different power densities in the heated phase, directly controlling the duration of the synthesis, something not possible in temperature controlled reactions.

During this work, the following observations were made:

a) The cuboidal morphology of the synthesised MFM-300 particles above 600 W was different both to the original conventional synthesis (nanometre plates)[41] and the microwave route developed in the commercial temperature controlled CEM microwave reactor.[2] (stubby cylinders, which were observed in 400 and 500 W experiments)
b) The crystals remained regularly shaped as opposed to forming irregular particles.
c) There was a correlation between the length of the particles and the power used for synthesis.

The impact of microwave heating on particle morphology is known, however, what was of particular note was that the crystals remained regularly shaped, and that this shape could be systemically altered. The elongation of the MOF particles is in contrast to the previous MIL-53 work[52] where the crystals became smaller, though largely retaining their regular cubic geometry. In the manuscript (Appendix 3) we present the hypothesis that this morphological control can be rationalised as a consequence of the selective heating mechanism; it is proposed that a growth step along the aluminium oxide backbone can occur without the linker present, whilst growth in any other direction requires addition of linker. Thus, since the aluminium salt is freely soluble and selectively heated and the linker sparingly soluble, the aluminium oxide growth along the crystal c axis is preferentially accelerated by microwave irradiation.

In the manuscript the possibility of defects within the crystal structure is also discussed, evidenced by the Renninger effect and the increased gas uptake seen in the previously published manuscript (Appendix 2). To further characterise possible defects, EDX (energy dispersive X-ray spectroscopy) analysis was conducted to see if chloride counter ions were present in the structure. The rational for investigating this was that a missing linker defect must be charged balanced, and this could entrap chloride ions in the structure. The total map EDX (Energy-dispersive X-ray spectroscopy) spectrum is shown in Figure 9. As with many analytical procedures the software can be forced to look for evidence of an element, and around the expected energy for chlorine (Kα1 = 2.622 keV)[53] there was a slight signal which could be discerned from the background noise. However, it was exceptionally small with

respect to the other elemental signals, with an estimated weight % of 0.01%. Mapping out these signals with respect to the SEM image (Figure 10) showed no coherent localisation in the data traces, (c.f. Appendix 3, ESI figure 1 where in definite shapes of MOF and linker particles are resolvable from the density of the elemental responses) indicating this to be nothing more than background noise.

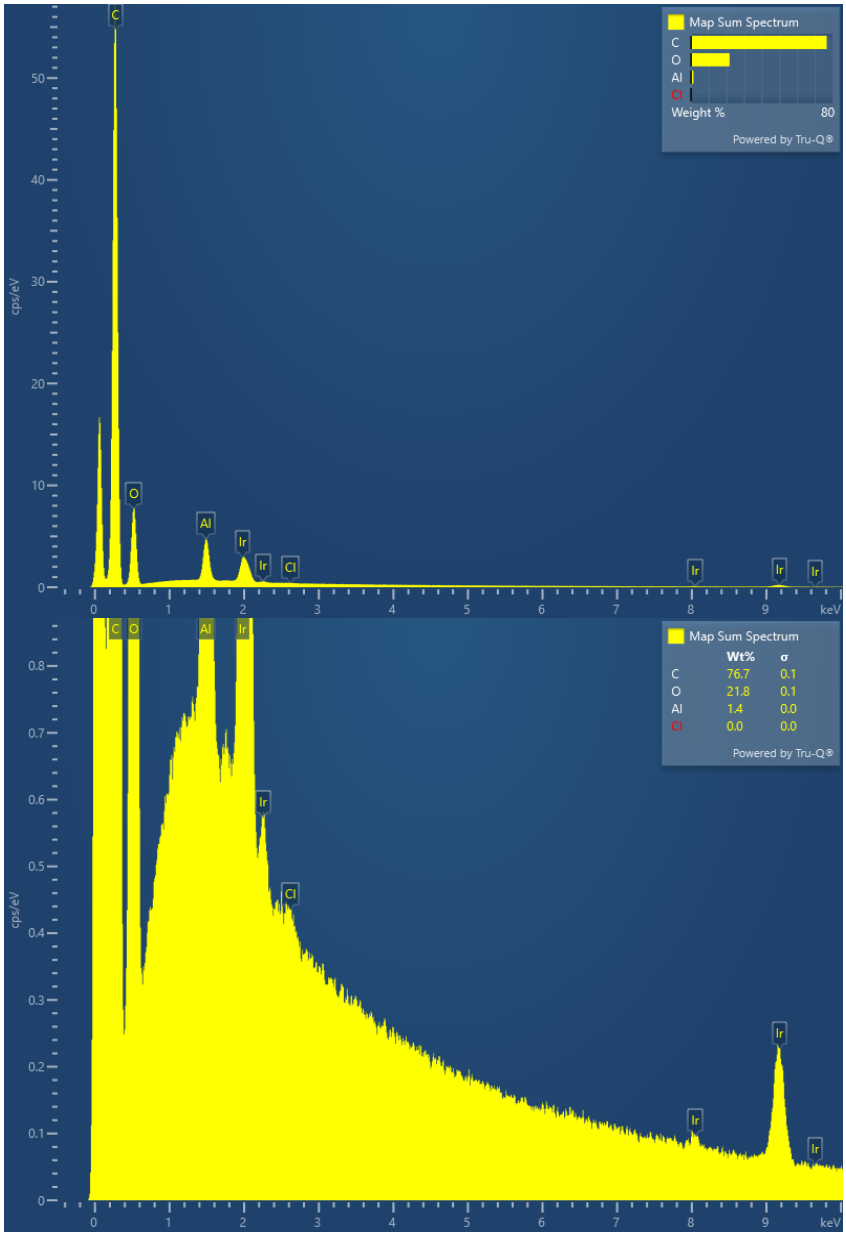


Figure 9: EDX spectrum of MFM-300(Al) synthesised in the P/EC reactor, corresponding to sample P/EC-8 (see Appendix 3 for details). Top: full spectrum scaled to the intensity of the carbon signal. Bottom: Zoomed in spectrum over an identical keV range to highlight the poor chlorine signal. Insert: Calculated composition expressed as weight %.

In order for the SBU to be charge balanced in defective systems this must necessitate coordinated hydroxides around the metal clusters. This would be potentially detectable by solid-state NMR (with the addition of a new O or H species) or IR/Raman spectroscopies.

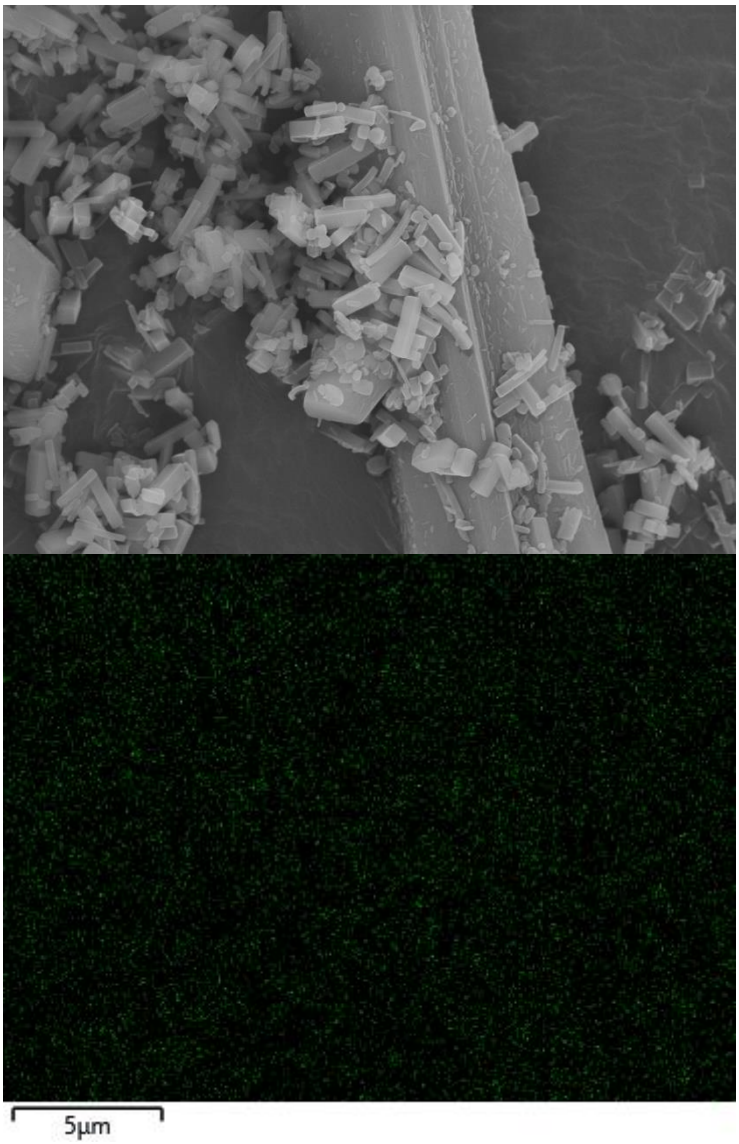


Figure 10: (Top) SEM micrograph of MFM-300(Al) synthesised in the P/EC reactor and (Bottom) the EDX map of the micrograph for chlorine. C.f. ESI figure 2 in the manuscript in appendix 3. The absence of any discernible grouping corresponding to either MOF or linker crystals leads to the conclusion that there is no chlorine in the sample, and the response in the EDX spectrum is simply background noise.

In the manuscript we state that PXRD showed no evidence of lower angle reflections. However, in samples obtained from the T/C (temperature controlled) reactor back when the original synthesis was being developed an errant reflection was observed at

low angle (Figure 11). This reflection (5.96 ° 2θ, 14.82 Å d-spacing) could not be fitted using the unit cell parameters and the $I4_122$ space group. The d-spacing is approximately the length of the *a* and *b* axis of the unit cell (14.83 Å).[41] Notably this reflection disappeared when the sample was left in air for an extended period of time, and thus this could possibly indicate a defect that is hydration dependent. Future investigation could involve temperature variable PXRD experiments.

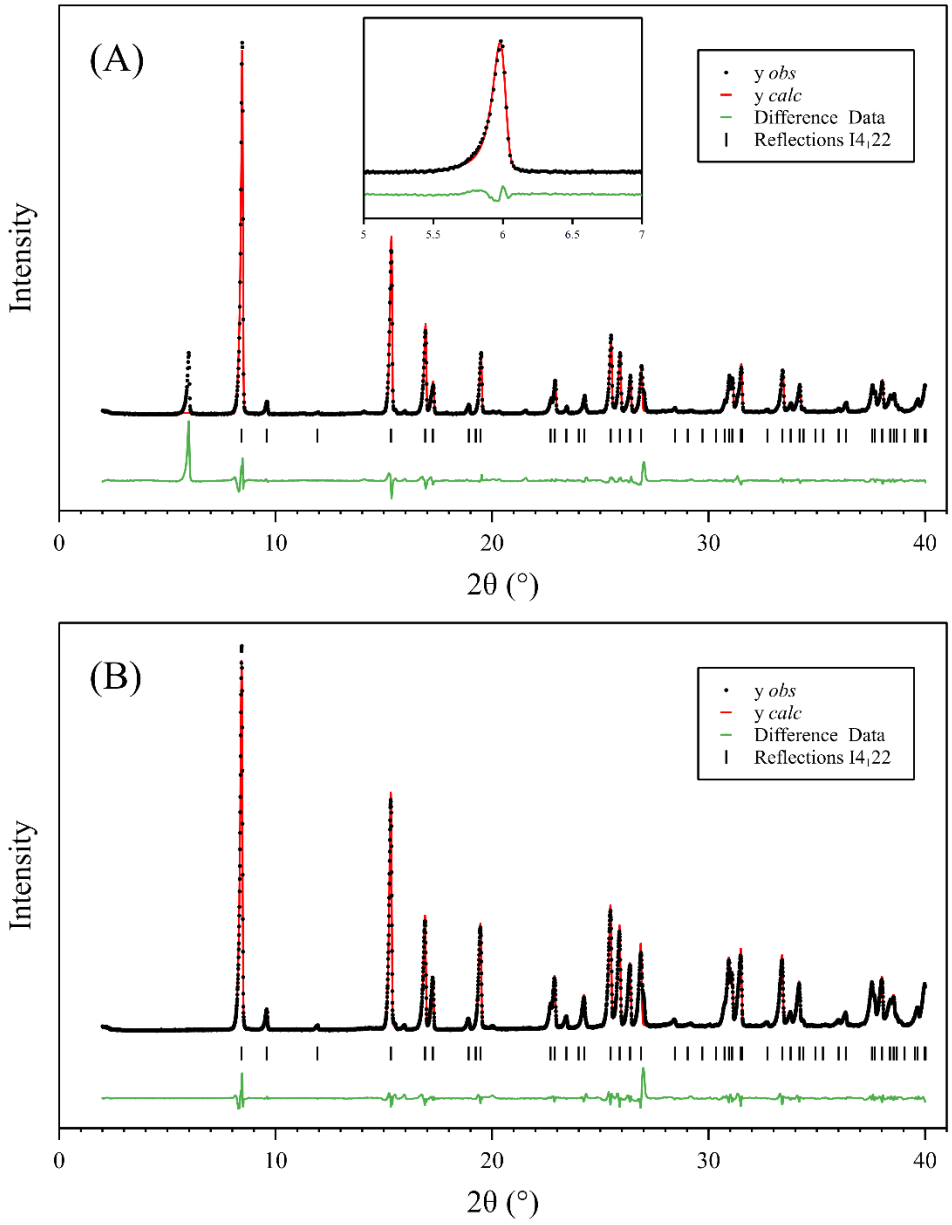


Figure 11: LeBail refinements of PXRD data for an MFM-300 sample (A) Initial experiment and (B) longer duration experiment after sample had been out on the diffractometer for ~ 30 minutes. Legends insert. Insert figure (A) zoomed in manual peak fit of the unidentified reflection at 5.95 °2θ.

A limitation of this work is that the batch reaction vessel, while less of a black box than the T/C reactor, is still limited by analysing the product of the reaction *ex situ*, after the reaction has occurred, cooled down and been worked up. Even with these limitations, however, significantly more understanding could be gained, and control levied from switching to P/EC (Power & Energy controlled) reactor, as the microwave delivery is now no longer controlled by an automated system relying on temperature readings. Because of this control, the effect microwave heating had on the morphology of the yielded particles could be rationalised mechanistically.

Microwave heating has been shown repeatedly to be capable of affecting important MOF properties. Here the morphology of MOF crystals is of importance to their potential application and further understanding of how this occurs can give insights into the mechanism of MOF synthesis. Thus control of these variables moving on is an important factor in reactor design. From a large-scale synthesis standpoint, the batch reactor is limited mostly by throughput. Although the reaction is exceptionally rapid the one and a half hour cooldown period leads to a low overall output of material. This provides an obvious motivation to move away from a batch reactor system and into a flow system, where the rapid reactions facilitated by microwave heating can lead to low residence times and high throughput. However, in both this manuscript and previous work[52] large amounts of linker were left over even in reactions which had the highest yield.

Chapter 4 – Purification of MFM-300(Al)

Appendix 4 contains a draft manuscript detailing a purification protocol for MFM-300(Al). In anticipation of transferring MFM-300(Al) from batch synthesis to flow, a method of purification was developed to enable recovery of any unreacted linker. Specifically the batch reactions had large amounts of linker left behind in the product as noted in previous studies on MIL-53[52] where large amounts of terephthalic acid remained as separate crystals in the produced powder (in addition to terephthalic acid occluded in the pores). The removal of this unreacted linker is essential for MOFs to be used in their intended applications as the nonporous mass of linker has a detrimental impact on the final product quality. Additionally, at £16800 a kg[54], reclamation of this unreacted linker for further use would be essential for the economic viability of any technology producing MFM-300(Al). Thus, a purification protocol must also be developed

In developing the purification protocol, the following requirements were considered essential:

a) Be achievable without the use of complicated process steps.
b) Occur at room temperature – energy intensive processing such as long duration calcination is less sustainable than a process which can occur in ambient conditions
c) Toxic solvents such as DMF need to be avoided as this would defeat the benefits of having a green water-based synthesis.
d) Ideally the removed linker should be reclaimable – linkers more complicated than single benzene rings require multistep organic synthesis, normally involving air sensitive cross coupling chemistry and so are exceptionally valuable.
e) Have a negligible effect on the MOF properties – There is zero utility in a purification protocol that causes extensive degradation of the material one desires to purify.

Based on these criteria a purification procedure was established using mild base. Purification with bases was attempted in the past by Haque *et al*.[55] and found to be inappropriate in the case of MIL-53(Al). However MFM-300(Al) was found to be sufficiently stable for the procedure.

Preliminary experiments were focused on removing the small excess of linker that was present after synthesis from the CEM microwave. Results from washing with a mild (0.01 M) aqueous piperazine (1,4-diazacyclohexane) solution (which was chosen due to its inclusion in the original MFM-300(Al) synthesis) were promising as there was no visible damage to the MOF crystals in the SEM images (Figure 12). While no reason is given in the original publication[41] for the addition of piperazine in the reaction it is plausible that its properties as a mild organic base aided in increasing the solubility of the organic acid linker in an otherwise acidic environment. Use of sodium hydroxide for washing, however, led to crystal degradation.

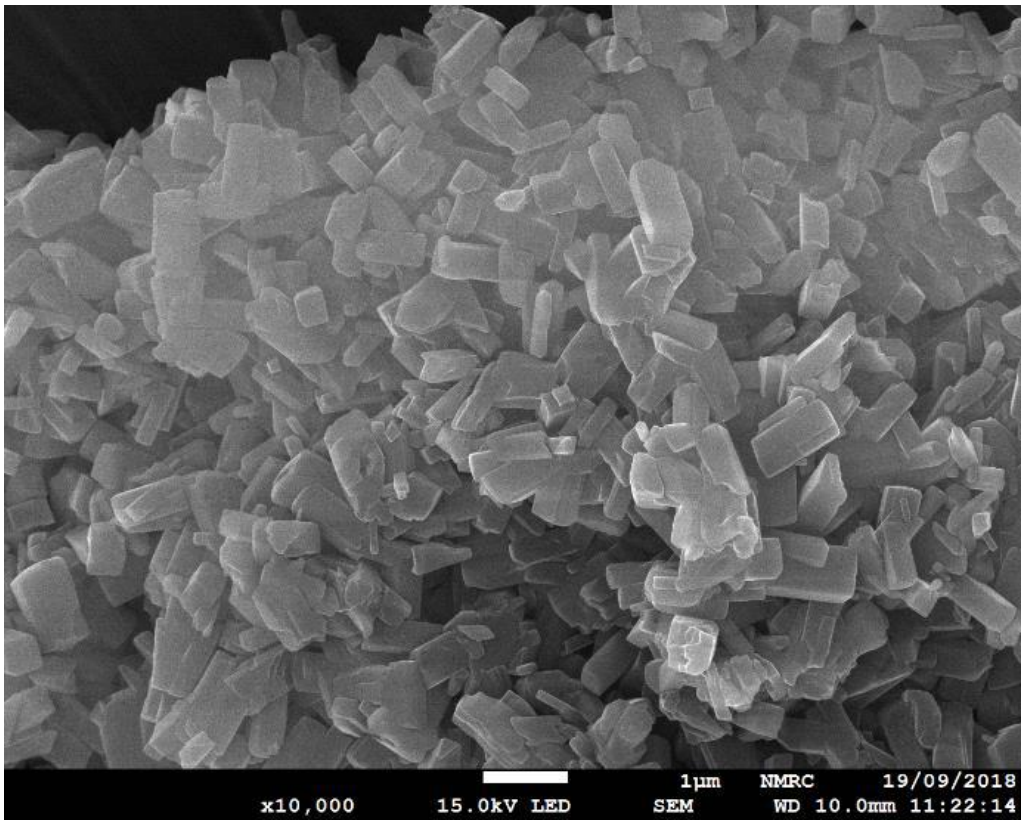


Figure 12 SEM of MFM-300(Al) washed with 0.1 M piperazine solution, the amount of linker in the experiment was not controlled, and the molar excess of piperazine therefore not characterised. The experiment was also sonicated for 20 minutes, which was removed with the subsequent switch to ammonia washing as the linker was shown to dissolve rapidly with no sonication required.

Ammonia was also trialled as it is a readily available mass-produced chemical synthesis (more so than piperazine) while having similar properties as a nitrogenous base. Ammonia is sufficiently basic to deprotonate and form conjugate salts with phenolic acids as a gas[56,57] and in aqueous solution. Additionally the pK_b of ammonia is marginally higher than piperazine (with a pK_b range of 4.83 to 4.73 from 5 to 40 °C

respectively[58]). For context, at 15 °C a 0.2 M ammonia solution has a concentration of only 0.0018 M hydroxide ions, whereas a 0.2 M solution of a sodium hydroxide base would formally be considered to dissociate completely and have 0.2 M concentration of hydroxide ions.

The methodical study in the prepared manuscript was designed to show not only a proof of concept but also detail the wide range of conditions with regards to ammonia concentration and relative quantity, as for a potential industrial scale procedure a degree of tolerance is desirable. Ammonia was found to be excellent at purifying the MOF, with negligible harm to the framework, recoverable of the linker and requiring nothing more complicated than a vessel and a centrifuge.

Ideally a wider range of alkaline solutions would be tested and compared to alternative solvents, and other MOFs tested as well. It is curious that MFM-300(Al) is resistant to ammonia in solution while MIL-53 was not.[55] Both MOFs are capable of taking ammonia in the gas phase, without suffering crystal degradation, and their structures are highly similar. A fundamental conclusion of the manuscript is that, while ammonia solution may not be suitable for all MOFs, it is worth investigating if it is usable for the purification of any particular target MOF.

Chapter 5 – Continuous flow microwave synthesis of MOFs

HKUST-1 is one of the most studied MOFs. The MOF is already available for commercial purchase, and its MW synthesis had already been reported using commercial microwaves, and in specifically designed microwave flow reactors. In our work, a thin MW reactor and OBR (Oscillatory Baffled Reactor) was used to synthesise high quality HKUST-1, achieving record space time yields. OBR's offer enhanced mixing within flow reactors by disrupting the flow and creating vortices within the reactor tube. The thinness of the tube minimised any negative impacts of microwave penetration depths being exceeded. COMSOL Multiphysics modelling presented in the manuscript indicated a largely homogenous distribution of electric field within the reactor, though with two distinct hotspots within the heating section. The reactor was not capable of pressurisation due to the glass construction, as such energy could only be supplied up to the boiling point of the ethanol reaction solvent.

Analysis of these samples with PXRD consistently showed the formation of HKUST-1, with gas adsorption experiments confirming that despite the high throughput synthesis the material was still porous. This is in contrast with previously reported HKUST-1 microwave synthesis which exhibited a significant reduction in gas capacity.[59] SEM analysis showed that at low flow rates (and consequently low powers) the crystals formed regular polyhedra similar to that observed in traditional synthesis methods. However, as flow rate increased (and so crystallisation occurred under higher power) the regular polyhedra were replaced with tiny highly irregular nanoparticles. Within each sample the distribution of morphology (shape and size) was significantly narrowed than that observed in the MFM-300 work, and this can be ascribed to the crystallisation environment being significantly more homogeneous. Also the lower energy requirement for HKUST-1 growth possibly led to a greater degree of Ostwald ripening in the cooling reaction mixture.

The exceptionally short residence time that was achieved (2.2 seconds) gave a record high space time yield form HKUST-1 (6.32×10^5 kg/m^3/day), which compares favourably to the previous record of 4.00×10^5 kg/m^3/day in a continuously stirred tank reactor. Additionally, a favourable comparison was drawn with regards to gas adsorption, where this product showed a significantly higher BET surface area. Yield was quite low at 27%, and it was suggested that altering the reactant ratio or

temperature may improve this – however, this would require a subsequent redesign of the reactor to account for penetration depth and pressure rise.

Taken together these two sets of experiments; (MFM-300(Al) batch reactions [appendix 3] and HKUST-1 flow reactor synthesis [appendix 5]) show two different trends in the resultant morphology from microwave heating. Though in both cases microwave heating could yield regular crystals this irregularity was not seen in the MFM-300 work. It is uncertain whether this difference stems from the MOF in question, the powers used, or the nature of the reactors. However, a key difference between the two experiments is the reaction time achieved, ~24 seconds for MFM-300 vs ~3 seconds for HKUST-1. It is possible that if MFM-300 synthesis was achieved in such a short reaction the resultant crystals would similarly be reduced to irregular nanoparticles. Though this is only one of a myriad of differences between the two case studies.

Chapter 6 – General conclusions and future work

6.1 – Conclusions of the attached manuscripts.

Overall, the manuscripts in appendices 2 -5 show a coherent set of efforts to develop a more fundamental understanding of the interaction of microwave energy with MOF chemistry and to also address some of the challenges associated with microwave MOF synthesis scale up. While the work presented here is mostly focused on MFM-300(Al), the methodology would be appropriate for any framework for which a large-scale microwave synthesis solution is desired:

1. Develop a microwave suitable synthesis. For some MOFs (such as HKUST-1 or MIL-53) the standard published synthesis is freely adaptable to a microwave reactor; however as seen here with MFM-300(Al) this is not always the case. Due to this, the development of MW synthesis could be as difficult as developing a successful synthesis from scratch. In this work the synthesis developed was an improvement on the original synthesis in terms of time (3 days down to 10 minutes) and material gas capacity.
2. Transfer from T/C reactors into P/EC reactions. This is an intermediate step to realising a flow reaction set up and demonstrates a proof of concept that a ramp only methodology will work for the reaction, whilst also enabling the characterisation of the effects different power deliveries have on the yielded framework. In the work presented here, this demonstrated a new capacity for control over the MOF crystallisation and for the first-time rationalised microwave synthesis of MOFs morphological control as a consequence of the selective heating mechanism.
3. Transfer into a suitable microwave flow reactor. The synthesis of HKUST-1 in a microwave flow reactor described in Chapter 5 demonstrates a gram per minute scale synthesis and the effects of different microwave powers with regards to the material properties. Efforts to realise this for MFM-300 were sadly curtailed (see section 6.2)
4. Address any problems with post synthetic work up. Here the immediate challenge was developing a purification protocol, however, for alternative MOFs it could be post synthetic modification to introduce additional functionality into the pore structure of the material, or a bulk post synthetic processing step such as pelletisation.

6.2 – Future work

This section details future work arising from the work conducted in this thesis.

6.2.1. – Flow synthesis of MFM-300(Al) and other frameworks

As identified throughout the manuscripts and commentary, microwave heating is an exciting area of MOF research due to its rapid reactions enabling larger scale synthesis than traditionally conventionally heated reactions. Whilst the CEM and bespoke batch reactors represent progress in this direction they are still limited to milligram quantities of MOF, albeit produced in significantly shorter time spans. Indeed at peak efficiency the batch reactor can realistically be operated 6 times during a standard working day, limiting the highest yield synthesis to ~1.8 g of MFM-300 per week, and with a degree of variability between batches due to penetration depth and the inherent instability with operating a pressurised batch reactor under such rapid heating conditions. To overcome these limitations, it was intended to shift the synthesis of MFM-300 (as well as other target MOFs) into a microwave flow reactor. A continuous flow reaction system is a proven method of process intensification, and with microwave MOF synthesis such short reaction times can translate to low residence times, thus compact reactors, and high throughputs. Once at steady state, a reactor can be run constantly as long as feedstocks are supplied, enabling a much greater degree of control over a large duration, thus a greater level of consistency can be achieved in the MOF product in comparison to a batch reactor. The reactor which was designed to achieve this has a narrow hot zone to achieve homogeneous heating, and this is believed to have led to some of the problems when attempting to get the reactor operational as it results in the reactor getting blocked, over pressurising and rupturing within the wave guide.

6.2.2. – Morphology & penetration depth.

A fundamental underlying theme of the presented investigations has been the desire to remove uncertainty in microwave heated MOF synthesis, that is to step away from temperature controlled reactions and transition into experiments where microwave radiation can be precisely delivered into the reaction mixture. Furthermore, it is also important to understand how microwave heating is facilitating MOF synthesis. While the work presented herein does step in this direction there are hindrances in interpretation from elements of the reaction which are difficult to characterise. This includes penetration depth, or more specifically how the microwave field attenuates as

it penetrates into the heated phase, which leads to uncertainty in the interpretation of results, as MOF synthesis is essentially occurring in different power environments depending on the nucleation site's location within the reaction, and so the very thing that is trying to be characterised is uncertain. This also leads to the problem of the batch rig as used being a chaotic system, where a subtle change in the initial conditions results in potentially very different behaviour by the end of the experiment.

To address this issue any further experimentation needs to better account for penetration depth as well as note the following recommendations:

a) The reactor must be as small as possible (depending on penetration depth < 1 cm) while being still able to adsorb microwave energy.
    - While penetration depth is a problem, a counter problem is experienced if there is insufficient mass within the cavity it will simply not be possible to match the microwave energy into the heating load.
    - A large reactor in which penetration depth remained an issue could be solved by diluting the sample (thus lowering the dielectric properties of the reaction mixture and increasing penetration depth)
    - An alternative frequency could also be used, as frequency reduces the penetration depth increases, leading to a larger penetration depth and thus more homogeneous distribution across the reaction (assuming no change in dielectric properties). For the MFM-300 reaction mixture used in chapter 3, switching to a 915 MHz results in a penetration depth increased to only 6.15 mm (c.f. 4.3 mm at 2.45 GHz)
b) The reactor must be able to hold pressure sufficient for the reaction temperature to be reached. In investigating MFM-300 this pressure is quite high at 19 bar, though obviously a degree of tolerance is desired both from a safe operating and a practicality standpoint. A higher-pressure tolerance would allow for resolution of the effects of microwave heating both in terms of power and energy (for example, experimenting with energies which result in a temperature of 250 °C; what occurs to the MOF under these circumstances)
c) The reactor would benefit for being transparent and in a waveguide in which macroscopic factors such as the distribution of insoluble/soluble species, stirring and boiling can all be observed.

- This final point is to further reduce the degree to which the reaction occurs in ‘black box’
- Compatible with forms of insitu analysis, such as IR and PXRD experiments.

6.2.3. – Synchrotron powder x-ray diffraction experiments, *in-situ* understanding

Alluded to in section 6.2.2, *in situ* PXRD has been used in the past to investigate MOF crystallisation in microwave reactors,[60,61] or for online measurements in microwave flow reactors.[40] A great disadvantage of the lab scale diffractometers is the reliance on *ex situ* analysis (preparing a multi-phase electrostatic material that sits on a wide shallow sample plate which tilts consistently is not a feasible endeavour). PXRD experiments with high quality data could be obtained with purified samples in a capillary on either a well focused lab diffractometer or a synchrotron beamline.

A possible application of PXRD in this research could be the investigation of defects within the crystals. Assuming high enough quality data could be taken, a rietveld refinement can reveal site occupancy, atomic displacement, and unassigned electron density within the unit cell. Thus, missing linker defects would be visible as a lower than expected site occupancy of linker carbons, and an expected increase in the anisotropic atomic displacement of the SBU atoms as their positions are allowed to move to compensate for the lack of linker. Additionally, it would be expected that there may be disordered electron density around defect sites from adsorbed species.

6.2.4. – Summary of future work

The future work arising from this thesis would best be focused on two main avenues of investigation. Firstly using microwave heating and building on the mechanistic understanding presented in chapter 3 to better understand the fundamental mechanism of MOF formation under microwave heating, by developing a reactor suitable for *insitu* investigations of the crystallisation. Secondly, to build on the rapid reactions facilitated in chapters 2 and 3, combined with the purification protocol presented in chapter 4 and drawing from similar work in chapter 5 to achieve large scale synthesis of MFM-300(Al).

References

1 I. Thomas-Hillman, A. Laybourn, C. Dodds and S. W. Kingman, *J. Mater. Chem. A*, 2018, **6**, 11564–11581.

2 I. Thomas-Hillman, L. A. Stevens, M. Lange, J. Möllmer, W. Lewis, C. Dodds, S. Kingman and A. Laybourn, *Green Chem.*, 2019, **21**, 5039-5045

3 A. Laybourn, A. M. López-Fernández, I. Thomas-Hillman, J. Katrib, W. Lewis, C. Dodds, A. P. Harvey and S. W. Kingman, *Chem. Eng. J.*, 2019, **356**, 170–177.

4 U. Mueller, M. Schubert, F. Teich, H. Puetter, K. Schierle-Arndt and J. Pastré, *J. Mater. Chem.*, 2006, **16**, 626–636.

5 A. U. Czaja, N. Trukhan and U. Müller, *Chem. Soc. Rev.*, 2009, **38**, 1284–1293.

6 M. Hirscher and B. Panella, *Scr. Mater.*, 2007, **56**, 809–812.

7 K. Konstas, T. Osl, Y. Yang, M. Batten, N. Burke, A. J. Hill and M. R. Hill, *J. Mater. Chem.*, 2012, **22**, 16698–16708.

8 W. Xuan, C. Zhu, Y. Liu and Y. Cui, *Chem. Soc. Rev.*, 2012, **41**, 1677–1695.

9 K. Xu, A. M. P. Moeljadi, B. K. Mai and H. Hirao, *J. Phys. Chem. C*, 2018, 122, 1, 503–514.

10 P. Silva, S. M. F. Vilela, J. P. C. Tomé and F. A. A. Paz, *Chem. Soc. Rev.*, 2015, **44**, 6774–6803.

11 V. Calvino-Casilda and R. M. Martín-Aranda, *Recent Pat. Chem. Eng.*, 2011, **4**, 1–16.

12 A. Dhakshinamoorthy, M. Alvaro and H. Garcia, *Chem. Commun.*, 2012, **48**, 11275–11288.

13 J. Lee, O. K. Farha, J. Roberts, K. A. Scheidt, S. T. Nguyen and J. T. Hupp, *Chem. Soc. Rev.*, 2009, **38**, 1450-1459.

14 L. E. Kreno, K. Leong, O. K. Farha, M. Allendorf, R. P. Van Duyne and J. T. Hupp, *Chem. Rev.*, 2012, **112**, 1105–1125.

15 P. Kumar, A. Deep and K.-H. Kim, *TrAC Trends Anal. Chem.*, 2015, **73**, 39–53.

16 R.-B. Lin, S.-Y. Liu, J.-W. Ye, X.-Y. Li and J.-P. Zhang, *Adv. Sci.*, 2016, **3**, 1500434

17 P. Horcajada, C. Serre, M. Vallet-Regí, M. Sebban, F. Taulelle and G. Férey, *Angew. Chem. Int. Ed.*, 2006, **45**, 5974–5978.

18 M. Arruebo, *WIREs Nanomedicine Nanobiotechnology*, 2012, **4**, 16–30.

19 M. Kotzabasaki and G. E. Froudakis, *Inorg. Chem. Front.*, 2018, **5**, 1255–1272.

20 J. Zhou and B. Wang, *Chem. Soc. Rev.*, 2017,**46**, 6927-6945.

21 X.-C. Xie, K.-J. Huang and X. Wu, *J. Mater. Chem. A*, 2018, **6**, 6754–6771.

22 E. S. Goda, S. Lee, M. Sohail and K. R. Yoon, *J. Energy Chem.*, 2020, **50**, 206–229.

23 S.-Y. Moon, Y. Liu, J. T. Hupp and O. K. Farha, *Angew. Chem. Int. Ed.*, 2015, **54**, 6795–6799.

24 H. Furukawa, K. E. Cordova, M. O'Keeffe and O. M. Yaghi, *Science*, 2013, **341**, 1230444.

25 D. M. D'Alessandro, B. Smit and J. R. Long, *Angew. Chem. Int. Ed.*, 2010, **49**, 6058–6082.

26 J.-R. Li, R. J. Kuppler and H.-C. Zhou, *Chem. Soc. Rev.*, 2009, **38**, 1477.

27 B. Yilmaz, N. Trukhan and U. Müller, *Chin. J. Catal.*, 2012, **33**, 3–10.

28 Statistics obtained from OICA (International organization of Motor Vehicle Manufacturers), http://www.oica.net, (accessed 25 February 2020).

29 M. S. Venkatesh and G. S. V. Raghavan, *Biosyst. Eng.*, 2004, **88**, 1–18.

31

30 C. Leonelli and T. J. Mason, *Chem. Eng. Process. Process Intensif.*, 2010, **49**, 885–900.

31 H. J. Kitchen, S. R. Vallance, J. L. Kennedy, N. Tapia-Ruiz, L. Carassiti, A. Harrison, A. G. Whittaker, T. D. Drysdale, S. W. Kingman and D. H. Gregory, *Chem. Rev.*, 2014, **114**, 1170–1206.

32 A. Buttress, A. Jones and S. Kingman, *Cem. Concr. Res.*, 2015, **68**, 112–123.

33 F. Wei, D. Chen, Z. Liang, S. Zhao and Y. Luo, *RSC Adv.*, 2017, **7**, 46520–46528.

34 S. Zhao, D. Chen, F. Wei, N. Chen, Z. Liang and Y. Luo, *J. Chem. Technol. Biotechnol.*, 2018, **93**, 698–709.

35 F. Wei, D. Chen, Z. Liang and S. Zhao, *Nanomaterials* **2018**, *8*(4), 248

36 N. Chen, D. Chen, F. Wei, S. Zhao and Y. Luo, *Chem. Phys. Lett.*, 2018, **705**, 23–30.

37 D. Chen, P. Feng and F. Wei, *Chem. Eng. Process. - Process Intensif.*, 2019, **135**, 63–67.

38 T. K. Vo, V. N. Le, K. S. Yoo, M. Song, D. Kim and J. Kim, *Cryst. Growth Des.*, 2019, **19**, 4949–4956.

39 T. K. Vo, V. N. Le, V. C. Nguyen, M. Song, D. Kim, K. S. Yoo, B. J. Park and J. Kim, *J. Ind. Eng. Chem.*, 2020, **86**, 178–185.

40 M. Taddei, D. A. Steitz, J. A. van Bokhoven and M. Ranocchiari, *Chem. - Eur. J.*, 2016, **22**, 3245–3249.

41 S. Yang, J. Sun, A. J. Ramirez-Cuesta, S. K. Callear, W. I. F. David, D. P. Anderson, R. Newby, A. J. Blake, J. E. Parker, C. C. Tang and M. Schröder, *Nat. Chem.*, 2012, **4**, 887–894.

42 X. Zhang, I. da Silva, H. G. W. Godfrey, S. K. Callear, S. A. Sapchenko, Y. Cheng, I. Vitórica-Yrezábal, M. D. Frogley, G. Cinque, C. C. Tang, C. Giacobbe,

C. Dejoie, S. Rudić, A. J. Ramirez-Cuesta, M. A. Denecke, S. Yang and M. Schröder, *J. Am. Chem. Soc.*, 2017, **139**, 16289–16296.

43 H. G. W. Godfrey, I. da Silva, L. Briggs, J. H. Carter, C. G. Morris, M. Savage, T. L. Easun, P. Manuel, C. A. Murray, C. C. Tang, M. D. Frogley, G. Cinque, S. Yang and M. Schröder, *Angew. Chem. Int. Ed.*, 2018, **57**, 14778–14781.

44 J. Carter, C. Morris, H. G. W. Godfrey, S. J. Day, J. Potter, S. P. Thompson, C. Tang, S. Yang and M. Schröder, *ACS Appl. Mater. Interfaces*, 2020, 12, 38, 42949–42954.

45 P. Z. Moghadam, A. Li, S. B. Wiggin, A. Tao, A. G. P. Maloney, P. A. Wood, S. C. Ward and D. Fairen-Jimenez, *Chem. Mater.*, 2017, **29**, 2618–2625.

46 X. Han, H. G. W. Godfrey, L. Briggs, A. J. Davies, Y. Cheng, L. L. Daemen, A. M. Sheveleva, F. Tuna, E. J. L. McInnes, J. Sun, C. Drathen, M. W. George, A. J. Ramirez-Cuesta, K. M. Thomas, S. Yang and M. Schröder, *Nat. Mater.*, 2018, **17**, 691–696.

47 C. G. Morris, N. M. Jacques, H. G. W. Godfrey, T. Mitra, D. Fritsch, Z. Lu, C. A. Murray, J. Potter, T. M. Cobb, F. Yuan, C. C. Tang, S. Yang and M. Schröder, *Chem. Sci.*, 2017, **8**, 3239–3248.

48 Unpublished structure, Crystallographic information file provided by private communication, .

49 T. Loiseau, C. Mellot-Draznieks, H. Muguerra, G. Férey, M. Haouas and F. Taulelle, *Comptes Rendus Chim.*, 2005, **8**, 765–772.

50 P. P. Reichertz and W. J. Yost, *J. Chem. Phys.*, 1946, **14**, 495–501.

51 S. P. Dubey, A. D. Dwivedi, M. Sillanpää, H. Lee, Y.-N. Kwon and C. Lee, *Chemosphere*, 2017, **169**, 99–106.

52 A. Laybourn, J. Katrib, R. S. Ferrari-John, C. G. Morris, S. Yang, O. Udoudo, T. L. Easun, C. Dodds, N. R. Champness, S. W. Kingman and M. Schröder, *J. Mater. Chem. A*, 2017,**5**, 7333-7338

53 E. C. Montenegro, G. B. Baptista and P. W. E. P. Duarte, *At. Data Nucl. Data Tables*, 1978, **22**, 131–177.

54 Personal communication - Sales representatives from Manchester organics - 24/01/2019, .

55 E. Haque, N. A. Khan, J. E. Lee and S. H. Jhung, *Chem. – Eur. J.*, 2009, **15**, 11730–11736.

56 R. S. Miller, D. Y. Curtin and I. C. Paul, *J. Am. Chem. Soc.*, 1974, **96**, 6329–6334.

57 W.-W. Yang, Y.-Y. Di, Y.-X. Kong, X.-Y. Guo and Z.-C. Tan, *Thermochim. Acta*, 2010, **502**, 14–19.

58 R. G. Bates and G. D. Pinching, *J. Res. Natl. Bur. Stand.*, 1949, **42**, 419.

59 C. McKinstry, E. J. Cussen, A. J. Fletcher, S. V. Patwardhan and J. Sefcik, *Chem. Eng. J.*, 2017, **326**, 570–577.

60 T. Ahnfeldt, J. Moellmer, V. Guillerm, R. Staudt, C. Serre and N. Stock, *Chem. – Eur. J.*, 2011, **17**, 6462–6468.

61 R. E. Osta, M. Feyand, N. Stock, F. Millange and R. I. Walton, *Powder Diffr.*, 2013, **28**, S256–S275.

Appendices:

These appendices contain manuscripts both published (1, 2 & 5) and prepared for publication (3 & 4). In the case of the published manuscripts, the appendices are copied from the published work with only minor formatting changes to the text and image sizes in order to incorporate them into the thesis format and aid in reading. No editorial changes have been made to either the text or the figures of these manuscripts. All figures are labelled as they appear in the published versions.

For the prepared manuscripts, the text and figures exist in a from intended for submission; but have not yet been peer reviewed and therefore will be subject to change between their current form and any subsequent versions published in peer reviewed literature.

All appendices contain their own references. All references retain the format of the original manuscripts.

Appendix 1: Realising the environmental benefits of metal–organic frameworks: recent advances in microwave synthesis

Ieuan Thomas-Hillman, Andrea Laybourn, Chris Dodds and Samuel W. Kingman
Faculty of Engineering, University of Nottingham, Nottingham, UK

Submitted 29th March 2018, Accepted 22nd May 2018

Published in Journal of Materials Chemistry A, 2018, 6, 11564-11581

DOI: 10.1039/C8TA02919A

Statement of contribution of joint authorship

Ieuan Thomas – Hillman conducted the review of the literature. Ieuan Thomas-Hillman and Andrea Laybourn wrote and iterated on manuscript drafts. Chris Dodds and Samuel Kingman proof-read, and critically commented on the manuscript. Andrea Laybourn submitted the manuscript for publication.

N.B. Figure 3, showing SEM of MOF synthesised in both conventional heating and microwave heating has been labelled incorrectly in the published manuscript. A minor correction is contained in a foot note next to the relevant figure.

Abstract

Metal–organic frameworks (MOFs) are a broad class of porous crystalline materials that show great potential for a wide-range of applications in areas such as energy and environmental sustainability. MOFs can show significant advantages in gas selectivity and separation over traditional adsorbents such as zeolites and activated carbons since they are tuneable both in terms of porosity and chemical functionality. The ability to control the pore environment of the MOF is one of their remarkable advantages and affords control over the structure and properties required for specific applications. Despite these advantages, the industrial adoption of MOFs is slow owing to the paucity of scalable, environmentally sustainable manufacturing methods and higher costs compared to zeolites. Microwave (MW) technology is an extremely promising method

of MOF production owing to significantly reduced reaction times and subsequently lower process energy consumption, control over MOF properties, and the ability to produce MOFs and MOF-hybrids otherwise difficult to isolate or unobtainable through other synthetic routes. However, the ability to produce the multiple kilogram or even tonne quantities of MOFs required by industry using MW technology is yet to be achieved owing to little or no understanding of the interaction(s) of reactants and MOFs with the electric field, and crucially, how this informs the design of the scale up processes. This review aims to bridge this gap in knowledge by (1) highlighting recent advances in understanding of MW–MOF interactions and areas for future focus; (2) providing an up-to-date and comprehensive summary of literature on MW synthesis of MOFs, focusing on examples where MW heating has facilitated novel and unique results in the laboratory; and (3) emphasising the advantages, challenges and current steps and methodologies required towards industrial-scale MW production of MOFs.

1. Introduction

Metal–organic frameworks (MOFs)[2] are a specific subset of coordination polymers, comprised of metal nodes/clusters and organic linkers, which combine together forming porous supramolecular networks analogous to zeolites in structure. The field of MOFs first emerged in the 1990s with preliminary work performed by Hoskins and Robson.[3,4] In 1995 Yaghi *et al.*[5–7] used the term "metal–organic framework" for the first time, showing selective accommodation of guest species in the porous material. Since these early reports, an exponentially increasing number of frameworks have been synthesised and studied, leading to the development of one of the hottest areas of chemical research with over 17 000 papers in the field published to date, as shown in Fig. 1.[8]

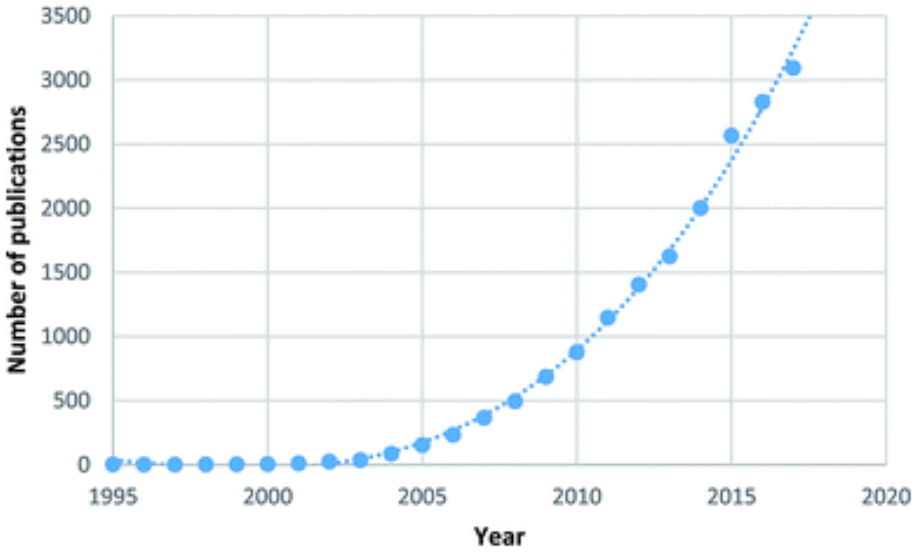


Fig. 1 Number of MOF papers published by year highlighting the high level of research interest.[8]

MOFs have attracted extensive and continually increasing interest from both academia and, more recently, industry owing to their unprecedented porosity and structural and functional diversity. Proposed applications of MOFs include separations,[9–11] gas storage,[11] catalysis,[11,12] sensing,[11,13–15] as synthetic precursors to porous materials[16,17] and as stimuli-responsive materials.[18,19] A significant advantage of MOFs over traditional adsorbents such as zeolites and activated carbons is the ability to tailor the pore environment of the MOF which affords control over the structure and properties required for any specific application.[20]

Typically MOFs are prepared by solvothermal batch reactions whereby solutions of metal salt and organic linker are heated above the boiling point of the solvent and retained under autogenous pressure for up to one week.[21] This synthetic route has inherent problems as it can produce MOFs of low quality (reduced crystallinity and porosity and non-uniform particle size and morphology, all of which are vital for processing to tailor practical applications). Additional problems include poor reproducibility between batches, long reaction times, large volumes of toxic solvent, and high cost of scale-up along with significant energy consumption.[22] The development of technologies that reproducibly give high-quality MOFs whilst reducing the cost of manufacture in an efficient and sustainable way is a key enabling step in the transfer of MOF research from the laboratory to industry and the ultimate realisation of the environmental process benefits that MOFs offer.

Over the past two decades microwave technology has been investigated as an alternative heating method in the preparation of MOFs with a rapidly growing number of publications in this field (over 200 papers published to date).[23] Microwave heating is a tremendously exciting route for MOF production as it offers the following benefits; considerably reduced synthesis times (from hours to seconds) and therefore significantly reduced energy consumptions[24,25] and control over MOF properties (particle size,[24,26,27] morphology[25] and phase-selectivity[28]). Importantly, through rapid and selective heating, microwave technology has been used to prepare MOFs and MOF-hybrids otherwise difficult to isolate or unobtainable through other synthetic routes. Despite this hugely exciting research, the majority of published approaches have involved generic lab microwave systems and experiments that essentially use microwaves as a mechanism for simply rapid heating of solvent. The same is also true of attempts to process zeolites using microwave heating where a number of laboratory-scale studies have been reported using domestic microwave ovens.[29] In order to facilitate future developments in microwave synthesis of MOFs (and zeolites) beyond the laboratory, greater understanding of the microwave parameters that are essential for scale-up is required. To this end, we present an up-to-date critical survey of literature relevant to MW synthesis of MOFs. This paper is organised as follows: first the theory of microwave heating and parameters that inform the design of scaled-up MW processes are discussed. Next we provide a comprehensive summary of MOF synthesis using microwave heating and compare materials prepared by this method to those obtained by conventionally heated solvothermal routes. Here we focus on reports of novel results exclusive to microwave heating as it is well-known that for economic impact MWs must be able to achieve outcomes that no other thermal processing method can due to high capital expenditure.[1] Finally we discuss the challenges and current progress towards industrial-scale MW production of MOFs. This review aims to assist the progression of microwave-assisted MOF synthesis research by systematically organising previous knowledge in this area across the reported literature in an accessible and informative manner and by identifying areas for future growth.

2. The theory of microwave heating and its application to MOF synthesis

In conventional heating energy is delivered to the material (or reaction mixture in the case of MOF synthesis) by conductive, convective or radiative heat transfer. In dielectric or microwave heating, energy is delivered through interaction of the electronic structure of the material with the alternating electric field. The extent to which the material interacts with the electric field can be characterised by the dielectric properties of the mixture (specifically the dielectric constant, ε', and dielectric loss, ε'').[30,31] ε' indicates the ability of the material to store energy through a form of polarisation, while ε'' is the ability of the material to convert the stored energy to heat.[30,31] At microwave frequencies, two polarisation or loss mechanisms occur, namely dipolar and ionic polarisation.[30,32,33] Dipolar mechanisms occur for molecules that have a permanent dipole, such as water and *N*,*N*-dimethylformamide. These molecules experience torque which forces them to reorient in the direction of the applied electric field.[32,33] Ionic mechanisms occur in solutions containing ions, such as dissolved salts; in this case the cations and anions are displaced by the oscillating electric field.[30,32,33] In both dipolar and ionic polarisation, the species in solution experience frictional forces from neighbouring molecules which is lost as heat.[30,32,33] It is important to note that the dielectric properties (ε' and ε'') greatly depend on a number of factors including, but not limited to, frequency of the electromagnetic field, temperature, physical state (solid, liquid, or gas), composition and concentration.[30,32,33] Therefore, ε' and ε'' may vary considerably during a microwave heating process and determination of their values for each reaction is required for detailed understanding of the interaction of the electric field with the material(s) of interest.[31]

The dielectric properties of individual components within the bulk reaction mixture indicate which reactants interact more strongly with the electric field and thus heat more effectively. Generally, reactants with high values of ε'' heat well and those with low ε'' heat poorly. If there are large differences in the dielectric properties, then individual components will be selectively heated and become much hotter than the bulk.[34] Through dielectric properties measurements, Laybourn *et al.*[34] showed that aqueous metal(III) salts interact strongly with the electric field ($\varepsilon'' > 35$), whereas

terephthalic acid exhibits little interaction ($\varepsilon'' < 0.03$). These results showed that the aqueous metal(III) salts will absorb more power and, therefore, heat more effectively than the ligand. This was the first indication of a selective heating process in MOF synthesis by microwaves. Further evidence of a selective heating mechanism in microwave synthesis of MOFs was also provided, for the first time, by Laybourn *et al.*[25] Using a specifically designed single mode microwave applicator capable of housing a pressure vessel in a well-defined electric field. The authors showed an increase in yield of MIL-53(Al) (MIL = Materials Institute Lavoisier) with increasing average absorbed power at a constant total absorbed energy. Importantly, the reports by Laybourn *et al.* showed that while still often conducted in pressurised vessels and with identical reaction mixtures, microwave synthesis of MOFs proceeds *via* a different heating mechanism to conventionally heated reactions. Selective heating can be advantageous as it may give reaction products unobtainable through conventional heating and can result in lower production of unwanted side-products; this is discussed further in Section 3. Crucially it also gives rise for the potential to significantly reduce energy consumption in a process as the whole bulk of the reaction mixture does not need to be heated to the same overall temperature as in a conventional process.

As well as governing the ability of the material/bulk reaction mixture to absorb and convert microwave energy to heat, the dielectric properties also directly affect the distribution of the electric field within the microwave cavity and the power density dissipation, as shown in eqn (1):

$$P_d = 2\pi f \varepsilon_0 \varepsilon'' E^2 \quad (1)$$

where P_d is the power density dissipation (W m^{-3}), f is frequency (Hz), ε_0 is the permittivity of free space (8.854×10^{12} F m^{-1}), E is the electric field strength in the material (V m^{-1}).

In addition, the temperature rise resulting from absorption of microwave energy by the material is related to the power density dissipation, as shown in eqn (2):

$$P_d = c\rho \frac{dT}{dt} \quad (2)$$

where c is the specific heat capacity (J kg^{-1} °C^{-1}), ρ is density of the material (kg m^{-3}), dT is the change in temperature (°C) and dt is the time increment (s).

From eqn (1), it is evident that the power density dissipation varies proportionally to ε'' and frequency, and by a power of two with the electric field. Consequently, significant increases in electric field strength, frequency and ε'' will result in greatly increased power dissipation densities and thus heating rates (see eqn (2)). Therefore, it is essential to quantify the dielectric properties and electric field distribution when designing microwave cavities as this will control the power density in the heated phases of the material under treatment.

The final parameter crucial to the development of microwave heated systems is the penetration depth. The penetration depth is defined as the point at which the electric field reaches 37% of its original value; the amplitude of the electric field diminishes owing to absorption of the field by the material and conversion into heat. The penetration depth depends greatly on the dielectric properties of the material, as shown in eqn (3):

$$D_p = \frac{\lambda_0}{2\pi\sqrt{2\varepsilon'}} \frac{1}{\sqrt{\left[\left\{1+\left(\frac{\varepsilon''}{\varepsilon'}\right)^2\right\}^{0.5}-1\right]}} \quad (3)$$

where D_p is the penetration depth (m), λ_0 is the free space wavelength of the incident radiation (m), ε' is the dielectric constant and ε'' is the dielectric loss.

The penetration depth is an important parameter in microwave cavity design as it gives an indication of heat distribution within the material, *i.e.* whether heating is taking place primarily on the surface of the reaction mixture/material or volumetrically (heating the bulk). To put this into perspective, a typical MIL-53(Al) reaction mixture containing $Al_2(SO_4)_3 \cdot 18H_2O$ (0.77 g, 1.2 mmol), terephthalic acid (0.19 g, 1.2 mmol) and deionized water (6.7 mL) has a penetration depth of 0.38 cm.[25]

From this section, it should now be clear that the dielectric properties, power density, electric field distribution and penetration depth are all vital in microwave processing as these variables underpin the successful integration of microwave energy with

chemical reactor systems capable of delivering the required materials, consistently at high quality and at the correct cost base and with minimal environmental impact. The literature presented in the following sections will be reviewed in this context.

3. Microwave synthesis of MOFs: a comparison of time with conventionally heated reactions

3.1. Background

With the prevalence of microwave heating in organic chemistry and the availability of 'off the shelf' microwave reactors, it is unsurprising that this technology has been increasingly applied to the synthesis of MOFs. Microwave technology has been used to prepare MOFs from transition metals[35–41] p-block metals (namely lead and indium),[42–44] alkali and alkaline earth metals,[45–50] lanthanides and actinides;[51–56] bimetallic MOFs;[57] and mixed-linker MOFs.[58–61] Additionally, microwave heating has been used in the synthesis of MOF linkers,[62–66] MOF thin films,[67–70] membranes,[71–76] for surface deposition[43,67,70,77–83] and for solvent-free synthesis of MOFs.[84,85] Early reports typically used microwave heating as a faster route to known MOFs by adapting the conventionally heated solvothermal reaction conditions. Only recently has microwave synthesis been used independently for discovery of new MOFs facilitated by the ability to screen many reaction conditions in a shorter period of time compared to conventional heating routes.[51,86–90]

The next sub-sections (3.2 to 3.6) of this paper summarise the effect of microwave heating on the reaction conditions and properties of MOFs produced. Where possible, information about microwave parameters such as power, treatment time, and type of cavity (or reactor) have been included and are discussed. However in all reported examples there is no information about the penetration depth and so it is not currently possible to determine whether the bulk synthesis mixture was heated by microwave energy or if the surface was heated by MW and the inside heated through conductive heat transfer. This is a major limitation in much of the literature currently published as it is impossible, without this knowledge, to determine if the systems were actually heated by microwave energy or a shell of the material heated by microwave energy

with the majority of the reaction mixture being heated through conductive heat transfer from a microwave heated zone into the bulk.

3.2. Influence of microwave heating on MOF reaction time

The shorter reaction time enabled by microwave treatment has been noted across all synthetic chemistry and was readily apparent in the first report of microwave synthesis of a MOF in 2005.[91] In this pioneering work Jhung *et al.* prepared MIL-100 *via* microwave and conventional routes by heating an aqueous mixture of metallic chromium, trimesic acid and hydrofluoric acid in a 1.0 : 0.67 : 2.0 molar ratio to 220 °C (the conditions for MIL-100 synthesis were previously established by Férey *et al.*[92]).[91] The significance of microwave heating was demonstrated by a marked reduction in synthesis time without affecting the yield; 44% after 4 hours reaction in a Mars-5 CEM multimode microwave reactor (power not given) compared to 45% after 4 days in a conventionally heated oven.[91] Thermo-gravimetric and X-ray diffraction analyses showed the MIL-100 products to be consistent regardless of heating method, however, a slightly reduced pore volume (from 1.16 to 0.97 cm^3 g^{-1}) was exhibited by the microwave-synthesised material.

Since 2005, microwave heating has continually been shown to facilitate a progressive reduction in MOF reaction time (in some cases the time is reduced by up to 99.8%, as presented in Table 1). Many papers show the ability to synthesise MOFs using microwave energy in the order of minutes.[86] Two reports have also demonstrated the synthesis of MOFs in as little as 25 (1 mL solution heated in a model 520A microwave reactor from Resonance Instrument Inc.)[24] and 4.3 seconds (6.7 mL solution heated in bespoke system with a cavity designed to enable precise control of the power and energy input to the reaction mixture);[25,34] with the latter representing the fastest reported synthesis of a MOF on the tens of milligram scale to date.[25,34]

Table 1 Summary of papers reporting a reduction in reaction time for MOF synthesis as a direct comparison with conventional heating[a]

MOF (trivial name)	Systematic name	Reaction time (minutes)		Reduction in synthesis time[b] (%)	Change in MOF yield (%)	Change in crystal size (%)	Change in surface area (%)	Microwave conditions			Ref.
		CH	MW					Cavity type	Power[c] (W)	Temp. (°C)	
HKUST-1	$Cu_3(BTC)_2$	1440	60	95.83	−5	−50	+21.35	CEM MARS-5[f]	1200	140	93
		1440	30	97.92	+2	[d]	+5.51	CEM discover[e]	200	180	94
		1200	4	99.67	[d]	[d]	+22.36	Domestic Galanz, PT021TP-6[f]	700	[g]	95
Ln-MOFs	$[Ln(TTTPC)(NO_2)_2(Cl)]\cdot(H_2O)_{10}$	2880	5	99.83	[d]	[d]	[d]	Biotage initiator 8EXP[e]	400	85	56
MIL-101	$[Cr_3OH(H_2O)_2(BDC)_3]$	1080	15	98.61	−9	−21.21	+15.72	CEM discover[e]	300	220	96
MIL-53	[Fe(OH)BDC]	4320	150	96.53	[d]	[d]	[d]	CEM MARS-5[f]	1200	70	97
MOF-5	$[Zn_4O(BDC)_3]$	1440	30	97.92	[d]	−95	−6.0	CEM MDS-2100[e]	1000	95–165	98
CPO-27	$Co_2(DHTP)(H_2O)_2\cdot 8H_2O$	510	47	90.78	[d]	[d]	+12.64	CEM MARS-5[f]	400	70	99
No trivial name given	Fe(1,4-naphthalene dicarboxylate)	4320	2	99.95	[d]	−70	+40.6	PreeKem Scientific Instruments WF-4000[e]	[d]	1500	100
UiO-66	$[Zr_6O_4(OH)_4(BDC)_6]$	1440	18	98.75	−3	+100	−10.5	CEM MARS-5[f]	Step 1 200 step 2 80	[d]	101

a All percentages calculated from (MW/CH) × 100 = *x*, *x* – 100. b Reaction time of microwave synthesis (MW) relative to conventional heating (CH) expressed as a percentage to two decimal places. c Power set on the microwave control unit; this will likely have changed once the target temperature was reached and does not reflect the actual power absorbed by the reaction mixture. d Quantitative data not reported in the original reference. e Single mode cavities. f Multi-mode cavities. g No data available, every minute the authors removed the vessel, stirred and re-heated to avoid overpressure.

3.3. Influence of microwave heating on MOF crystal size

A consequence of the shorter reaction times afforded by microwave heating is the reduction in crystal and/or particle size of MOFs compared to those produced using conventionally heated solvothermal routes. In some cases a 50% reduction in crystal size is observed (see Table 1 above).[93] Unlike conventionally heated routes, a narrower crystal size distribution is also exhibited by MOFs produced using microwave-assisted synthesis.[25] Many research groups have highlighted the importance of particle size and distribution for environmental applications such as chromatographic separations,[102] adsorption,[42,103] catalysis[104–106] as well as for making multiferroics.[107] These results (small crystals and narrow size distribution) have been ascribed to faster kinetics of crystal nucleation and growth owing to hot-spots (or selective heating of components) in the reaction mixture.[97] It has been hypothesised that the hot-spots give rise to a high concentration of nucleation points and thus a large nuclei to reactant ratio. As the crystals grow on these nuclei, remaining reactant is rapidly consumed, resulting in crystal size reduction.[108] In attempts to quantify the effect of heating source on the crystallisation of MOFs, Haque *et al.* followed a two-step synthesis of MIL-53(Fe) prepared by ultrasound, conventional, and microwave heating methods using *ex situ* powder X-ray diffraction (PXRD).[97] The authors reported increased acceleration factors (calculated from the pre-exponential factor in the Arrhenius equation) of 14.8 and up to 53.1 for crystal nucleation and growth, respectively, under microwave conditions (CEM Mars 5 reactor, up to 1200 W, 70 °C) compared to conventional heating (70 °C).[97] Ultrasound (VCX 750 ultrasonic generator from Sonics & Materials, Inc; power varied at fixed reaction temperatures) was also found to have increased acceleration factors (48.7 and 284.2 for the nucleation and crystal growth steps, respectively) compared to conventional heating.[97] However, in the case of ultrasound synthesis, the mode of acceleration is ascribed to cavitation whereby formation, growth, and instantaneous collapse of bubbles in the reaction mixture generates local hot spots.[109] Further kinetic studies by *ex situ* PXRD have also shown significant acceleration of crystal nucleation and growth by microwave heating for a range of MOFs.[99,110] However, all kinetic studies conducted thus far carry a level of inherent inaccuracy. No consideration is given to the influence of power absorbed by the reaction mixture in the microwave or ultrasound experiments. These approaches also do not take into account the effect of localised microwave heating and simply measure

average bulk temperature arising from the differential heating of individual components, coupled with subsequent heat transfer.

In addition to a reduction in crystal size and distribution, many groups have demonstrated the ability to control the crystal size during microwave synthesis. Ni and Masel were able to fine-tune the crystals of IRMOF-1, -2 and -3 on the sub-micrometre scale by altering the concentration of the reaction mixtures, more dilute mixtures being preferable.[24] Bag *et al.* showed control over crystal size for a series of isostructural lanthanide MOFs by careful manipulation of the reaction time; 5 minute reactions yielded micro-crystals and longer times (>30 minutes) gave larger crystals similar in size to the conventionally heated solvothermal route.[56] Similarly, Li *et al.* reported control over IRMOF-3 crystal size by varying the synthesis time.[111] Bunzen *et al.*[112] and Liu *et al.*[113] demonstrated control over particle size for MFU-4 and a cyclodextrin MOF, respectively, by variation of reaction time and addition of chemical modulators to the reaction mixture. Reactions involving addition of a modulator with the same chemical functionality as the linker to the reaction mixture in varying amounts is referred to as coordination modulation.[114] Finally, Laybourn *et al.* tuned the particle size and distribution of MIL-53(Al) during microwave synthesis by altering the absorbed power at a fixed energy (250–4000 W; 56 kJ mol^{-1}, based on water as the solvent) showing smaller crystals and narrower size distributions with increasing absorbed power.[25]

3.4. Influence of microwave heating on the morphology of MOFs

In most instances of microwave synthesis of MOFs, the morphology (*i.e.* crystal or particle shape) of products is the same as those produced using conventionally heated solvothermal methods. However, few examples of differences in morphology have been reported. Taylor *et al.* showed a change from spiral rods (1–2 μm) to smaller (300 nm) block-like particles for the room temperature and microwave-assisted syntheses, respectively.[115] Using microwave-assisted coordination modulation (for further explanation see Section 3.3), Sakata *et al.* altered the morphology of $Zn_2(ndc)_2(dabco)$ (ndc: 1,4-naphthalenedicarboxylate; dabco: 1,4-diazabicyclo[2,2,2]octane) from large micron-sized cubic crystals to nano-sized rods by changing the quantity of modulator added to the reaction mixture.[114] Guo *et al.* demonstrated morphological control over MIL-53(Fe), and the resultant iron oxide nanostructures produced from the calcined

MOF, by varying the reaction time in the MOF synthesis step.[116] Reaction times of 0.5 and 2 hours gave 1.5 μm long spindles and shorter, fatter spindles, for the iron oxide materials respectively (see Fig. 2).[116] At longer times, the microwave reaction led to the production of yolk–shell octahedra with increasing size until 12 hours where large rod structures were observed (Fig. 2).[116] In all cases PXRD confirmed production of MIL-53(Fe) in the microwave-synthesis step[116] except for the 12 hour reaction which produced a different, though previously reported phase.[117]

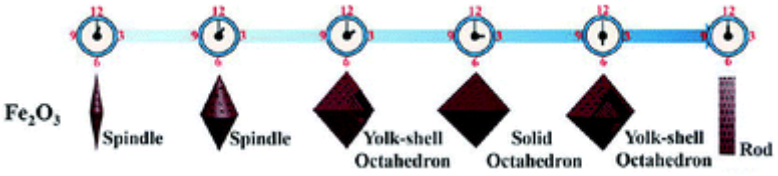


Fig. 2 Morphological progression of iron oxide produced from MIL-53(Fe) in a two-step synthesis. Step 1 involved microwave synthesis of the MOF. In step 2, the MOF is calcined. Control of morphology was demonstrated by altering the reaction time in step 1. Reprinted (adapted) with permission from (W. Guo, W. Sun, L.-P. Lv, S. Kong and Y. Wang, *ACS Nano*, 2017, 11, 4198–4205). Copyright (2017) American Chemical Society.

Finally, Chouhan *et al.* reported aggregated rhomboidal crystals and thin needle crystals for a MOF based on 2-pyridyltetrazole and zinc produced by conventional and microwave heating methods, respectively;[118] and rhomboidal (Fig. 3a) and bundled fibrous (Fig. 3b) nano-sized crystals for the conventional and microwave synthesis of the isostructural cadmium analogue, respectively.[119]

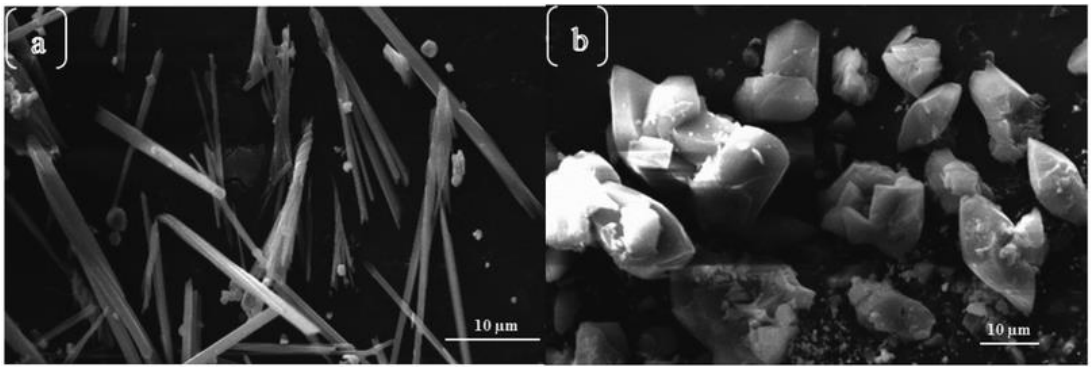


Fig. 3 Morphological differences between microwave (a) and conventionally heated (b) syntheses of a 2-pyridyltetrazole cadmium MOF.[119] Reprinted from *Chinese Journal of Chemistry*, A. Chouhan, G. Pilet, S. Daniele, *et al.*, Shape Controllable Preparation of Submicronic Cadmium Tetrazole-Based Metal–Organic Frameworks *via* Solvothermal or Microwave-Assisted Methods and Their Photocatalytic Studies, with permission from John Wiley and Sons. Copyright 2017 SIOC, CAS, Shanghai & WILEY-VCH Verlag GmbH & Co. KGaA, Weinheim.[ℵ]

Interestingly, although PXRD analyses of the zinc and cadmium 2-pyridyltetrazole MOFs indicated identical crystal structures, the materials produced *via* microwave and conventional methods exhibited subtly different properties (BET surface areas, UV-vis absorption, and luminescence).[119] As a result of these differences, the microwave products performed better in the studies of photo-catalytic degradation of methylene blue, which the authors attributed to the higher surface area and therefore more accessible reactive sites in the microwave-synthesised MOFs.[119] Although changes in morphology as a result of microwave heating have been reported, the effect of microwave heating on the growth mechanism is yet to be established.

3.5. Influence of microwave heating on the surface area of MOFs

The surface area varies largely for any given MOF. For example, MIL-53(Al) from commercial sources (tradename: Basolite® A100) is supplied with a surface area ranging from 1100 to 1500 $m^2\ g^{-1}$.[120] Many factors are known to affect the surface area, including solvent choice, quantity of solvent in the reaction mixture, ratio of

[ℵ] In the published manuscript this figure is incorrectly referenced in the text as shown. The caption is correct, however the text in the preceding paragraph should read "…and bundled fibrous nano-sized crystals (Fig. 3a) and rhomboidal (Fig. 3b) for the microwave and conventional synthesis of the isostructural cadmium analogue…"

metal to linker, choice of metal salt and reaction temperature.[121–123] Therefore, in order to make a fair assessment of the effect of heating method (conventional solvothermal *vs.* microwave) on the surface area, comparison between reactions involving the same chemical conditions are required. In these cases, microwave synthesis of MOFs has generally been shown to give products with higher surface areas than those produced *via* conventional heating routes (see Table 1 and Fig. 4).

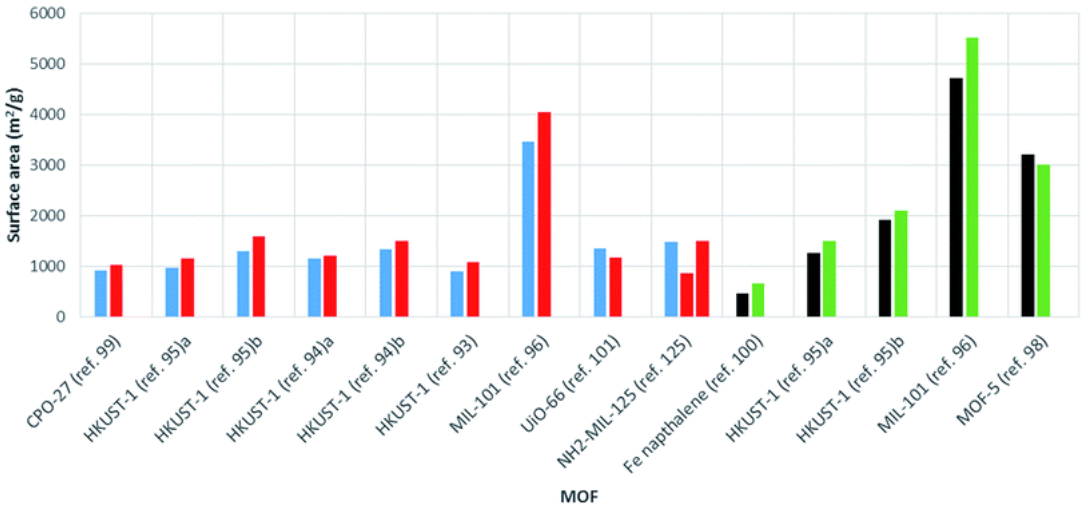


Fig. 4 Bar chart showing comparative surface areas between MOFs prepared using microwave (red, BET; green, Langmuir) and conventionally heated solvothermal (blue, BET; black, Langmuir) synthesis. Ref. 95[a] MOF activated by dissolution in $CHCl_3$. Ref. 95[b] MOF activated using supercritical carbon dioxide. Synthesis conducted in ethanol and water (ref 94[a]) and DMF (ref 94[b]).

In a comparative study, Khan and Jhung found HKUST-1 synthesised using microwave heating to have a larger surface area and pore volume than the conventionally heated solvothermal product (1080 $m^2\ g^{-1}$ and 0.39 $cm^3\ g^{-1}$ compared to 890 $m^2\ g^{-1}$, 0.32 $cm^3\ g^{-1}$, respectively, see Table 1).[93] Increased surface areas and pore volumes for MOFs produced by microwave heating compared to conventional heating have also been reported for MIL-101 [96] and further examples of HKUST-1 [94,95] values are given in Table 1. The largest increase in surface area with microwave heating to date was reported by Lou *et al.* for a 1,4-naphthalene di-carboxylate based iron MOF synthesised using a WF-4000 microwave reactor (PreeKem Scientific Instruments).[100] In this case a surface area increase of around 40% was observed (see Table 1).[100]

An increase in surface area for microwave-synthesised MOFs has been attributed to the production of smaller crystals compared to those resulting from conventional heating methods.[99] There are many cases where nano-sized crystals have been found to exhibit greater surface areas than larger MOF crystals.[124] However, few examples of reduced surface areas for MOFs produced by microwave heating have been reported. These include MOF-5,[98] UiO-66 [101] and MIL-53(Al)[25] where the reduction in surface area was attributed to trapping of oxidised reaction solvent in the pores of the MOF,[98] a reduction in linker defects,[101] and thermally-induced deterioration of crystal quality at high absorbed powers,[25] respectively. Finally, Kim *et al.* reported both larger and smaller surface areas for MIL-125 and NH_2-MIL-125 materials produced using microwave heating (power and reaction time varied) compared to conventionally heated reactions with no clear trend.[125] This result suggests that any effect microwave heating has on surface area is dependent on the specifics of the particular synthesis (reactant ratios, solvent systems).

3.6. Summary

In Section 3 we have shown that microwave synthesis is an extremely promising route for MOFs as it potentially offers shorter reaction times, and therefore, lower energy consumptions, control over crystallite size and morphology, and can also produce MOFs with higher surface areas than those produced by conventional solvothermal methods. However, despite the huge activity in this area, gaps in fundamental understanding are still prevalent. For example, the underlying effect of microwave heating on morphology, crystal growth and surface area are still not fully understood. Additionally, many of the reported studies use the average temperature of the reaction mixture as a key indicator for microwave heating. In order for the area to move forward the effect of microwave parameters such as electric field strength and distribution and the dielectric properties must be considered in order to determine if the bulk synthesis mixture was heated by microwave energy.

4. Microwave synthesis of new MOFs and MOF-hybrids

4.1. Background

Microwave heating is advantageous for MOF discovery owing to the ability to screen many reaction conditions in a short time-frame. Additionally, selective heating offers the potential to produce new MOF structures through kinetically driven reactions. This section discusses the use of microwave technology in the preparation of new MOFs and MOF-hybrids.

4.2. Phase-selective synthesis of MOFs

MOFs can exhibit multiple phases; that is different arrangements of the same metal nodes and linkers, resulting in fundamentally different crystal structures. In some instances up to 5 separate structural phases have been produced from the same reactants.[126,127] Different MOF phases often exhibit different properties, notably surface area, therefore production of specific phases is essential for targeting precise properties.[128] Synthesis of specific MOF phases can be achieved through control of pH and temperature, by templating and by microwave heating.[21] For example, Khan and Jhung[28] investigated phase selective synthesis of two MOFs, namely MIL-53(Cr) and MIL-101(Cr), from aqueous reaction mixtures of chromium chloride hexahydrate and terephthalic acid (H_2BDC).[28] The reaction mixtures were heated to 210 °C under autogenous pressure using either conventional or microwave heating for specific time intervals (daily and hourly, respectively) and the ratio of phases was determined by *ex situ* PXRD analysis.[28] In the early stages of reaction, <1 day for conventional and <3 hours for microwave heating, the kinetically favourable MIL-101(Cr) product was dominant.[28] Longer reaction times (>3 hours) resulted in greater quantities of the thermodynamically favourable MIL-53(Cr) product.[28] The authors proposed a mechanism for the formation of these two phases; MIL-101 forms first, disassembles, re-assembling to form the MIL-53 phase, as shown in Fig. 5.[28,129] Exclusive synthesis of the MIL-101(Cr) phase (termed ‘phase-pure’) was achieved using microwave heating with reaction times of 1 hour.[28]

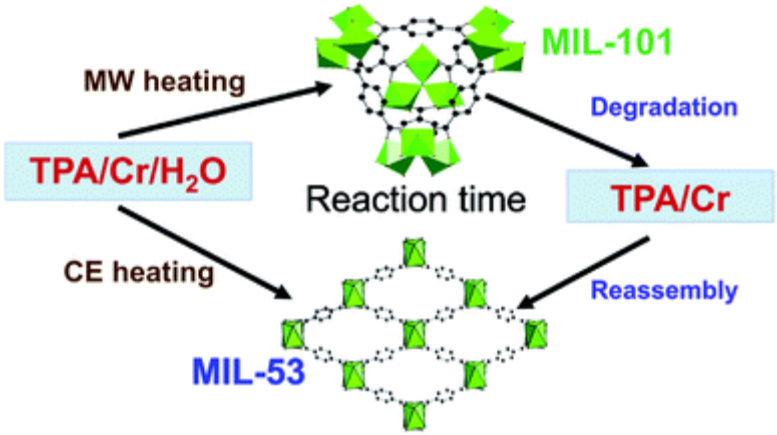


Fig. 5 Schematic representation for the formation of two MOF phases (MIL-101 and MIL-53) from reaction between $CrCl_3 \cdot 6H_2O$ and H_2BDC in water using microwave and conventional heating. Reprinted from *Coordination Chemistry Reviews*, **285**, N. A. Khan, S. H. Jhung, Synthesis of metal–organic frameworks (MOFs) with microwave or ultrasound: rapid reaction, phase-selectivity, and size reduction, 11–23, Copyright (2015), with permission from Elsevier.

Further work by Khan *et al.* focused on a series of three frameworks based on aluminium metal nodes and trimesic acid, namely MIL-96(Al), MIL-100(Al) and MIL-110(Al).[128] Alteration of the reaction time and pH during microwave heating enabled isolation of the separate phases; MIL-110(Al) < 2 h, 2.3 M equivalents of base; MIL-100(Al) < 2 h, 2.3 M equivalents of nitric acid and reactions conducted above 2 hours afforded the thermodynamically stable MIL-96(Al) phase.[128] Interestingly, the authors identified a downward trend in porosity with BET surface areas of 1056, 639 and 216 $m^2\ g^{-1}$, for MIL-100, MIL-110 and MIL-96, respectively, indicating that more porous structures are inherently less thermodynamically stable.[128] Finally, during the microwave synthesis of MIL-77 (a cubic nickel glutarate MOF, previously prepared by Guillou *et al.*[130]), Jhung and co-workers discovered a new tetragonal phase.[26] Alteration of the reaction conditions showed that the cubic phase preferentially forms at low pH, low temperature and especially under conventional heating whereas the tetragonal phase is obtained favourably at high pH, high temperature and particularly using microwave heating (Mars-5 CEM multimode reactor, power input was varied at different stages of the reaction).[26] This result was unexpected as previous reports had shown the denser tetragonal phase to be thermodynamically favourable and the less dense cubic phase to be kinetically favourable and so one would expect the cubic and tetragonal phases to dominate in microwave and conventionally heated reactions,

respectively.[26] The authors hypothesised the formation of the denser tetragonal phase under microwave heating to be the result of changes in crystallisation rates for the two phases.[26]

4.3. "One pot" synthesis of MOF hybrids

In chemistry, a one-pot synthesis involves carrying out successive chemical reactions in one reactor. This strategy is often employed to improve the efficiency of reactions as multiple work-up steps are avoided. In MOF chemistry, one-pot synthesis is often used to prepare MOF-hybrids or MOFs with additional functionality as the porous structure can be further functionalised by the secondary reaction. Examples of one-pot microwave-assisted syntheses of MOF hybrids include; MOF–silica[131,132] and MOF–alumina[131] composites; a photochromic indium trimesate (trivial MOF name, JUC-120) hybrid film produced by entrapping guest molecules within the framework;[133] a catalyst for alcoholysis of styrene oxide produced by doping MIL-101(Cr) with phosphotungstic acid;[134] and a heterogeneous catalyst for microwave heated organic coupling reactions comprising of IRMOF-3 doped with silver nanoparticles synthesised from the MOF precursor solution and silver nitrate.[111] In the latter example the sizes of silver nanoparticles were controlled by altering the reaction time.[111] All of these reports are summarised in Table 2.

Table 2 Summary of hybrid MOF materials produced using one-pot synthesis and microwave heating

Classification of material produced	**Details**	**Ref.**
Core–shell hybrid	MIL-53-Cr/V	135
Inorganic composites	Silica/HKUST-1	131
	Alumina/HKUST-1	131
	Silica (MCM-41)/HKUST-1	132
	Spiropyran incorporation in thin film JUC-120	133
	Keggin phosphotungic acid doped MIL-101	134
Entrapped molecules/'doped' hybrid MOFs	IRMOF-3 doped with silver nanoparticles	111
	Cu-BDC/reduced graphene oxide composite as a precursor for hybrid metal oxide	136

Recently Depauw *et al.* used microwave heating to prepare a mixed metal MIL-53 MOF *via* a one-pot reaction containing a mixture of chromium and vanadium salts and H_2BDC linker.[135] Under conventionally heated solvothermal conditions a homogenous framework was produced, however microwave heating led to the formation of an "egg yolk" structure comprising of a Cr/V core surrounded by a pure chromium MIL-53 shell as determined by energy-dispersive X-ray (EDX) spectroscopy mapping shown in Fig. 6.[135]

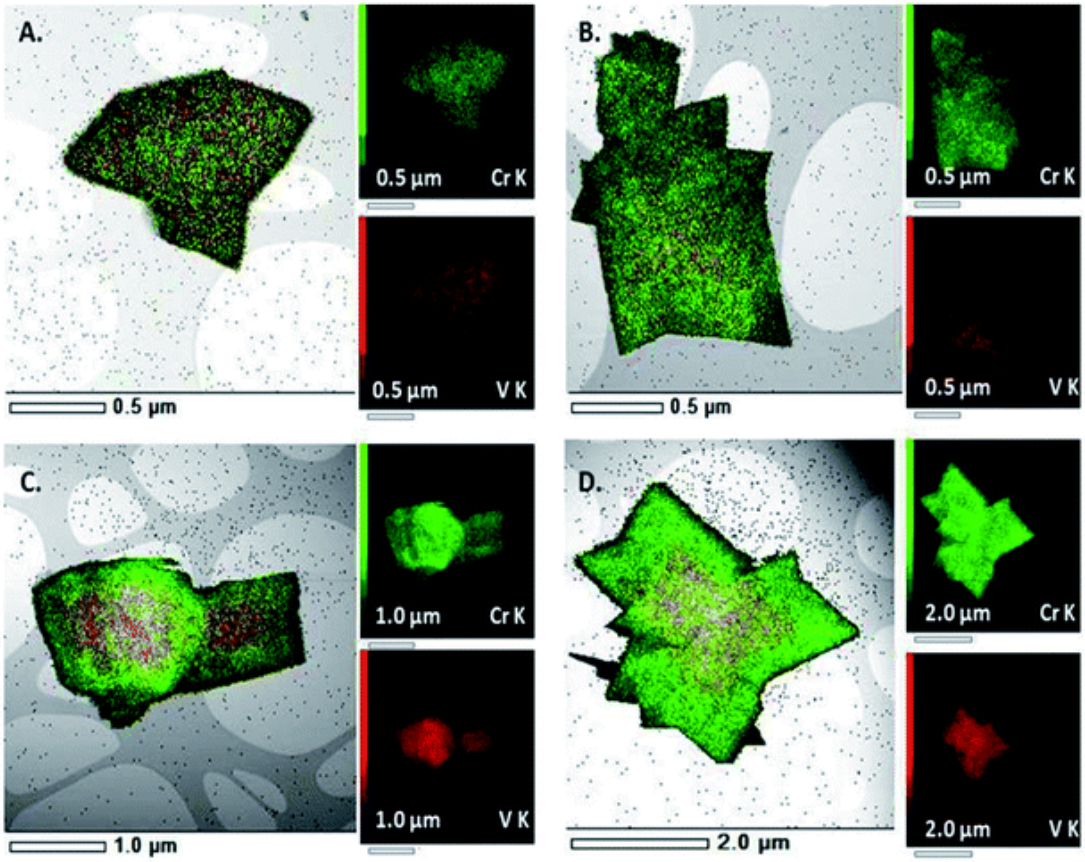


Fig. 6 EDX spectroscopy mapping of a homogenous (A and B) and "egg yolk" (C and D) mixed metal MIL-53(Cr/V) MOF synthesised by conventional and microwave heating, respectively.[135] Reproduced from ref. 135 with permission from the Royal Society of Chemistry.

4.4. Post-synthetic modification of MOFs

Microwave heating has also been used for the post-synthetic modification (PSM) of MOFs, whereby a pre-formed MOF is altered. PSM is a particularly important technique as it enables further enhancement and fine-tuning of MOF properties for a wide range of applications through inclusion of alternative chemical species/functionalities.[137–139] Post synthetic modification can be categorised into several types, including modification of the linkers (without changing the structure of the MOF) or metal nodes, incorporation of additional chemical species (also called doping, often into the pores of the MOF), or modification of the whole MOF structure. Examples of PSM facilitated by microwave heating are now discussed and a summary is presented in Table 3.

Table 3 Summary of PSM of MOFs using microwave heating

Type of PSM	Details	Comment	Ref.
Incorporation of catalytic nanoparticles	MIL-101@Pd, MIL-101@Cu and MIL-101@Pd/Cu (bimetallic nanoparticles incorporated)	Catalytic oxidation of CO	140
	ScBTC@Pd	Cross coupling reactions	141
	MIL-101@Cu	Catalytic reduction of nitro-aromatics	142
	UiO-66@Pd	Cross coupling reactions	143
Incorporation of catalytically active nanoparticles	MIL-101@Cu and MIL-101@Ni	Augmented CO_2 storage	144
	MIL-101@Fe_2O_3	Catalytic oxidation of alcohols and alkenes	145
Incorporation of graphene oxide	ZIF-8 derived ZnO with incorporated graphene oxide	Photo-catalytic degradation of methylene blue	146
Linker functionality modification	UiO-66-Br → UiO-66-CN	90% yield, route to otherwise unobtainable linker functionality	147
	De-protection of an amine functionalised with *tert*-butoxycarbonyl (Boc) group IRMOF-74 (Mg)		148
	MIL-101-NH_2 → MIL-101-peptide MIL-68-NH_2 → MIL-68-peptide UiO-66-NH_2 → UiO-66-peptide	Up to tetra-amino acids grafting onto the linkers without racemization of the amino acids	149
	MIL-53-NH_2 functionalised with an alkyl halide	Catalytic synthesis of cyclic carbonates	150

Type of PSM	Details	Comment	Ref.
	IRMOF-74-III	Multivariate in pore tri-peptide functionality	151
	De-protection of IRMOF-74-III-Boc to give the primary amine	Carbon capture	152
	MIL-101	Chromatography	153
MOF–polymer monoliths	MIL-101(Fe), MIL-101(Al), MIL-100(Cr), UiO-66, MIL-88B(Cr), MIL-53(Al)	Solid phase extraction of penicillin	154
	MIL-53		155
	Ni-BTC → Ni/Cu-BTC	Base for production of hybrid metal oxides	156
Cation exchange	UiO-66 → UiO-66(Zr/Ti)	Photocatalysis	157
	Ni-BTC to mixed metal Ni/Sn-BTC	Base for production of hybrid metal oxides	158
	MIL-100 → magnetic Fe_2O_3/C composite	Ionothermal synthesis with doped zinc chloride	159
Synthetic precursor to hybrid metal oxide	MIL-53 → magnetic Fe_2O_3/C composite	Ionothermal synthesis with doped zinc chloride, for dye removal and degradation	160
	Prussian blue: $Zn(CO_3)$	Precursor for a porous ZnO/$ZnFe_2O_4$ composite	161

An example of PSM by doping was reported by El-Shall *et al.*[140] In their work a catalyst for the oxidation of CO gas was prepared by doping MIL-101 with metallic and bimetallic nanocrystals.[140] During the PSM step, metal salts of palladium and copper were allowed to diffuse into the pores of MIL-101 before addition of a hydrazine hydrate reducing agent.[140] This was followed by a 2 minute microwave reaction to yield the final MOF@nanoparticle materials.[140] Several examples of PSM involving the MOF linker have been reported, in this case an exposed pendant functional group on the linker undergoes chemical reaction. For instance, Bonnefoy *et*

al. successfully grafted oligopeptides onto the linker of 3 MOFs using microwave heating.[149] The authors highlighted the diversity of peptide chemistry as a potential route to a large library of MOF-oligopeptide materials with potential applications in sensing, catalysis and separation.[149] It is important to note that the ability to produce MOFs with numerous different pendant functional groups on the linker is particularly powerful as it is conceivably possible to perform countless reactions to augment MOFs using this method of PSM. A final notable example of PSM by microwave heating involves preparation of MOF–polymer monoliths reported by Lin *et al.*[154] The various MOFs (see Table 3 'MOF–polymer monoliths' for exact details) were suspended in a monomer mixture, loaded into a column and then polymerised by microwave heating to give the MOF–polymer monoliths.[154] The monoliths were tested for their ability to extract and recover penicillin-type compounds in solid phase extraction, with excellent results.[162]

4.5. Summary

From the many examples discussed in Section 4 and summarised in Tables 2 and 3, it is clear that microwave heating is an effective method for the production of new MOFs and MOF hybrids by phase-selective or one-pot synthesis or through PSM. However, as identified in Section 3 of this paper, there is little understanding of the mechanisms of microwave heating. In particular the effect of microwave energy on MOF crystallisation is yet to be determined.

5. Towards industrial scale microwave synthesis of MOFs

5.1. Background

The diverse and tuneable properties of MOFs offer immense opportunities for economic and environmental impact; for example in the field of ambient pressure CO_2 capture,[163,164] an industry which is estimated to be worth between $128 billion and $221 billion by 2030.[165] However, current state of the art in industrial manufacture has restricted widespread adoption of MOFs for commercial applications, as at scale they deliver poor quality materials, whilst incurring high energy and capital costs, meaning

that many applications are not economically viable. The production of MOFs at large scales is hindered by a combination of chemical, environmental and engineering challenges including; dependence on high temperatures and pressures to give solvothermal synthesis conditions; use of large quantities of toxic, corrosive and highly flammable chemicals; production of acidic by-products, long times required for crystal growth; cost and availability of large scale reaction rigs; and energy requirements.[22] Additional challenges also exist in materials handling, such as; heterogeneous reaction conditions, mixing requirements, reactions that form precipitates; and separation of products after synthesis.

In order to address these challenges, microwave reactions under continuous flow conditions have recently been developed. This production route has several advantages; the combination of rapid microwave heating and high surface area-to-volume ratio for a reaction mixture in a flow reactor leads to improvements in heat and mass transfer and thus significant reduction in synthesis time; typically less solvent is required; process intensification leads to less energy consumption and safer implementation of harsh reaction conditions; improved control over the synthesis parameters allows faster optimisation of reactions to give reproducible MOF products of high quality; and continuous flow reactors are more scalable and often greener compared to batch systems.[22]

This section focuses on recent research efforts involving the production of MOFs beyond the laboratory scale using microwave technology. Current microwave systems for MOF synthesis on the gram to kilogram scale are presented and their advantages and limitations are discussed. Additionally, the successful development of industrial scale microwave reactors in other sectors is described in order to highlight important considerations and learnings transferrable to the development of an industrial scale microwave process for the synthesis of MOFs. Finally, the economic and environmental implications of industrial scale microwave reactors are discussed.

5.2. Current efforts in scaling-up MOF synthesis using microwave heating

The first continuous flow microwave reactor for the synthesis of MOFs was reported in 2015.[166] The pioneering work by Albuquerque *et al.* involved laboratory scale

preparation of MOF-74(Ni) using a gas liquid segmented flow reactor.[166] Gas liquid segmented flow was used to improve mixing and to prevent blockages in the reactor.[166] The reactor comprises a 1/16 inch tube fed through two sections; a microwave heated zone (see Table 4 for specific details) used for nucleation, and a conventionally heated oil bath zone for crystal growth, as shown in Fig. 7.[166] Both sections were found to be necessary for MOF production as broad peaks were observed in the PXRD patterns of MOF-74(Ni) prepared without the oil bath zone.[166] The authors reported high conversion of reagents (*ca.* 96.5%) and space time yields (STY) of (~90 g h^{-1} L^{-1} or 720 kg m^{-3} d^{-1}, where 1 day is equivalent to 8 hours),[166] a significant improvement on the conventional heated batch process (STY of 28.5 g L^{-1} h^{-1}).[167]



Fig. 7 Schematic diagram of the gas liquid segmented continuous flow reactor for synthesis of MOF-74(Ni) developed by Albuquerque *et al.*[166] Reproduced from ref. 166 with permission from the Royal Society of Chemistry.

Table 4 Summary of parameters used in continuous flow microwave reactors for synthesis of MOFs

Name of continuous flow system	**MOFs prepared using the reactor**	**Reaction conditions**	**Microwave conditions**		**Production rate (g h^{-1})**	**Space time yield (kg m^{-3} d^{-1})[d]**	**Ref.**
			Cavity type	**Power (W)**			
Segmented flow reactor	MOF-74 (Ni)	2.5 bar, DMF[a]	Teflon tube with 1/16 inch inner diameter fed through a WR340 waveguide (single mode)	<3000	4.5	—[e]	166
Plug flow reactor	MIL-53(Al)	6 bar, DMF,[a] H_2O	PTFE tube with 4.35 mm inner diameter fed through the cavity of a CEM MARS 5 multimode synthesizer. Reactor volume altered by changing the number of coils in the tube	200	7.1	3168[c]	168
	UiO-66	3 bar, DMF,[a] H_2O, acetic acid[b]		200	14.4	7204[c]	
	HKUST-1	6 bar, DMF[a]		360	79.4	64 800[c]	
Continuous tubular microwave reactor	HKUST-1	Ethanol, 3% solids	PTFE tube (1 mm internal diameter) fed through the side vents of a of a domestic microwave oven (Logik L20MS10)	*ca.* 80	Not given	80 000	169
	HKUST-1	Ethanol, 15% solids				400 000	

a DMF = *N*,*N*-dimethylformamide. b Acetic acid was used as a modulator. c Based on a 53 mL microwave heated zone and production rate in g h^{-1} (in the adjacent column). d Number of hours equivalent to 1 day is variable, depending on the source, and not formally given. e STY not stated, 80–90 g L^{-1} h^{-1} given instead.

Building upon their batch process involving simultaneous heating of multiple discrete vessels containing MOF reaction in a multimode microwave reactor (CEM MARS 5 synthesizer),[101] Taddei *et al.* investigated the continuous flow microwave synthesis of three MOFs, namely UiO-66, HKUST-1 and MIL-53.[168] The reactor comprises a coiled PTFE tube fed through a CEM MARS 5 synthesizer.[168] The volume of the microwave section of the reactor was altered by changing the number of coils in the tube.[168] Downstream of the microwave heated section, the tube is introduced into a custom-built pressurised 'collector' made of glass, as shown in Fig. 8.[168] The collector negates the need to flow slurries containing reactants and products through the back pressure regulator, preventing blockages in the reactor.[168] Specific reaction conditions (pressures, solvent systems) and microwave parameters are given in Table 4, above. STYs of 3618, 7204, 64 800 kg m^{-3} d^{-1} for MIL-53, UiO-66, and HKUST-1, respectively were achieved.[168]

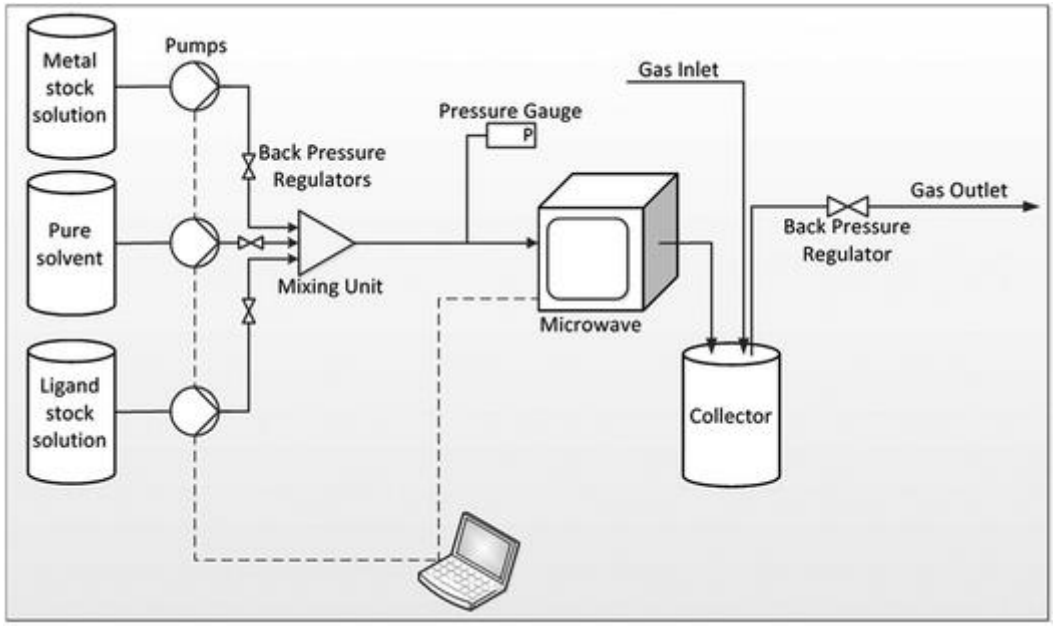


Fig. 8 Schematic diagram of the plug flow microwave reactor developed by Taddei *et al.*[168] Reprinted from *Chemistry A European Journal*, M. Taddei, D. A. Steitz, J. A. van Bokhoven, *et al.* Continuous-Flow Microwave Synthesis of Metal–Organic Frameworks: A Highly Efficient Method for Large-Scale Production, with permission from John Wiley and Sons. Copyright 2016 WILEY-VCH Verlag GmbH & Co. KGaA, Weinheim.

Using the same reactor (Fig. 8),[168] Taddei *et al.* investigated the crystallisation of UiO-66 using high-resolution powder X-ray diffraction by placing the outlet tube (coming out of the microwave heated section) in the focus of the X-ray beam.[170] This experimental set-up enabled *in situ* monitoring of the reaction after microwave heating had taken place. The effect of varying quantities of water and acetic acid modulator in the reaction mixture on the yield and crystallite size of UiO-66 was investigated over a range of residence times. No consideration was given to the effect of absorbed microwave energy on the reaction. A constant power of 280 W was applied in all experiments, therefore the reaction mixtures were subjected to varying amounts of microwave energy depending upon the flow rate. Results showed the rate of product formation, yield and crystallite size to be highly dependent on the water/acetic acid ratio and age of metal salt stock solution.[170]

Most recently, McKinstry *et al.* reported the continuous flow microwave synthesis of HKUST-1 using a PTFE tube (1 mm internal diameter) fed through the side vents of a domestic microwave oven (Logik L20MS10, 800 W).[169] The authors highlighted that alterations to the microwave cavity casing were avoided for safety reasons,[169] however, it is extremely important to note that microwave leakage may still occur even without modification. As electromagnetic wave is attenuated by the reaction mixture (*i.e.* the amplitude of the electric field diminishes owing to absorption of the field by the reaction mixture, see Section 2 for further details) it is possible for the wave to be small enough to pass along the tube and out of the microwave cavity. Consideration and mitigation of microwave leakage is discussed further in Section 5.3. Using their continuous flow microwave system, McKinstry *et al.* investigated the effect of varying concentration (reported as % of solids) and residence times on the yield and surface area of HKUST-1 with a constant power input of 80 W; a summary of these results is given in Table 4.[169] As the production rate was found to greatly affect the surface area (a key indicator of MOF quality), the authors used surface area production rates (SAPRs, the amount of surface area of MOF produced per reactor volume and time, m^2 per m^3 per day, where a day is equivalent to 24 hours)[169] to compare between experiments and other reported methods of production. A residence time of 6 minutes with 3% solids gave an STY of 2700 kg m^{-3} d^{-1} with an SAPR of 5.2×10^6 m^2 m^{-3} d^{-1} (BET surface area of 1930 m^2 g^{-1}). A residence time of 13 seconds and solids of 3 and 15% gave STYs of 80 000 and 400 000 kg m^{-3} d^{-1}, respectively.[169] However, in both

cases a decrease in surface area was observed; 1550 and 600 $m^2\ g^{-1}$ (corresponding to an SAPR of 240 000 × 10^6 $m^2\ m^{-3}\ d^{-1}$) for 3 and 15% reaction solids, respectively.[169] Although an STY of 400 000 kg $m^{-3}\ d^{-1}$ is, to the best of our knowledge, the highest value for any MOF produced to-date *via* any synthesis method, a significant reduction in surface area indicates production of poor quality MOF. The trade-off between product quality and rapid, scalable bulk production of MOFs is an important consideration for industrial manufacture.

5.3. Development of industrial scale microwave reactors; important factors to consider

Scaling-up microwave systems from the laboratory to industry requires a multi-disciplinary approach and many factors must be considered from a materials processing, microwave design, chemical, environmental and economic perspective. It is beneficial to transfer key learning outputs from successful development of industrial scale microwave reactors in other processing sectors. An example of this is the microwave treatment of ores for the mining industry, work which has led to the largest mass throughput microwave processing systems ever developed. In their work, Buttress *et al.*[171] and Batchelor *et al.*[172] demonstrated the necessity for understanding the fundamental parameters required for designing microwave systems capable of a stable and reliable treatment that also meets with occupational health and safety (OHS) and electromagnetic compatibility (EMC) regulations. These parameters (discussed in this paper in Section 2) include (i) dielectric properties, defining the efficiency of power coupling and distribution of the electric field within the heating cavity; (ii) penetration depth and relationship with reactor design and specification; (iii) power density in the heated phase, which is a direct function of the dielectric loss, the applied frequency and the electric field strength. All of these variables underpinned the design of microwave cavities capable of delivering the power density distribution (energy per unit volume over the treatment time) needed to produce the required material effect, consistently at high quality and with maximum treatment efficiency. Buttress *et al.* also noted the importance of using single mode cavities as the interaction between the applied microwave energy and the material is very difficult to characterise in multi-mode systems owing to the complexity of the electric field pattern.[171] Integration of the microwave cavity with a materials handling system based on flow requirements

(*e.g.* mixing), and chemical compatibility was also essential. For continuous flow reactors, the design of choking structures to confine the electric field within the microwave system is paramount in order to achieve compliance with safety standards. All of these factors support the successful integration of microwave energy with chemical reactor systems capable of delivering the economic large-scale manufacturing processes at the correct cost and minimal environmental impact.

Current state of the art in industrial manufacture of MOFs has restricted widespread adoption of MOFs for commercial applications, as at scale they deliver poor quality materials, whilst incurring high energy and capital costs, meaning that many applications are not economically viable. Microwave technology can address these challenges through rapid and selective heating, which can increase production rates by orders of magnitude, give controllable product quality and at a reduced energy and potentially capital cost. Furthermore, the cost of MOF production varies considerably depending on the type of MOF, reagents, synthesis temperature, energy and recyclability of reagents; to ensure that the MOFs and reactors being developed are sustainable on a life cycle basis, it is necessary to evaluate their environmental and economic implications from an early stage of development using life cycle assessment (LCA) and techno-economic analysis (TEA). At present, life cycle, environmental and commercial data in the literature are scarce for conventionally heated well-established MOFs and are non-existent for MOFs synthesised using microwave heating and so further work in this area is much needed. In order for the breakthroughs in research to occur it is our view that there is a requirement to integrate expertise in microwave technology, process engineering design, techno-economic and environmental analyses, and MOF chemistry to deliver a fundamental understanding of the interactions between microwave energy and commercially and scientifically important MOF systems. This knowledge could then be used to deliver the highest quality scientific and engineering breakthroughs to underpin the development of novel scalable and sustainable chemical reactor manufacturing technologies based upon integration of advanced electromagnetic design and process intensification techniques. For successful delivery, this work requires innovation at the boundaries of process assessment and engineering, microwave and materials interaction, process design and materials chemistry. If it can be delivered, we propose that it will commercially unlock the use of MOFs for a number of high impact energy and environmental applications.

6. Conclusions

MOFs are an incredibly large and diverse class of materials. The potentially high commercial value of MOFs arises from their high porosity and tuneable pore environment which gives them an extremely high capacity and high selectivity for gas and hydrocarbon applications. Their proposed applications address challenges in energy, environmental sustainability and innovative healthcare. However, challenges in scaling-up MOF production and their high product and environmental cost compared to traditional sorbents has restricted widespread adoption in industry. Therefore, the development of technologies that reduce the cost of manufacture in an efficient and sustainable way is a key enabling step in the transfer of MOF research from the laboratory to industry.

Microwave (MW) technology shows great promise for scale up of MOF synthesis as it offers benefits over other methods including significantly reduced reaction times (from hours to seconds), high space time yields, and improved energy efficiency. However the most noteworthy advantage of microwave heating is the high level of control over MOF properties such as morphology, particle size and phase; achieved by altering the applied power and treatment time. Further control is realised by altering the reaction chemistry through addition of modulators and/or co-reactants and by varying the solvent. Additionally, microwave heating has been shown to facilitate MOF discovery and has the ability to produce new MOFs and MOF-hybrids that are otherwise difficult to prepare or inaccessible by other synthetic approaches. These advantages demonstrate the applicability and value of microwave heating both at laboratory and industrial scales, through acceleration of MOF design and discovery and as a route to large scale production. However, research in the field of microwave synthesis of MOFs is dominated by the use of commercially available multi-mode microwave systems and a lack of understanding of the interactions of reactants and MOFs with the electric field, and crucially, how this informs the design of the scale up processes. MOFs are potential “step-change” materials, but failure to determine this fundamental knowledge thus far explains the general failure in scale-up from the laboratory and to the non-realization of the potential benefits offered.

Conflicts of interest

There are no conflicts of interest to declare.

List of abbreviations for linkers and MOFs

DHTP
: 1,5-Dihydroxyterephthalic acid

TTTPC
: 1,1′,1″-Tris(2,4,6-trimethylbenzene-1,3,5-triyl)-tris(methylene)-tris(pyridine-4-carboxylic acid)

BTC
: Trimesic acid (1,3,5-benzenetricarboxylic acid)

BDC
: Terephthalic acid (1,4-benzenedicarboxylic acid)

HKUST
: Hong Kong University of Science and Technology

Ln MOF
: Lanthanide metal–organic framework

MIL
: Materials of Institut Lavoisier

IRMOF
: Isoreticular MOF

JUC
: Jilin University, Changchun

UiO
: University of Oslo

Acknowledgements

Andrea Laybourn acknowledges the University of Nottingham for the award of a Nottingham Research Fellowship.

References

1. R. J. Meredith *Engineers' handbook of industrial microwave heating*, IET, UK, 1998,
2. S. R. Batten, N. R. Champness, X.-M. Chen, J. Garcia-Martinez, S. Kitagawa, L. Öhrström, M. O'Keeffe, S. M. Paik and J. Reedijk, *Pure Appl. Chem.*, 2013, **85**, 1715 —1724
3. B. F. Hoskins and R. Robson, *J. Am. Chem. Soc.*, 1989, **111**, 5962 —5964
4. B. F. Hoskins and R. Robson, *J. Am. Chem. Soc.*, 1990, **112**, 1546 —1554
5. O. M. Yaghi, G. Li and H. Li, *Nature*, 1995, **378**, 703 —706
6. O. M. Yaghi and H. Li, *J. Am. Chem. Soc.*, 1995, **117**, 10401 —10402
7. O. M. Yaghi and G. Li, *Angew. Chem., Int. Ed. Engl.*, 1995, **34**, 207 —209
8. Scopus database search for “Metal–Organic Framework” or “Metal Organic Framework” – Total results 17759-retrieved 01/12/17.
9. J.-R. Li, R. J. Kuppler and H.-C. Zhou, *Chem. Soc. Rev.*, 2009, **38**, 1477
10. Y. Cui, B. Li, H. He, W. Zhou, B. Chen and G. Qian, *Acc. Chem. Res.*, 2016, **49**, 483 —493
11. S. Qiu and G. Zhu, *Coord. Chem. Rev.*, 2009, **253**, 2891 —2911
12. J. Lee, O. K. Farha, J. Roberts, K. A. Scheidt, S. T. Nguyen and J. T. Hupp, *Chem. Soc. Rev.*, 2009, **38**, 1450
13. L. E. Kreno, K. Leong, O. K. Farha, M. Allendorf, R. P. Van Duyne and J. T. Hupp, *Chem. Rev.*, 2012, **112**, 1105 —1125
14. D. Liu, K. Lu, C. Poon and W. Lin, *Inorg. Chem.*, 2014, **53**, 1916 —1924
15. P. Kumar, A. Deep and K.-H. Kim, *TrAC, Trends Anal. Chem.*, 2015, **73**, 39 —53
16. L. Zhang, H. B. Wu and X. W. (David) Lou, *J. Am. Chem. Soc.*, 2013, **135**, 10664 —10672
17. K. J. Lee, J. H. Lee, S. Jeoung and H. R. Moon, *Acc. Chem. Res.*, 2017, **50**, 2684 —2692

18. C. L. Jones, A. J. Tansell and T. Easun, *J. Mater. Chem. A*, 2016, **4**, 6714 — 6723

19. F.-X. Coudert *Chem. Mater.*, 2015, **27**, 1905 —1916

20. H.-C. Zhou, J. R. Long and O. M. Yaghi, *Chem. Rev.*, 2012, **112**, 673 —674

21. N. Stock and S. Biswas, *Chem. Rev.*, 2012, **112**, 933 —969

22. M. Rubio-Martinez, C. Avci-Camur, A. W. Thornton, I. Imaz, D. Maspoch and M. R. Hill, *Chem. Soc. Rev.*, 2017, **46**, 3453 —3480

23. Scopus database search for "Metal–Organic Framework" or "Metal Organic Framework" and "Microwave" – Total results 284-retrieved 20/03/18.

24. Z. Ni and R. I. Masel, *J. Am. Chem. Soc.*, 2006, **128**, 12394 —12395

25. A. Laybourn, J. Katrib, R. S. Ferrari-John, C. G. Morris, S. Yang, O. Udoudo, T. L. Easun, C. Dodds, N. R. Champness, S. W. Kingman and M. Schröder, *J. Mater. Chem. A*, 2017, **5**, 7333 —7338

26. S. H. Jhung, J.-H. Lee, P. M. Forster, G. Férey, A. K. Cheetham and J.-S. Chang, *Chem.–Eur. J.*, 2006, **12**, 7899 —7905

27. Y. K. Hwang, J.-S. Chang, S.-E. Park, D. S. Kim, Y.-U. Kwon, S. H. Jhung, J.-S. Hwang and M. S. Park, *Angew. Chem., Int. Ed.*, 2005, **44**, 556 —560

28. N. A. Khan and S. H. Jhung, *Cryst. Growth Des.*, 2010, **10**, 1860 —1865

29. R. Xu, W. Pang and Q. Huo, *Modern Inorganic Synthetic Chemistry*, Elsevier, 2011,

30. J. B. Hasted *Aqueous dielectrics*, Chapman and Hall, 1973,

31. A. Metaxis and R. J. Meredith, *Industrial Microwave Heating*, IET, UK, 1983,

32. G. B. Dudley, R. Richert and A. E. Stiegman, *Chem. Sci.*, 2015, **6**, 2144 — 2152

33. U. Kaatze and R. Behrends, *Tech. Mess.*, 2009, **69**, 5

34. A. Laybourn, J. Katrib, P. A. Palade, T. L. Easun, N. R. Champness, M. Schröder and S. W. Kingman, *Phys. Chem. Chem. Phys.*, 2016, **18**, 5419 — 5431

35. W. Liu, L. Ye, X. Liu, L. Yuan, X. Lu and J. Jiang, *Inorg. Chem. Commun.*, 2008, **11**, 1250 —1252

36. S. Biswas, M. Grzywa, H. P. Nayek, S. Dehnen, I. Senkovska, S. Kaskel and D. Volkmer, *Dalton Trans.*, 2009, 6487 —6495

37. A. Centrone, T. Harada, S. Speakman and T. A. Hatton, *Small*, 2010, **6**, 1598 —1602

38. J. L. Crane, K. E. Anderson and S. G. Conway, *J. Chem. Educ.*, 2015, **92**, 373 —377

39. M. Ma, A. Bétard, I. Weber, N. S. Al-Hokbany, R. A. Fischer and N. Metzler-Nolte, *Cryst. Growth Des.*, 2013, **13**, 2286 —2291

40. G. Y. Yoo, W. R. Lee, H. Jo, J. Park, J. H. Song, K. S. Lim, D. Moon, H. Jung, J. Lim, S. S. Han, Y. Jung and C. S. Hong, *Chem.–Eur. J.*, 2016, **22**, 7444 —7451

41. Y.-Y. Liu, S. Couck, M. Vandichel, M. Grzywa, K. Leus, S. Biswas, D. Volkmer, J. Gascon, F. Kapteijn, J. F. M. Denayer, M. Waroquier, V. Van Speybroeck and P. Van Der Voort, *Inorg. Chem.*, 2013, **52**, 113 —120

42. L. Hashemi and A. Morsali, *CrystEngComm*, 2012, **14**, 779 —781

43. S. Khanjani and A. Morsali, *CrystEngComm*, 2012, **14**, 8137 —8142

44. L. M. Aguirre-Díaz, M. Iglesias, N. Snejko, E. Gutiérrez-Puebla and M. Á. Monge, *Chem.–Eur. J.*, 2016, **22**, 6654 —6665

45. H.-K. Liu, T.-H. Tsao, Y.-T. Zhang and C.-H. Lin, *CrystEngComm*, 2009, **11**, 1462 —1468

46. P.-C. Liang, H.-K. Liu, C.-T. Yeh, C.-H. Lin and V. Zima, *Cryst. Growth Des.*, 2011, **11**, 699 —708

47. M. Mazaj, V. Kaucic, A. Golobic and N. Zabukovec Logar, *Acta Crystallogr., Sect. C: Cryst. Struct. Commun.*, 2012, **68**, m4 —m6

48. C.-T. Yeh, W.-C. Lin, S.-H. Lo, C.-C. Kao, C.-H. Lin and C.-C. Yang, *CrystEngComm*, 2012, **14**, 1219 —1222

49. C.-Y. Wu, D. S. Raja, C.-C. Yang, C.-T. Yeh, Y.-R. Chen, C.-Y. Li, B.-T. Ko and C.-H. Lin, *CrystEngComm*, 2014, **16**, 9308 —9319

50. C. P. Cabello, C. O. Arean, J. B. Parra, C. O. Ania, P. Rumori and G. T. Palomino, *Dalton Trans.*, 2015, **44**, 9955 —9963

51. P. Silva, F. Vieira, A. C. Gomes, D. Ananias, J. A. Fernandes, S. M. Bruno, R. Soares, A. A. Valente, J. Rocha and F. A. A. Paz, *J. Am. Chem. Soc.*, 2011, **133**, 15120 —15138

52. Z.-J. Lin, Z. Yang, T.-F. Liu, Y.-B. Huang and R. Cao, *Inorg. Chem.*, 2012, **51**, 1813 —1820

53. S. M. F. Vilela, D. Ananias, A. C. Gomes, A. A. Valente, L. D. Carlos, J. A. S. Cavaleiro, J. Rocha, J. P. C. Tomé and F. A. A. Paz, *J. Mater. Chem.*, 2012, **22**, 18354 —18371

54. P. Silva, D. Ananias, S. M. Bruno, A. A. Valente, L. D. Carlos, J. Rocha and F. A. Almeida Paz, *Eur. J. Inorg. Chem.*, 2013, **2013**, 5576 —5591

55. R. F. Mendes and F. A. Almeida Paz, *Inorg. Chim. Acta*, 2017, **460**, 99 —107

56. P. P. Bag, X.-S. Wang and R. Cao, *Dalton Trans.*, 2015, **44**, 11954 —11962

57. H. Li, M. Liang, W. Sun and Y. Wang, *Adv. Funct. Mater.*, 2016, **26**, 1098 —1103

58. Y.-S. Bae, K. L. Mulfort, H. Frost, P. Ryan, S. Punnathanam, L. J. Broadbelt, J. T. Hupp and R. Q. Snurr, *Langmuir*, 2008, **24**, 8592 —8598

59. S. Bernt, M. Feyand, A. Modrow, J. Wack, J. Senker and N. Stock, *Eur. J. Inorg. Chem.*, 2011, **2011**, 5378 —5383

60. A. C. Kathalikkattil, R. Roshan, J. Tharun, H.-G. Soek, H.-S. Ryu and D.-W. Park, *ChemCatChem*, 2014, **6**, 284 —292

61. A. C. Kathalikkattil, D.-W. Kim, J. Tharun, H.-G. Soek, R. Roshan and D.-W. Park, *Green Chem.*, 2014, **16**, 1607 —1616

62. S. Mukhopadhyay, B. G. Mukhopadhyay, M. F. C. G. da Silva, J. Lasri, M. A. J. Charmier and A. J. L. Pombeiro, *Inorg. Chem.*, 2008, **47**, 11334 —11341

63. W. Karuehanon, W. Fanfuenha, A. Rujiwatra and M. Pattarawarapan, *Tetrahedron Lett.*, 2012, **53**, 3486 —3489

64. W. Funfuenha, W. Phakhodee and M. Pattarawarapan, *Tetrahedron*, 2014, **70**, 5415 —5419

65. L. Martins, R. Nasani, M. Saha, S. Mobin, S. Mukhopadhyay and A. Pombeiro, *Molecules*, 2015, **20**, 19203 —19220

66. A. D. Martin, T. L. Easun, S. P. Argent, W. Lewis, A. J. Blake and M. Schröder, *CrystEngComm*, 2017, **19**, 603 —607

67. Y. Yoo and H.-K. Jeong, *Chem. Commun.*, 2008, **0**, 2441 —2443

68. Z.-Q. Li, M. Zhang, B. Liu, C.-Y. Guo and M. Zhou, *Inorg. Chem. Commun.*, 2013, **36**, 241 —244

69. Y. Abdollahian, J. L. Hauser, I. R. Colinas, C. Agustin, A. S. Ichimura and S. R. J. Oliver, *Cryst. Growth Des.*, 2014, **14**, 1506 —1509

70. W.-J. Li, J.-F. Feng, Z.-J. Lin, Y.-L. Yang, Y. Yang, X.-S. Wang, S.-Y. Gao and R. Cao, *Chem. Commun.*, 2016, **52**, 3951 —3954

71. H. Bux, F. Liang, Y. Li, J. Cravillon, M. Wiebcke and J. Caro, *J. Am. Chem. Soc.*, 2009, **131**, 16000 —16001

72. Y. Yoo, Z. Lai and H.-K. Jeong, *Microporous Mesoporous Mater.*, 2009, **123**, 100 —106

73. J. Caro *Curr. Opin. Chem. Eng.*, 2011, **1**, 77 —83

74. H. T. Kwon and H.-K. Jeong, *Chem. Commun.*, 2013, **49**, 3854 —3856

75. Y. Zhu, Q. Liu, J. Caro and A. Huang, *Sep. Purif. Technol.*, 2015, **146**, 68 —74

76. S. Shahid, K. Nijmeijer, S. Nehache, I. Vankelecom, A. Deratani and D. Quemener, *J. Membr. Sci.*, 2015, **492**, 21 —31

77. Y.-S. Li, F.-Y. Liang, H. Bux, A. Feldhoff, W.-S. Yang and J. Caro, *Angew. Chem., Int. Ed.*, 2010, **49**, 548 —551

78. A. Centrone, Y. Yang, S. Speakman, L. Bromberg, G. C. Rutledge and T. A. Hatton, *J. Am. Chem. Soc.*, 2010, **132**, 15687 —15691

79. S. Xiao, P. Liu, W. Zhu, G. Li, D. Zhang and H. Li, *Nano Lett.*, 2015, **15**, 4853 —4858

80. M. Bechelany, M. Drobek, C. Vallicari, A. A. Chaaya, A. Julbe and P. Miele, *Nanoscale*, 2015, **7**, 5794 —5802

81. C. Liu, Y. Wu, C. Morlay, Y. Gu, B. Gebremariam, X. Yuan and F. Li, *ACS Appl. Mater. Interfaces*, 2016, **8**, 2552 —2561

82. N. E. Tari, A. Tadjarodi, J. Tamnanloo and S. Fatemi, *J. CO2 Util.*, 2016, **14**, 126 —134

83. R. D. Arrua, A. Peristyy, P. N. Nesterenko, A. Das, D. M. D'Alessandro and E. F. Hilder, *Analyst*, 2017, **142**, 517 —524

84. H. Zhang, J. Zhong, G. Zhou, J. Wu, Z. Yang and X. Shi, *J. Nanomater.*, 2016, **2016**, 9648386

85. H. J. Kitchen, S. R. Vallance, J. L. Kennedy, N. Tapia-Ruiz, L. Carassiti, A. Harrison, A. G. Whittaker, T. D. Drysdale, S. W. Kingman and D. H. Gregory, *Chem. Rev.*, 2014, **114**, 1170 —1206

86. J. Klinowski, F. A. Almeida Paz, P. Silva and J. Rocha, *Dalton Trans.*, 2011, **40**, 321 —330

87. P. Maniam and N. Stock, *Inorg. Chem.*, 2011, **50**, 5085 —5097

88. T. Ahnfeldt, J. Moellmer, V. Guillerm, R. Staudt, C. Serre and N. Stock, *Chem.–Eur. J.*, 2011, **17**, 6462 —6468

89. H. Reinsch and N. Stock, *Microporous Mesoporous Mater.*, 2013, **171**, 156 —165

90. S. Halis, N. Reimer, A. Klinkebiel, U. Lüning and N. Stock, *Microporous Mesoporous Mater.*, 2015, **216**, 13 —19

91. S. H. Jhung, J.-H. Lee and J.-S. Chang, *Bull. Korean Chem. Soc.*, 2005, **26**, 880

92. G. Férey, C. Serre, C. Mellot-Draznieks, F. Millange, S. Surblé, J. Dutour and I. Margiolaki, *Angew. Chem., Int. Ed.*, 2004, **43**, 6296 —6301

93. N. A. Khan and S. H. Jhung, *Bull. Korean Chem. Soc.*, 2009, **30**, 2921 —2926

94. M. Schlesinger, S. Schulze, M. Hietschold and M. Mehring, *Microporous Mesoporous Mater.*, 2010, **132**, 121 —127

95. Z. Xiang, D. Cao, X. Shao, W. Wang, J. Zhang and W. Wu, *Chem. Eng. Sci.*, 2010, **65**, 3140 —3146

96. L. Bromberg, Y. Diao, H. Wu, S. A. Speakman and T. A. Hatton, *Chem. Mater.*, 2012, **24**, 1664 —1675

97. E. Haque, N. A. Khan, J. H. Park and S. H. Jhung, *Chem.–Eur. J.*, 2010, **16**, 1046 —1052

98. J.-S. Choi, W.-J. Son, J. Kim and W.-S. Ahn, *Microporous Mesoporous Mater.*, 2008, **116**, 727 —731

99. E. Haque and S. H. Jhung, *Chem. Eng. J.*, 2011, **173**, 866 —872

100. Y. Lou, J. Chen, J. Jiang and Q. Bao, *Dalton Trans.*, 2013, **43**, 1261 —1266

101. M. Taddei, P. V. Dau, S. M. Cohen, M. Ranocchiari, J. A. van Bokhoven, F. Costantino, S. Sabatini and R. Vivani, *Dalton Trans.*, 2015, **44**, 14019 —14026

102. D. Cabooter, A. Fanigliulo, G. Bellazzi, B. Allieri, A. Rottigni and G. Desmet, *J. Chromatogr. A*, 2010, **1217**, 7074 —7081

103. H. Uehara, S. Diring, S. Furukawa, Z. Kalay, M. Tsotsalas, M. Nakahama, K. Hirai, M. Kondo, O. Sakata and S. Kitagawa, *J. Am. Chem. Soc.*, 2011, **133**, 11932 —11935

104. M. Tonigold, Y. Lu, B. Bredenkötter, B. Rieger, S. Bahnmüller, J. Hitzbleck, G. Langstein and D. Volkmer, *Angew. Chem., Int. Ed.*, 2009, **48**, 7546 —7550

105. A. Dhakshinamoorthy, M. Alvaro, Y. K. Hwang, Y.-K. Seo, A. Corma and H. Garcia, *Dalton Trans.*, 2011, **40**, 10719 —10724

106. K. Hindelang, A. Kronast, S. I. Vagin and B. Rieger, *Chem.–Eur. J.*, 2013, **19**, 8244 —8252

107. N. Abhyankar, M. Lee, M. Foley, E. S. Choi, G. Strouse, H. W. Kroto and N. S. Dalal, *Phys. Status Solidi RRL*, 2016, **10**, 600 —605

108. C. Carlucci, H. Xu, B. Federica Scremin, C. Giannini, D. Altamura, E. Carlino, V. Videtta, F. Conciauro, G. Gigli and G. Ciccarella, *CrystEngComm*, 2014, **16**, 1817 —1824

109. M. Yaser Masoomi, A. Morsali and P. C. Junk, *RSC Adv.*, 2014, **4**, 47894 —47898

110. E. Haque, N. A. Khan, C. M. Kim and S. H. Jhung, *Cryst. Growth Des.*, 2011, **11**, 4413 —4421

111. D. Li, X. Dai, X. Zhang, H. Zhuo, Y. Jiang, Y.-B. Yu, P. Zhang, X. Huang and H. Wang, *J. Catal.*, 2017, **348**, 276 —281

112. H. Bunzen, M. Grzywa, M. Hambach, S. Spirkl and D. Volkmer, *Cryst. Growth Des.*, 2016, **16**, 3190 —3197

113. B. Liu, Y. He, L. Han, V. Singh, X. Xu, T. Guo, F. Meng, X. Xu, P. York, Z. Liu and J. Zhang, *Cryst. Growth Des.*, 2017, **17**, 1654 —1660

114. Y. Sakata, S. Furukawa, C. Kim and S. Kitagawa, *Chem. Lett.*, 2012, **41**, 1436 —1438

115. K. M. L. Taylor, W. J. Rieter and W. Lin, *J. Am. Chem. Soc.*, 2008, **130**, 14358 —14359

116. W. Guo, W. Sun, L.-P. Lv, S. Kong and Y. Wang, *ACS Nano*, 2017, **11**, 4198 —4205

117. C. Zhang, L. Ai and J. Jiang, *J. Mater. Chem. A*, 2015, **3**, 3074 —3081

118. A. Chouhan, P. Mayer and A. Pandey, *Indian J. Chem.*, 2015, **54A**, 851 —857

119. A. Chouhan, G. Pilet, S. Daniele and A. Pandey, *Chin. J. Chem.*, 2017, **35**, 209 —216

120. Calculated from the advertised surface area range of Basolite MOFs on Sigma Aldrich, retrieved 18/09/17.

121. R. Sabouni, H. Kazemian and S. Rohani, *Chem. Eng. Technol.*, 2012, **35**, 1085 —1092

122. M. Märcz, R. E. Johnsen, P. D. C. Dietzel and H. Fjellvåg, *Microporous Mesoporous Mater.*, 2012, **157**, 62 —74

123. M. R. DeStefano, T. Islamoglu, S. J. Garibay, J. T. Hupp and O. K. Farha, *Chem. Mater.*, 2017, **29**, 1357 —1361

124. A. Carné, C. Carbonell, I. Imaz and D. Maspoch, *Chem. Soc. Rev.*, 2011, **40**, 291 —305

125. S.-N. Kim, J. Kim, H.-Y. Kim, H.-Y. Cho and W.-S. Ahn, *Catal. Today*, 2013, **204**, 85 —93

126. F.-L. Yuan, Y.-Q. Yuan, M.-Y. Chao, D. J. Young, W.-H. Zhang and J.-P. Lang, *Inorg. Chem.*, 2017, **56**, 6522 —6531

127. S. R. Caskey, A. G. Wong-Foy and A. J. Matzger, *Inorg. Chem.*, 2008, **47**, 7751 —7756

128. N. A. Khan, J. S. Lee, J. Jeon, C.-H. Jun and S. H. Jhung, *Microporous Mesoporous Mater.*, 2012, **152**, 235 —239

129. N. A. Khan and S. H. Jhung, *Coord. Chem. Rev.*, 2015, **285**, 11 —23

130. N. Guillou, C. Livage, M. Drillon and G. Férey, *Angew. Chem., Int. Ed.*, 2003, **42**, 5314 —5317

131. J. Górka, P. F. Fulvio, S. Pikus and M. Jaroniec, *Chem. Commun.*, 2010, **46**, 6798 —6800

132. N. E. Tari, A. Tadjarodi, J. Tamnanloo and S. Fatemi, *Microporous Mesoporous Mater.*, 2016, **231**, 154 —162

133. F. Zhang, X. Zou, W. Feng, X. Zhao, X. Jing, F. Sun, H. Ren and G. Zhu, *J. Mater. Chem.*, 2012, **22**, 25019 —25026

134. L. H. Wee, F. Bonino, C. Lamberti, S. Bordiga and J. A. Martens, *Green Chem.*, 2014, **16**, 1351 —1357

135. H. Depauw, I. Nevjestic, J. D. Winne, G. Wang, K. Haustraete, K. Leus, A. A. Verberckmoes, C. Detavernier, F. Callens, E. D. Canck, H. M. Vrielinck and P. V. D. Voort, *Chem. Commun.*, 2017, **53**, 8478 —8481

136. D. Li, D. Yan, X. Zhang, J. Li, T. Lu and L. Pan, *J. Colloid Interface Sci.*, 2017, **497**, 350 —358

137. Z. Wang and S. M. Cohen, *Chem. Soc. Rev.*, 2009, **38**, 1315 —1329

138. K. K. Tanabe and S. M. Cohen, *Chem. Soc. Rev.*, 2011, **40**, 498 —519

139. S. M. Cohen *Chem. Rev.*, 2012, **112**, 970 —1000

140. M. S. El-Shall, V. Abdelsayed, A. E. R. S. Khder, H. M. A. Hassan, H. M. El-Kaderi and T. E. Reich, *J. Mater. Chem.*, 2009, **19**, 7625 —7631

141. L. Zhang, Z. Su, F. Jiang, Y. Zhou, W. Xu and M. Hong, *Tetrahedron*, 2013, **69**, 9237 —9244

142. F. Wu, L.-G. Qiu, F. Ke and X. Jiang, *Inorg. Chem. Commun.*, 2013, **32**, 5 —8

143. W. Dong, C. Feng, L. Zhang, N. Shang, S. Gao, C. Wang and Z. Wang, *Catal. Lett.*, 2016, **146**, 117 —125

144. M. Montazerolghaem, S. F. Aghamiri, S. Tangestaninejad and M. R. Talaie, *RSC Adv.*, 2015, **6**, 632 —640

145. A. M. Balu, C. S. K. Lin, H. Liu, Y. Li, C. Vargas and R. Luque, *Appl. Catal., A*, 2013, **455**, 261 —266

146. G. Zhu, X. Li, H. Wang and L. Zhang, *Catal. Commun.*, 2017, **88**, 5 —8

147. M. Kim, S. J. Garibay and S. M. Cohen, *Inorg. Chem.*, 2011, **50**, 729 —731

148. A. M. Fracaroli, H. Furukawa, M. Suzuki, M. Dodd, S. Okajima, F. Gándara, J. A. Reimer and O. M. Yaghi, *J. Am. Chem. Soc.*, 2014, **136**, 8863 —8866

149. J. Bonnefoy, A. Legrand, E. A. Quadrelli, J. Canivet and D. Farrusseng, *J. Am. Chem. Soc.*, 2015, **137**, 9409 —9416

150. H.-G. Seok, D.-W. Kim, J.-G. Yang, M.-I. Kim and D.-W. Park, *J. Nanosci. Nanotechnol.*, 2016, **16**, 4612 —4619

151. A. M. Fracaroli, P. Siman, D. A. Nagib, M. Suzuki, H. Furukawa, F. D. Toste and O. M. Yaghi, *J. Am. Chem. Soc.*, 2016, **138**, 8352 —8355

152. R. W. Flaig, T. M. Osborn Popp, A. M. Fracaroli, E. A. Kapustin, M. J. Kalmutzki, R. M. Altamimi, F. Fathieh, J. A. Reimer and O. M. Yaghi, *J. Am. Chem. Soc.*, 2017, **139**, 12125 —12128

153. H.-Y. Huang, C.-L. Lin, C.-Y. Wu, Y.-J. Cheng and C.-H. Lin, *Anal. Chim. Acta*, 2013, **779**, 96 —103

154. C.-L. Lin, S. Lirio, Y.-T. Chen, C.-H. Lin and H.-Y. Huang, *Chem.–Eur. J.*, 2014, **20**, 3317 —3321

155. S. Lirio, W.-L. Liu, C.-L. Lin, C.-H. Lin and H.-Y. Huang, *J. Chromatogr. A*, 2016, **1428**, 236 —245

156. W. Guo, W. Sun and Y. Wang, *ACS Nano*, 2015, **9**, 11462 —11471

157. J. Tu, X. Zeng, F. Xu, X. Wu, Y. Tian, X. Hou and Z. Long, *Chem. Commun.*, 2017, **53**, 3361 —3364

158. R. Dai, W. Sun, L.-P. Lv, M. Wu, H. Liu, G. Wang and Y. Wang, *Small*, 2017, **13**, 1700521

159. J.-D. Xiao, L.-G. Qiu, X. Jiang, Y.-J. Zhu, S. Ye and X. Jiang, *Carbon*, 2013, **59**, 372 —382

160. C. Zhang, F. Ye, S. Shen, Y. Xiong, L. Su and S. Zhao, *RSC Adv.*, 2015, **5**, 8228 —8235

161. X. Yang, H. Xue, Q. Yang, R. Yuan, W. Kang and C.-S. Lee, *Chem. Eng. J.*, 2017, **308**, 340 —346

162. C. L. Arthur and J. Pawliszyn, *Anal. Chem.*, 1990, **62**, 2145 —2148

163. Z. Zhang, Z.-Z. Yao, S. Xiang and B. Chen, *Energy Environ. Sci.*, 2014, **7**, 2868 —2899

164. A. Samanta, A. Zhao, G. K. H. Shimizu, P. Sarkar and R. Gupta, *Ind. Eng. Chem. Res.*, 2012, **51**, 1438 —1463

165. Carbon Capture and Sequestration Market Could Reach $128 Billion by 2030, https://www.navigantresearch.com/newsroom/carbon-capture-and-

sequestration-market-could-reach-128-billion-by-2030, accessed May 16, 2017.

166. G. H. Albuquerque, R. C. Fitzmorris, M. Ahmadi, N. Wannenmacher, P. K. Thallapally, B. P. McGrail and G. S. Herman, *CrystEngComm*, 2015, **17**, 5502 —5510

167. S. Cadot, L. Veyre, D. Luneau, D. Farrusseng and E. A. Quadrelli, *J. Mater. Chem. A*, 2014, **2**, 17757 —17763

168. M. Taddei, D. A. Steitz, J. A. van Bokhoven and M. Ranocchiari, *Chem.–Eur. J.*, 2016, **22**, 3245 —3249

169. C. McKinstry, E. J. Cussen, A. J. Fletcher, S. V. Patwardhan and J. Sefcik, *Chem. Eng. J.*, 2017, **326**, 570 —577

170. M. Taddei, N. Casati, D. A. Steitz, K. C. Dümbgen, J. van Bokhoven and M. Ranocchiari, *CrystEngComm*, 2017, **19**, 3206 —3214

171. A. J. Buttress, J. Katrib, D. A. Jones, A. R. Batchelor, D. A. Craig, T. A. Royal, C. Dodds and S. W. Kingman, *Miner. Eng.*, 2017, **109**, 169 —183

172. A. R. Batchelor, A. J. Buttress, D. A. Jones, J. Katrib, D. Way, T. Chenje, D. Stoll, C. Dodds and S. W. Kingman, *Miner. Eng.*, 2017, **111**, 5 —24

Appendix 2: Developing a sustainable route to environmentally relevant metal–organic frameworks: ultra-rapid synthesis of MFM-300(Al) using microwave heating

Ieuan Thomas-Hillman, Lee A. Stevens, Marcus Lange, Jens Möllmer, William Lewis, Chris Dodds, Samuel W. Kingman, and Andrea Laybourn.

Faculty of Engineering, University of Nottingham, Nottingham, UK
Institut für Nichtklassische Chemie e.V., Permoserstrasse 15, 04318 Leipzig, Germany
School of Chemistry, University of Nottingham, Nottingham NG7 2RD, UK
School of Chemistry, The University of Sydney, New South Wales 2006, Australia

Submitted 11th July 2019, Accepted 1st August 2019

Published in Green Chemistry, 2019, 21, 5039-5045

DOI: 10.1039/C9GC02375E

Statement of contribution of joint authorship

Ieuan Thomas – Hillman conducted laboratory experiments developing the synthesis of MFM-300(Al) and performed SEM, PXRD and TGA analysis of the reported sample. Lee Stevens conducted CO_2 and N_2 gas adsorption experiments and aided Ieuan Thomas-Hillman with BET, PSD analysis and interpretation. Marcus Lange and Jens Möllmer conducted SO_2 and NO_2 gas adsorption experiments and provided interpretation. William Lewis aided with PXRD characterisation of samples both published and in development. Andrea Laybourn, Chris Dodds and Samuel Kingman provided overall experimental supervision and development of the synthesis. All authors contributed to writing of the manuscript and responding to reviewers. Andrea Laybourn submitted the manuscript for publication.

Abstract

NO_2, SO_2 and CO_2 are major air pollutants causing significant environmental and health problems. Metal–organic frameworks (MOFs), in particular $[Al_2(OH)_2(C_{16}O_8H_6)](H_2O)_6$ (trivial names: NOTT-300/MFM-300(Al)), have shown great promise for capturing these gases. However MOF syntheses often involve toxic

solvents and long durations which are inherently energy intensive, an environmental burden, and have serious safety risks. There is a pressing need to develop environmentally-friendly routes to MOFs that require less energy and implement safer solvents particularly when considering scale-up beyond the laboratory for industrial application. We report the rapid synthesis of MFM-300(Al) in aqueous conditions and 10 minutes using microwave heating. This is the fastest reported synthesis of MFM-300(Al) to date with a 99.77% reduction in reaction time compared to the current reported 3-day conventionally heated route. The microwave synthesized sub-micron crystalline material exhibits gas uptake capacities of 8.8 mmol g^{-1} at 273 K and 1.0 bar for CO_2, 8.5 mmol g^{-1} at 298 K and 0.17 bar for SO_2, and 1.9 mmol g^{-1} at 298 K and 0.01 bar for NO_2. These are 26%, 70%, and 90% greater for CO_2, SO_2, and NO_2, respectively, when compared to previously reported MFM-300(Al) materials produced *via* a 3-day conventionally heated route demonstrating the production of high quality materials in a fraction of the time with enhanced gas properties. Crucially, this offers an opportunity to move from batch to continuous processing owing to reduced reaction times underpinned by targeted heating.

Main text of paper

The dioxides of nitrogen, sulfur and carbon (NO_2, SO_2 and CO_2, respectively) are regarded as three of the most problematic air pollutants generated by anthropogenic activity.[1–3] NO_2 and SO_2 are particularly detrimental to the environment[3–5] and human health[1,6,7] as they contribute to toxic photochemical smog and acid rain.[8] Additionally, the escalating level of atmospheric CO_2 is a major environmental concern due to its implication in global warming.[3,9] The harmful effects of NO_2, SO_2 and CO_2 have provided significant impetus for their removal and the development of a sustainable low-carbon economy.

Metal–organic frameworks (MOFs) are subset of co-ordination polymers that show great potential for gas storage and separation owing to their exceptionally high surface areas and tuneable pore environment and functionalities.[8,9] Notably $[Al_2(OH)_2(C_{16}O_8H_6)](H_2O)_6$ (trivial names: NOTT-300/MFM-300(Al)) has shown exceptional selective reversible adsorption and uptake capacity of CO_2, SO_2, low-concentration NO_2 (5000 to <1 ppm), and ammonia.[10–17] A highly sensitive SO_2 sensor

based on the indium analogue of MFM-300 was also recently reported.[18] However, current methods of preparing MFM-300 and indeed many other MOFs, hinders their adoption in industrial gas storage and separation applications.[19] MOFs are commonly synthesised *via* solvothermal batch reactions which involve large volumes of toxic solvent and long reaction times (up to one week).[20] The development of routes that reduce the product cost and environmental burden of MOFs is critical for the transfer of these materials from the laboratory to industry and the realisation of the environmental benefits that these materials offer.[21] In order to address these synthetic challenges, electrochemical, sonochemical, mechanochemical, spray drying, continuous flow, and microwave methods have been developed.[20,22] Of these routes, microwave heating has been shown to offer highly significant benefits such as exceptionally rapid reactions (on the order of seconds),[23] control over particle morphology and size, and phase selectivity.[21]

In this paper we describe an aqueous microwave-assisted method for synthesising MFM-300(Al) on the tens of milligrams scale in 10 minutes. This is the first time a microwave route to MFM-300(Al) has been reported. This route requires significantly less time than the current procedure (3-day solvothermal synthesis at 210 °C)[12] and negates the requirement for a corrosive piperazine additive,[12] whilst delivering MFM-300(Al) at a higher percentage yield (83 *cf.* 75%) with a highly uniform particle size and morphology and significantly enhanced uptake capacities for CO_2, SO_2 and NO_2.

A 4 : 1 mixture of aluminium chloride hexahydrate and biphenyl-3,3′,5,5′-tetracarboxylic acid (H_4BPTC) in deionized water was heated, with stirring, at 210 °C in a commercial CEM Discover microwave cavity for 10 minutes. Further synthetic details, including method development, are given in the Experimental section. Note: Temperature was determined by an in-built infra-red sensor and therefore represents the average temperature of the reaction mixture. The resulting suspended particles of microwave synthesised MFM-300(Al) (hereby denoted MFM-300(Al)-MW) were found to be 249–790 nm long and between 74–964 nm wide, with a stubby cylindrical to cuboidal morphology (Fig. 1). This differs from the plate-like sub-micron particles previously reported for MFM-300(Al)[12] prepared using conventional heating (hereby denoted MFM-300(Al)-CH) and is a likely consequence of the different heating mechanism promoting a different mode of crystal growth.[21,23] Reflections in the

powder X-ray diffraction (PXRD) pattern of MFM-300(Al)-MW were indexed to the $I4_122$ tetragonal space group, corresponding to the reported crystal structure of MFM-300(Al)-CH (Fig. 2).[12] A simulated Le Bail fit[24] to the $I4_122$ space group revealed the presence of a low intensity extra reflection at around 27° 2θ (Fig. 2) attributed to residual unreacted linker (H_4BPTC). However, there was no detectable evidence of unreacted linker by thermogravimetric analysis, *i.e.* no loss at the decomposition temperature of H_4BPTC (340 °C) was observed (Fig. 3). No peaks corresponding to γ-Al(O)OH[25] or other MOF phases beyond MFM-300(Al) were observed. Attempts to synthesise MFM-300(Al) using these conditions with conventional heating for 24 to 72 hours (rather than rapidly using microwaves) gave a mixture of MOF phases and γ-Al(O)OH.[25]

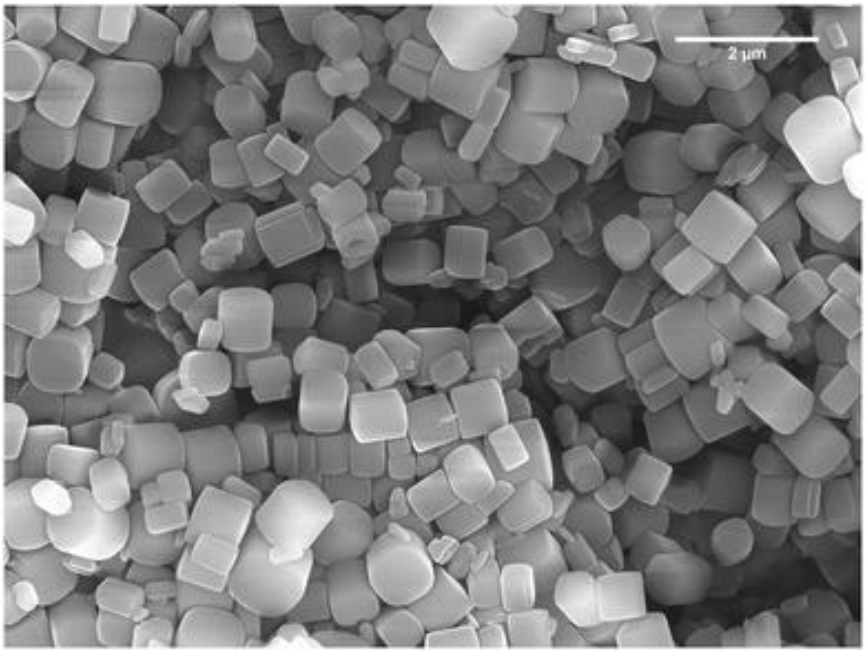


Fig. 1 SEM image of MFM-300(Al)-MW synthesised in deionized water in 10 minutes. The material exhibits average particle dimensions of 604 ± 111 × 520 ± 234 nm.

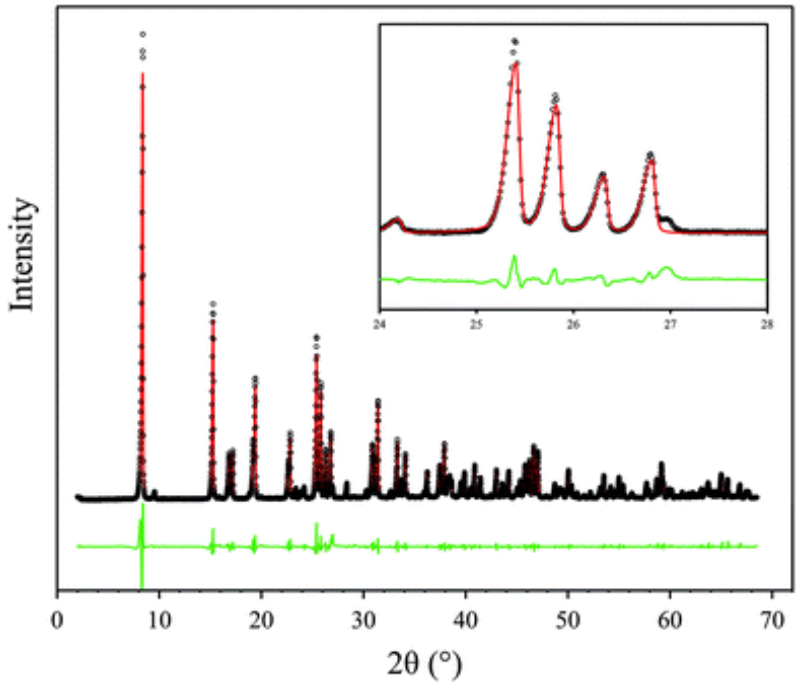


Fig. 2 PXRD pattern of MFM-300(Al)-MW. Black = observed; red = simulated pattern Le Bail fit; green = difference plot. Inset: Plot of the PXRD pattern between 24 and 28° 2θ; an extra reflection attributed to unreacted linker is visible at ~27° 2θ in the difference plot.

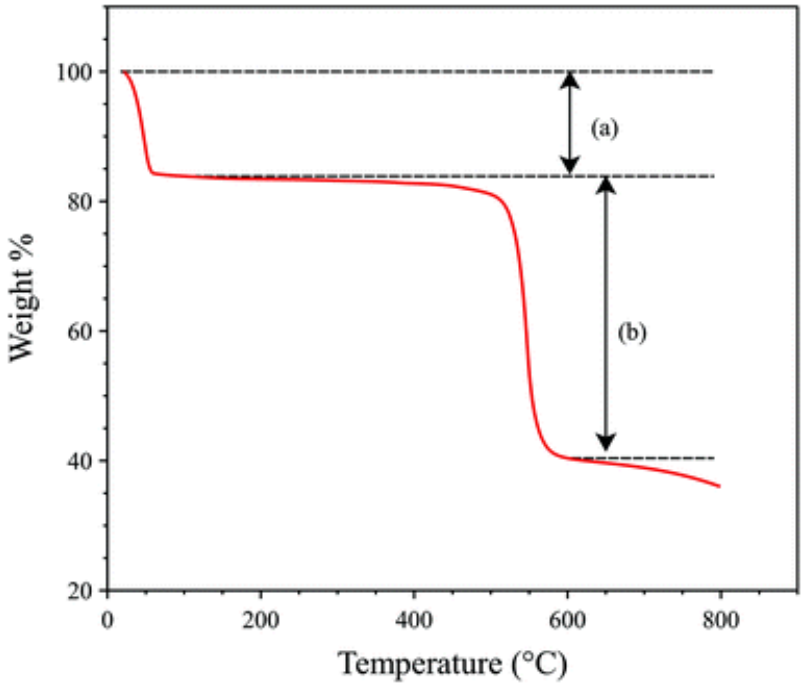


Fig. 3 TGA thermogram of MFM-300(Al)-MW. (a) 30–100 °C = loss of adsorbed water (15.85%) from the MOF. (b) 465–600 °C = thermal decomposition of MFM-300(Al)-MW (40.23%). Slow MOF decomposition is observed beyond 600 °C.

Low pressure CO_2 adsorption–desorption isotherms of MFM-300(Al)-MW at ambient temperatures (273–303 K, Fig. 4a) show very high uptake capacities, with a maximum value of 8.8 mmol g^{-1} at 273 K and 1.0 bar and 4.7 mmol g^{-1} at 303 K and 1.0 bar. Analysis of the adsorption branch of the CO_2 isotherm at 273 K gave a BET surface area of 1272 ± 25 m^2 g^{-1}. The non-local density functional theory (NLDFT) model for carbon slit pores[26–28] gave a pore size distribution centred at 0.5 nm whereby the total pore volume is reached at 0.6 nm, indicative of a solely microporous material,[26] and a cumulative pore volume of 0.58 cm^3 g^{-1} (Fig. 4b). These results differ from the CO_2 sorption properties of MFM-300(Al)-CH whereby a maximum uptake of 7.0 mmol g^{-1} at 273 K and 1.0 bar and cumulative pore volume of 0.38 cm^3 g^{-1} were reported.[12] MFM-300(Al)-MW shows negligible N_2 sorption at 298 K up to 1 bar (see Fig. 5a), however at 77 K a Type I isotherm, with some Type IV character, is observed (Fig. 5b). From these data, an N_2 uptake of 135 cm^3 g^{-1} at *ca.* 0.5 bar and BET surface area of 515 ± 1 m^2 g^{-1} were calculated (Fig. 5b). These results are significantly different compared to MFM-300(Al)-CH which does not adsorb dinitrogen.[10–12] The lack of N_2 porosity demonstrated by MFM-300(Al)-CH is not expected for an open porous structure and was ascribed by Yang *et al.* to restricted diffusion at low temperatures as a result of the narrow pore channels.[12] Further work is ongoing to investigate the difference in porosity between microwave and conventionally heated MFM-300(Al) materials.

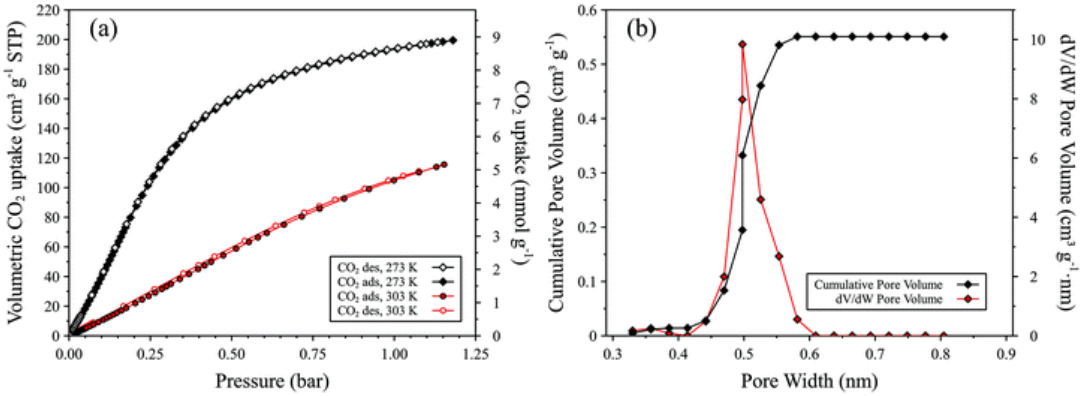


Fig. 4 (a) Manometric carbon dioxide gas sorption isotherms (legend inset) and (b) pore size distribution (PSD, red) and cumulative pore volume plot (black) for MFM-300(Al)-MW. Data calculated from the adsorption branch of the CO_2 isotherm at 273 K using the NLDFT model for carbon slit pores.[26–28]

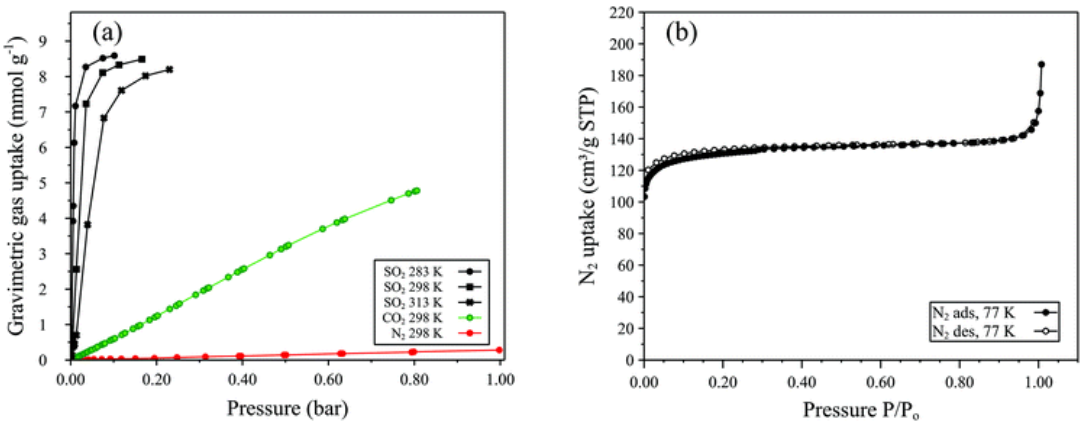


Fig. 5 (a) Gravimetric SO_2 and manometric CO_2, and N_2 gas adsorption isotherms and (b) manometric N_2 gas sorption isotherm at 77 K for MFM-300(Al)-MW. Legends inset. SO_2 data were collected using 25% SO_2 in N_2 as the sorbate.

We also determined the SO_2 and NO_2 sorption properties of MFM-300(Al)-MW which, like MFM-300(Al)-CH, exhibits exceptional uptake capacities for these environmentally detrimental gases. The high uptake of SO_2 and NO_2 exhibited by MFM-300(Al) are a result of multiple formal interactions between the bridging μ_2-OH functionality of the aluminium secondary building unit with guest molecules, resulting in an efficient packing of SO_2 and NO_2 within the pore.[12,15,16] SO_2 adsorption isotherms at 283 K, 298 K and 303 K for MFM-300(Al)-MW collected using 25% SO_2 in N_2 are shown in Fig. 5a and are summarised in Table 1. As can be seen, MFM-300(Al)-MW exhibits high SO_2 uptakes, 8.49 mmol g^{-1} at 298 K and 0.17 bar partial pressure (*P*), exceeding the previously reported ~5 mmol g^{-1} at the same temperature and pressure,[16] and 8.1 mmol g^{-1} at 273 K and *P* = 1.0 bar.[12] As with the previously reported MFM-300(Al)-CH, the SO_2 uptake for MFM-300(Al)-MW (Fig. 5a) shows a steep increase at low pressure (<0.01 bar *P*) followed by a less steep increase up to 0.1 bar *P*, indicative of a Type I isotherm.[12] At a *P* of 0.10 bar and 298 K, MFM-300(Al)-MW exhibits the second highest reported SO_2 uptake capacity compared to other MOFs (Table 1) which is promising for potential applications in SO_2 capture from flue gas where the concentration of SO_2 is typically <500 ppm [29] or for low concentration SO_2 gas detection.[17] NO_2 uptake by MFM-300(Al)-MW was confirmed by measuring single point adsorption at 273 K, 298 K and 313 K using a mixture of 1% NO_2 in N_2 (see Fig. 6). At a *P* of 0.01 bar and 298 K, MFM-300(Al)-MW shows an NO_2 uptake of 1.89 mmol g^{-1} which exceeds the reported NO_2 uptake of 1.02 mmol g^{-1} for MFM-300(Al)-CH at the equivalent pressure.[16]

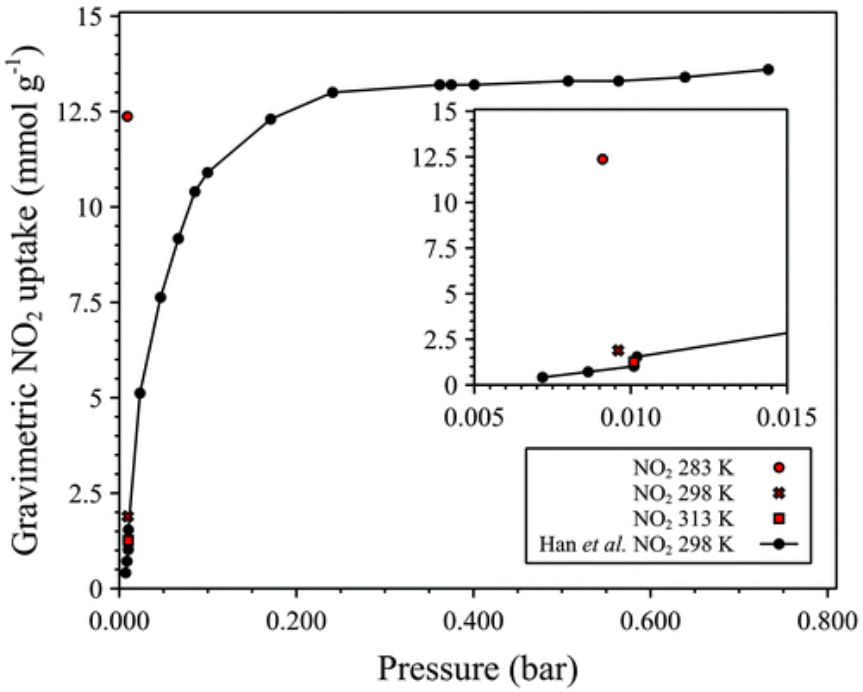


Fig. 6 Single point NO_2 sorption data collected for MFM-300(Al)-MW at 283 K, 298 K, and 313 K corresponding to partial pressures between 0.009 and 0.01 bar using 1% NO_2 in N_2 as the sorbate (in red). NO_2 isotherm at 298 K reported by Han *et al.* (ref. 10) for MFM-300(Al)-CH for comparison in black (sorbate is pure NO_2). Legend inset.

Table 1 Comparison of SO_2 uptake of selected MOFs

Material	SO_2 uptake (mmol g^{-1})					Ref.
	Pressure (bar)				Temperature (K)	
	0.01	0.10	0.17	1.00		
MFM-300(Al)-MW	7.2	8.6	—	—	283	This work
	2.6[b]	8.1[c]	8.5	—	298	This work
	0.5	7.6[d]	8.0	—	313	This work
MFM-300(Al)-CH	—	—	—	8.1	273	12
		~4.5[a]	~5[a]	~5[a]	298	16
MFM-300(In)	—	—	—	8.3	298	34
MOF-177	0.3	1.0	1.5[a]	25.7	293	29
NH_2-MIL-125(Ti)	3.0	7.9	~8.6[a]	10.8	293	29
	—	5[a]	~7[a]	9.7[a]	298	35
MIL-160	4.2	5.5	~5.8[a]	10.8	293	29
SIFSIX-1-Cu	3.4	8.7	—	11.0	298	36
SIFSIX-2-Cu-i	4.2	6.0	—	6.9	298	36

a Taken from isotherm. b At 0.013 bar. c At 0.074 bar. d At 0.12 bar.

In conclusion, the rapid synthesis of MFM-300(Al) in aqueous conditions using microwave heating has been developed. This route yields MFM-300(Al) on the tens of milligram scale in just 10 minutes with significantly enhanced uptake of polluting dioxides (8.8 *cf.* 7.0 mmol g^{-1} CO_2 at 273 K and 1 bar,[10–12] 8.5 *cf.* ~5 mmol g^{-1} SO_2 at 298 K and 0.17 bar,[12,16] and 1.9 *cf.* 1.0 mmol g^{-1} NO_2 at 298 K and 0.01 bar.[17] Other essential properties of MFM-300(Al) such as surface area (1272 ± 26 m^2 g^{-1}) and temperature of decomposition (>500 °C) are maintained. This is the fastest reported synthesis of MFM-300(Al) to date with a 99.77% reduction in reaction time compared to current solvothermal methods (3 days). The efficient and facile procedure in this work represents a key step towards the development of a sustainable route to MFM-300(Al), and possibly other MOFs, by reducing the environmental burden (use of aqueous solvent and very short reaction times). This new method also offers favourable conditions (*e.g.* short timescales) for development of a continuous and

scalable production route using microwave heating. Industry has identified the need for new sustainable routes to MOFs[30] as a prerequisite for their use in real-world applications addressing major world-wide concerns in environmental air pollution.

Experimental section

Materials and methods

Synthesis of MFM-300(Al)-MW

Aluminium trichloride hexahydrate (99%) and biphenyl-3,3′,5,5′-tetracarboxylic acid (95%) were obtained from Alfa Aesar and Manchester Organics Limited, respectively, and used as received. Milli-Q plus 18.2 MΩ cm deionized water was used.

$AlCl_3 \cdot 6H_2O$ (250 mg, 1.04 mmol), biphenyl-3,3′,5,5′-tetracarboxylic acid (H_4BPTC, 85 mg, 0.26 mmol) and deionized water (15.0 mL) were added to a 35 mL vial. The vial was sealed and contents stirred to facilitate dissolution of the metal salt. The vial was then placed into a CEM Discover microwave cavity and heated to 210 °C for 10 minutes (300 W, maximum forward power) under autogenous pressure and with stirring. After the reaction time had elapsed the vial was cooled in the microwave cavity with air and the resultant suspension was centrifuged (4200 revolutions per minute, 20 minutes) and washed with distilled water (*ca.* 50 mL). The centrifugation and wash step was repeated twice and the supernatant decanted. The white powder product was then dried in an oven at 50 °C for 18 hours. After this time the sample was allowed to rehydrate in the fumehood under ambient atmospheric conditions for 8 hours. Yield (89 mg, 83.5%; for the dehydrated MOF, *i.e.* $[Al_2(OH)_2(C_{16}O_8H_6)]$, calculated based on the linker and TGA analyses). Further details on synthetic development can be found in the ESI.†

Characterisation

Powder X-ray diffraction

Diffraction patterns were collected using a PANalytical MPD diffractometer equipped with a PIXcel DKIW179H1 detector and a conventional sealed tube Cu X-ray source (operating at 40 kV and 40 mA), equipped with an α1 monochromator. Scans were

conducted between 2° and 70° 2θ and data were analysed using TOPAS Academic[31] and are plotted using Veusz.[32]

Thermogravimetric analyses

Thermogravimetric analyses were carried out using either a TA instruments TGA 550 or Q5000IR analyser. Samples were heated at a rate of 2 K min^{-1} under a nitrogen atmosphere to a maximum of 800 °C. Data plotted using Veusz.[32]

Scanning electron microscopy

High-resolution SEM images of MFM-300(Al) were collected using a JEOL 7100F FEG-scanning electron microscope. Samples were prepared on machined aluminium stubs with carbon adhesive tabs. The samples were coated with a 10 nm layer of iridium using a Quorum QISOT ES coater. Imaging was conducted at a working distance of 10 mm with an electron gun accelerating potential of 15 kV. Frame captures of the sample morphologies were obtained using Jeol PC-SEM software. Average particle size and standard deviation were determined by measuring the length and diameter of a total of 50 particles using ScionImage software.[33]

Gas sorption

Manometric CO_2 sorption isotherms were recorded at 273 K and 303 K up to 1.2 bar using either a Micromeritics 3Flex or a Micromeritics ASAP 2420 adsorption analyser. In a typical measurement between 100 and 150 data points were collected. Surface areas were calculated in the relative pressure (P/P_0) range from 0.01 to 0.015 which corresponds to a pressure of <0.5 bar; in this region all of the micropores are filled. PSD and cumulative pore volume were calculated from the adsorption branch of the CO_2 isotherm at 273 K using the NLDFT pore model for carbon slit pore geometry.[26–28] Manometric N_2 sorption was recorded at 77 K up to 1.0 bar using a Micromeritics ASAP 2420 adsorption analyser; *ca.* 100 data points were collected. Samples were degassed at 120 °C for 15 hours under vacuum (10^{-5} bar) before analysis. Data were analysed using Micromeritics MicroActive software (V5) and plotted using Veusz.[32]

Gravimetric SO_2 and NO_2 adsorption isotherms were recorded using a magnetic suspension balance working in the dynamic flow mode at ambient pressure. Therefore,

an inert gas flow of dry nitrogen was used to balance the SO_2 concentration between SO_2 partial pressure 0.002–0.2. SO_2 data were collected at temperatures of 283 K, 298 K, and 313 K and partial pressures up to 0.10, 0.17 and 0.232 bar using 25% SO_2 in N_2 as the sorbate. Single point NO_2 sorption data were collected at 283 K, 298 K, and 313 K corresponding to partial pressures between 0.009 and 0.01 bar using 1% NO_2 in N_2 as the sorbate. Samples were degassed in a nitrogen flow at 120 °C until no further decrease in weight was observed.

Manometric CO_2 and N_2 sorption isotherms were recorded using a stainless-steel version of the BELSORP-max sorption analyser at 298 K and up to 0.81 and 1.0 bar, respectively. In a typical measurement between 30 and 60 data points were collected. Samples were degassed at 120 °C for 15 hours under vacuum (10^{-7} bar) before analysis. Data were plotted using Veusz.[32]

Conflicts of interest

There are no conflicts of interest to declare.

Acknowledgements

SEM analyses in this work were supported by the Engineering and Physical Sciences Research Council (EPSRC) [under grant EP/L022494/1] and the University of Nottingham. Andrea Laybourn gratefully acknowledges the University of Nottingham for the award of a Nottingham Research Fellowship.

References

1. M. Kampa and E. Castanas, Human health effects of air pollution, *Environ. Pollut.*, 2008, **151**, 362 —367
2. J. N. Galloway Acid deposition: Perspectives in time and space, *Water, Air, Soil Pollut.*, 1995, **85**, 15 —24
3. D. W. Keith Why Capture CO_2 from the Atmosphere?, *Science*, 2009, **325**, 1654 —1655

4. P. M. Edwards, S. S. Brown, J. M. Roberts, R. Ahmadov, R. M. Banta, J. A. deGouw, W. P. Dubé, R. A. Field, J. H. Flynn, J. B. Gilman, M. Graus, D. Helmig, A. Koss, A. O. Langford, B. L. Lefer, B. M. Lerner, R. Li, S.-M. Li, S. A. McKeen, S. M. Murphy, D. D. Parrish, C. J. Senff, J. Soltis, J. Stutz, C. Sweeney, C. R. Thompson, M. K. Trainer, C. Tsai, P. R. Veres, R. A. Washenfelder, C. Warneke, R. J. Wild, C. J. Young, B. Yuan and R. Zamora, High winter ozone pollution from carbonyl photolysis in an oil and gas basin, *Nature*, 2014, **514**, 351 —354

5. J. Lelieveld, T. M. Butler, J. N. Crowley, T. J. Dillon, H. Fischer, L. Ganzeveld, H. Harder, M. G. Lawrence, M. Martinez, D. Taraborrelli and J. Williams, Atmospheric oxidation capacity sustained by a tropical forest, *Nature*, 2008, **452**, 737 —740

6. Z. Chen, J.-N. Wang, G.-X. Ma and Y.-S. Zhang, China tackles the health effects of air pollution, *Lancet*, 2013, **382**, 1959 —1960

7. V. L. Feigin, G. A. Roth, M. Naghavi, P. Parmar, R. Krishnamurthi, S. Chugh, G. A. Mensah, B. Norrving, I. Shiue, M. Ng, K. Estep, C. J. L. Cercy, M. H. Murray and I. Forouzanfar, Global Burden of Diseases, Risk Factors Study 2013, Stroke Experts Writing Group. Global burden of stroke and risk factors in 188 countries, during 1990–2013: a systematic analysis for the Global Burden of Disease Study 2013, *Lancet Neurol.*, 2016, **15**, 913 —924

8. E. Barea, C. Montoro and J. A. R. Navarro, Toxic gas removal – metal–organic frameworks for the capture and degradation of toxic gases and vapours, *Chem. Soc. Rev.*, 2014, **43**, 5419 —5430

9. K. Sumida, D. L. Rogow, J. A. Mason, T. M. McDonald, E. D. Bloch, Z. R. Herm, T.-H. Bae and J. R. Long, Carbon Dioxide Capture in Metal–Organic Frameworks, *Chem. Rev.*, 2012, **112**, 724 —781

10. X. Han, H. G. W. Godfrey, L. Briggs, A. J. Davies, Y. Cheng, L. L. Daemen, A. M. Sheveleva, F. Tuna, E. J. L. McInnes, J. Sun, C. Drathen, M. W. George, A. J. Ramirez-Cuesta, K. M. Thomas, S. Yang and M. Schröder, Reversible adsorption of nitrogen dioxide within a robust porous metal–organic framework, *Nat. Mater.*, 2018, **17**, 691 —696

11. S. Yang, A. J. Ramirez-Cuesta, R. Newby, V. Garcia-Sakai, P. Manuel, S. K. Callear, S. I. Campbell, C. C. Tang and M. Schröder, Supramolecular binding and separation of hydrocarbons within a functionalized porous metal–organic framework, *Nat. Chem.*, 2015, **7**, 121 —129

12. S. Yang, J. Sun, A. J. Ramirez-Cuesta, S. K. Callear, W. I. F. David, D. P. Anderson, R. Newby, A. J. Blake, J. E. Parker, C. C. Tang and M. Schröder, Selectivity and direct visualization of carbon dioxide and sulfur dioxide in a decorated porous host, *Nat. Chem.*, 2012, **4**, 887 —894

13. C. G. Morris, N. M. Jacques, H. G. W. Godfrey, T. Mitra, D. Fritsch, Z. Lu, C. A. Murray, J. Potter, T. M. Cobb, F. Yuan, C. C. Tang, S. Yang and M. Schröder, Stepwise observation and quantification and mixed matrix membrane separation of CO_2 within a hydroxy-decorated porous host, *Chem. Sci.*, 2017, **8**, 3239 —3248

14. C. P. Krap, R. Newby, A. Dhakshinamoorthy, H. García, I. Cebula, T. L. Easun, M. Savage, J. E. Eyley, S. Gao, A. J. Blake, W. Lewis, P. H. Beton, M. R. Warren, D. R. Allan, M. D. Frogley, C. C. Tang, G. Cinque, S. Yang and M. Schröder, Enhancement of CO_2 Adsorption and Catalytic Properties by Fe-Doping of $[Ga_2(OH)_2(L)]$ (H_4L = Biphenyl-3,3′,5,5′-tetracarboxylic Acid), MFM-300(Ga_2), *Inorg. Chem.*, 2016, **55**, 1076 —1088

15. H. G. W. Godfrey, I. da Silva, L. Briggs, J. H. Carter, C. G. Morris, M. Savage, T. L. Easun, P. Manuel, C. A. Murray, C. C. Tang, M. D. Frogley, G. Cinque, S. Yang and M. Schröder, Ammonia Storage by Reversible Host–Guest Site Exchange in a Robust Metal–Organic Framework, *Angew. Chem., Int. Ed.*, 2018, **57**, 14778 —14781

16. X. Han, S. Yang and M. Schröder, Porous metal–organic frameworks as emerging sorbents for clean air, *Nat. Rev. Chem.*, 2019, **3**, 108 —118

17. T. Jurado-Vázquez, E. Sánchez-González, A. E. Campos-Reales-Pineda, A. Islas-Jácome, E. Lima, E. González-Zamora and I. A. Ibarra, MFM-300: From air pollution remediation to toxic gas detection, *Polyhedron*, 2019, **157**, 495 —504

18. V. Chernikova, O. Yassine, O. Shekhah, M. Eddaoudi and K. N. Salama, Highly sensitive and selective SO_2 MOF sensor: the integration of MFM-300 MOF as a sensitive layer on a capacitive interdigitated electrode, *J. Mater. Chem. A*, 2018, **6**, 5550 —5554

19. U. Mueller, M. Schubert, F. Teich, H. Puetter, K. Schierle-Arndt and J. Pastre, Metal-organic frameworks-prospective industrial applications, *J. Mater. Chem.*, 2006, **16**, 626 —636

20. N. Stock and S. Biswas, Synthesis of Metal-Organic Frameworks (MOFs): Routes to Various MOF Topologies, Morphologies, and Composites, *Chem. Rev.*, 2012, **112**, 933 —969

21. I. Thomas-Hillman, A. Laybourn, C. Dodds and S. W. Kingman, Realising the environmental benefits of metal-organic frameworks: recent advances in microwave synthesis, *J. Mater. Chem. A*, 2018, **6**, 11564 —11581

22. M. Rubio-Martinez, C. Avci-Camur, A. W. Thornton, I. Imaz, D. Maspoch and M. R. Hill, New synthetic routes towards MOF production at scale, *Chem. Soc. Rev.*, 2017, **46**, 3453 —3480

23. A. Laybourn, J. Katrib, R. S. Ferrari-John, C. G. Morris, S. Yang, O. Udoudo, T. L. Easun, C. Dodds, N. R. Champness, S. W. Kingman and M. Schroder, Metal-organic frameworks in seconds *via* selective microwave heating, *J. Mater. Chem. A*, 2017, **5**, 7333 —7338

24. A. Le Bail, H. Duroy and J. L. Fourquet, *Ab initio* structure determination of $LiSbWO_6$ by X-ray powder diffraction, *Mater. Res. Bull.*, 1988, **23**, 447 —452

25. X. Bokhimi, J. A. Toledo-Antonio, M. L. Guzmán-Castillo, B. Mar-Mar, F. Hernández-Beltrán and J. Navarrete, Dependence of Boehmite Thermal Evolution on Its Atom Bond Lengths and Crystallite Size, *J. Solid State Chem.*, 2001, **161**, 319 —326

26. K. S. W. Sing Reporting physisorption data for gas/solid systems with special reference to the determination of surface area and porosity (Recommendations 1984), *Pure Appl. Chem.*, 1985, **57**, 603

27. J. J. Manyà, B. González, M. Azuarab and G. Arner, Ultra-microporous adsorbents prepared from vine shoots-derived biochar with high CO_2 uptake and CO_2/N_2 selectivity, *Chem. Eng. J.*, 2018, **345**, 631 —639

28. A. C. Dassanayake and M. Jaroniec, Activated polypyrrole-derived carbon spheres for superior CO_2 uptake at ambient conditions, *Colloids Surf., A*, 2018, **549**, 145 —154

29. P. Brandt, A. Nuhnen, M. Lange, J. Möllmer, O. Weingart and C. Janiak, Metal–Organic Frameworks with Potential Application for SO_2 Separation and Flue Gas Desulfurization, *ACS Appl. Mater. Interfaces*, 2019, **11**, 17350 — 17358

30. P. A. Julien, C. Mottillo and T. Friščić, Metal–organic frameworks meet scalable and sustainable synthesis, *Green Chem.*, 2017, **19**, 2729 —2747

31. A. A. Coelho TOPAS and TOPAS-Academic: an optimization program integrating computer algebra and crystallographic objects written in C++, *J. Appl. Crystallogr.*, 2018, **51**, 210 —218

32. https://veusz.github.io/2019.

33. https://scion-image.software.informer.com/2019.

34. M. Savage, Y. Cheng, T. L. Easun, J. E. Eyley, S. P. Argent, M. R. Warren, W. Lewis, C. Murray, C. C. Tang, M. D. Frogley, G. Cinque, J. Sun, S. Rudić, R. T. Murden, M. J. Benham, A. N. Fitch, A. J. Blake, A. J. Ramirez-Cuesta, S. Yang and M. Schröder, Selective Adsorption of Sulfur Dioxide in a Robust Metal–Organic Framework Material, *Adv. Mater.*, 2016, **28**, 8705 —8711

35. W. P. Mounfield, C. Han, S. H. Pang, U. Tumuluri, Y. Jiao, S. Bhattacharyya, M. R. Dutzer, S. Nair, Z. Wu, R. P. Lively, D. S. Sholl and K. S. Walton, Synergistic Effects of Water and SO_2 on Degradation of MIL-125 in the Presence of Acid Gases, *J. Phys. Chem. C*, 2016, **120**, 27230 —27240

36. X. Cui, Q. Yang, L. Yang, R. Krishna, Z. Zhang, Z. Bao, H. Wu, Q. Ren, W. Zhou, B. Chen and H. Xing, Ultrahigh and Selective SO_2 Uptake in Inorganic Anion-Pillared Hybrid Porous Materials, *Adv. Mater.*, 2017, **29**, 1606929

Supporting Information

Starting from the conventional solvothermal route,1-3 a reproducible microwave-assisted synthetic procedure to MFM-300(Al) was developed. The aims of developing the new route were to reduce the reaction time, negate the requirement for additional chemicals (piperazine and nitric acid), and to minimise the amount of unwanted side products (i.e.γ-Al(O)OH)and unreacted starting materials. A summary of the method development steps is given in TableS1 below.

Table S1. Summary of method development for a microwave-assisted route to MFM-300(Al). All reactions performed in deionised water without piperazine or nitric acid.

Synthetic modification	Aluminium chloride source	Reactant ratio Aluminium: H_4BPTC	Reaction time (minutes)	Synthetic outcome
1	Anhydrous	2:1	120	γ-Al(O)OH produced.
2	Anhydrous	2:1	30	γ-Al(O)OH produced.
3	Hexahydrate	2:1	10	Unreacted linker, *ca.* 5.4 – 10.4% from TGA.
4*	Hexahydrate	4:1	10	Unreacted linker present in PXRD pattern but none detected by TGA.
5	Hexahydrate	> 4:1	10	High intensity peak corresponding to unreacted linker in PXRD pattern.

*Desired synthetic outcome achieved; results presented in main paper.

References:

(1) Han, X.; Godfrey, H. G. W.; Briggs, L.; Davies, A. J.; Cheng, Y.; Daemen, L. L.; Sheveleva, A. M.; Tuna, F.; McInnes, E. J. L.; Sun, J.; Drathen, C.; George, M. W.; Ramirez-Cuesta, A. J.; Thomas, K. M.; Yang, S.; Schröder, M. Reversible adsorption of nitrogen dioxide within a robust porous metal–organic framework. Nature Materials 2018, 17, 691-696.

(2) Yang, S.; Ramirez-Cuesta, A. J.; Newby, R.; Garcia-Sakai, V.; Manuel, P.; Callear, S. K.; Campbell, S. I.; Tang, C. C.; Schröder, M. Supramolecular binding and separation of hydrocarbons within a functionalized porous metal–organic framework. Nature Chemistry 2015, 7, 121-129.

(3) Yang, S.; Sun, J.; Ramirez-Cuesta, A. J.; Callear, S. K.; David, W. I. F.; Anderson, D. P.; Newby, R.; Blake, A. J.; Parker, J. E.; Tang, C. C.; Schröder, M. Selectivity and direct visualization of carbon dioxide and sulfur dioxide in a decorated porous host. Nature Chemistry 2012, 4, 887-89

Appendix 3: Crystallisation mechanism of a microwave-synthesised metal-organic framework: the long and the short of it.

Ieuan Thomas-Hillman, Yuchun Zhang, Ricardo Caldas, Zhehao Huang, Xiaodong Zou, Chris Dodds, Samuel Kingman, and Andrea Laybourn

Faculty of Engineering, University of Nottingham, Nottingham, UK
School of Chemistry, University of Nottingham, Nottingham, UK
Department of Materials and Environmental Chemistry, Berzeli Center EXSELENT on Porous Materials, Stockholm University, Stockholm, SE-106 91, Sweden

Manuscript prepared for publication awaiting submission.

Statement of contribution of joint authorship

Ieuan Thomas – Hillman modified and assembled the power/energy controlled batch reactor. Ieuan Thomas – Hillman operated the reactor synthesising MFM-300(Al). Yuchun Zhang and Ricardo Caldas assisted with experimental procedures. Ieuan Thomas-Hillman collected and interpreted SEM, EDX, PXRD and TGA data. Zhehao Huang and Xiaodong Zou collected and interpreted TEM-ED data and provided helpful discussions interpreting the significance of the data. Ieuan Thomas-Hillman, Andrea Laybourn and Samuel Kingman compiled and edited the manuscript. Andrea Laybourn, Chris Dodds and Samuel Kingman supervised the project. Ieuan Thomas-Hillman would like to acknowledge Matt Nichols for assistance in setting up and modifying experiment equipment.

Abstract

Microwave heating is a tremendously exciting route for the synthesis of metal-organic frameworks (MOFs) owing to significantly reduced reaction times (from hours to seconds) and enhanced control over MOF properties (particle size, morphology, phase-selectivity) compared to conventional heating. Despite this hugely exciting research, many reports involve generic non-specific microwave heating cavities that simply use the average temperature of the reaction mixture to control the microwave energy supplied to the reaction mixture. Furthermore, these reports do not consider the interactions between electromagnetic waves and the electronic structure of the reaction

mixtures which ultimately influences the synthetic outcome. Here we show that control of the microwave energy and power delivery, using a single mode cavity, can be used to control the morphology of an aluminium MOF ($[Al_2(OH)_2(C_{16}O_8H_6)](H_2O)_6$) by preferential growth along one distinct crystallographic axis. From our results we provide, for the first time, a mechanistic rationalisation of MOF crystallisation in a microwave field.

Introduction

Metal-organic frameworks (MOFs) are a broad class of highly porous materials comprised of metal nodes and organic linkers. Through variation of constituent metal ions and organic linkers, the pore environment of MOFs can be tailored for any specific application including gas storage [1-5], catalysis [5-7], chemical separation [2, 8] and drug delivery [1, 9]. In addition to chemical structure and functionalities, a further important property of MOFs is morphology, *i.e.* the shape and size of MOF particles, since this influences availability of internal surface area, mass transfer kinetics, and diffusion pathways. These factors have huge implications for gas-sorption [10] and catalysis where substrates must diffuse in and out of the MOF structure [11]. Morphology also affects how MOF particles pack together, essential in applications and MOF devices where packing efficiency and tessellation are required, such as in cylinder filling, fixed bed applications, and pelletisation [12].

Morphology is affected by numerous chemical parameters [12] and can be controlled using surfactants [12-15], modulators [16-18], templates [19-21], or physical casting methods [22, 23]. Surfactants and modulators (which can also lead to defects [24]) are additional chemical components which need to be added into a reaction, templates rely on being able to fabricate a desired morphology of a different species which then remains after the reaction and physical casting methods in microfluidics are inherently difficult to scale up. These methods can be difficult to scale up, and involve extra external chemical or physical effects rather than exploiting the MOFs inherent self-assembly.

In contrast to these chemical methods many MOF structures naturally self-assemble in a way which exhibits anisotropic preferential phase and morphological growth due

to the chemical mechanism of linker and metal ion fragment nucleation by which they form[25, 26]. For example, the synthesis of MIL-88 forms well-ordered nanorods [27] and a recent study by Lee et al. [28] on hybridising the (B) and (C) variants of the structure used TEM electron diffraction to explore the structure of the hybrids, showing all their materials to be growing along the crystallographic c-axis, however no mechanistic rational is given. Along with morphology, the presence of defects in the MOF crystal structure can further augment a MOFs properties by enhancing gas adsorption [29] or leading to catalytic behaviour [30, 31], and offering additional opportunities to tune the overall properties of the MOF framework [32].

Microwave synthesis [33], which is gaining popularity in MOF chemistry due to the fast reactions it enables, has also been reported showing a morphological change with respect to a conventional synthesis [33-36], though why this occurs is left unexplained. Additionally, microwave synthesis often yields MOF particles that are smaller than their conventionally synthesised counterparts [33, 37], which is an attractive trait for applications due to the previously mentioned increase in accessibility of the MOF's internal volume [12, 33]. In microwave heated synthesis energy is delivered into a reaction via an oscillating electric field, which induces translational and rotational motion of ionic and polar species within the load, respectively, and thus heat via friction. In the case of MOF synthesis mixtures this leads to preferential heating of the area around solvated metal ions, or 'hotspots' [33, 38, 39] which drive the reaction significantly faster than conventionally heated reactions [33, 38, 39]. This affects morphology as it changes the nucleation and crystallisation kinetics of MOF formation, often leading to small nanoscale MOF crystals.

However, while morphological changes brought on by MW processing have been documented, conclusions drawn from such experiments are limited, as the experiments relied on temperature controlled commercial microwave systems. In these temperature controlled (TC) systems, software is typically used to control the power delivery, and the actual power that the reaction solution is exposed to, and thus the environment that MOF crystallisation is actually occurring in is not accurately characterised [33, 40]. Additionally, in any discussion of microwave heated synthesis the penetration depth is an essential factor which must be considered. In its simplest form a formal definition of penetration depth gives the point at which the intensity of the electric field is reduced

to 1/e of its original value at the surface of the sample (Equation 1) [41]. This can be calculated from the dielectric properties of the heating load using the penetration depth equation [42] However it is important to consider that this value actually represents a continuous attenuation of the electric field strength within the sample. Due to the limitation in understanding of these TC microwave systems there is an impetus to move to power & energy controlled (P/EC) systems where the energy delivery can be precisely controlled.

By switching to P/EC based experimentation we have previously been able to show the effects of different power deliveries onto MOF synthesis both in batch processing and continuous flow production, in both cases there was a clear influence on yield and particle morphology from varying the incident power delivered to the reaction [39, 43]. These effects can be ascribed to the "hotspot" mechanism and its dependence on the microwave deilvery, since the temperature rise in a material is directly related to the power density (Equation 2) and thus intensity of the electric field (Equation 3). When using higher power (and control of the electronic field by impedence matching) the power density is higher, thus the localised heating of the hotspot is maximised and the heat transfer to the bulk is minimised [41, 43].

$$D_p = \frac{\lambda_0}{2\pi\sqrt{2\varepsilon'}} \frac{1}{\sqrt{\left[\left\{1+\left(\frac{\varepsilon''}{\varepsilon'}\right)^2\right\}^{0.5}-1\right]}} \qquad \text{(Equation 1)}$$

$$P_d = c\rho\frac{dT}{dt} \qquad \text{(Equation 2)}$$

$$P_d = 2\pi f\varepsilon_0\varepsilon'' E^2 \qquad \text{(Equation 3)}$$

(Where e' is the dielectric constant, e'' is the dielectric loss, D_p is the penetration depth (m), λ_0 is the wavelength of the microwave radiation (m), P_d is the power density (W m^{-3}), c is the specific heat capacity of the material (J kg^{-1} °C^{-1}), ρ is the density (kg m^{-3}), $\frac{dT}{dt}$ is the temperature change over time, f is frequency (Hz) and E is the electric field strength in the material (V m^{-1}).)

Recently we reported the microwave synthesis of the aluminium MOF NOTT/MFM-300 using a commercial microwave system; representing a synthesis time reduction of 98%, yielding a product superior to that previously reported [44-46], and showing uniform morphology of stubby sub-micron sized cylinders (604 ± 111 x 520 ± 234 nm). Noticing how this morphology differed from the plates previously reported from conventional heating, we were keen to see how more controlled microwave energy delivery effected the morphology of the yielded MFM-300. As a comparison, reactions are performed both in a commercial TC reactor, and a purpose-built P/EC MW rig, to better illustrate the difference between the two systems.

By investigating the impact of energy delivery for the synthesis of $[Al_2(OH)_2(C_{16}O_8H_6)](H_2O)_6$ (also known as NOTT-300/MFM-300(Al)) we show how microwave heating directly affects the morphology of the crystals with preferential growth along one crystallographic axis offering insight into the crystallisation mechanism of MOFs in a microwave field. The framework is synthesised in short times (28 seconds), high yields (up to 70%) and we show how the adsorbed power by the reaction mixture directly affects the morphology of the crystals, with the microwave energy delivery preferentially accelerating crystal growth along one crystallographic axis. We ascribe oriented crystal growth as a consequence of a selective heating mechanism. To our knowledge this is the first time a mechanistic rationalisation of microwave heated MOF synthesis has been provided.

Experimental Procedures

General experimental notes:

Aluminium trichloride hexahydrate (99%) and biphenyl-3,3',5,5'-tetracarboxylic acid (95%) were obtained from Alfa Aesar and Manchester Organics Limited, respectively. Both chemicals were used as received without further purification. Deionized water (18.2 $M\Omega cm^{-1}$) was obtained from a Milli-Q plus ultra-pure water purifier.

Synthesis of MFM-300 in a TC commercial microwave system

In a typical synthesis, aluminium trichloride hexahydrate, biphenyl-3,3',5,5'-tetracarboxylic acid and 10 mL of deionised water were combined in a 35 mL glass pressure vial. The required masses of reactants varied according to experiment and are

fully detailed in Table 1. This was then placed in a CEM Discover microwave cavity and heated to 210 °C for 10 minutes (300 W maximum power) under autogenous pressure and with stirring. After the reaction time had elapsed the vial was cooled using compressed air and the resultant suspension transferred to a centrifuge tube. The white product was collected via centrifuge, washed twice with distilled water (ca. 50 mL per wash) and dried in an oven (50 °C / 18 hours).

Synthesis of MFM-300 in a bespoke P/EC single mode cavity

In a typical synthesis, aluminium trichloride hexahydrate, biphenyl-3,3',5,5'-tetracarboxylic acid and 10 mL of deionised water were combined in a 45 mL PTFE cup, and sealed in a Parr instruments 4782 microwave pressure digestion vessel. This was then placed in the single mode microwave applicator. [39] Reactant masses, microwave power and experimental duration were varied according to experiment and are detailed in Table 2. The 2.45 GHz electric field was pre-matched into the cold reaction load using a network analyser and an S-TEAM HOMER [47] 3 stub auto tuner. During this experiment this auto tuner was used to continually match the power into the reaction mixture as heating changed its dielectric characteristics, and to measure the forward and reflected power during the microwave treatment. From this data the total adsorbed energies could be calculated and averaged with the generator reported power. After treatment, the vessel was allowed to cool and the white product was collected following a centrifuge step, washed twice with distilled water (ca 50. mL per wash) and dried in an oven (50 °C / 18 hours). Experiments were performed in triplicate at each given power, and yield determination per sample likewise performed in triplicate, and the results detailed in the results section and Table 2.

In both synthesis procedures the MOF powder was allowed to re-hydrate in the centrifuge tube at ambient lab conditions in a fume cupboard before weighing.

Pressure warning:

Syntheses were conducted in superheated conditions, and so are kept under autogenous pressure. In the CEM discover microwave reactor the equipment comes built in with pressure monitoring and pressure relief, to ensure safe handling. In the bespoke P/EC microwave applicator pressure monitoring is not possible. The pressure vessel was

equipped with emergency pressure release (a compression disk and vent port) and the applicator was designed to allow safe release of pressure in the event of a pressure release, with the entire set up contained within a bullet-proof polycarbonate box and sealed extraction hood for the duration. After treatment the reaction was left for 90 minutes to cool before handling.

SEM / EDX

High-resolution SEM images of MFM-300(Al) were collected using a JEOL 7100F FEG-scanning electron microscope, with a Field Emission Gun (FEG), a secondary electron detector and a backscatter electron detector. Samples were prepared on machined aluminium stubs with carbon adhesive tabs. The samples were coated with a 10 nm layer of iridium using a Quorum QISOT ES coater. Imaging was conducted at a working distance of 10 nm with an electron gun accelerating potential of 15 kV or 5 kV depending on the image charging. Frame captures of the sample morphologies were obtained using Jeol PC-SEM software, and sizing was conducted with the freeware ImageJ [48].

EDX analyses were conducted using an attached Oxford Instruments EDX spectrometer. Data for regional analysis was collected and processed in the Oxford Instruments INCA software, while elemental maps were collected and analysed in the oxford instruments AZTEC software. Due to the high degree of three-dimensionality in the samples and coating EDX cannot be considered to be reliably quantitative, and its inclusion here is as a qualitative tool to support the assignment of various species within the SEM images. Examples of EDX results are shown in the ESI figures. (ESI Figure 2)

TEM analysis

Samples for transmission electron microscopy observation were diluted in acetone. A droplet of the suspension was transferred onto a carbon-coated copper grid. Observation was performed on a JEOL JEM2100 microscope, and operated at 200 kV (Cs 1.0 mm, point resolution 0.23 nm). Images were recorded with a Gatan Orius 833 CCD camera (resolution 2048 x 2048 pixels, pixel size 7.4 µm) under low dose conditions.

TGA

Thermogravimetric analyses were performed on a Thermal analysis Q550 using high temperature platinum pans. A ramp rate of 2 °C min^{-1} to 100 °C, then at a rate of 5 °C a minute up to 800 °C, all under an N_2 flowrate of 25 ml min^{-1}. A final isothermal stage at 800 °C was used to burn off organic material leaving behind aluminium oxide residue for yield determination. Data were analysed using the TA TRIOS software v5.

Powder X-ray diffraction (PXRD)

Diffraction patterns were recorded on a PANalytical powder X-ray diffractometer, with a CuKα1 (1.5406 Å) X-ray source, and a PIXcel DKIW179H1 detector. Samples were loaded onto zero background silicon plates and patterns collected in a range of 2-70° 2θ for 2 hours. Data conversion was performed with PowDLL [49]. Whole pattern fitting and refinement, along with individual peak fitting were conducted using TOPAS academic [50], using the split pseudo-Voigt peak function to account for reflection asymmetry, and starting from space group and unit cell parameters retrieved from entries NIRPIQ and PUYTEI in the Cambridge structural database [51].

Results and discussion:

Detailing the differences between TC and P/EC reactions

In the TC reactions while a nominal 300 W is applied into the reaction in order to heat it this refers only to a maximum. The reaction in these reactors is controlled via on-board software, which reduces the power as the target temperature is approached, and reapplies power as temperature begins to drop, such that during the 10 minutes of maintaining temperature the reaction is actually being continuously hit with short pulses of MW energy at 300 W (Figure 1 A). This is contrasted with the P/EC reactions, where MW power is applied until a target energy is delivered (30.5 kJ, to achieve a reaction temperature of 210°C). Once this threshold is reached the energy delivery is halted and the reaction is allowed to cool (Figure 1 B). We hypothesise that the MOF crystallisation is occurring in the final moments of the energy delivery, when the bulk temperature has risen enough to not immediately quench the localised hotspots.

Our bespoke cavity was designed to give control over the position of the highest electric field intensity so that the load could be positioned correctly to ensure a homogeneous distribution of electric field within the sample. Automatic impedance matching was used to ensure minimisation of reflection of power from the load. In our experiments we regularly achieved reflected powers so close to 0 that the readings can be considered to be within the error of the power monitor; this is due to the high dielectric properties of the sample (dielectric constant e' = 60.8 ±1.3 and dielectric loss e'' = 36.8 ±2.0) and the precise matching of the system prior to heating coupled with a well characterised applicator. However, such a high dielectric loss leads to a limiting penetration depth [33, 41, 42], which is the attenuation of the electric field within the heating load as energy is stored and converted to heat. A formal definition of penetration depth gives the point at which the intensity of the electric field is reduced to 1 over its original value within a sample [41]. In our case this is at a depth of 4.3 ±0.1 mm within the sample, compared to 10 ml of water in a 31.3 mm ID cup and with 12.8 mm vertical height (considering stirring to cause only minor deformation of this shape). This inhomogeneity of the electric field is important to consider, as while a formal power is delivered into the reaction mixture, different parts of the reaction are actually experiencing a power delivery that is less than this formal value.

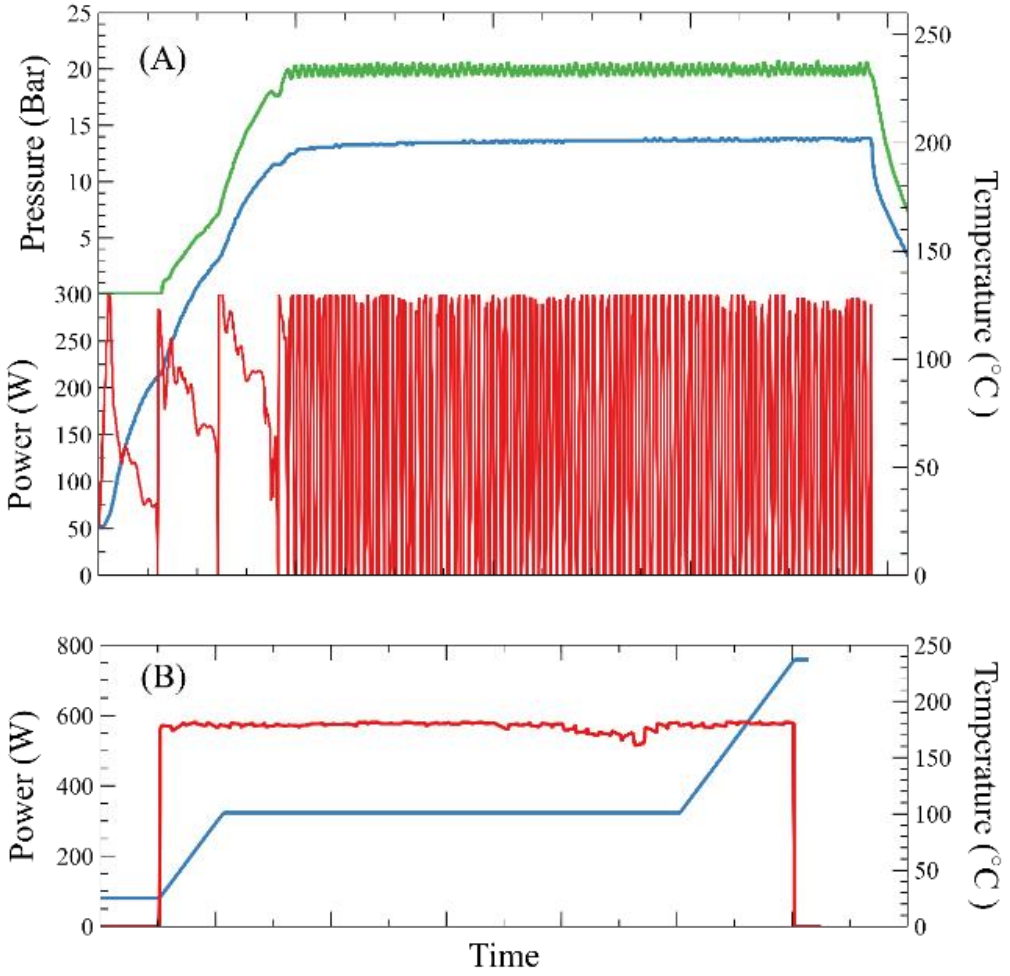


Figure 1: Temperature heating profiles of the reactions, illustrating the difference between thermal control (A) and power & energy control (B). Graph A is taken from the readouts of an experiment in the TC reactor (experiment TC-1), while graph B is shows the recorded energy delivery from the HOMER 3 stub auto tuner/power monitor (see experimental) and a temperature profile calculated from the specific heat capacity/latent heat of vaporisation (experiment P/EC - 12). Red = Power, Blue = Temperature, Green = Pressure, Time axis not to scale.

The effects of reactant ratio and applied microwave power on synthesised MFM-300(Al): Identity & Yield

Two sets of experiments were conducted, one with a 2:1 metal:linker reactant ratio, and a second with a 4:1 metal:linker reactant ratio, based on our previous reports [44]. Reactions were conducted in a T/C reactor at 210 °C for 10 minutes, with a maximum forward power during heating of 300 W followed by rapid power on/off to maintain temperature. In P/EC reactions the target energy was kept at 30.5 kJ with energy

delivered to within 1 kJ of that. Between the two different reactant ratios the aluminium trichloride concentration was maintained at 69 mmol/dm^3. Both TC and P/EC reactions yielded MFM-300(Al), along with residual linker that was not consumed in the reaction, which was confirmed by PXRD analysis. A common impurity in aluminium MOF synthesis is γ-AlO(OH), though no evidence of this was present in any of the samples in PXRD [52]. At 300 W P/EC no MOF was synthesised in detectable amounts for crystallographic analysis. As power delivery increased the intensity of the reflections corresponding to the MOF likewise increased. (Figure 2) Relative crystallinity measurements on the 110 reflection in the PXRD data were not able to resolve any difference between the samples and indistinguishable from the peak profile resultant of the instrument optics and sample preparation. (ESI Figure 4 & 5)

Yield was determined from the final aluminium oxide residue left after TGA experiments. (Figure 3) As would be expected, in the TC reactor, synthesis with an excess of aluminium trichloride showed a higher yields (87.6 ± 0.8%) than those with a stoichiometric 2:1 reactant yield (63.3 ± 1.2%). Figure 4 A and Figure 4 B show the crude yield (hydrated mass collected) and percentage yield (determined by TGA) for the P/EC experiments, respectively. Crude yield represents the mass of all material that was reclaimed from the reaction after sequential washings, drying, and subsequent rehydration; while % yield was determined by TGA, using the final mass of the aluminium oxide residue and back calculating the equivalent mass of MFM-300 in the sample. As with our previous studies [39] increasing power generally increased the yield of MOF. Negligible yields were obtained from 300 W experiments, showing no mass gain from the experiment and limited % yield (<6% -Figure 4 B) as determined by TGA, in agreement with PXRD results. Yields rapidly rose as power increased, to optimal yields (~60%) around 900 W. As would be expected, reactions taking place in an excess of aluminium resulted in higher yield, by approximately 15% at 900 W (50.62 ± 4.97 at a 2:1 reactant ratio vs 64.99 ± 7.38% at a 4:1 reactant ratio). We attribute this increase in yield with increased incident power to the selective heating mechanism, [33, 39] wherein thermal energy is gradually transferred out of the hotspots into the bulk solution. At higher powers the rate at which the hotspots are heated is increased, reducing the ability of the bulk solution to thermally quench them [39, 53, 54], resulting in a higher local temperature and therefore faster reaction. Both sets of reaction yielded less MOF than their corresponding synthesis in the TC reactor;

this is attributed to a limit in various aspects of the synthesis such as migration of the linker throughout the bulk solution, which in such fast reactions becomes a greater limitation than total reactant availability. An increasing variance in yield was observed as power increased (up to ± 14.8% at 1250 W c.f. 4-7% at 900 W), this can be attributed to the fact that at higher powers minor fluctuations in the reaction mixture have a greater effect on the matching and subsequent delivery of energy.

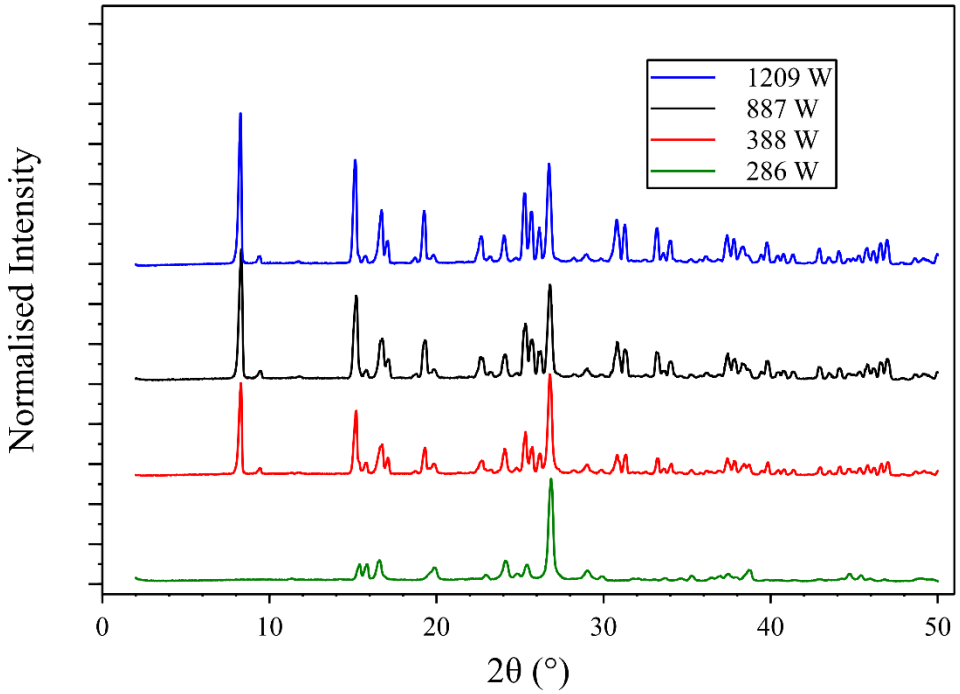


Figure 2: PXRD patterns of PE/C The reflections corresponding to MFM-300(Al) are not present at 300 W (PE/C-9), while one (8.3 °2 θ) is just barely visible at 400 W (PE/C-10). Reactions which had a noticeable yield of MFM-300(Al) show the expected reflections clearly.

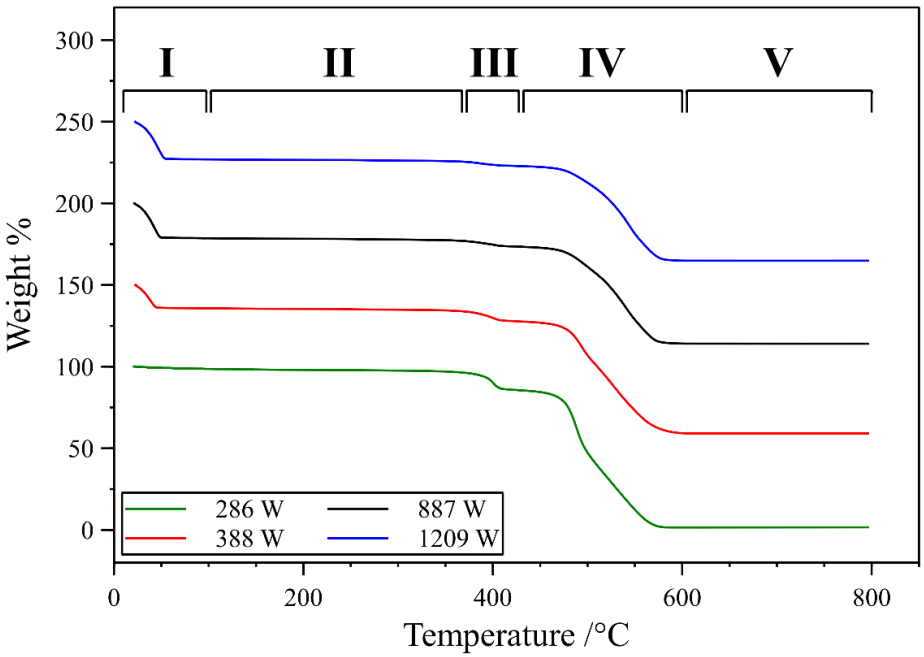


Figure 3: TGA thermograms of samples yielded from both the P/EC reactor (denoted by powers) and T/C reactor (experiment TC-1), shifted by 50 weight percent between each trace. (I) loss of adsorbed water from MFM-300 in the sample, (II) Region of thermal stability in both MFM-300 and the H_4BPTC linker, (III) first thermal mass loss of the linker – visible in all samples retrieved from the P/EC reactor, (IV) Region of thermal mass loss of both MFM-300 and the linker. (V) Final residue of decomposition – used to back calculate % yield. The increase in water mass (I) and decrease in unreacted linker mass (III) shows the progressively increased conversion of linker to MOF.

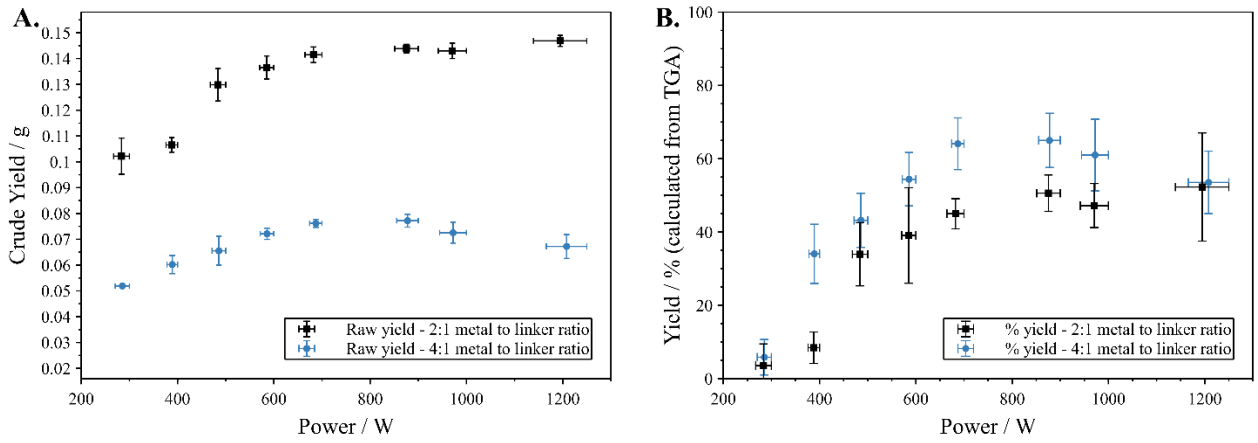


Figure 4: **A.** Raw yield and **B.** Percentage yields from the two sets of experiments relative to power. The mass gain in the raw yields can be ascribed to the combined effect of aluminium in the structure of the MOF and adsorbed water in the pores. Percentage yields are determined from TGA experiments, where the final residue. Vertical error bars represent standard deviation, horizontal error bars represent the uncertainty in the adsorbed power, i.e. the calculated difference from power monitoring using a HOMER 3 stub auto tuner and the internal power monitoring of the generator.

Table 1: Experiments conducted using thermal control in an off the shelf microwave system. The reactor was set to a target temperature of 210°C for 10 minutes and the power delivery was controlled by the inbuilt software to maintain this temperature (See Figure 1)

Code	Ratio Metal salt : Linker	Conc. $AlCl_3$ ($mmol/dm^3$)	Raw Yield / g	%Yield/TGA
TC-1	4:1	69.0	0.0869	87.57±0.79
TC-2	2:1	69.0	0.1531	63.32±1.25

Table 2: Summary of experiments performed using direct power & energy control. Aluminium trichloride concentration was fixed at 69 mmol/dm^3 while linker amount was determined by the chosen reactant ratio. Target energy delivery was kept to 30.5 kJ, and reaction time determined by the incident power setting. Experiments were repeated 3 times, and subsequent yield determination also performed in triplicate, and the resulting averages presented & discussed in the main text. *± represents standard deviation.

Ratio Metal salt: Linker	Linker Mass / g	Code	Power / W	Time / s	Raw yield* / g	% Yield* calc. TGA
2:1	0.114	P/EC-1	300	101.8	0.1022±0.0070	3.56±5.89
		P/EC-2	400	76.4	0.1065±0.0028	8.45±4.30
		P/EC-3	500	61.1	0.1299±0.0063	33.95±8.61
		P/EC-4	600	50.9	0.1365±0.0045	39.06±13.01
		P/EC-5	700	43.6	0.1415±0.0030	44.99±4.13
		P/EC-6	900	33.9	0.1438±0.0017	50.62±4.97
		P/EC-7	1000	30.5	0.1430±0.0029	47.23±6.03
		P/EC-8	1250	24.4	0.1469±0.0021	52.29±14.76
4:1	0.057	P/EC-9	300	101.8	0.0519±0.0005	5.84±4.83
		P/EC-10	400	76.4	0.0602±0.0035	34.06±8.05
		P/EC-11	500	61.1	0.0655±0.0056	43.20±7.39
		P/EC-12	600	50.9	0.0721±0.0022	54.40±7.27
		P/EC-13	700	43.6	0.0762±0.0015	64.09±7.05
		P/EC-14	900	33.9	0.0772±0.0025	64.99±7.38
		P/EC-15	1000	30.5	0.0726±0.0040	61.01±9.80
		P/EC-16	1250	24.4	0.0672±0.0047	53.53±8.54

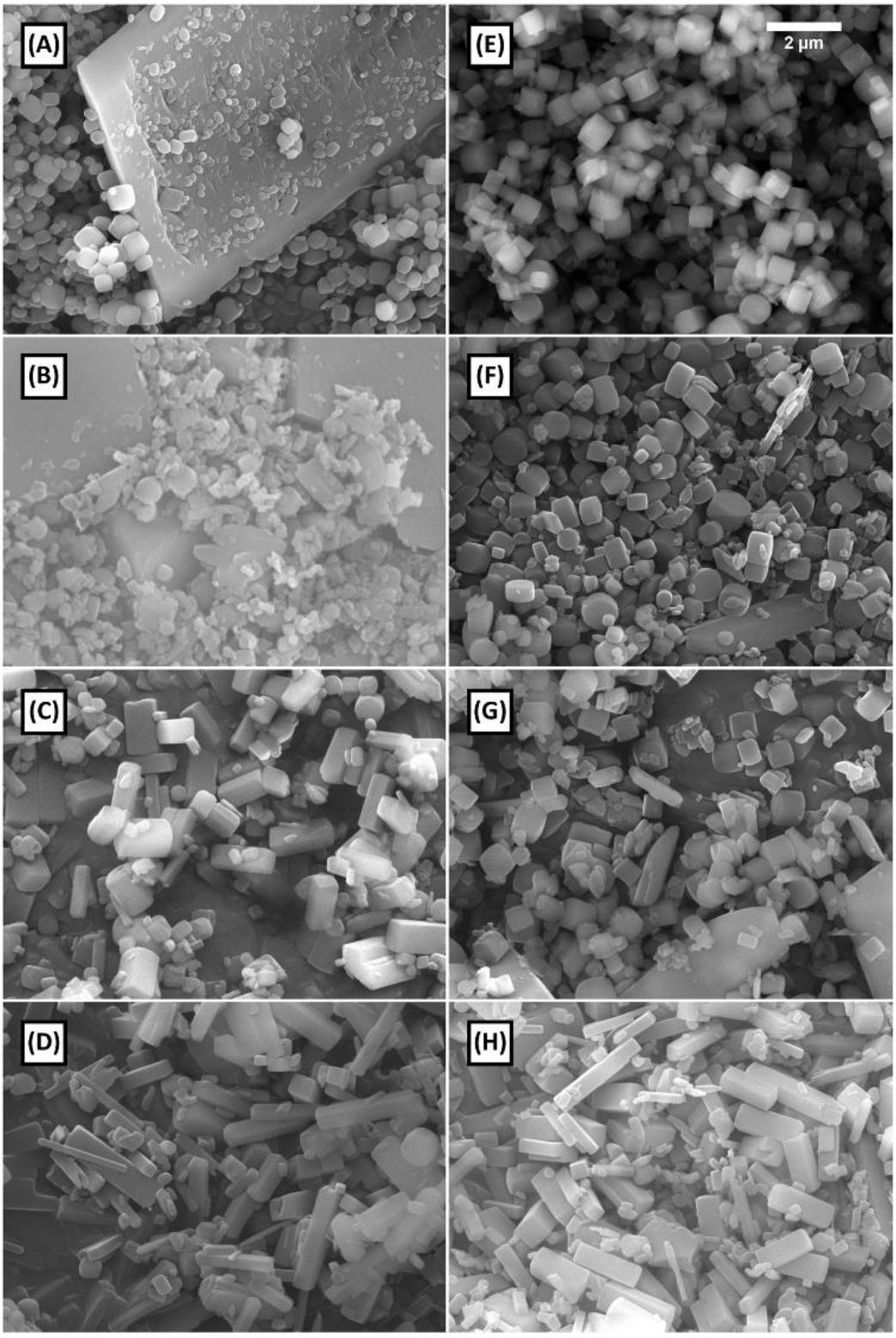
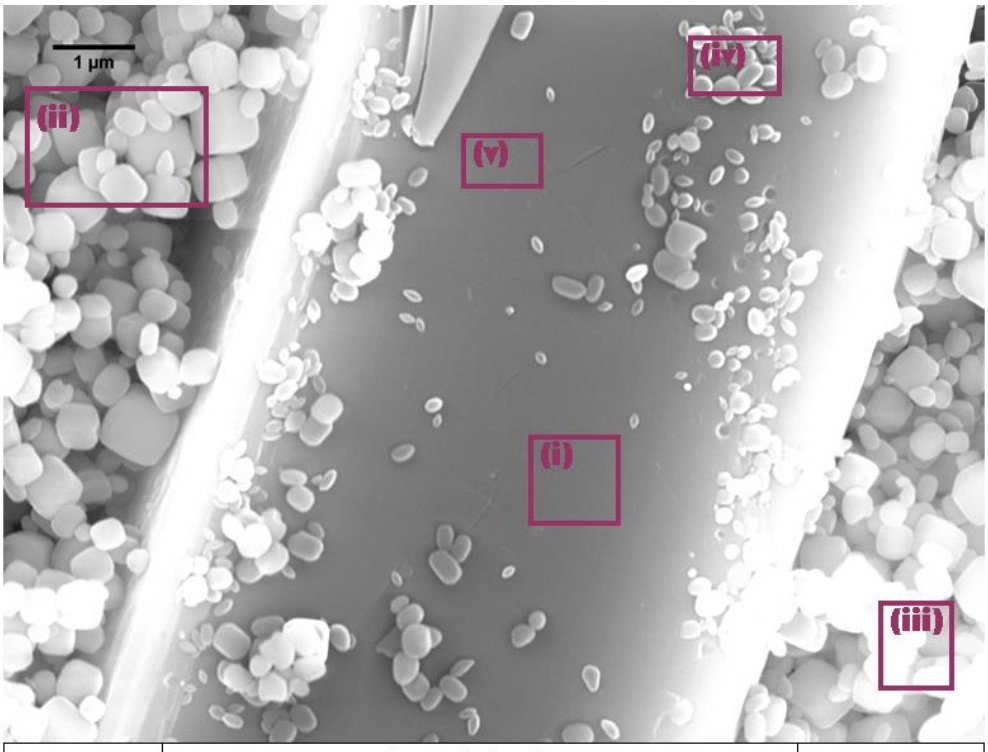


Figure 5: SEM images of MFM-300 crystals, produced using various reaction conditions. Right (A-D) – 2:1 reactant ratio experiments. Left (E-H) - 4:1 reactant ratio experiments. A & E - TC synthesis (10 minutes), B & F - 400 W P/EC experiments, C & G - 500 W PE/C experiments, D & H - 1250 W PE/C experiments. All powers listed as target forward power. Right: Identifying MOF and linker,



Sample Location	Elemental Abundance				Identity
	Oxygen	Carbon	Aluminium	Iridium	
(i)	36.84	59.43	0.21	3.52	Linker
(ii)	37.27	55.00	4.46	3.27	MOF
(iii)	34.31	53.73	6.09	5.87	MOF
(iv)	31.98	64.17	0.47	3.38	MOF/Linker
(v)	33.44	63.10	0.12	3.34	Linker

Figure 6: Energy-dispersive X-ray spectroscopy experiments of TC-2 showing the presence of aluminium in the species we have assigned as the MOF, and a lack of aluminium in the large species we attribute to remaining linker. Boxes and labels in the image correspond to the table. Iridium presence from conductive coating is also shown.

Morphology of yielded MOF particles from different powers and reactant ratios.

SEM was used to characterise the effect of microwave power on the resultant morphology of the MFM-300 crystals (Figure 5 A to H). The synthesis in the PE/C reactor (and TC-2) had left over linker, and this was visible in PXRD experiments where sufficient linker was present to perform a enable a 2 phase Le Bail refinement [55] to the tetragonal $I4_122$ and monoclinic p21/c space group (based on entries NIRPIQ and PUYTEI from the Cambridge structural database [51], for the MOF and the linker, respectively). A representative example of this fitting is shown in ESI

Figure 1, where the presence of two phases, and their contribution to the total pattern is clearly visible in the region around 27 ° 2Θ.

Altering the reaction ratio yielded clear morphological changes (Figure 5 A & E). At a 4:1 reaction ratio the morphology is as previously described [44], with stocky cylinders to rounded off cuboids (560±89 by 610±208 nm) with an average crystal aspect ratio of 1.05. Here we have defined aspect ratio as the ratio of the length (unique crystal dimension) vs width (symmetric crystal dimension). At a 2:1 reactant ratio, where there is no excess of aluminium trichloride the predominant morphology present was cubes with well-defined edges with a size range of 340 to 730 nm (Average 499 ± 83 nm), combined with many smaller more irregular crystals, which resembled grains of rice to pill like cylinders (Average size 252 x 147 nm). Smaller crystals were mostly in conjunction with large crystals of linker, the identity of which was inferred from EDX experiments and PXRD (Figure 6, ESI Figure 2 & ESI Figure 3). All samples also contained these large species.

For 2:1 ratio experiments (P/EC-1 to P/EC-8) a clear progression in morphology was observed. At low powers (300/400 W) there was no evidence of MOF crystals. With assorted broken species being attributed to linker that had been broken up by the heating effect of the microwave. However, at power levels above this (500 W) cuboidal species (~1400 nm long with an aspect ratio of 2.7) formed. As power increased further (at 1250 W) the crystals exhibited an elongated morphology along a singular axis, resulting in long and thin (2500 nm long with an aspect ratio of 7.6) needle-like crystals (Figure 5 D).

In 4:1 ratio experiments (P/EC-9 to P/EC-16, Figure 2 E-H) a similar behaviour was observed. 300 W gave MOF crystals. 400 W experiments showed many MOF particles, taking the form of stubby cylinders (530 nm with an aspect ratio of 0.59), similar to the cylinders seen in TC reactions (Figure 5 F), however with the crystal length being shorter than the width/diameter. As power increased beyond 500 W the crystals morphology rapidly changed. At 600 W and above the predominant morphology returned to the large cuboids seen in 2:1 reactions, with the crystal edges becoming well defined. Finally, at the maximum experimental power the long and thin (2760 nm with an aspect ratio of 8.5) needle like crystals were again seen (Figure 5

H). It is significant that the intensity of the incident MW energy is capable of exerting a greater influence on morphology than chemical effects in this way.

In each sample a large range of sizes and dimensions of the MOF crystals was apparent. Crystal aspect ratio was found to increase (averages from 0.63 to 3.70 for the crystals obtained from the 4:1 reactions) in line with target forward power (Figure 7 C). However as power increased there remained crystals with the lower aspect ratios characteristic of the lower power experiments, (seen clearly in the histogram plots, with widening distributions in the box and whisker diagrams) we attribute this to the attenuation of the electric field intensity (and thus power application) as the microwaves penetrate into the reaction mixture. Assuming MOF crystallisation to be occurring in the last seconds of the reaction, and mixing to be highly inefficient, we propose that crystals can be presumed to have formed in a relative static power environment. Thus, the images represent a range of crystals that have been formed at the incident power down to the lowest power present in the reaction. Selecting the longest 10% of crystals in each sample and calculating the aspect ratio of those showed a trend in line with what a visual assessment of the crystal morphology indicated, with both average particle length and average particle aspect ratio increasing with incident power (Figure 7). 4:1 reactions showed the greatest change; MOF particles grew from stubby cylinders (533 nm long with an aspect ratio of 0.59 @ 400 W [PE/C 10]) to long cuboids (2758 nm long with an aspect ratio of 8.48 @ 1250 W [P/EC 16]). 2:1 reactions showed a slightly less pronounced change, going from stubby cuboids (1438 nm with an aspect ratio of 2.68 @ 500 W [P/EC 3]) to long cuboids (2480 nm long with an aspect ratio of 7.60 @ 1250 W [P/EC 8]). Calculating averaged particle volume of the longest crystals showed no overall trend. This crystal lengthening and thinning can be seen in histogram plots of the crystal sizing data.

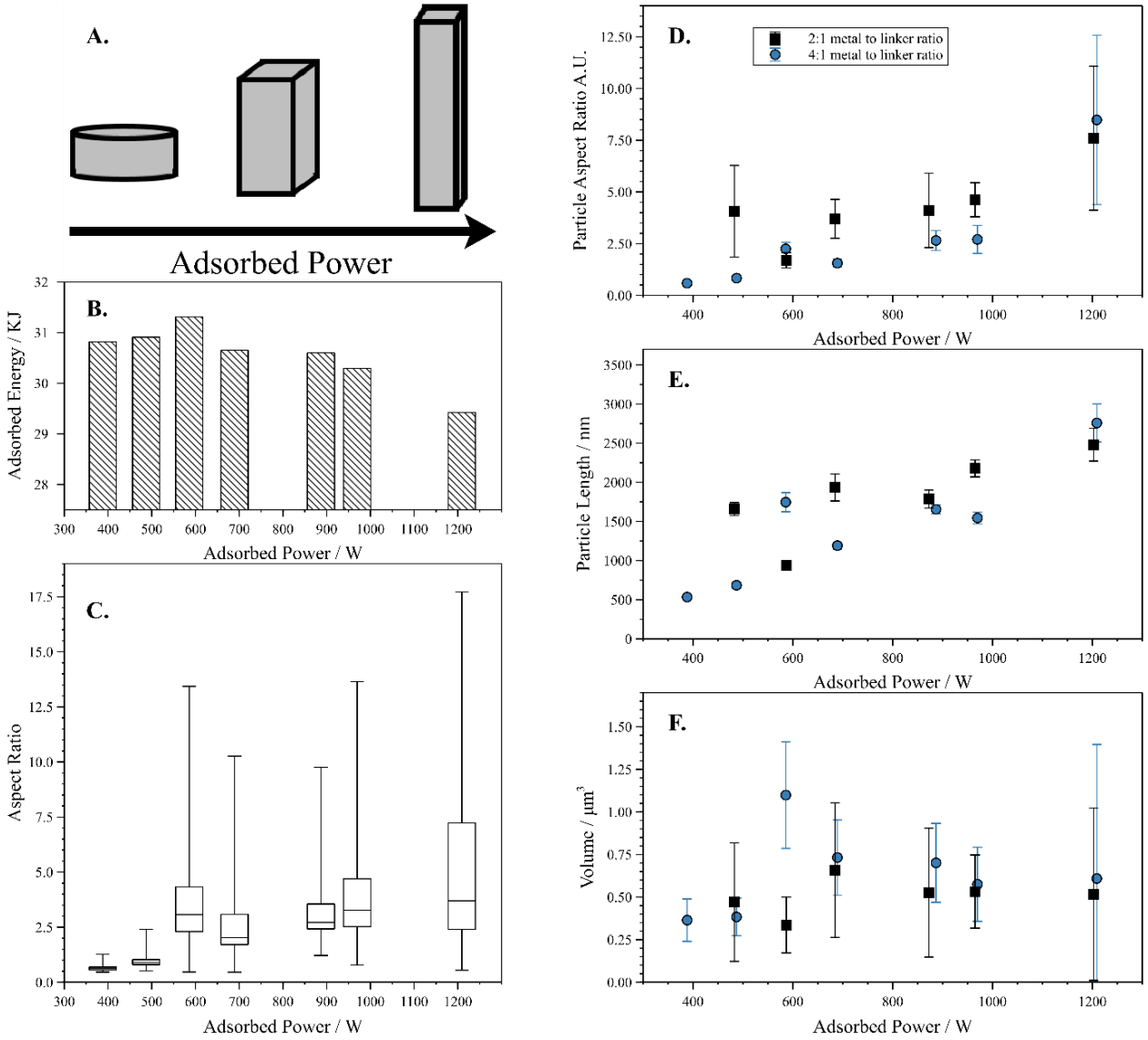


Figure 7: MOF Morphology, A. Scheme of the overall relationship between adsorbed power and the crystal morphology of the yielded MFM-300 crystals, we have defined the length of the crystal to be the unique axis around which the particle has rotational symmetry (thus the vertical length in this diagram) Aspect ratio is defined as the ratio of the length to the width. B. Total adsorbed energy by the samples for which crystal sizing was conducted (4:1 metal to linker ratio). C. Box and whisker plot of the total distribution of MFM-300 aspect ratio relative to average adsorbed power, with particle elongation apparent across the samples (4:1 metal to linker ratio). D. Particle aspect ratio, E. Particle Length and F. Particle Volumes of the longest 10% of particles in each sample relative to average adsorbed power, the elongation and thinning with increase power is apparent. However no showing no apparent correlation exists between crystal volume and adsorbed power over the power range tested. Data points around 400, 500 and 1250 W correspond to images taken from the same samples as shown in figure 2. 400 W experiments were not analysed for the 2:1 reactant ratio experiments as PXRD/TGA showed little MOF in the sample and it was not possible in SEM/EDX to reliably identify what was MOF and what was broken up linker.

In summary, when moving into a P/EC reaction we see that control over the incident microwave power (and therefore the power density in the heated phase) can facilitate control over the crystal morphology. In general, microwave based synthesis of metal-organic frameworks gives smaller crystals than those yielded from conventionally heated reactions [22, 26]. Additionally, our previous studies using P/EC reactions have shown a trend of higher powers producing smaller crystals than lower powers while at constant total delivered energy [28, 32]. However, in this work we see the contrary to this and indeed, see a direct effect on once direction of crystal growth. (Figure 3 + Figure 4 A) We propose that this preferential growth is along the *c* axis of the crystal as it is the unique axis in the tetragonal crystal lattice, and thus the unique crystallographic direction for growth. This axis lies along the aluminium oxide backbone secondary building unit of the MOF, with the other two faces of the cuboids representing equal and orthogonal crystallographic planes (we suggest the 1,1,0 plane, as this lies across the pore and would give a surface of the benzene rings of the linker).

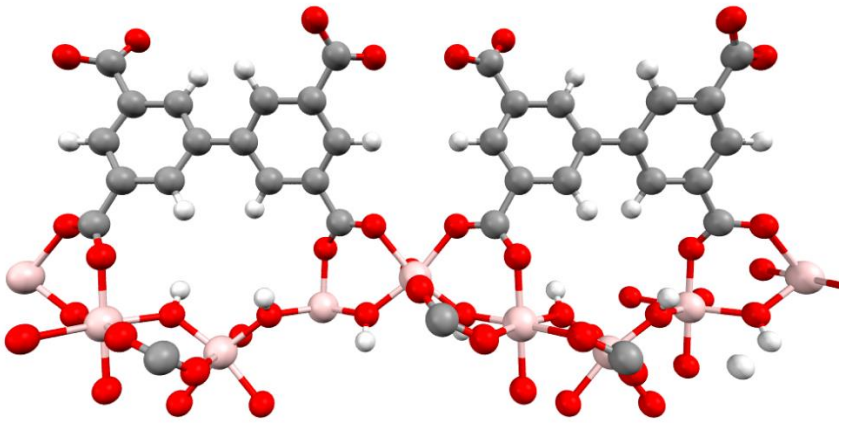


Figure 8: View of the *bc* face (down the *a* axis) of the MFM-300(Al) crystal structure with the *c* axis running along the aluminium oxide backbone SBU of the structure (left to right) we propose that MOF growth is being preferentially accelerated along this axis.

TEM and electron diffraction

To determine which direction crystal growth was being affected in (thus to support our supposition of the crystal rods to be along the *c* axis) TEM electron diffraction experiments were used. Transmission electron microscopy images of samples showed the rod-like morphology with different length/diameter ratios. (Figure 9). To identify

the crystal orientation, electron diffraction (ED) patterns were obtained along main projection. D-values were measured from ED patterns, and compared the calculated d-values from MFM-300 structure, with the results shown in Table 3. This supports the speculative crystal orientation in which the *c* axis is along the rods. Electron diffraction patterns also showed d_{002} reflections (red circle Figure 9-F), which is an expected systemic absence in the space group $I4_122$.[56] This reflection is strong in samples representing PE/C 8 and 13, and is weak (though still present) in TC 1. We attribute this to secondary diffraction, or the Renninger effect [57, 58], possibly indicating the presence of defects within the crystal structure. TGA, PXRD and LeBail refinement of these samples is included in the ESI (ESI Figure 1, 11 and 12.)

Table 3: Predicted d-spacings of select reflections from the MFM-300(Al) crystal and the measured d spacing by electron diffraction, all values in angstrom. Good agreement between the predicted and measured d-spacing supports the assignment of the crystallographic orientation which has the c-axis running along the crystal length.

Reflection	110	200	004
Calculated d-spacing	10.48	7.41	2.95
TC 1	Not Measured	7.54	2.98
PE/C 13	10.45	Not Measured	2.95
PE/C 8	10.61	Not Measured	2.99

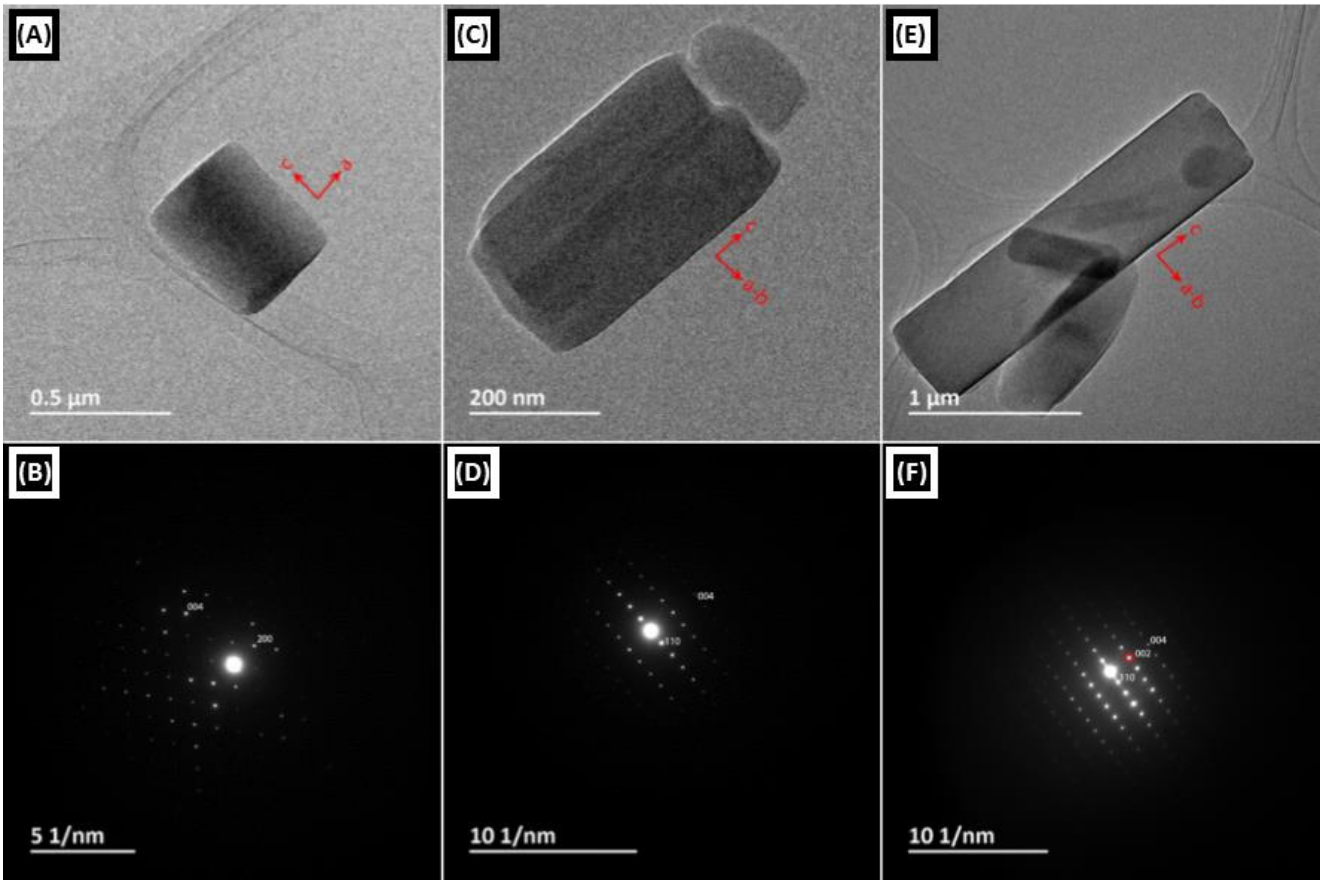


Figure 9: TEM images (Top) and corresponding electron diffraction Laue photographs (bottom) of microwave synthesised MFM-300(Al). A&B = TC 1 (viewed along the [010] axis), C&D = PE/C 13 (viewed along the [1-10] axis) and E&F = PE/C 8 (viewed along the [1-10] axis). Crystal orientation and view direction determined by electron diffraction and represented on TEM photographs. In all cases a 002 reflection is faintly present, despite being an expected systemic absence in the $I4_122$ crystal space group.[56]

Rationalisation of observed morphological control

Clearly, microwave heating is preferentially accelerating growth in one crystallographic direction. There is also the possibility of defects, indicated by the high intensity forbidden reflection in ED experiments and enhanced gas adsorption data collected in our previous study, where the uptakes of CO_2, SO_2 and NO_2 were increased above that seen from conventionally heated reaction, and the crystals were porous to nitrogen at cryogenic temperatures[44]. In that paper we did not offer an explanation for this, however the ability for N_2 to permeate into the structure notably suggests the presence of larger pores (defects), though PXRD experiments lacked evidence of long range order in these defects as seen in studies on the defects UiO-

66[32, 59]. Similar effects have been seen before, for example Chouhan et al. [34, 35] observed a similar shift in morphology induced by microwave heating, where rhombohedral crystals were synthesised from conventional systems, and long needle like particles were synthesised via microwave heating. In their case the crystal structure of their material crystallised in the triclinic P-1 space group, thus with all crystallographic directions inequivalent. However, the authors did not attempt to ascertain the direction in which crystal growth was being affected or provide a mechanistic explanation of the change. Additionally understanding of the material crystallisation is limited by reliance on a TC reactor [60].

In our case we have determined that the crystal growth is being preferentially accelerated along the *c* axis, the unique crystallographic direction. Additionally it is known that crystallisation is occurring rapidly, with the fastest reactions taking place over 25 seconds, it is also known that while sufficient energy to take the bulk temperature to 210°C the selective heating mechanism that is proposed for MW heated reactions leads to the formation of super-heated hot spots in a colder than expected bulk, with the temperature rise of the bulk reaction relying on heat transfer.

We believe that the elongate growth can be rationalised with (and provides further evidence of) the selective heating mechanism of MW MOF synthesis where in aluminium addition is accelerated due to the selective heating (of which the actual temperature is unknown) of the aluminium ion. Recently Yeung et al. [26] presented a model of MOF growth crystallisation in which growth occurs through a series of interconnected prereaction equilibria starting from solvated metal ions and growing from fragments into the 3D framework. We argue that within our system, MFM-300's unique crystallographic axis, which lies along the 1D secondary building unit, can be constructed without the need for linker-metal fragments, as the bridging hydroxides come from the solvent (Figure 10). Since the formation of the backbone does not require linker molecules rapid growth can occur in this direction, as these species are the source of the 'hotspots' which are enhanced through higher power densities. Conversely growth in any other crystallographic direction requires addition of linker, which SEM images suggests is sparingly soluble even in the superheated water (in comparison to the freely soluble aluminium ion), and the ability for this to occur will be dependent on bulk temperature as the solid linker is largely dielectrically inactive.

To summarise, the morphology can be understood as the consequence of two simultaneous reaction mechanisms in which one (the aluminium addition) is accelerated by increased temperature and reactant availability.

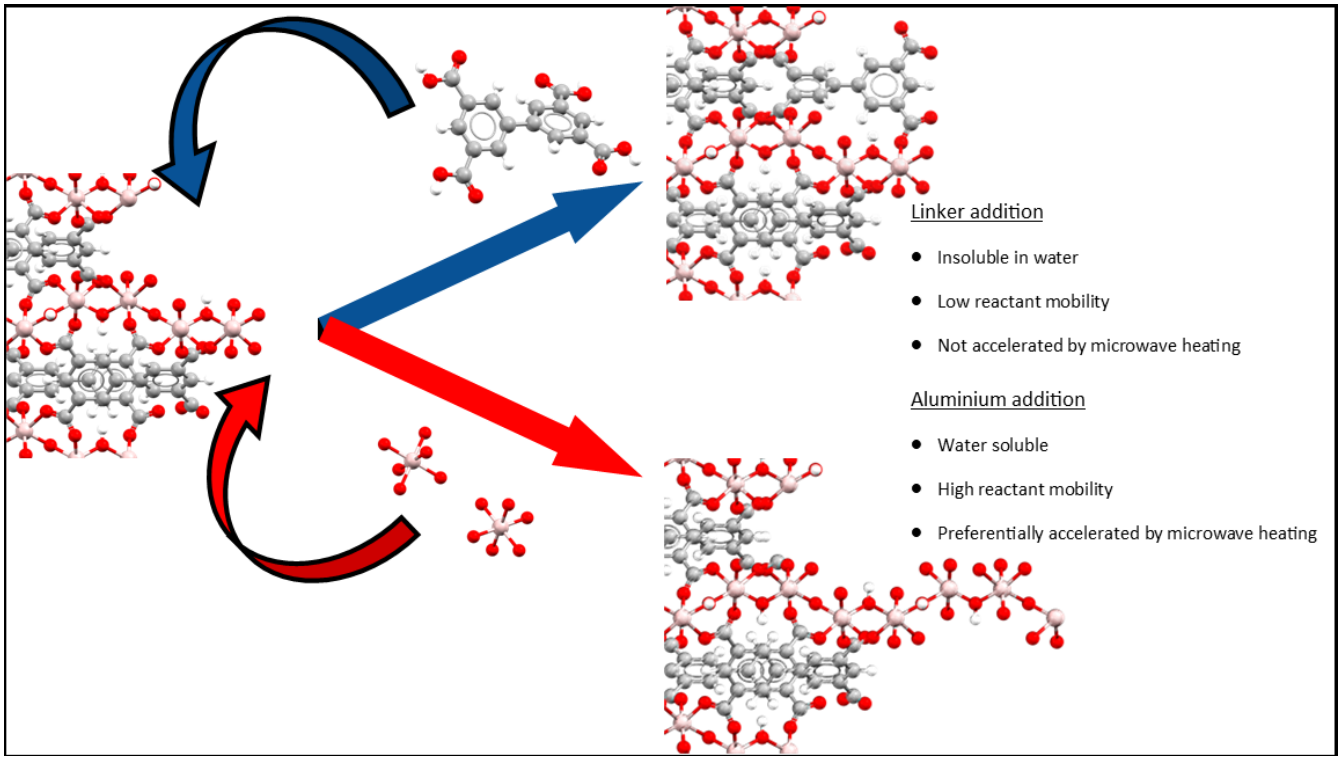


Figure 10: The elongated growth along the c-axis can be rationalised with the selective heating mechanism. Crystal images derived from CCDC entry NIRPIQ, Grey = Carbon, Red = Oxygen, Beige = Aluminium and White = Hydrogen. Solvated aluminium ions are represented as their hexaaqua complexes (not an empirically derived crystal structure)

Conclusions

The present study shows the controlled delivery of microwave energy for the synthesis of MFM-300(Al). In comparison to a thermally controlled system our reactor is able to synthesise the MOF in exceptionally short times (24.4 seconds) and with comparable yields (~60% c.f. ~80% based on linker). We have characterised the products in relation to the power adsorbed by the reaction mixture, focusing on the effect this has on the MOF morphology. It is shown that higher microwave powers appear to preferentially accelerate crystal growth in one crystallographic direction, resulting in longer and thinner crystals, and where a threshold power level exists in which the yielded MOF crystals change from cylinders to cuboids. TEM electron

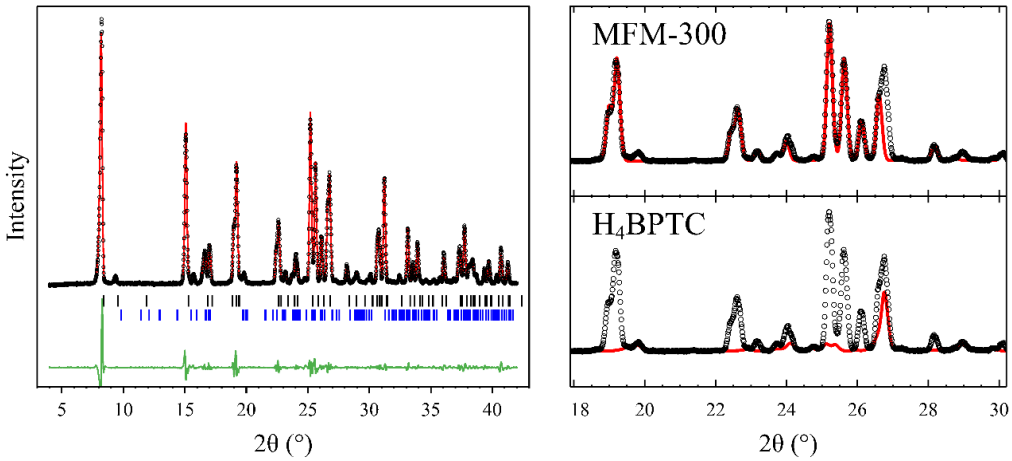
diffraction was used to confirm that this preferential growth occurred along the *c* axis (the unique crystallographic axis of the framework) along which lies the aluminium backbone secondary building unit of the MOF.

We provide a hypothetical mechanistic explanation of this phenomena with regards to the selective heating of microwave synthesis, in which metal-ion species are able to form the aluminium oxide backbone SBU without intermediate linker due to the relative availability of the two species in such short reactions and the preferential heating around the ionic species. *To the best of our knowledge this is the first time a mechanistic rationalisation of microwave heated MOF synthesis has been provided*. Exploiting and manipulating inherent aspects of MOF self-assembly can potentially offer a route to better understanding and greater control over MOF crystallisation. This tool is offered by microwave heating, however in contrasting TC and P/EC reactions we demonstrate that correct utilisation of microwave heating is important for future work on both fundamental study and practical application with regards to MOF synthesis.

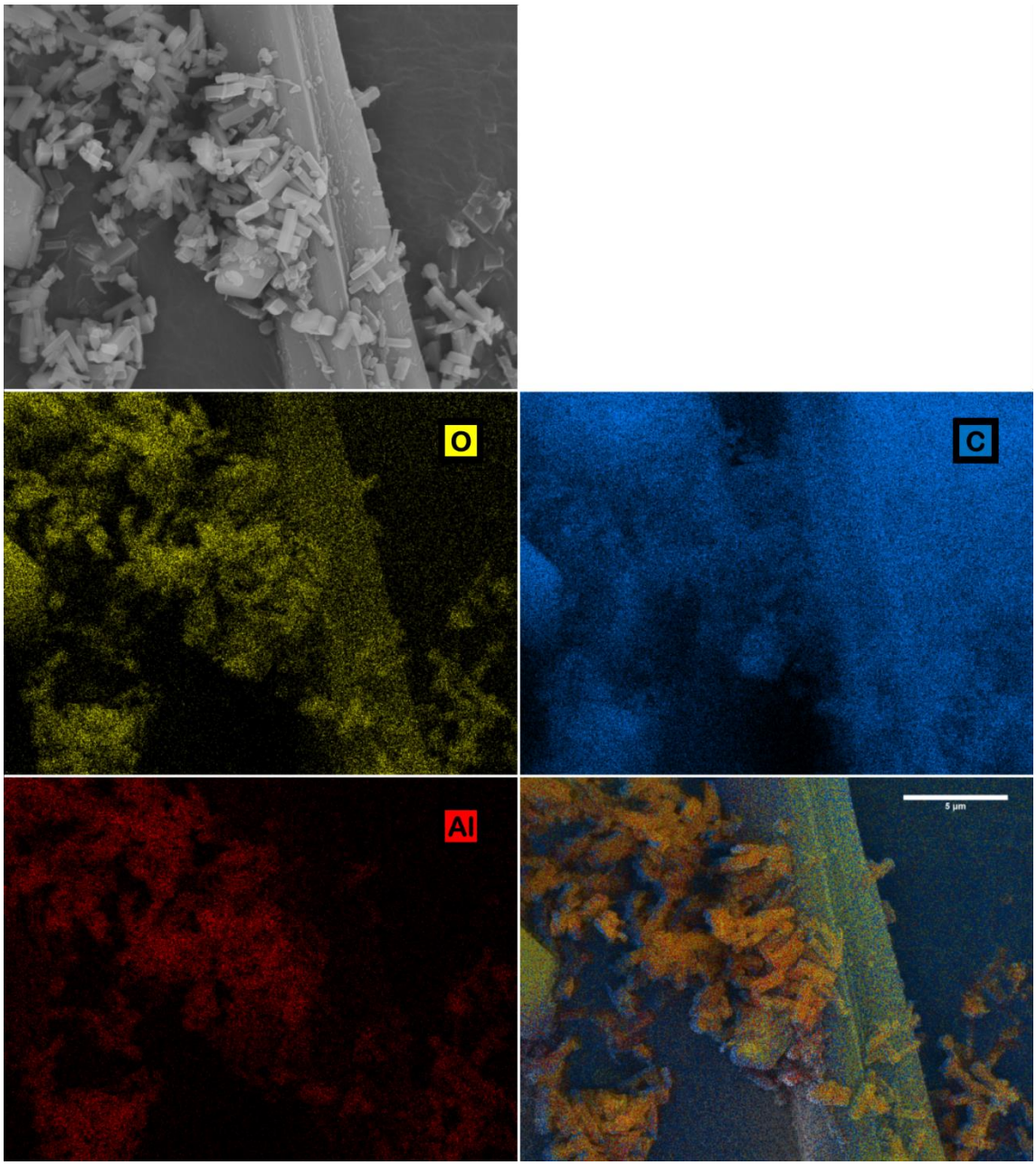
Acknowledgements

SEM analyses in this work were supported by the Engineering and Physical Sciences Research Council (EPSRC) [under grant EP/L022494/1] and the University of Nottingham.

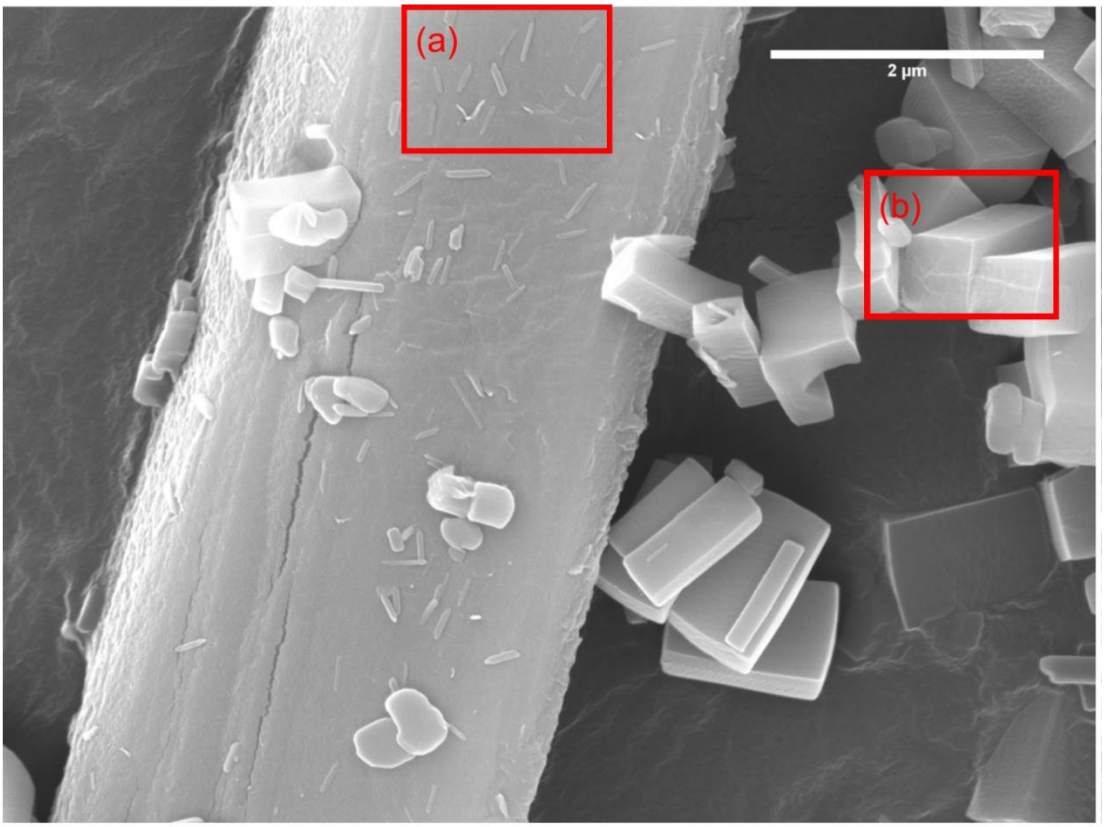
Supplementary Information



ESI Figure 1: PXRD of MFM-300 from a PE/C microwave heated reaction (sample P/EC-8), showing a simulated pattern for a 2 phase leBail refinement. Zoomed in patterns for the region 18-30°, show the contributions of the two phases; the space groups $I4_122$ (MFM-300) and $P2_1/c$ (H4BPTC) were used in the refinement, and together show a good match with the experimental pattern. Pattern from sample sent for ED analysis (Figure 6 E). Black circles = Observed intensity, Red line = Calculated intensity, Green line = $y_{obs} - y_{calc}$ Black and blue tick marks show allowed brag reflections for the MOF and Linker, respectively.

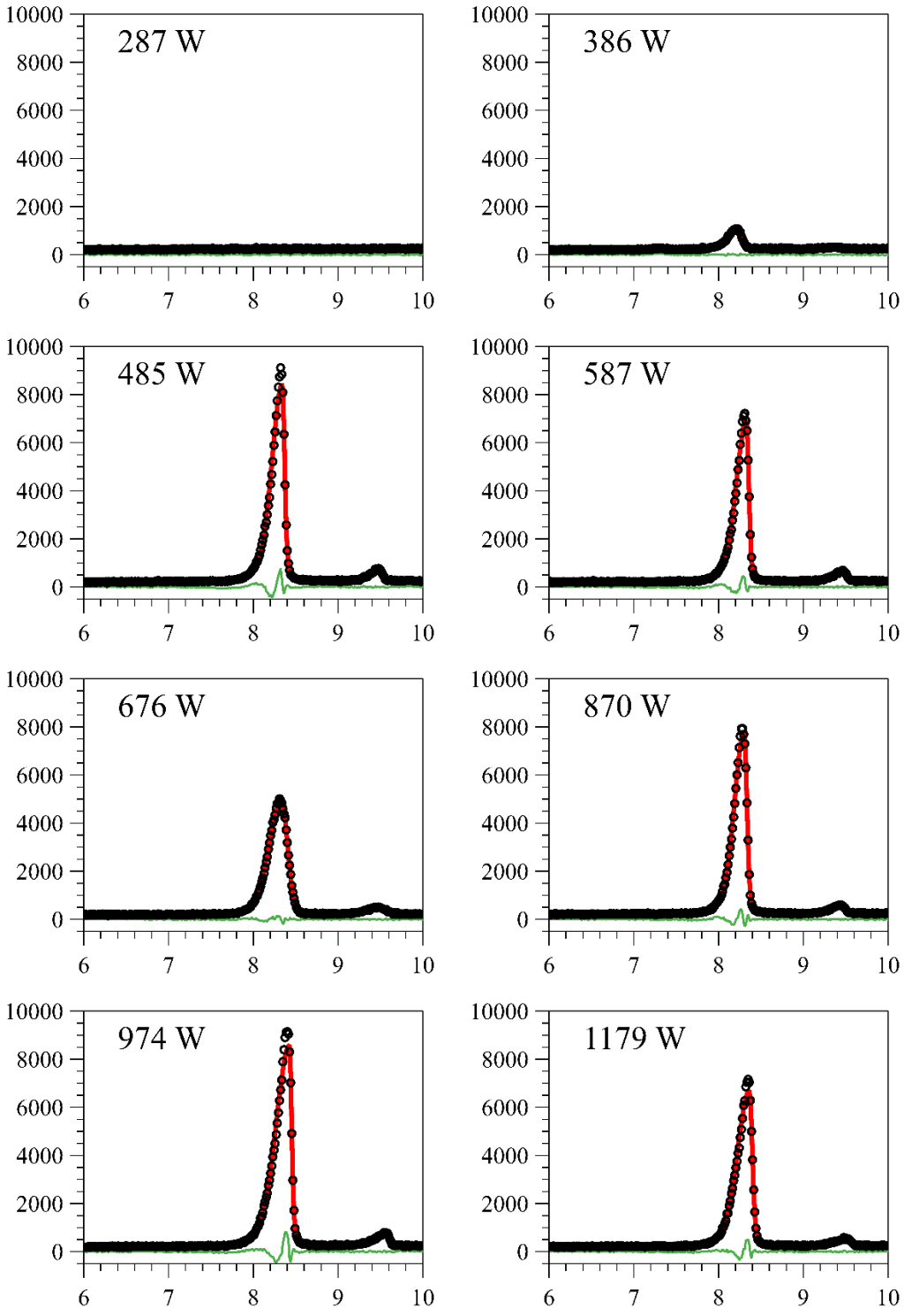


ESI Figure 2 EDX map of a P/EC-8 sample. In the Oxygen (yellow) and Carbon (blue) maps all features are visible (with the carbon map also showing a great degree of signal from the carbon adhesive tab. However Aluminium signals (red) are only featured in the smaller species, supporting the assignment of the large species as unreacted linker.

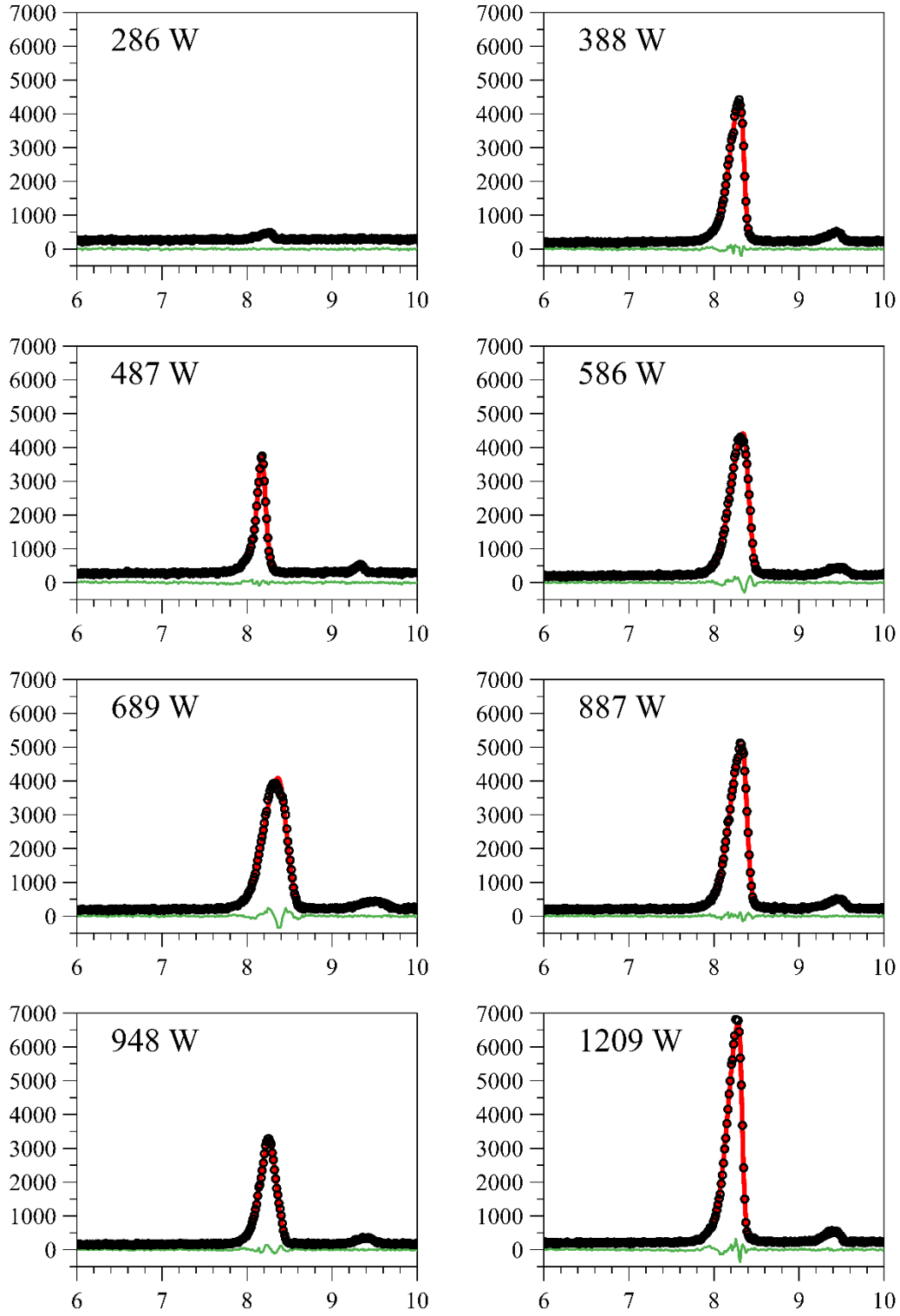


Sample Location	Elemental abundance				Identity
	Oxygen	Carbon	Aluminium	Iridium	
(a)	23.47	72.62	0.61	3.31	Linker
(b)	26.91	65.50	3.32	4.27	MOF

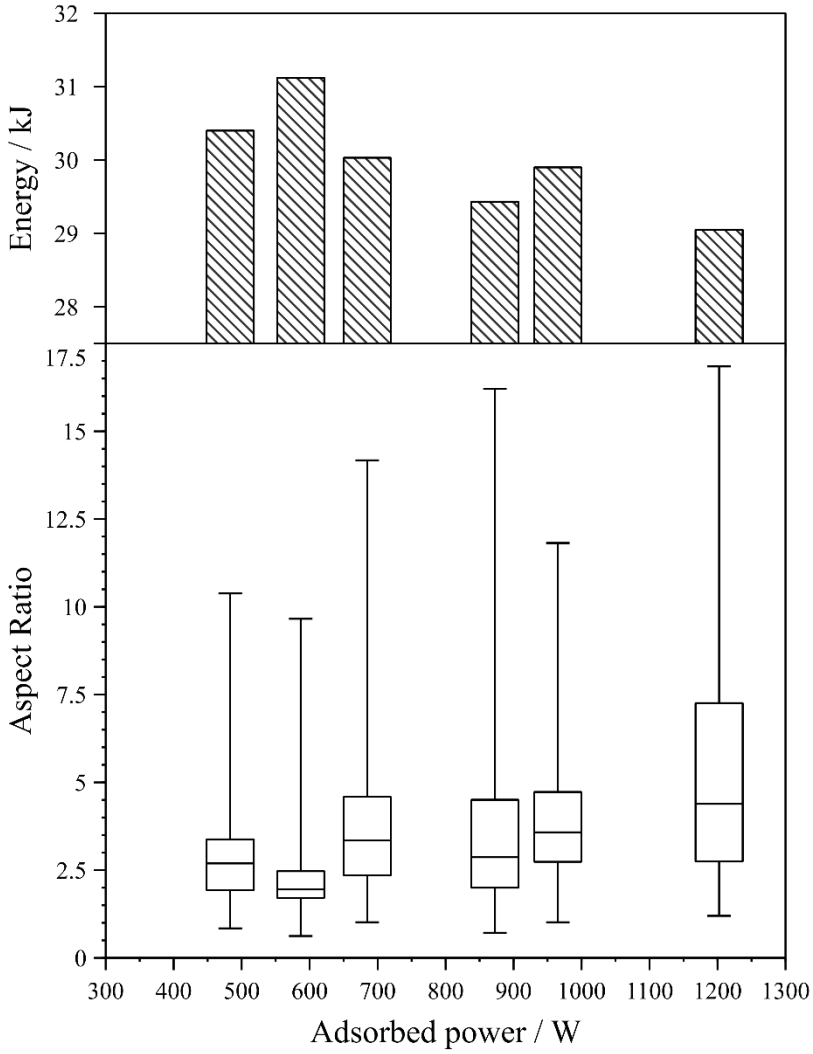
ESI Figure 3: Energy-dispersive X-ray spectroscopy experiments of P/EC-13 showing the presence of aluminium in the species we have assigned as the MOF, and a lack of aluminium in the large species we attribute to remaining linker. Boxes and labels in the image correspond to the table. Iridium presence from conductive coating is also shown.



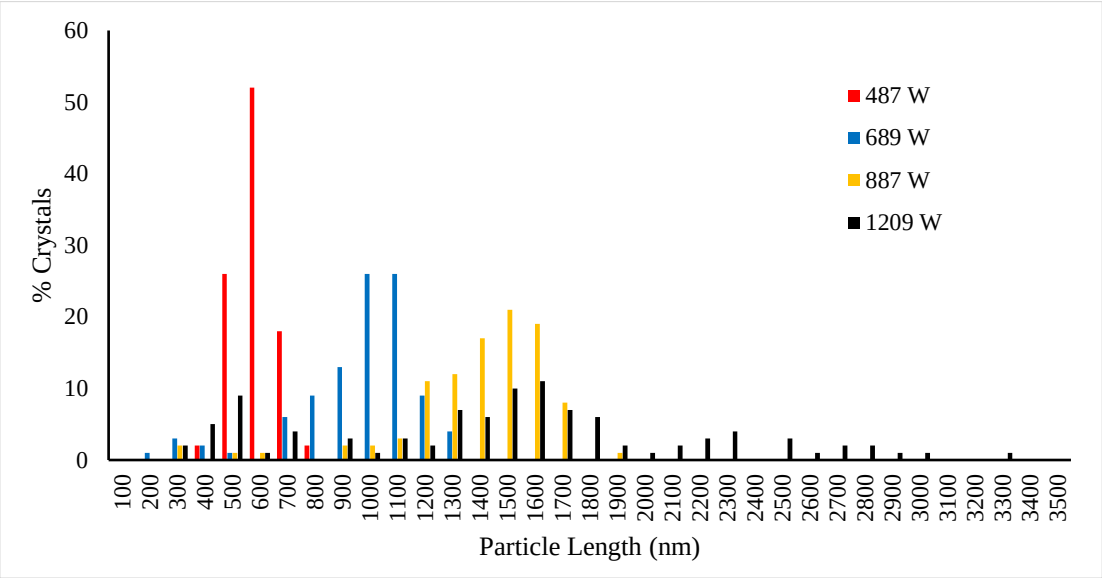
ESI Figure 4: Individual peak fits of the (1 1 0) and (1 0 1) reflections in the powder pattern of MFM-300(Al) synthesised in the P/EC reactions, with respective powers insert. Black circles, red line and green line represent observed intensity, calculated intensity and difference profile, respectively. X-axis = 2 theta angle in degrees, Y axis = intensity. The experiments correspond to representative samples of P/EC-1 to 8.



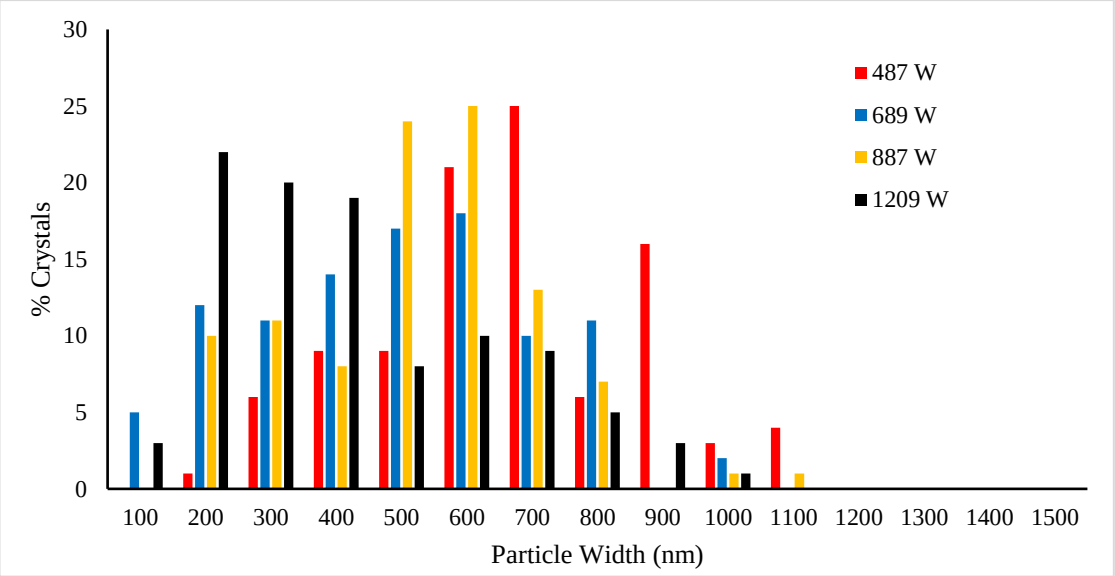
ESI Figure 5: Individual peak fits of the (1 1 0) and (1 0 1) reflections in the powder pattern of MFM-300(Al) synthesised in the P/EC reactions, with respective powers insert. Black circles, red line and green line represent observed intensity, calculated intensity, and difference profile, respectively. X-axis = 2 theta angle in degrees, Y axis = intensity. The experiments correspond to representative samples of P/EC-9 to 16.



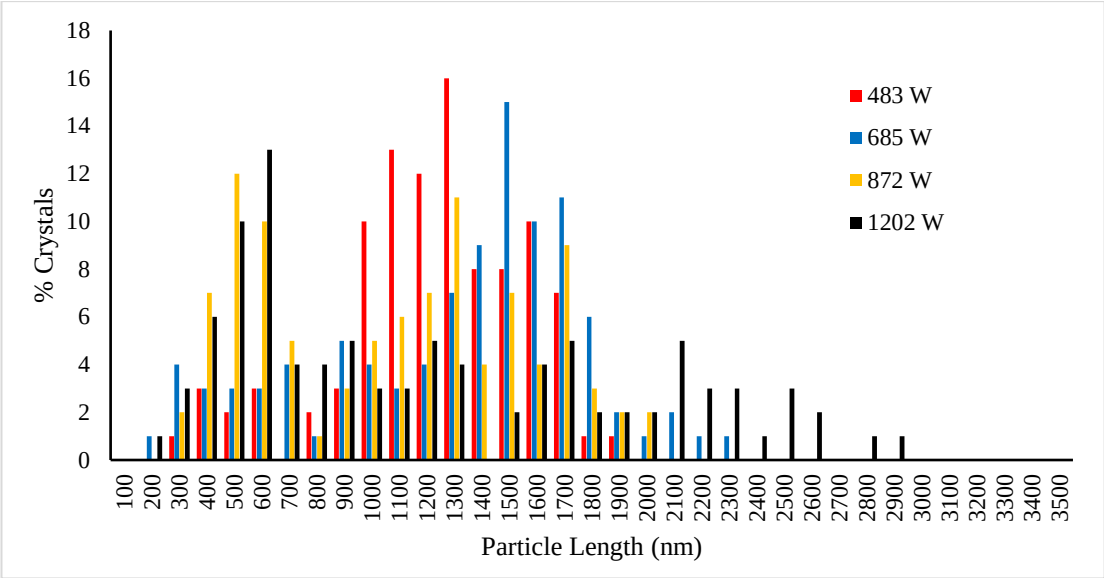
ESI Figure 6: Data of particle aspect ratio and energy for the 2:1 reactant ratio experiments. Top: total energy adsorbed by the samples for which sizing was conducted. Bottom: Box and whisker plot of the total distribution of MFM-300 aspect ratio relative to nominal forward power, with particle elongation apparent across the full samples. The trend of elongation is less apparent than in the 4:1 reactant ratio experiments.



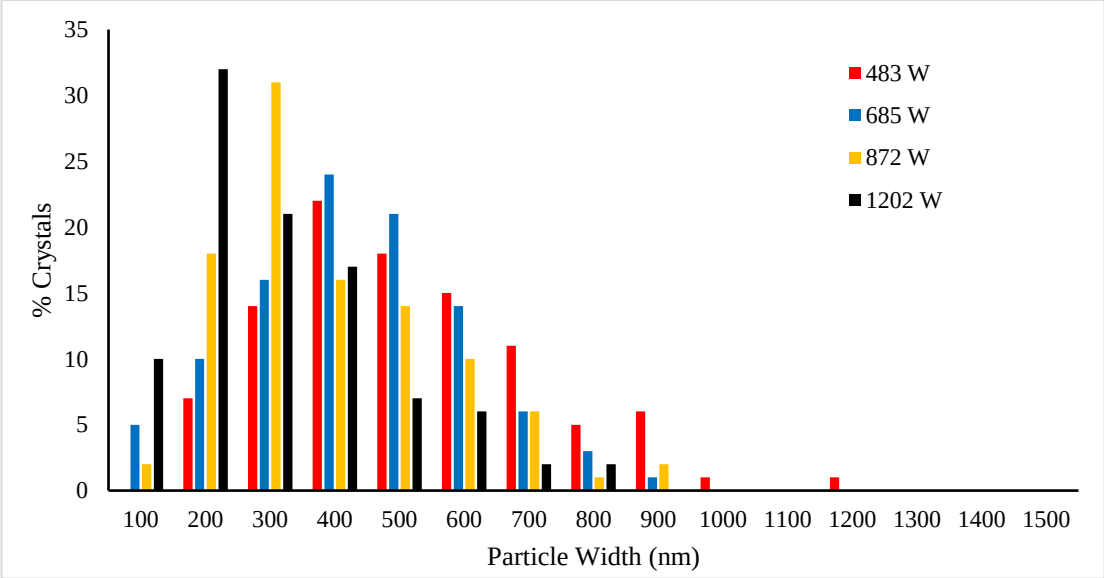
ESI Figure 7: Histogram plot of the lengths of MFM-300 crystals at select powers at a 4-1 reaction ratio (Legend insert). Values rounded to the nearest 100 nm.



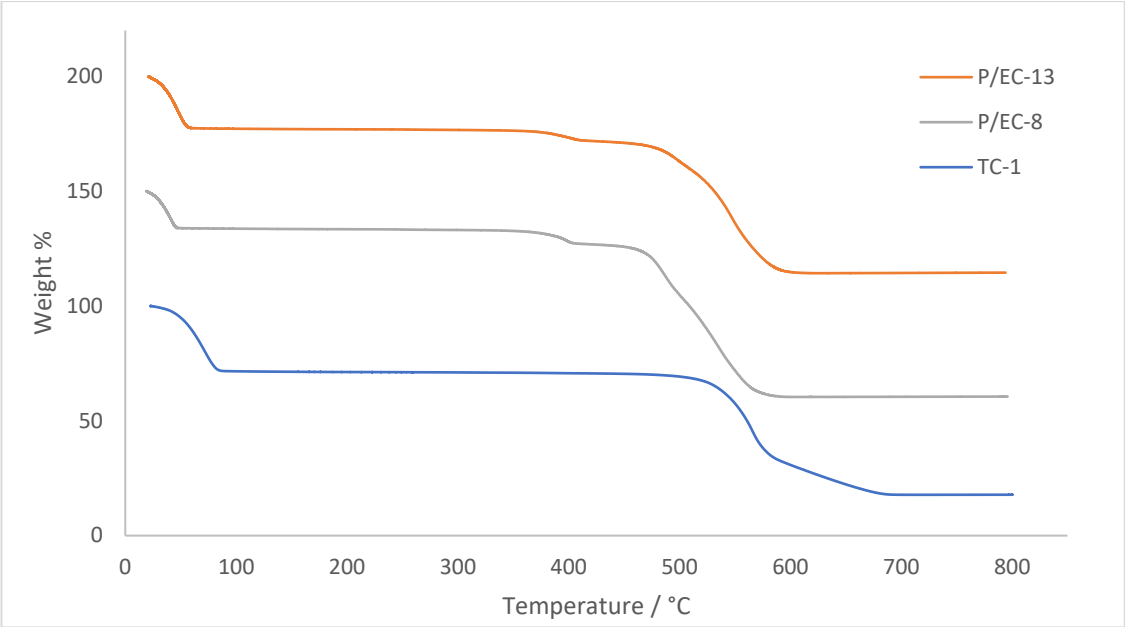
ESI Figure 8: Histogram plot of the widths of MFM-300 crystals at select powers at a 4-1 reaction ratio (Legend insert). Values rounded to the nearest 100 nm.



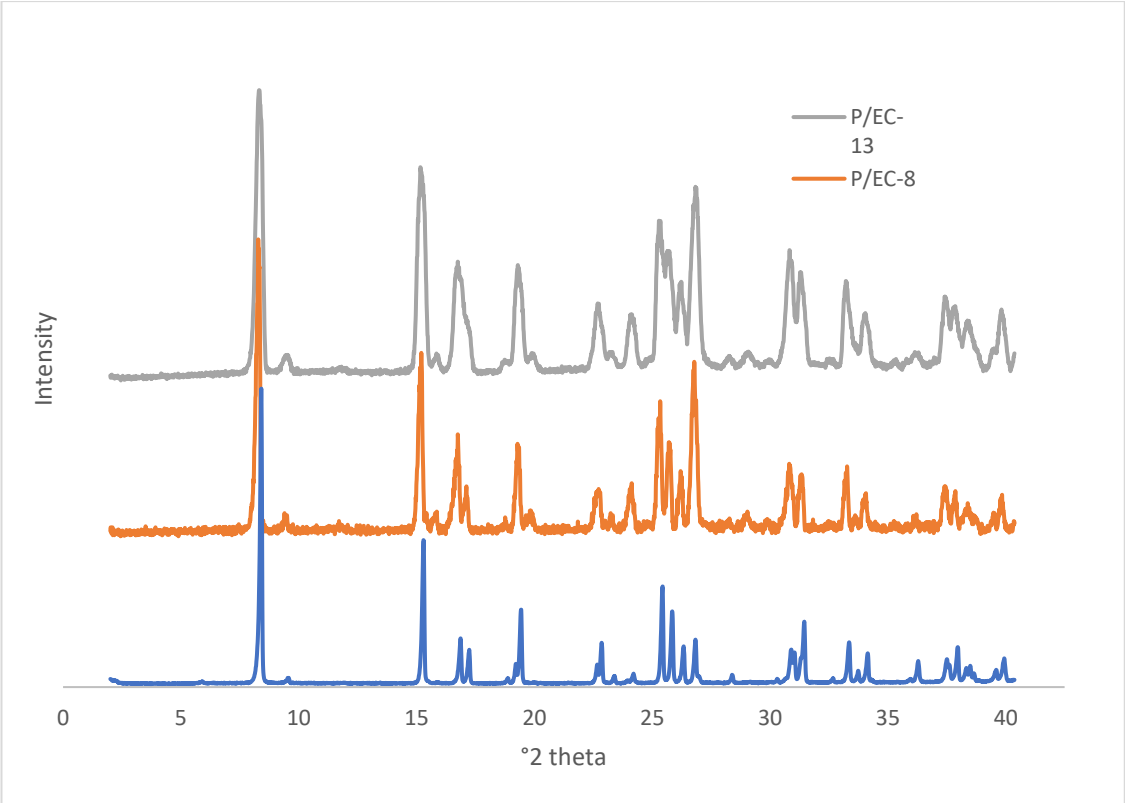
ESI Figure 9: Histogram plot of the lengths of MFM-300 crystals at select powers at a 2-1 reaction ratio (Legend insert). Values rounded to the nearest 100 nm.



ESI Figure 10: Histogram plot of the widths of MFM-300 crystals at select powers at a 2-1 reaction ratio (Legend insert). Values rounded to the nearest 100 nm.



ESI Figure 11: TGA thermograms of MFM-300(Al) samples used in ED experiments. Staggered by 50 weight % for clarity.



ESI Figure 12: PXRD diffractograms of MFM-300(Al) samples used in ED experiments.

References

1. Kuppler, R.J., et al., *Potential applications of metal-organic frameworks.* Coordination Chemistry Reviews, 2009. **253**(23): p. 3042-3066.

2. Li, J.-R., R.J. Kuppler, and H.-C. Zhou, *Selective gas adsorption and separation in metal–organic frameworks.* Chemical Society Reviews, 2009. **38**(5): p. 1477-1504.

3. Li, W., et al., *Metal−organic framework composite membranes: Synthesis and separation applications*. Chemical Engineering Science, 2015. **135**: p. 232-257.

4. Silva, P., et al., *Multifunctional metal–organic frameworks: from academia to industrial applications*. Chemical Society Reviews, 2015. **44**(19): p. 6774-6803.

5. Czaja, A.U., N. Trukhan, and U. Müller, *Industrial applications of metal–organic frameworks.* Chemical Society Reviews, 2009. **38**(5): p. 1284-1293.

6. Dhakshinamoorthy, A., M. Alvaro, and H. Garcia, *Commercial metal–organic frameworks as heterogeneous catalysts.* Chemical Communications, 2012. **48**(92): p. 11275-11288.

7. Lee, J., et al., *Metal–organic framework materials as catalysts.* Chemical Society Reviews, 2009. **38**(5): p. 1450-1459.

8. Cui, Y., et al., *Metal–Organic Frameworks as Platforms for Functional Materials.* Accounts of Chemical Research, 2016. **49**(3): p. 483-493.

9. Ma, Z. and B. Moulton, *Recent advances of discrete coordination complexes and coordination polymers in drug delivery*. Coordination Chemistry Reviews, 2011. **255**(15): p. 1623-1641.

10. Haque, E., et al., *Facile Purification of Porous Metal Terephthalates with Ultrasonic Treatment in the Presence of Amides.* Chemistry – A European Journal, 2009. **15**(43): p. 11730-11736.

11. Wu, C.-D., et al., *A Homochiral Porous Metal−Organic Framework for Highly Enantioselective Heterogeneous Asymmetric Catalysis*. Journal of the American Chemical Society, 2005. **127**(25): p. 8940-8941.

12. A. Flügel, E., et al., *Synthetic routes toward MOF nanomorphologies.* Journal of Materials Chemistry, 2012. **22**(20): p. 10119-10133.

13. Pan, Y., et al., *Tuning the crystal morphology and size of zeolitic imidazolate framework-8 in aqueous solution by surfactants*. CrystEngComm, 2011. **13**(23): p. 6937-6940.

14. Rieter, W.J., et al., *Nanoscale Metal−Organic Frameworks as Potential Multimodal Contrast Enhancing Agents.* Journal of the American Chemical Society, 2006. **128**(28): p. 9024-9025.

15. Taylor, K.M.L., W.J. Rieter, and W. Lin, *Manganese-Based Nanoscale Metal−Organic Frameworks for Magnetic Resonance Imaging.* Journal of the American Chemical Society, 2008. **130**(44): p. 14358-14359.

16. Marshall, R.J., et al., *Amino acids as highly efficient modulators for single crystals of zirconium and hafnium metal–organic frameworks*. Journal of Materials Chemistry A, 2016. **4**(18): p. 6955-6963.

17. Wang, F., et al., *The controlled regulation of morphology and size of HKUST-1 by "coordination modulation method".* Microporous and Mesoporous Materials, 2013. **173**: p. 181-188.

18. Griffin, S.L., C. Wilson, and R.S. Forgan, *Uncovering the Structural Diversity of Y(III) Naphthalene-2,6-Dicarboxylate MOFs Through Coordination Modulation*. Frontiers in Chemistry, 2019. **7**:36

19. Cai, G., et al., *Template-Directed Growth of Well-Aligned MOF Arrays and Derived Self-Supporting Electrodes for Water Splitting*. Chem, 2017. **2**(6): p. 791-802.

20. Jahan, M., et al., *Structure-Directing Role of Graphene in the Synthesis of Metal−Organic Framework Nanowire.* Journal of the American Chemical Society, 2010. **132**(41): p. 14487-14495.

21. Rad, M. and S. Dehghanpour, *ZnO as an efficient nucleating agent and morphology template for rapid, facile and scalable synthesis of MOF-46 and ZnO@MOF-46 with selective sensing properties and enhanced photocatalytic ability*. RSC Advances, 2016. **6**(66): p. 61784-61793.

22. Ameloot, R., et al., *Direct Patterning of Oriented Metal–Organic Framework Crystals via Control over Crystallization Kinetics in Clear Precursor Solutions*. Advanced Materials, 2010. **22**(24): p. 2685-2688.

23. Sorrenti, A., et al., *Growing and Shaping Metal–Organic Framework Single Crystals at the Millimeter Scale*. Journal of the American Chemical Society, 2020. 142, 20, 9372–9381

24. Li, H., et al., *Crystal-Growth-Dominated Fabrication of Metal–Organic Frameworks with Orderly Distributed Hierarchical Porosity.* Angewandte Chemie International Edition, 2020. **59**(6): p. 2457-2464.

25. Marshall, C.R., S. Staudhammer, and C. Brozek, *Experimental Evidence for a General Model of Modulated MOF Nanoparticle Growth*. Chemical Science, 2020, **11**, 11539-11547

26. Yeung, H.H.M., et al., *Control of Metal–Organic Framework Crystallization by Metastable Intermediate Pre-equilibrium Species.* Angewandte Chemie International Edition, 2019. **58**(2): p. 566-571.

27. Cho, W., S. Park, and M. Oh, *Coordination polymer nanorods of Fe-MIL-88B and their utilization for selective preparation of hematite and magnetite nanorods.* Chemical Communications, 2011. **47**(14): p. 4138-4140.

28. Lee, G., et al., *Tip-To-Middle Anisotropic MOF-On-MOF Growth with a Structural Adjustment.* Journal of the American Chemical Society, 2020. **142**, 6, 3042–3049

29. Wu, H., et al., *Unusual and Highly Tunable Missing-Linker Defects in Zirconium Metal–Organic Framework UiO-66 and Their Important Effects on Gas Adsorption. Journal of the American Chemical Society*, 2013. **135**(28): p. 10525-10532.

30. Gutov, O.V., et al., *Metal–Organic Framework (MOF) Defects under Control: Insights into the Missing Linker Sites and Their Implication in the Reactivity of Zirconium-Based Frameworks. Inorganic Chemistry*, 2015. **54**(17): p. 8396-8400.

31. Valvekens, P., F. Vermoortele, and D.D. Vos, *Metal–organic frameworks as catalysts : the role of metal active sites.* Catalysis Science & Technology, 2013. **3**(6): p. 1435-1445.

32. Shearer, G.C., et al., *Defect Engineering: Tuning the Porosity and Composition of the Metal–Organic Framework UiO-66 via Modulated Synthesis*. Chemistry of Materials, 2016. **28**(11): p. 3749-3761.

33. Thomas-Hillman, I., et al., *Realising the environmental benefits of metal–organic frameworks: recent advances in microwave synthesis*. Journal of Materials Chemistry A, 2018. **6**: p. 11564-11581.

34. Chouhan, A., P. Mayer, and A. Pandey, *A comparative study of the morphologies and photocatalytic performances of bis[5-(2-pyridyltetrazolato)]diaquazinc(II) framework synthesized by hydrothermal and microwave methods*. Indian Journal of Chemistry, 2015: **54A** , 851 —857

35. Chouhan, A., et al., *Shape Controllable Preparation of Submicronic Cadmium Tetrazole-Based Metal–Organic Frameworks via Solvothermal or Microwave-Assisted Methods and Their Photocatalytic Studies.* Chinese Journal of Chemistry, 2017. **35**(2): p. 209-216.

36. Lou, Y., et al., *Rapid synthesis of iron 1,4-naphthalenedicarboxylate by microwave irradiation with enhanced gas sorption*. Dalton Transactions, 2013. **43**(3): p. 1261-1266.

37. Klinowski, J., et al., *Microwave-Assisted Synthesis of Metal–Organic Frameworks.* Dalton Transactions., 2011. **40**(2): p. 321-330.

38. Khan, N.A. and S.H. Jhung, *Synthesis of metal-organic frameworks (MOFs) with microwave or ultrasound: Rapid reaction, phase-selectivity, and size reduction*. Coordination Chemistry Reviews, 2015. **285**: p. 11-23.

39. Laybourn, A., et al., *Metal-organic frameworks in seconds via selective microwave heating.* Journal of Materials Chemistry A, 2017. **5**(16): p. 7333-7338.

40. Robinson, J., et al., *Understanding microwave heating effects in single mode type cavities—theory and experiment.* Physical Chemistry Chemical Physics, 2010. **12**(18): p. 4750-4758.

41. Meredith, R.J., *Engineers' handbook of industrial microwave heating*. 1998, UK: IET.

42. Metaxas, A.C. and R.J. Meredith, *Industrial Microwave Heating*. 1983: IET. 380.

43. Laybourn, A., et al., *Combining continuous flow oscillatory baffled reactors and microwave heating: Process intensification and accelerated synthesis of metal-organic frameworks.* Chemical Engineering Journal, 2019. **356**: p. 170-177.

44. Thomas-Hillman, I., et al., *Developing a sustainable route to environmentally relevant metal-organic frameworks: ultra-rapid synthesis of MFM-300(Al) using microwave heating*. Green Chemistry, 2019. **21**(18). 5039-5045

45. Han, X. et al. *Reversible adsorption of nitrogen dioxide within a robust porous metal–organic framework.* Nature Materials, 2018. **17**(8): p. 691-696.

46. Yang, S., et al., *Selectivity and direct visualization of carbon dioxide and sulfur dioxide in a decorated porous host*. Nature Chemistry, 2012. **4**: p. 887-894.

47. Engen, G.F., *A (historical) review of the six-port measurement technique.* IEEE Transactions on Microwave Theory and Techniques, 1997. **45**(12): p. 2414-2417.

48. Schneider, C.A., W.S. Rasband, and K.W. Eliceiri, *NIH Image to ImageJ: 25 years of image analysis.* Nature Methods, 2012. **9**(7): p. 671-675.

49. PowDLL, a reusable .NET component for interconverting powder diffraction data: Recent developments, N. Kourkoumelis, ICDD Annual Spring Meetings (ed. Lisa O'Neill), Powder Diffraction, 28 (2013) 137-48.

50. Coelho, A.A., TOPAS and TOPAS-Academic: an optimization program integrating computer algebra and crystallographic objects written in C++. Journal of Applied Crystallography, 2018. **51**(1): p. 210-218.

51. Groom, C.R., et al., *The Cambridge Structural Database.* Acta Cryst., 2016. **B72**: p. 171-179.

52. Bokhimi, X., et al., Dependence of Boehmite Thermal Evolution on Its Atom Bond Lengths and Crystallite Size. Journal of Solid State Chemistry, 2001. **161**(2): p. 319-326.

53. Vallance, S.R., S. Kingman, and D.H. Gregory, *Ultrarapid Materials Processing: Synthesis of Tungsten Carbide on Subminute Timescales.* Advanced Materials, 2007. **19**(1): p. 138-142.

54. Whittles, D.N., S.W. Kingman, and D.J. Reddish, *Application of numerical modelling for prediction of the influence of power density on microwave-assisted breakage.* International Journal of Mineral Processing, 2003. **68**(1): p. 71-91.

55. Le Bail, A., H. Duroy, and J.L. Fourquet, *Ab-initio structure determination of LiSbWO6 by X-ray powder diffraction.* Materials Research Bulletin, 1988. **23**(3): p. 447-452.

56. International Tables for Crystallography Volume A: Space-group symmetry. 2nd ed. 2016.

57. Renninger, M., *"Umweganregung", eine bisher unbeachtete Wechselwirkungserscheinung bei Raumgitterinterferenzen.* Zeitschrift für Physik, 1937. **106**(3): p. 141-176.

58. Kambe, K., *Study of Simultaneous Reflexion in Electron Diffraction by Crystals I. Theoretical Treatment*. Journal of the Physical Society of Japan, 1957. **12**(1): p. 13-25.

59. Cliffe, M.J., et al., *Correlated defect nanoregions in a metal–organic framework.* Nature Communications, 2014. **5**(1): p. 4176.

60. Li, H., et al., *Nucleation–Elongation Dynamics of Two-Dimensional Covalent Organic Frameworks.* Journal of the American Chemical Society, 2020, **142**, 3, 1367–1374

Appendix 4: Basic removal of residual linker from metal organic framework synthesis

Ieuan Thomas-Hillman, Lee Stevens, Chris Dodds, Sam Kingman, Andrea Laybourn

Faculty of Engineering, University of Nottingham, Nottingham, UK

Manuscript prepared for publication awaiting submission.

Statement of contribution of joint authorship

Ieuan Thomas-Hillman conducted laboratory experiments synthesising MFM-300(Al), performing purification experiments and performed SEM, PXRD and TGA analysis of the samples. Lee Stevens conducted CO_2 and N_2 gas adsorption experiments and Ieuan Thomas-Hillman performed BET, PSD analysis and interpretation. Andrea Laybourn, Chris Dodds and Samuel Kingman provided overall experimental supervision. All authors were consulted in proof-reading and critically commented on the manuscript.

Abstract

The facile purification of MFM-300(Al) using ammonium hydroxide solution is presented. In MOF syntheses that terminate with large amounts of unreacted linker a purification method to obtain MOF is essential in maximising the properties of the bulk material. Our method results in rapid MOF purification at room temperature and with easy reclamation of unreacted linker for further synthesis. The purification method used causes no damage to the MOF material, and is compared to using the 'hard' base sodium hydroxide, which results in digestion of the MOF crystals.

Introduction

Metal-organic frameworks are a large class of porous materials constructed from metal nodes and organic linkers [1-4]. A common subset of these is constructed from carboxylic acid linkers, which can cause purity problems post synthesis as even small (based on a single benzene ring) carboxylic acids are often exceptionally insoluble. At an industrial scale, the use of hazardous solvents or calcination to purify product leads

to high energy and environmental costs, if such methods are even possible considering linkers which are neither soluble or calcinable. For example, MFM-300(Al), for which we recently developed a rapid synthetic method [5] is a MOF with a potential applications in the capture of environmentally polluting dioxides (CO_2, SO_2 & NO_2) however the linker in MFM-300(Al) (biphenyl-3,3',5,5'-tetracarboxylic acid, H_4BPTC) is insoluble in alcohols and DMF, and cannot be separated from the MOF by calcination. With the continual drive within the chemical industry for environmentally benign synthesis methods [6, 7], purification methods should similarly be developed to be as green as possible. For gram scale synthesis a method of removing gram amounts of linker is required, both allowing for MOF purification and reclamation and reuse of potentially valuable and difficult to synthesises feedstocks, important developments in the realisation of sustainable production of these materials. Additionally, such a purification method would best be versatile, not requiring excessively precise procedures in order to successfully purify the material as the quantity of linker and framework in a bulk powder may be difficult to precisely determine, therefore a method which requires high precision is impractical.

A possible alternative to solvent washing is removing the linkers with alkaline solutions. Haque et al. [8] previously discussed purification of MOFs using base and found that 5% ammonia hydroxide solution was capable of digesting the MOF MIL-53(Al), therefore leading to a recommendation of activation of MOFs with DMF. For MFM-300(Al), DMF is highly impractical, as the H_4BPTC linker is sparingly soluble even at elevated temperatures, and so cause is given to reinvestigate ammonium hydroxide solution washing, which is able to dissolve the linker, H_4BPTC, rapidly in a <4 molar equivalent quantity of an ammonia solution. In the interests of maintaining as economical a method as possible sodium hydroxide is also a possibility.

Experimental:

Synthesis of MFM-300(Al).

MFM-300 was synthesised in a series of batch reactions based on a modified version of our previously reported method [7]. Aluminium trichloride hexahydrate (250 mg, 1.04 mmol), H_4BPTC (85 mg, 0.258 mmol) and deionised water (15 ml) were placed

in a glass vial and heated to 210 °C in a CEM discover microwave reactor for 10 minutes (maximum forward power 300 W, maximum allowed pressure 20 bar). Following a compressed air cool, the product was transferred to a centrifuge tube and diluted with deionised water, centrifuged, and then decanted and washed with deionised water (with 2 x centrifugations and 2 x washing). Average yield 135 mg, 88.5% for the dehydrated MOF, *i.e.* $[Al_2(OH)_2(C_{16}O_8H_6)]$, calculated based on the linker and TGA analyses).

Ammonia, NaOH, washing experiments

As synthesised MFM-300(Al) (39 mg) and H_4BPTC linker (40 mg) were added to a 50 mL centrifuge tube (all masses ± 1 mg) to which was added a quantity of ammonia solution (0.2M / 0.5M or 1 M) corresponding to a desired excess of base to linker (it was determined by titration that a 4:1 ratio of base to linker was required for solvation, indicating all 4 carboxylic acids need to react to pull the aromatic components into aqueous solution). The solutions were shaken manually for 15 minutes then transferred to a centrifuge and centrifuged (4200 RPM, 15 °C) for 30 minutes. The supernatant liquid was decanted and the remaining solid washed once with deionised water (20 mL). The solid was then dried in an oven (50 °C) over night and allowed to rehydrate in a fume hood for one day before being collected. All experiments conducted at room temperature (approx. 15°C).

Molar equivalent of base – relative to free linker	Volume of alkaline solution added (cm^3)			
	Ammonium hydroxide			NaOH
	0.2 M	0.5 M	1 M	0.2 M
4	2.4	/	/	2.4
4.8	2.9	/	/	2.9
5.6	3.4	/	/	3.4
6.4	3.9	/	/	3.9
8	4.8†	1.9	/	4.8
10	6.0	2.4	1.2	6.0
12	7.2	2.9	1.5	7.2
16	9.7	3.9	1.9	9.7
40	24.2	9.7	4.8	24.2

Table 1: Table of experiments: All samples contained MFM-300(Al) (39 ± 1 mg, 0.067 mmol) and H_4BPTC linker (40 ± 1 mg, 0.12 mmol). The volume of alkaline solution added to each sample was determined by the desired molar equivalence of basic species and the molar concentration of the solution. Volumes accurate to 0.1 cm^3. †Experiment carried forward for linker reclamation and reuse experiment.

Linker reclamation

MFM-300(Al) (114 mg) and H_4BPTC (117 mg) were combined in a centrifuge tube and then mixed with a 2 fold molar excess of ammonia solution (0.2 M, 14.2 ml) as a scaled up version of the experiment marked in table 1† After centrifugation the supernatant liquid, containing linker and ammonia, was collected and acidified to pH 4 using HCl (37%) and additional distilled water to precipitate the H_4BPTC linker. This linker slurry was then centrifuged and washed twice with distilled water to remove ammonium chloride before being dried in an oven (115 mg, 98.3%). This linker was then used to synthesis MFM-300 as per the established synthetic technique.

PXRD

Powder X-ray diffraction experiments were performed on a Bruker D8 Advance Da Vinci diffractometer with a CuKα X-ray source, LYNXEYE XE-T high energy

resolution 1D x-ray detector. Patterns were collected between 5 and 50° 2 theta with a step size of 0.010°. Patterns were analysed with the TOPAS academic software (version 6) [15].

TGA

Thermogravimetric analysis was performed on a TA instruments Discovery TGA 550. Samples were heated to 800 °C with a ramp rate of 5°C/min under a compressed air flow. Data were analysed in TRIOS v5 and plotted in Veusz 3.2 [16].

Scanning electron microscopy

High-resolution SEM images of MFM-300(Al) were collected using a JEOL 7100F FEG-scanning electron microscope. Samples were prepared on machined aluminium stubs with carbon adhesive tabs. The samples were coated with a 10 nm layer of iridium using a Quorum QISOT ES coater. Imaging was conducted at a working distance of 10 mm with an electron gun accelerating potential of 15 kV. Frame captures of the sample morphologies were obtained using Jeol PC-SEM software.

Gas sorption analysis

Gas sorption analyses were performed on a Micromeritics ASAP 2420 adsorption analyser. CO_2 isotherms were collected at 273 K from between 0.5 and 1190 mbar (or P/P_o $1.6*10^{-5}$ to $3.5 * 10^{-2}$). 83 points were collected for the adsorption branch, and 44 for the desorption. BET analyses were conducted using the data points between the relative pressures 0.010 and 0.015 (348.5 and 522.8 mbar). PSD analyses were conducted using the NLDFT pore model for carbon slit pore geometry at 10 atm / 273 K; regularization was kept constant between all samples. Samples were degassed at 120 °C for 15 hours under vacuum (10^{-5} bar) before analysis. Isotherm data were analysed with the micromeritics MicroActive software Version 5.00 and plotted using Veusz 3.2 [16]. Ads branches are shown in the main text, with full isotherms in ESI Figure 5.

Results and discussion

The MOFs were synthesised in a slight adaption (50% increased quantity per reaction) of our previously published literature procedures [7] and analysed by PXRD (ESI Figure 2), indicating that MFM-300 was synthesised in almost phase purity with a small amount of linker reflections visible when the data was fit with a LeBail refinement [17] for the $I4_122$ space group. Thermogravimetric analysis showed no linker.

Mass out

In each experiment a mass of MFM-300(Al) was combined with fresh linker, followed by mixing with an appropriate amount of base solution as detailed in Table 1. Samples are referred to by the molar ratio of free linker to the molar equivalent of base. It was determined by titration that a 1:4 molar ratio of ammonium hydroxide was required to dissolve the solid linker, indicating that all 4 carboxylic acid groups must react with ammonium hydroxide for the linker to become water soluble. After centrifugation, all samples consisted of solid pellets. Samples dispersed and washed with deionised water followed by centrifugation twice before being dried and allowed to rehydrate as per the normal synthetic procedure. As a purely qualitative observation, samples washed with base are significantly less electrostatic, thus much easier to retrieve reliably from the polypropylene centrifuge tubes, and the pellets were easier to break apart than those formed from the as synthesised MOF. Deionised water was used as a control. Sample weight, PXRD and TGA analysis were used to check for evidence of free linker, SEM was used to check for any signs of damage to the MOF crystals and gas adsorption analysis was used to ensure that the MOF retained its porosity.

The effects of washing can be seen directly from the mass of the sample post washing, compared with the mass of MOF put into the experiment (Figure 1). A mass gain indicates incomplete removal of the excess linker, where as a mass loss indicates the framework itself is being lost. Powder X-ray diffraction confirmed that all samples washed with ammonium hydroxide matched the expected powder pattern of MFM-300 and contained no H_4BPTC (Figure 2). When washed with DI as a control the added linker was not removed, as shown by the positive mass difference of 34 mg and

continued contribution in the PXRD pattern, (some mass loss occurs simply from sample handling.)

When washed with ammonium hydroxide (0.2 M) the linker is removed by solvation to the point where the there is no detectable peak in the PXRD pattern (Figure 2) and no linker decomposition is evidenced by TGA (Figure 3). At a stoichiometric 0.7:1:4 ratio a small mass gain (+1 mg) is observed, indicating possible incomplete removal of the linker. By a 0.7:1:8 ratio all linker is removed and some mass loss (-2 mg) from the MOF sample is occurring, which we can attribute to MOF digestion that worsens as the excess of ammonia increases (to a total loss of 6 mg at 0.7:1:40 ratio. Figure 1). At higher concentrations (0.5 & 1 M ammonium hydroxide) this trend was the same. With the Mass, PXRD and TGA evidence we conclude that ammonium hydroxide preferentially reacts with free linker and its subsequent attack on the MOF is slow enough to be scarcely noticeable in the time frame of the experiment.

By comparison, NaOH washing experiments with even a slight molar excess (MOF:Linker:NaOH = 0.7:1:4.8) show large quantities of mass loss (-10 mg, c.f. 0 mg if the MOF remained intact and the linker all removed. Figure 1), representing a large degree of MOF digestion (as evidenced by both the mass loss shown in Figure 1 and backed up by visible crystal degradation in Figure 4 SEM). By a 0.7:1:40 ratio of free linker to NaOH the MOF is almost completely gone (<1 mg recovered, Fig 1) this was visible as mass in centrifuge tube disappeared during experiment (total time < 15 minutes, kept constant between different bases used).

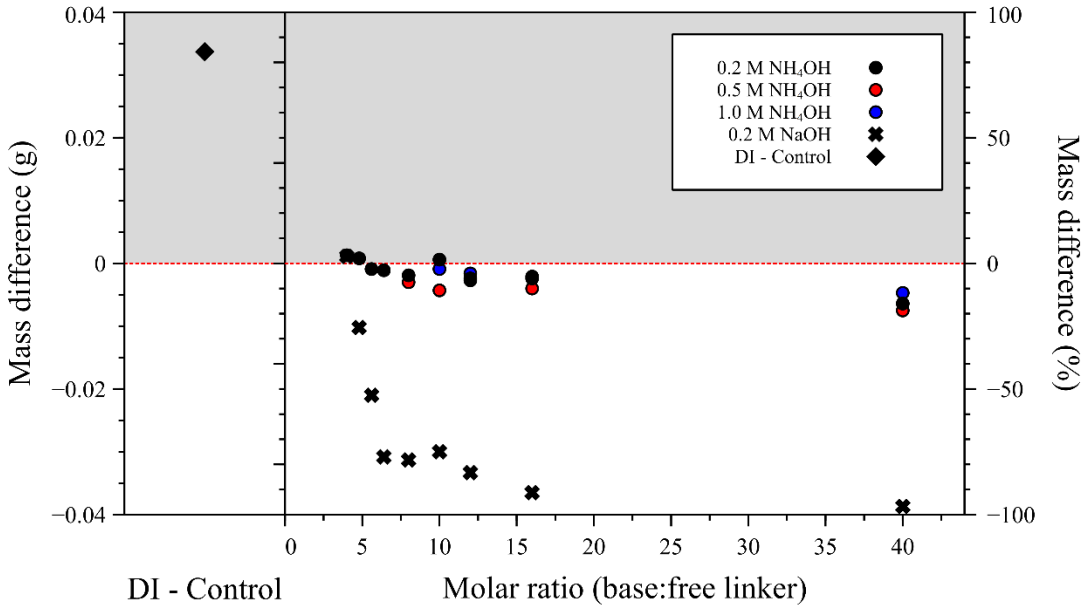


Figure 1: Mass differences from washing experiments (Legend insert). Data represent difference between the mass after washing c.f. the input mass of 39 mg MFM-300(Al). Values above zero indicate remaining free linker. Values below zero indicate loss of mass of MOF. Control experiment conducted with pure DI indicated by black diamond. Washing with ammonium hydroxide results in small mass (-2 mg, 0.7:1:8 MOF : linker : ammonium hydroxide ratio) loss even at large molar excesses, while NaOH caused large amounts of MOF digestion at only a minor excess (-31 mg, 0.7:1:8 MOF : linker :NaOH ratio).

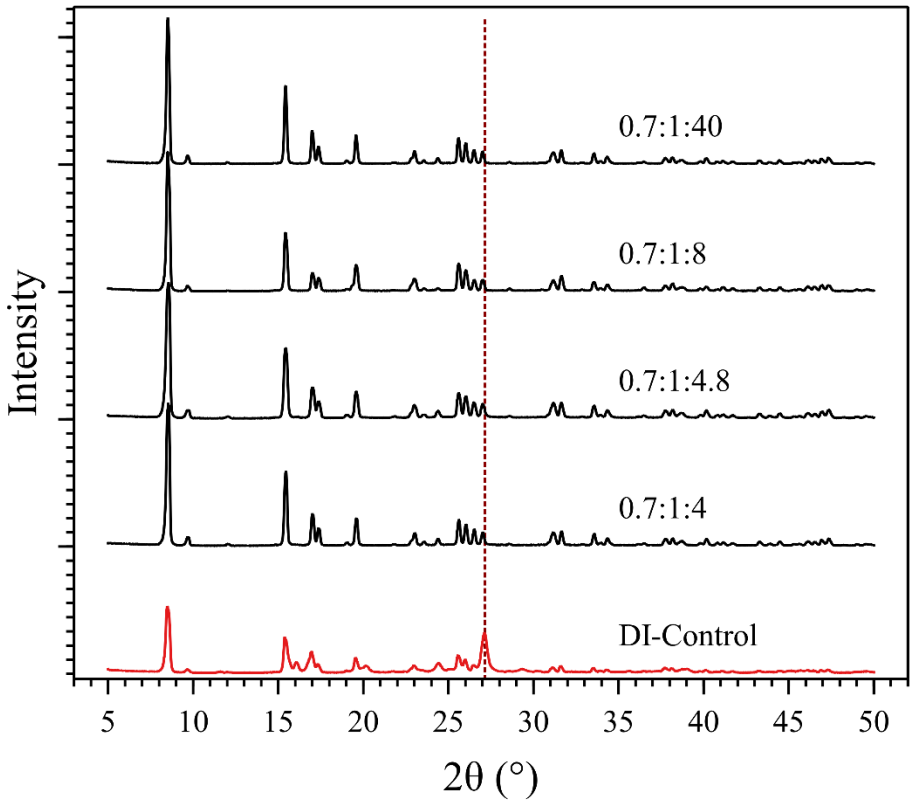


Figure 2: PXRD patterns of MFM-300(Al) and H_4BPTC mixes after washing: Red – Deionised water control experiment, Black – 0.2 M Ammonia solution (labelled according to the ratio MOF : Linker : Ammonium hydroxide.), Dotted line shows the primary reflection of H_4BPTC which is clearly visible in a sample washed only with water, but absent in samples washed with ammonium hydroxide, indicating removal of the free H_4BPTC while retaining MOF structure.

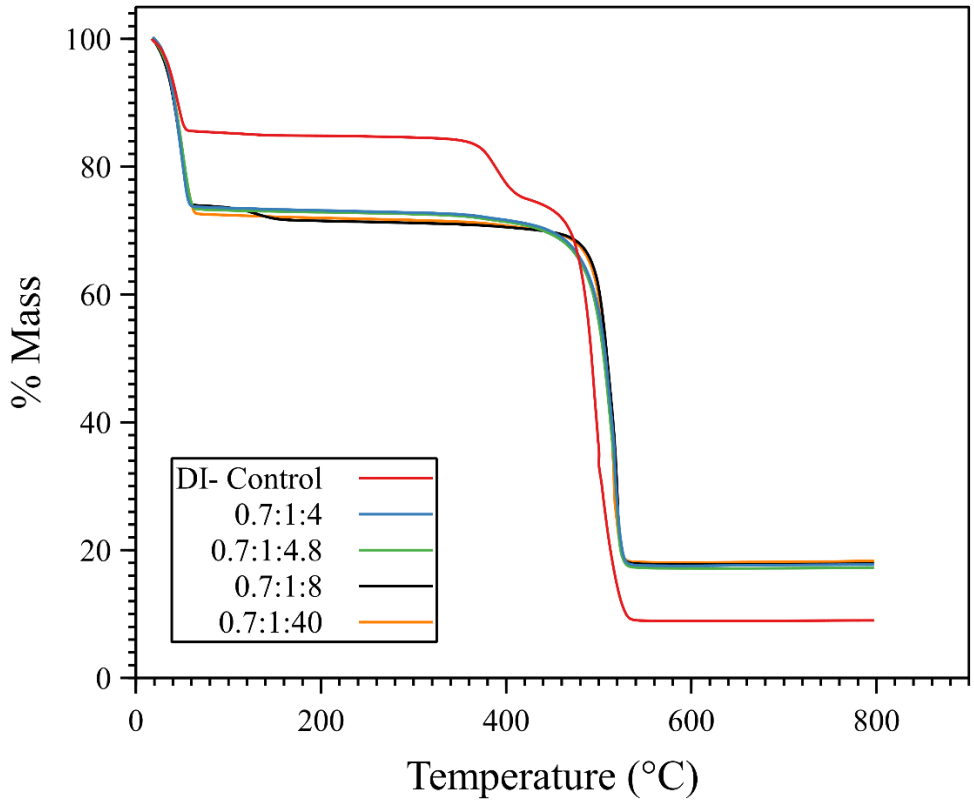


Figure 3: TGA thermograms of MFM-300 samples under air (Legend insert). The first step of mass loss is adsorbed water from the pores of the framework. In the case of the water control experiment the next mass loss (ca.350-450°C) is a component of the decomposition of the pure linker. Following this rapid mass loss occurs from the decomposition of the MOF leaving behind aluminium oxide. The data show a slight increase in H_2O content (approximately 4%) in samples washed with a larger excess of ammonia in conjunction with an increased onset point of decomposition (approx. 5 °C).

Crystal surface damage

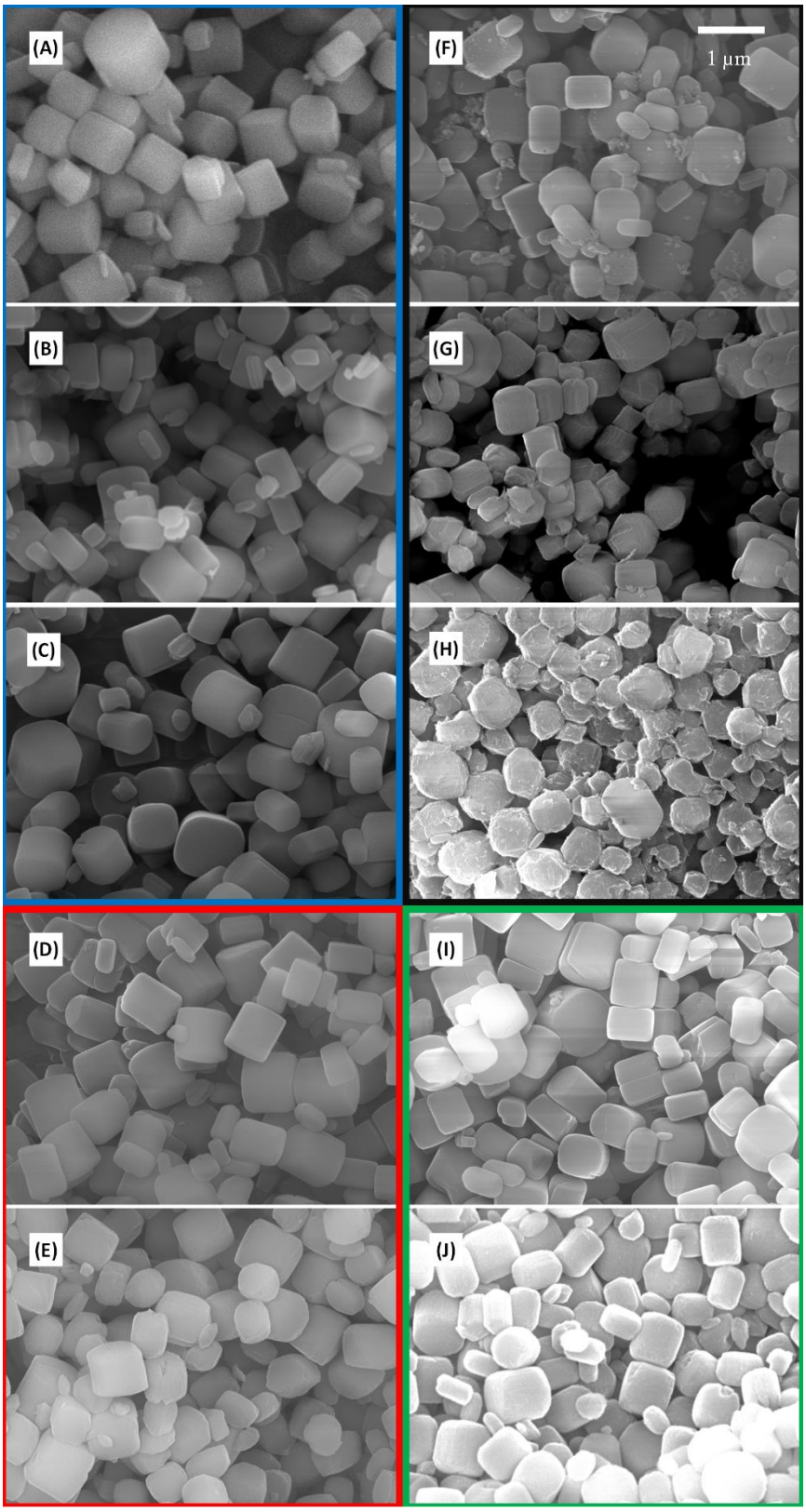


Figure 4: SEM micrographs of MFM-300 samples washed with alkaline solutions, grouped by solution used. Blue – ammonium hydroxide 0.2 M. (A)-0.7:1:4, (B)-

0.7:1:8, (C)-0.7:1:40. Red – ammonium hydroxide 0.5 M. (D)-0.7:1:8, (E)-0.7:1:40. Black – NaOH 0.2 M. (F)-0.7:1:4, (G)-0.7:1:8, (H)-0.7:1:40. Green – ammonium hydroxide 1 M. (I)-0.7:1:10, (J)-0.7:1:40. No damage is visible when washing with 0.2 M ammonium hydroxide (blue) but is seen clearly in comparison experiments, in the samples washed with NaOH (Black). Scale bar represents 1μm and is consistent for all images.

Scanning electron microscopy was used to determine potential damage to the surface of the crystals (Figure 4). When washing with 0.2 molar ammonia solution none of the crystals showed any visible signs of damage to the external surface of the MOF in the ratio's tested (from 0.7:1:4 to 0.7:1:40, Figure 4 A B & C). NaOH washing experiments at the same concentration and ratios (0.2 M, Figure 4 F, G & H) all showed damage to the crystals, indicative of the MOF digestion which was responsible for the experimental mass loss. Experiments using 0.5 M and 1 M ammonium hydroxide within this range were also investigate with SEM, it was found that at these concentrations low ratios (0.7:1:8 @ 0.5 M & 0.7:1:10 @ 1 M) also showed no visible signs of damage, however at the maximum amount tested (0.7:1:40 – both concentrations) some limited damage was visible.

Gas adsorption

CO_2 sorption measurements were conducted at 273 K to analyse the adsorption properties, and ensure that uptake was minimally effected by washing, which would indicate damage to the crystal structure through crystal defects (enhanced adsorption) or possible pore collapse/blocking (reduced adsorption) (Figure 5). The as-synthesised sample has a capacity of 8.85 mmol g^{-1} at ~1070 mbar [7] and when combined with excess linker and washed with distilled water, this was greatly reduced to 3.51 mmol g^{-1} at the same pressure due to the extra mass of non-porous linker. Samples washed with 0.2 M ammonium hydroxide solutions showed that with a molar equivalent or slight molar excess (0.7:1:4 & 0.7:1:4.8) the linker was mostly removed and the porosity of the framework largely unaffected, resulting in an uptake of 7.54 mmol g^{-1} at ~1070 mbar. When washed with a full 2 fold excess (0.7:1:8) an uptake of 8.13 mmol g^{-1} was achieved. A highest excess of ammonia tested (0.7:1:40) did not show any adsorption gain beyond that, indicating that a 2 fold excess was sufficient to

remove all the linker present. BET analysis between the relative pressures 0.010 and 0.015 (348.5 and 522.8 mbar), gave a surface area of 1164 m^2g^{-1} for this sample (0.7:1:8) compared to 1272 m^2g^{-1} for the previously synthesised sample [7]. PSD (Pore size distribution) determination by a Non Linear Density functional theory (NLDFT) model based on carbon slit pores (Figure 5 B) showed a narrow PSD centred on 0.5 nm in all cases, in line with our previously reported results indicating no change in the pore size as a result of washing with ammonium hydroxide solutions.

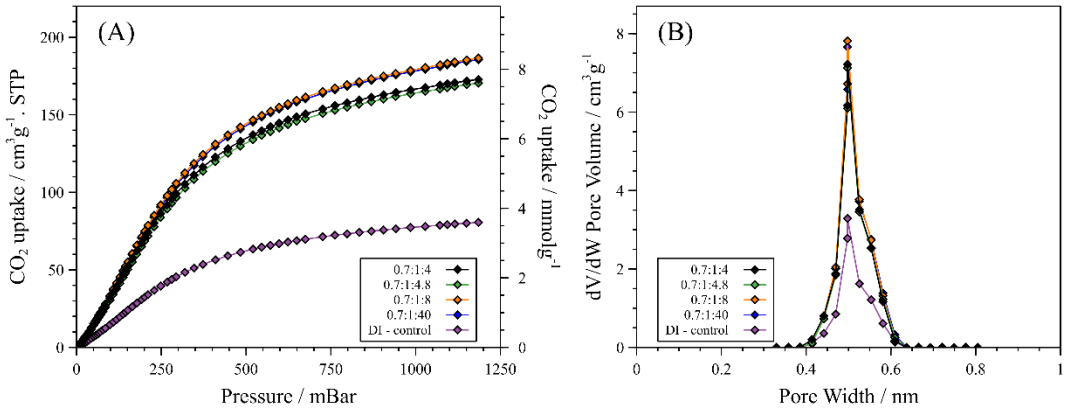


Figure 5: Gas adsorption of MFM-300 samples (A) Adsorption branches of CO_2 isotherms at 273 K. (B) PSD calculated using NLDFT for carbon slit pores. Legends insert When linker is added the per gram gas uptake of total material is reduced, as the linker mass is non-porous (purple trace). Washing with ammonia hydroxide solution removes the linker and therefore increases the capacity of the sample (black and green traces), a slight further increase of ~0.5 mmol g^{-1} is observed when washing with greater quantities of base (blue and orange traces). The pore width and profile of the material remain constant over the course of washing experiments.

Reusing reclaimed linker for further synthesis

A great benefit of our method of purification over washing with a solvent such as DMF is the ease with which material can be reclaimed from the solution. Linker was precipitated from ammonium hydroxide solution with the addition of HCl and collected via centrifugation. 98.3% of the linker was reclaimed based on mass of linker added. After washing with deionised water and drying, the reclaimed linker used to synthesise a new sample of MFM-300. (ESI Figure 3)

Conclusions:

The ability to purify MFM-300(Al) with basic solutions is assessed. In contrast with sodium hydroxide solution, ammonium hydroxide solution was demonstrated to offer a facile method of dissolving the linker without causing damage to the MOF. The use of ammonium hydroxide in removing linker is versatile in that a large excess of base can be used (0.7 : 1 : 40) without damaging the MOF, therefore if the exact quantity of unreacted linker is not known an excess of this base can be used to ensure complete removal of linker without fear of degrading the MOF product.

The method can potentially be applied at large scale, simply involving dispersing the MOF and linker in the basic solution in which the linker then dissolves leaving behind the solid MOF product. The linker can then be easily reclaimed via acidification of the solution and reused for further synthesis, an important consideration when choosing a purification technique so that valuable and difficult-to-synthesise feedstocks can be reclaimed and reused. In this paper, we have shown that it is possible to purify MFM-300(Al) using ammonium hydroxide which was previously shown to damage other MOFs (e.g. MIL-53(Al)). This work highlights that the selection of a purification method is dependent on the MOF and so it is worth analysing the stability of a candidate MOF when choosing a purification protocol.

References

1. L. James, S., *Metal-organic frameworks.* Chemical Society Reviews, 2003. **32**(5): p. 276-288.

2. Pettinari, C., et al., *Application of metal − organic frameworks.* Polymer International, 2017. **66**(6): p. 731-744.

3. Sun, Y. and H.-C. Zhou, *Recent progress in the synthesis of metal–organic frameworks.* Science and Technology of Advanced Materials, 2015. **16**(5): p. 054202.

4. Czaja, A.U., N. Trukhan, and U. Müller, *Industrial applications of metal–organic frameworks.* Chemical Society Reviews, 2009. **38**(5): p. 1284-1293.

5. Thomas-Hillman, I., et al., *Developing a sustainable route to environmentally relevant metal-organic frameworks: ultra-rapid synthesis of MFM-300(Al) using microwave heating.* Green Chemistry, 2019. **21**(18). 5039-5045

6. Clark, J.H., *Green chemistry: challenges and opportunities.* Green Chemistry, 1999. **1**(1): p. 1-8.

7. Poliakoff, M., et al., *Green Chemistry: Science and Politics of Change.* Science, 2002. **297**(5582): p. 807-810.

8. Haque, E., et al., *Facile Purification of Porous Metal Terephthalates with Ultrasonic Treatment in the Presence of Amides.* Chemistry – A European Journal, 2009. **15**(43): p. 11730-11736.

9. Chen, Y., et al., *Recyclable ammonia uptake of a MIL series of metal-organic frameworks with high structural stability.* Microporous and Mesoporous Materials, 2018. **258**: p. 170-177.

10. Kajiwara, T., et al., *A Systematic Study on the Stability of Porous Coordination Polymers against Ammonia.* Chemistry – A European Journal, 2014. **20**(47): p. 15611-15617.

11. Godfrey, H.G.W., et al., *Ammonia Storage by Reversible Host–Guest Site Exchange in a Robust Metal–Organic Framework.* Angewandte Chemie International Edition, 2018. **57**(45): p. 14778-14781.

12. Bates, R.G. and G.D. Pinching, *Acidic dissociation constant of ammonium ion at 0 to 50 C, and the base strength of ammonia.* Journal of Research of the National Bureau of Standards, 1949. **42**(5): p. 419.

13. Miller, R.S., D.Y. Curtin, and I.C. Paul, *Reactions of molecular crystals with gases. I. Reactions of solid aromatic carboxylic acids and related compounds with ammonia and amines.* Journal of the American Chemical Society, 1974. **96**(20): p. 6329-6334.

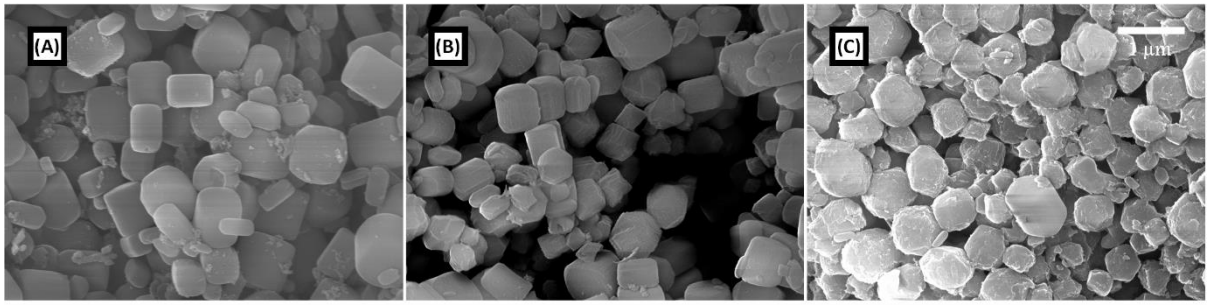
14. Yang, W.-W., et al., *Synthesis, characterization, and thermodynamic study of ammonium benzoate C7H5O2NH4(s).* Thermochimica Acta, 2010. **502**(1): p. 14-19.

15. Coelho, A.A., *TOPAS and TOPAS-Academic: an optimization program integrating computer algebra and crystallographic objects written in C++*. Journal of Applied Crystallography, 2018. **51**(1): p. 210-218.

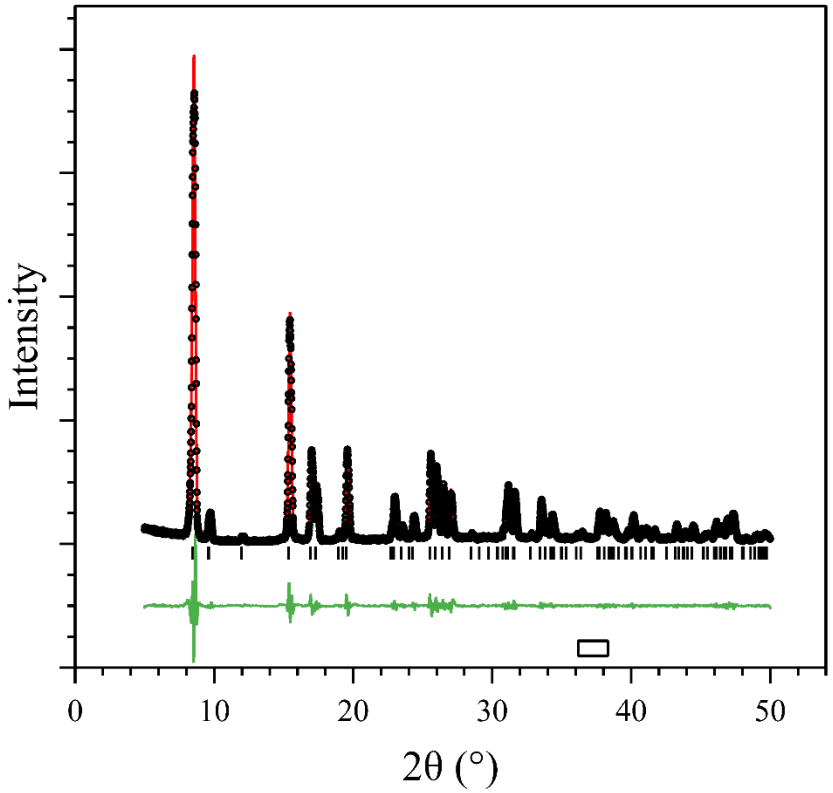
16. Sanders, J., *https://veusz.github.io/.*

17. Le Bail, A., H. Duroy, and J.L. Fourquet, *Ab-initio structure determination of LiSbWO6 by X-ray powder diffraction.* Materials Research Bulletin, 1988. **23**(3): p. 447-452.

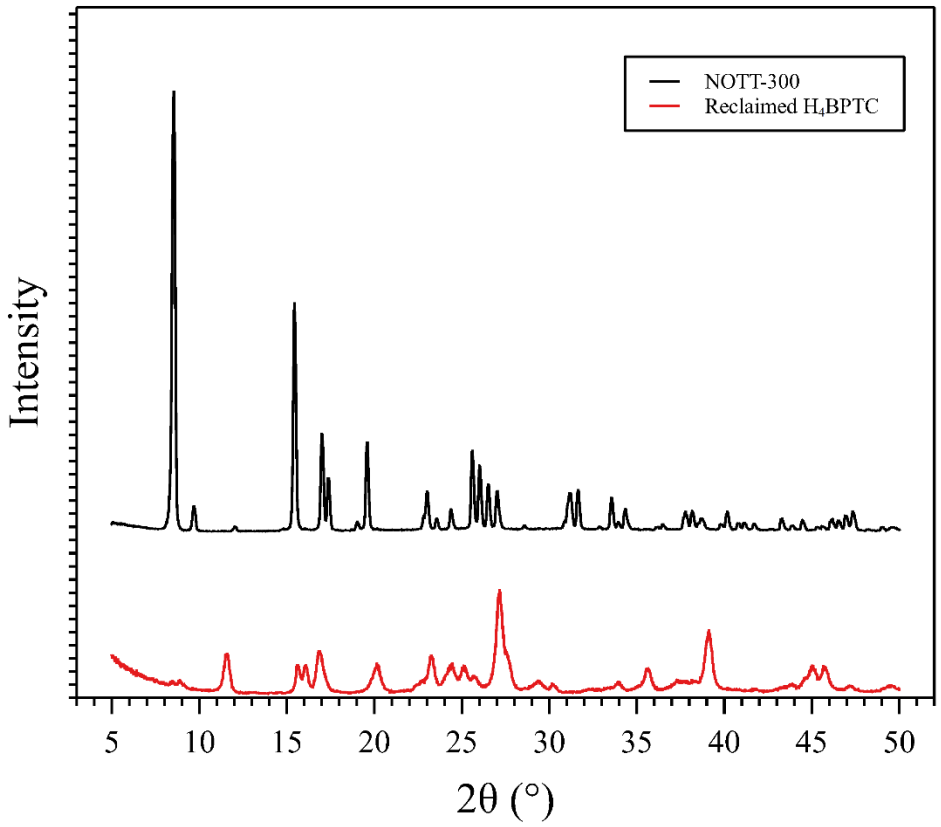
Supplementary Information



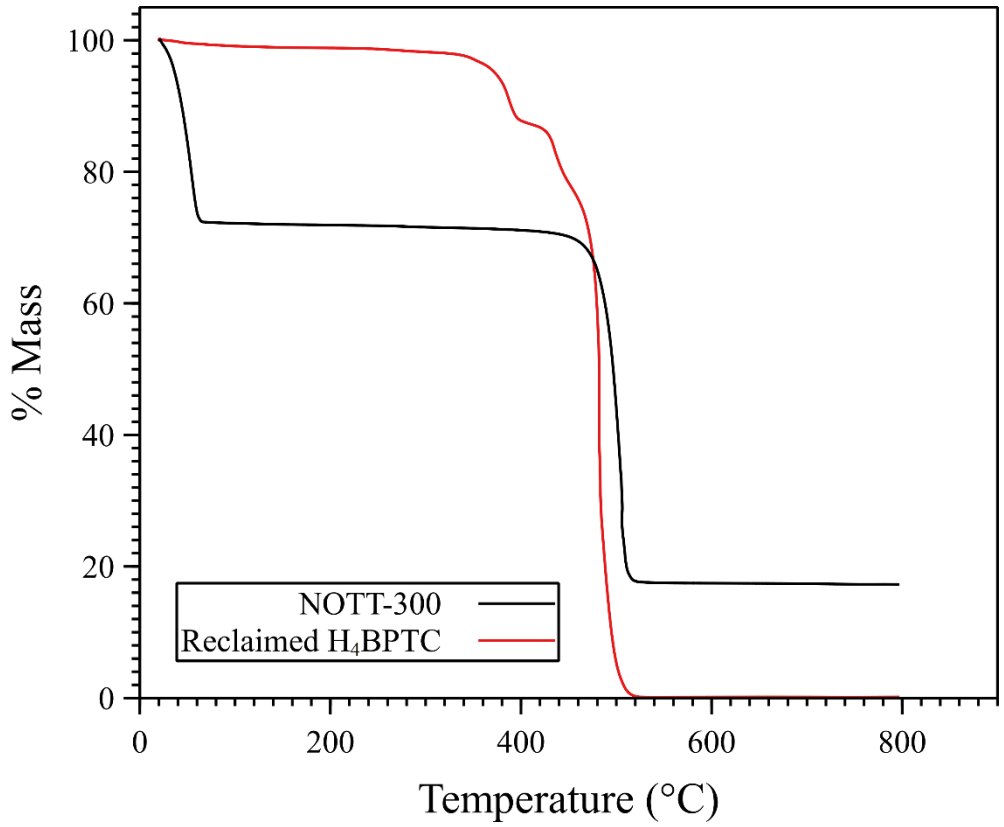
ESI Figure 1: SEM micrographs of samples washed with 0.2 M NaOH solution: (A) an equimolar quantity of NaOH, (B) a 100% excess, (C) a 900% excess. In all experiments the surviving crystals show visible signs of damage from NaOH. Scale bar represents 1 μm. Direct comparison experiments with Figure 4.



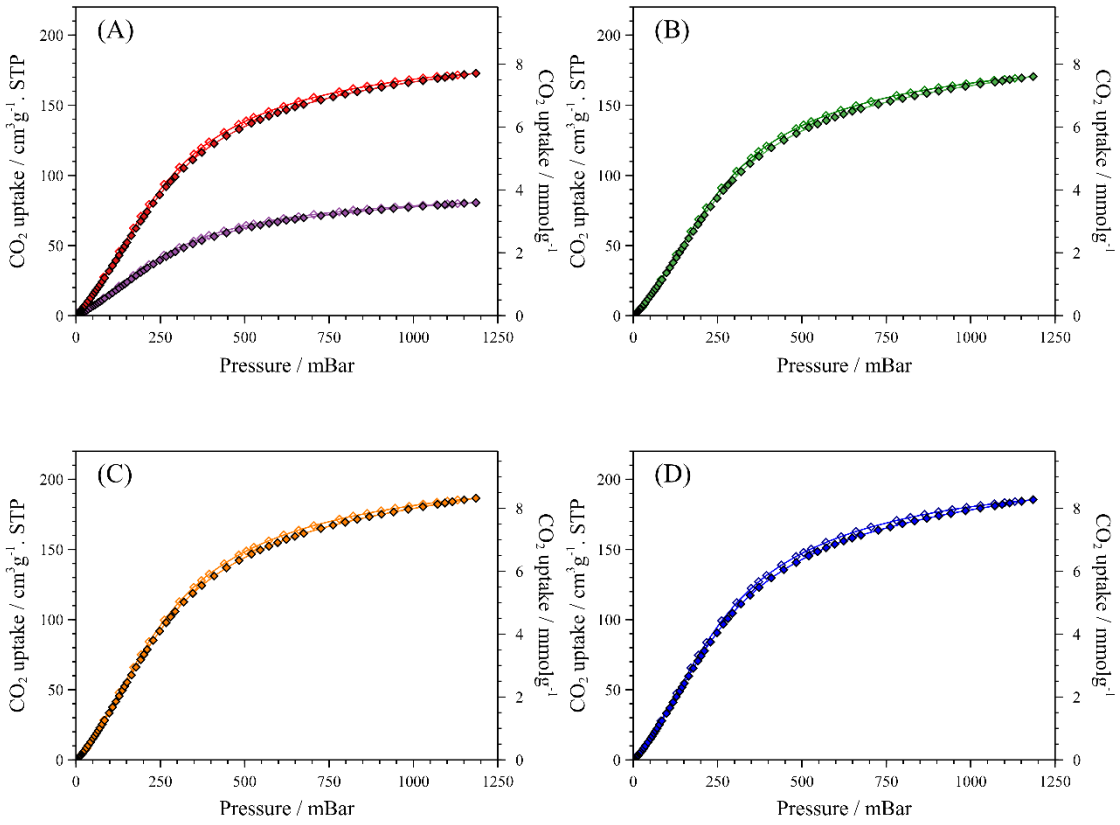
ESI Figure 2: PXRD of the as synthesised MFM-300(Al) and modelled patterns using a LeBail refinement; Black circles = Observed intensities, red = simulated pattern by LeBail refinement, green = difference plot. Tick marks represent possible Bragg reflections of the $I4_122$ space group, associated with the MOF.



ESI Figure 3: PXRD of reclaimed H_4BPTC linker and MFM-300 synthesised from this reclaimed material.



ESI Figure 4: TGA thermograms of reclaimed H_4BPTC linker and MFM-300 synthesised from this reclaimed material.



ESI Figure 5: Expanded Gas adsorption isotherms showing both adsorption and desorption branches (A – purple) DI-control, (A – red) 0.7:1:4, (B) 0.7:1:4.8, (C) 0.7:1:8 & (D) 0.7:1:40.

Appendix 5: Combining continuous flow oscillatory baffled reactors and microwave heating: Process intensification and accelerated synthesis of metal-organic frameworks

Andrea Laybourn, Ana María López-Fernández, Ieuan Thomas-Hillman, Juliano Katrib, William Lewis, Chris Dodds, Adam P.Harvey and Samuel W.Kingman

Faculty of Engineering, University of Nottingham, Nottingham, UK
School of Engineering, Newcastle University, Newcastle Upon Tyne, UK
School of Chemistry, University of Nottingham, Nottingham, UK

Submitted 29th May 2018, Accepted 2nd September 2018

Published in Chemical Engineering Journal, 2019, 356, 170-177

DOI: 10.1016/j.cej.2018.09.011

Statement of contribution of joint authorship

Andrea Laybourn and Ana Maria Lopez-Fernandez designed the experimental plan and designed, built, and operated the reactor. Andrea Laybourn collected and interpreted gas adsorption, PXRD and TGA data. Ieuan Thomas-Hillman assisted with experimental procedures, provided analysis of collected PXRD powder patterns, collected SEM images of synthesised MOF particles and characterised and sized the samples based on those images. William Lewis provided support with PXRD characterisation. Juliano Katrib performed electromagnetic simulations and assisted with reactor design. Andrea Laybourn, Chris Dodds, Adam Harvey, and Samuel Kingman designed and supervised project and developed protocols. All authors contributed to writing of the manuscript and responding to reviewers. Andrea Laybourn submitted the manuscript for publication.

Abstract

We have constructed a continuous flow oscillatory baffled reactor (CF-OBR) equipped with a homogeneous and controllable microwave applicator in an entirely novel design. This affords a new route to chemical production incorporating many of the principles of process intensification and allows, for the first time, investigation of the

synergistic benefits of microwave heating and CF-OBRs such as; faster and continuous processing; improved product properties and purity; improved control over the processing parameters; and reduced energy consumption. The process is demonstrated by the production of a metal-organic framework (MOF), HKUST-1, a highly porous crystalline material with potential applications in gas storage and separation, catalysis, and sensing. Our reactor enabled the production of HKUST-1 at the 97.42 g/h scale, with a space time yield (STY) of 6.32×10^5 kg/m^3/day and surface area production rate (SAPR) of 1.12×10^{12} m^2/m^3/day. This represents the highest reported STY and fastest reported synthesis (2.2 s) for any MOF produced *via* any method to-date and is an improvement on the current SAPR for HKUST-1 by two orders of magnitude owing to the superior porosity exhibited by HKUST-1 produced using our rig (Langmuir surface area of 1772 compared to 600 m^2/g).

Keywords

Metal-organic framework; Microwave; Oscillatory baffled reactor; Process intensification; Ultra-fast synthesis; Continuous flow

1. Introduction

Microwave heating is an established process intensification method used in industrial sectors such as rubber vulcanizing [1] and for drying food and wood [2]. During microwave heating, energy is delivered instantaneously through interaction of an alternating electromagnetic field with a material rather than by conductive, convective or radiative heat transfer [3]. Microwave heating enables selective and targeted heating to specific components during the reaction; this is particularly attractive for chemical processing as an alternative to conventional heating owing to the following benefits; significantly reduced production times (many hours to minutes), increase in product yield and purity, and enhancement of product properties [4], [5], [6], [7], [8].

A continuous flow oscillatory baffled reactor (CF-OBR) is a proven process intensification method in the laboratory for reactions such as biodiesel production [9], bioprocessing [10] and saponification [11], and is increasingly being commercialised [12]. CF-OBRs are tubular reactors containing equally spaced baffles presented transversely to an oscillatory/pulsed flow, as shown in Fig. 1. Fluid inside the CF-OBR

is oscillated by a pump placed at one or both ends of the tube. The baffles disrupt the boundary layer at the tube wall, whilst the oscillation creates vortices, resulting in improved mixing. Superposition of net flow on to the oscillatory motion allows control over mixing and residence times by altering the oscillation conditions, *i.e.* oscillation amplitude and frequency [13]. Unlike a conventional tubular reactor, the degree of mixing in an OBR is independent of the net flow, therefore it is possible to achieve a high level of mixing at low flow rates and what would otherwise be low Reynolds numbers [13]. An advantage of this is the ability to use tubular reactors with a greatly reduced length-to-diameter ratio thus decreasing the size of the process. Size reductions of up to 99.6% compared to continuous stirred tank reactors (CSTRs) with equivalent throughput are possible [14]. Furthermore, OBRs are scalable as the mixing mechanisms do not alter between the laboratory and industrial scale, given geometric and dynamic similarity [13].

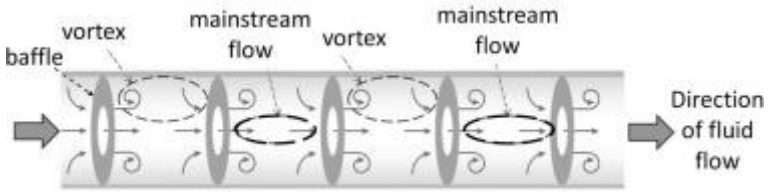


Fig. 1. Schematic representation of fluid flow in an oscillatory baffled reactor (OBR).

As with microwave heating, CF-OBRs offer huge opportunities for intensifying chemical production. The uniform mixing environment and enhanced heat transfer in OBRs enable considerable reduction in processing times (by up to 80%), better temperature control, and consistent product properties (*i.e.* particles with uniform size and morphology) [14].

Microwave heating and CF-OBRs individually show great potential for energy savings, enhanced process control and optimization, and improved product quality compared to other processing methods, such as CSTRs, as a result of reduced solvent and energy usage, faster and continuous processing, smaller processing equipment, and safer implementation of harsh production conditions [13]. Therefore, a production route that combines microwave heating and CF-OBR technology has the potential to deliver synergistic benefits to scalable chemical processing with exceptional process intensification attributes. In particular, the CF-OBR is able to provide plug flow in a

compact design whilst uniformly suspending solid particles. The solid particles are suspended by the oscillatory flow mixing structures. They will be in constant motion, hence they will be exposed to the same dose of microwave energy. This is an advantage over packed bed catalytic reactors, for example, where it can be challenging to heat large beds homogeneously using the microwave field. In other designs of laboratory-scale plug flow reactors, such as microchannel reactors, it is difficult to operate with solid particles without blockages, or time-consuming development of catalyst washcoats (carriers to disperse particles).

Metal-organic frameworks (MOFs) are highly porous crystalline materials composed of metal nodes and organic linkers [15]. MOFs have received marked attention from academia and industry owing to their unprecedented porosity (surface areas up to 7000 m^2/g) [16] and diverse structures and functionalities. The properties of MOFs offer immense opportunities for economic and environmental impact in areas such as gas storage and separation [17], catalysis [18], sensing [19], and drug delivery [20]. In particular, the tuneable nature of MOFs could enhance their performance in gas and petrochemical separations compared to other adsorbents, such as activated carbons and zeolites.

MOFs are not currently used in industry owing to the inability to produce these materials at the required quality, purity, quantity and cost for application [6], [21]. The main reason for this is the demanding MOF synthesis conditions; *i.e.* use of large amounts of toxic, corrosive and highly flammable chemicals, high temperatures and autogenous pressures (typically above the boiling point of the solvent), long reaction times (hours or days), acidic by-products, high energy requirements, and heterogeneous reaction mixtures that require mixing [6]. Additional challenges include reproducibility between batches and cost and availability of large scale reaction rigs [6]. The development of technologies that address these issues in an efficient and sustainable way is a key enabling step in the transfer of MOFs from the laboratory to industrial application.

As methods for scaling up MOF production evolve, parameters for comparing and assessing their efficiency and practicality and have become important. Two key parameters include production rate (mass of dry MOF product per hour, g/hr) and

space time yield (STY, quantity of MOF produced per unit volume of reactor in a 24 h period, kg/m^3/day) [6]. Another important factor is the quality of MOF produced; this is dependent upon their intended use. For example, the overall surface area exhibited by MOFs is important for gas capture and storage [6], [22] whereas uniformity of size and morphology of the crystals are important for separations [23], [24], [25] and controlled drug release [26]. Surface area production rate (SAPR), which is defined as the amount of surface area of MOF produced per unit volume of reactor per day, m^2/m^3/day, has recently been developed to indicate the quality of MOF obtained from different production methods [21]. This criterion will be used in this paper to evaluate the production methods discussed and developed herein.

Few examples of combined microwave heating and continuous flow systems for MOF synthesis at the laboratory scale have been reported. These include; a gas liquid segmented flow reactor capable of producing ~90 g/h/L of MOF-74(Ni) with a STY of 2160 kg/m^3/d; [27] a plug flow reactor shown to produce three MOFs, namely MIL-53(Al), UiO-66, and HKUST-1 at production rates of 7.1, 14.4 and 79.4 g/h respectively [28]; and a tubular microwave reactor with a high reported STY of up to 400,000 kg/m^3/d for HKUST-1 [21]. In the latter system, a significant decrease in surface area from *ca.* 2100 [29] to 600 m^2/g [21] is observed which would render the MOF with little or no commercial value, highlighting the importance of assessing the quality of MOF produced as well as the production rate. However, these systems do not fully assess the effect of microwave energy on the reaction mixture and rely upon mixing provided by small internal diameters (i.d. <4.4 mm) [21], [27], [28] tubes. In order to facilitate developments in continuous flow microwave synthesis of MOFs beyond the laboratory, greater understanding of the effect of microwave and mixing parameters that are essential for scale-up is required. Microwave parameters include; the efficiency of power coupling and distribution of the electric field within the heating cavity; penetration depth and relationship with reactor design and specification; and the required power density distribution (energy per unit volume over the treatment time, see references [7], [30] for a more in-depth explanation) to produce MOFs consistently at high quality and at the required production rates and STYs [7]. Mixing parameters include; fluid mechanics, formation and dissipation of vortices, velocity profiles, shear rate distribution, residence times, and scale-up correlations aimed at producing MOFs with a desired particle size distribution and morphology [11]. All of

these variables underpin the successful integration of microwave energy with chemical reactor systems capable of delivering the economic large-scale manufacturing processes needed to produce MOFs, consistently at high quality and at the correct cost base and minimal environmental impact.

We have constructed a CF-OBR system equipped with a homogeneous and controllable microwave applicator in an entirely novel design, as CF-OBRs have not been used in conjunction with controllable microwave heating before. This affords a new route to MOF production incorporating many of the principles of process intensification and allows, for the first time, investigation of the synergistic benefits of microwave heating and CF-OBRs. Using our system, herein referred to as the 'MW-CF-OBR' rig (Fig. 2), we have, for the first time, quantified experimentally the amount of microwave energy absorbed by a MOF reaction mixture in continuous flow thus allowing investigation of the effect of mixing and microwave heating on continuous MOF production. We report the effect of flow rate and baffle material on the production rate, STY and quality (SAPR, porosity, crystallinity, particle size and morphology) of an archetypal MOF, HKUST-1 [31]. This particular MOF was chosen to enable comparison with other production routes. Using our MW-CF-OBR rig we have produced HKUST-1 at the 97.42 g/h scale and with a space time yield (STY) of 6.32×10^5 kg/m^3/day. This is >50% higher than the previously reported STY [21] and represents the highest reported STY for any MOF produced *via* any method to-date. Additionally, all the HKUST-1 materials produced were highly porous and exhibited Brunauer–Emmett–Teller surface areas (SA_{BET}) over 1300 m^2/g (*i.e.* at the desired level/ according to specification) resulting in a surface area production rate (SAPR) of 1.12×10^{12} m^2/m^3/day. This is two orders of magnitude more than the highest reported SAPR for HKUST-1 and shows that the materials produced using the MW-CF-OBR rig are of high quality.

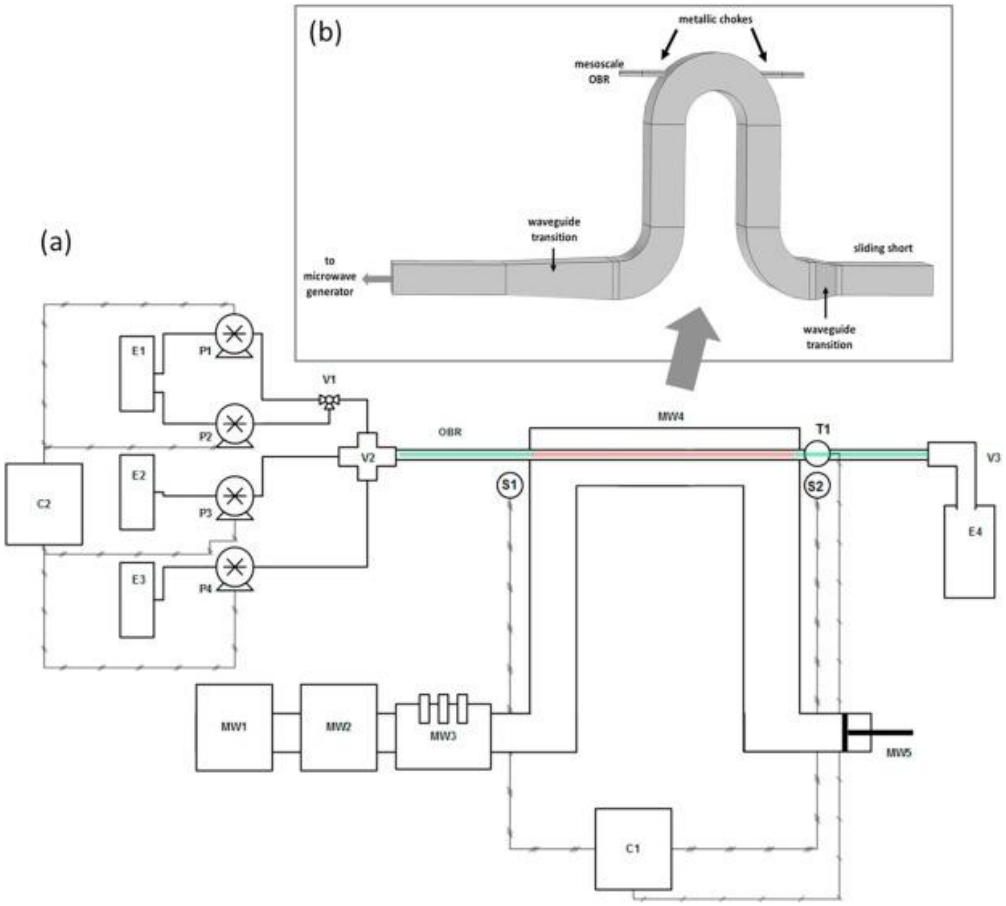


Fig. 2. Schematic of MW-CF-OBR rig; (a) Whole rig; (b) 3D model of MW4 section. MW1: microwave generator; MW2: power meters; MW3: automatic 3-stub tuner; MW4: microwave cavity; MW5: sliding short; E1: vessel containing ethanol; E2 vessel containing metal salt dissolved in ethanol; E3: vessel containing linker dissolved in ethanol; E4: collection vessel; P1 to P4: syringe pumps; V1, V2, V3: Teflon connectors; T1: thermocouple; S1 and S2; microwave leakage meters; OBR: green corresponds to plastic baffle, red corresponds to interchangeable baffle section (metal or plastic); C1 and C2: PC controllers. Further information about the components is given in the Supplementary Information (SI). (For interpretation of the references to colour in this figure legend, the reader is referred to the web version of this article.)

2. Experimental

The schematic of the MW-CF-OBR rig is given in Fig. 2. The rig consists of four continuous syringe pumps (labelled P1-P4 in Fig. 2), three feedstocks (E1-E3, Fig. 2), a mesoscale-oscillatory baffled reactor (consisting of two individual tubes connected

together fitted with a helical plastic perfluoroalkoxyalkane, PFA, baffle; labelled OBR in Fig. 2) fed through a choked microwave cavity (MW4, Fig. 2) and a product collection vessel (E4, Fig. 2). PFA was used for the baffles as it is compatible with the reaction mixtures and is microwave transparent. The microwave cavity was designed to ensure homogeneity of the treatment by considering the electromagnetic properties of the reaction mixture. This was achieved *via* electromagnetic simulations performed using COMSOL Multiphysics [32] (see SI, for further details and model). Fig. 3 shows the power density distribution inside the material (including baffles and reaction mixture). Power density variation was ±6% across the treatment zone (Fig. 3), indicative of uniform heating in the microwave applicator zone. Chokes were designed by considering the electromagnetic properties of the reaction mixture to prevent any microwave leakage and are compliant with health and safety legislation [33]. A thermocouple located directly after the microwave cavity (T1, Fig. 2) was used to monitor the bulk temperature of the suspension following heating in order to ensure no disruption to the oscillatory flow in the microwave heated zone.

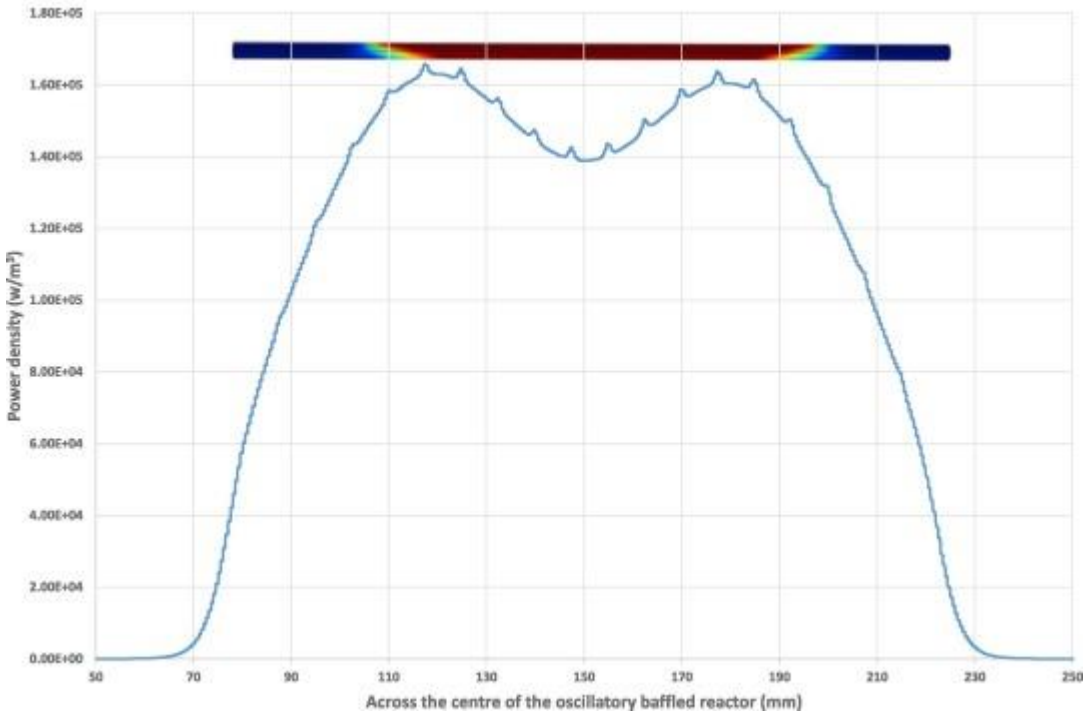


Fig. 3. Power density distribution across the centre of the oscillatory baffle reactor simulated using the electromagnetic properties of the reaction mixture and COMSOL Multiphysics [32]. Further details are given in the SI.

As mentioned in the introduction, HKUST-1 was selected as it has been produced *via* many different routes (*e.g.* electrochemical, mechanochemical/extrusion, spray drying, microwave heated reactions, conventional heated continuous flow synthesis and in batch systems such as CSTRs) [6]. This enables direct comparison of production rate, STY and quality (SAPR, porosity, particle size and morphology, crystallinity) for which some data already exist. For example, production of HKUST-1 in ethanol in a CSTR at 60 °C takes 5 h with a yield of 32.3%, STY of 41 kg/m^3/day, and an SAPR of 91 × 10^6 kg/m^3/day [21].

Feedstocks were prepared according to previously reported stochiometries and concentrations for HKUST-1 synthesis [21]. Feedstock one (E1, Fig. 2) consisted of an 8.94 mM solution of copper salt, made from copper nitrate hemipentahydrate (13.86 g) dissolved in ethanol (150 mL). Feedstock two (E2, Fig. 2) comprised of a 4.75 mM solution of linker made from trimesic acid (6.66 g) dissolved in ethanol (150 mL). Both solutions were stirred prior to pumping to ensure complete dissolution of the solid into ethanol. Feedstock 3 (E3, Fig. 2) was pure ethanol used by pumps P1 and P2 for oscillatory flow (Note: this liquid is used for oscillation only and not added to the net flow). Oscillation frequency was controlled by adjusting the speed of the piston movement and the amplitude was adjusted by setting the amount of volume dispensed. The parameters were monitored and controlled using the "SAPPHIRE" engineering software.

During treatment, feedstocks one and two were dispensed in equal proportion (in accordance with reported synthesis conditions) [34] at the desired flow rate (5, 10, 30, 50, 80 and 100 mL/min) and the oscillation was initiated. Further details about the oscillation conditions are provided in the SI. These flow rates correspond to residence times in the microwave heated zone of 2.2–44.4 s, covering a broad range of residence times and energy inputs. Next, the total volume of the OBR was completely filled with the reaction mixture at the respective flow rate and the mixture heated to 65 ± 5 °C (heating above this temperature resulted in 'boil off' owing to slightly hotter temperatures inside the microwave heated zone) by adjusting the microwave power at a frequency of 2.45 ± 0.0025 GHz (consistent with penetration depth measurements).

An automatic 3-stub tuner (S-TEAM) [35] was used for impedance matching to minimize reflected power and maximize energy absorption by the reaction mixture during microwave treatment. Once temperature had stabilized and the system had reached steady state (approximately 5 reactor volumes), samples were collected at the OBR outlet (after V3, Fig. 2) at approximately 15 mL intervals during continuous HKUST-1 production. Power meters were used to measure the forward and reflected power from which the average absorbed power (forward minus reflected) and total absorbed energy were determined.

In order to assess the effect of localised electromagnetic heating of the baffles, both PFA and stainless steel baffles were used in the interchangeable baffle section (as indicated by the red zone in Fig. 2). When metals are exposed to microwave energy, the majority of the microwave current flows in a thin layer (an eddy current) of the surface known as skin depth. The skin depth for stainless steel is 8.48 μm [3]. The remaining OBR length was fitted with PFA baffles (highlighted green in Fig. 2) to ensure that the metal baffle did not protrude beyond the chokes of the microwave cavity thus preventing microwave leakage. Experiments conducted with stainless were performed at two flow rates, 10 and 50 mL/min.

After microwave treatment, the resulting blue suspensions were centrifuged for 10 min at 4200 revolutions per minute at 5 °C. The supernatant was then decanted and the blue powder washed with ethanol (*ca.* 10 mL) and re-centrifuged using the same conditions. The decant, wash and centrifugation step was repeated once more. After this, the supernatant was decanted and the powder was dried in an oven at 50 °C for 5 h. A minimum of five samples from three separate reactions were obtained for analysis at each flow rate. The average yields of HKUST-1 at each flow rate were determined by thermogravimetric analysis of 2 samples from 3 separate experiments (*i.e.* the 'average yield' is determined from a total of 6 samples per flow rate). Data are given in Table S2 in the SI.

3. Results and discussion

Using our novel MW-CF-OBR rig (Fig. 2), the effect of synthesis conditions, namely flow rate, applied power (and therefore energy), and baffle material, on the yield and properties (porosity, crystallinity and morphology) of HKUST-1 were investigated.
173

Reactions were conducted in ethanol as this solvent does not decompose during HKUST-1 synthesis and can be recycled, thus reducing the cost, inherent safety issues, and environmental burden of the process [36]. The applied power was varied with flow rate to maintain a bulk reaction temperature of 65 ± 5 °C, as displayed in Table 2. Temperatures beyond 65 ± 5 °C were not investigated in order to prevent build-up of pressure from the boiling reaction mixture. Data in Table 2 show that an increase in energy is required to maintain the target temperature with decreasing flow rate and in presence of a metal baffle; this is due to heat losses to the surrounding areas. Future experiments need to consider insulating the OBR if flow rates below 30 mL/min are required.

Table 1. Summary of relative crystallinity of HKUST-1 produced using the MW-CF-OBR rig. High values of 1/full width half maximum indicate highly crystalline materials.

Flow rate (mL/min)	**Relative crystallinity (1/FWHM) of 220 peak**
5	4.6
10	4.9
10[#]	4.1
50	4.2
50[#]	5.2
100	3.5

#Metal baffle used during microwave treatments.

Table 2. Summary of gas sorption data collected at 77 K using N_2 as the sorbate for HKUST-1 produced in the MW-CF-OBR rig and oscillation conditions.

Flow rate (mL/min)	**Velocity ratio (Ψ)= Re_o/Re_n #,*1**	**Average absorbed power (W)*1**	**Average absorbed energy (kJ)*2**	**Average absorbed energy per volume of reaction mixture (kJ/mL)*2**	**Langmuir surface area (m^2g^{-1})*a**	**BET surface area (m^2g^{-1})*b**	**$V_{0.1}/V_{Tot}$ *c**
5	27.76	53 ± 1	6.56 ± 0.13	0.52 ± 0.01	1893	***1850***	0.91
10	13.88	51 ± 5	3.49 ± 1.25	0.28 ± 0.13	1661	***1621***	0.90
10*d	13.88	95 ± 5	5.84 ± 0.31	0.58 ± 0.03	1964	***1916***	0.90
30	4.63	86 ± 4	1.85 ± 0.07	0.18 ± 0.00	2054	***2004***	0.86
50	2.78	104 ± 1	2.22 ± 0.02	0.13 ± 0.00	1386	1345	0.81
50*d	2.78	158 ± 2	3.39 ± 0.30	0.20 ± 0.02	1734	***1686***	0.76
80	1.73	128 ± 0	1.70 ± 0.01	0.12 ± 0.00	1728	***1680***	0.65
100	1.39	156 ± 2	1.75 ± 0.02	0.10 ± 0.00	1772	***1751***	0.68

*a P/P_0 range 0.001‑0.01.

*b The Rouquerol plot was used in the P/P_0 range 0.001‑0.01 to give positive C values for the BET surface area.

*c Pore volume at $P/P_0 = 0.1$ divided by the total pore volume at $P/P_0 = 0.99$; values are written to two decimal places.

*d Metal baffle used during microwave treatments. BET surface areas in italics and bold are within the reported range of commercially available HKUST-1 [55].

*2 Values written to two decimal places.

*1 Values written to nearest integer.

Calculation and explanation of velocity ratio given in the SI.

3.1. Yield of HKUST-1

Products synthesised using the MW-CF-OBR rig exhibit powder X-ray diffraction (PXRD) peaks corresponding to pure HKUST-1, showing that no other MOF phases or impurities were produced (see Fig. S4, SI). As mentioned in the introduction, it is important to calculate yield in terms of the production rate and STY as these parameters are typically used to evaluate process efficiency and to compare between different production routes. Fig. 4 shows an increase in production rate with increasing flow rate. The highest production rate of 97.42 g/h is observed at the maximum flow rate, 100 mL/min, with a residence time of 2.2 s in the microwave heated zone of the MW-CF-OBR rig. This is shortest reported synthesis time for any MOF produced *via* any method to-date. The corresponding STY is 6.32×10^5 kg/m^3/day which is the highest reported for HKUST-1, 1.58 times higher than the previous maximum reported STY, of 4.00×10^5 kg/m^3/day. An average yield of 27.03% based on the theoretical conversion was achieved. This percentage yield is consistent with the recent work of McKinstry *et al.* in which a maximum yield of 32.3% was reported using the same conditions as that used in our study, *i.e.* 1.5:1 of BTC:$Cu(NO_3)_2$ in ethanol [21]. It may be possible to improve the conversion by altering the concentration of reactants [21], the metal:linker ratio [37], or by increasing the reaction temperature [21] but our current experimental set-up is limited by the reduced penetration depths observed for more concentrated metal salt solutions and by the pressure generated at elevated temperatures. Further work is ongoing to investigate these factors.

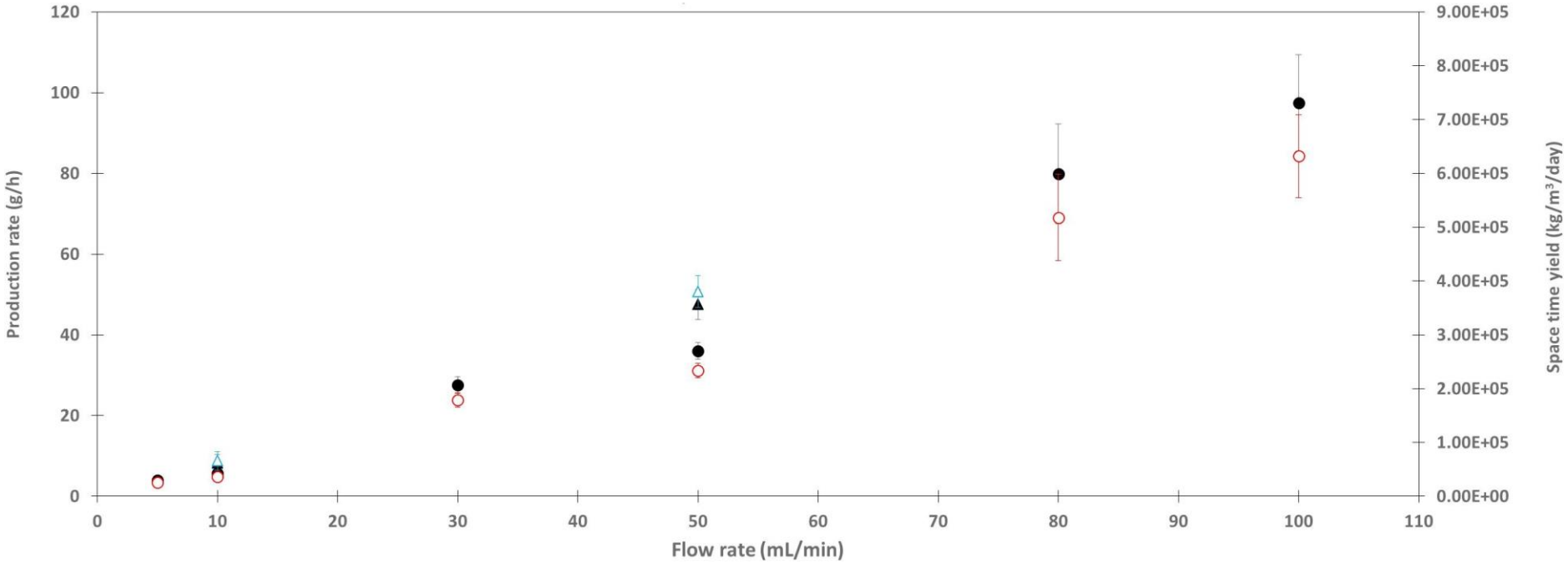


Fig. 4. Plot of flow rate *vs.* production rate (left axis; filled in symbols) and space time yield (right axis; red and blue hollow symbols) for HKUST-1 produced using the MW-CF-OBR rig. Circles and triangles represent experiments conducted with a plastic and metal baffle, respectively. Error bars represent the largest absolute experimental deviation from the mean/average values. (For interpretation of the references to colour in this figure legend, the reader is referred to the web version of this article.)

3.2. Quality of HKUST-1: crystallinity, morphology and porosity

The effect of treatment conditions on the quality of HKUST-1 was also investigated by analysing the crystallinity, morphology and porosity of HKUST-1 produced using the MW-CF-OBR rig. As mentioned in the introduction, MOFs that exhibit high surface areas are particularly desirable for gas storage and capture [6], [22] whereas MOFs consisting of highly crystalline particles of uniform size and morphology are appropriate for separations [23], [24], [25] and controlled drug release [26].

3.2.1. Crystallinity and morphology

SEM analyses show that HKUST-1 materials recovered from the MW-CF-OBR rig mainly consist of nano-sized crystals below 15 μm^2. This is consistent with previous reports in which microwave heating produces smaller crystals than conventional heating owing to nucleation at hotspots that form due to local superheating of the solvent [8] and solvated metal ions [7], [30]. In this work, five dominant morphologies namely, plates, circular, irregular, triangular based prisms and octahedral crystals are observed (see Section 4, SI). Irregular [38], circular [38] and octahedral shaped crystals have been reported previously for HKUST-1 with octahedral crystals >5 μm being the most common [38], [39], [40], [41], [42]. The shape of the crystals is unlikely to be critical for industrial applications of MOFs, however, the production of crystals with uniform size and shape is desirable. Using an aforementioned particle size distribution analysis method [7], [43], our present work shows that HKUST-1 particle size and morphology is dependent on the flow rate and, therefore, mixing effects and microwave treatment (power and time, consistent with previous reports [7], [44]). However, there is no obvious correlation between the yield of HKUST-1 and particle size (see Table S2 in SI).

Materials recovered from the MW-CF-OBR rig show a reduction in median particle size with increasing flow rate. For example, at a flow rate of 5 mL/min (plastic baffles) HKUST-1 particles consist of triangular based prisms and octahedral crystals with a median crystal size of 0.78 μm^2 as observed by scanning-electron microscopy (SEM, see Fig. 5 and SI). However at a flow rate of 100 mL/min (plastic baffles) HKUST-1 particles consist of much smaller irregular and circular shaped crystals with a median

size of 0.016 μm^2 (see Fig. 5). The same trend is observed for HKUST-1 produced using metal baffles; the median particle size decreases from 0.15 (octahedral and triangular prisms) to 0.019 μm^2 (irregular and circular crystals) between flow rates of 10 and 50 mL/min, respectively (see Fig. 5). The smaller and irregular shaped crystals recovered at high flow rates are likely the result of decreased reaction time, *i.e.* crystals are earlier in the crystallisation process, or crystal breakage due to rapid and harsh mixing. Further work is ongoing to investigate these effects.

The relative crystallinity of HKUST-1 materials were determined using the method of Vivani *et al.* [45] by comparing the reciprocals of the full width half maximum (1/FWHM) for a selected peak in the PXRD patterns. FWHM were calculated using a split pseudo-Voigt peak fitting function (Fig. S5, SI). Data in Table 1 show no obvious correlation between treatment conditions and relative crystallinity. HKUST-1 produced at 100 mL/min shows the lowest 1/FWHM (see Table 1) and therefore is the least crystalline material produced using the MW-CF-OBR rig. This is consistent with SEM analyses in which irregular shaped crystals were produced at 100 mL/min and is an acceptable level of crystallinity compared to other commercially available materials [46], [47].

3.2.2. Porosity

A summary of N_2 gas sorption data for HKUST-1 produced in the MW-CF-OBR rig is given in Table 2. HKUST-1 prepared at flow rates of 5 and 10 mL/min exhibit Type I isotherms with little hysteresis [48], characteristic of microporous materials and typically exhibited by HKUST-1 [49], [50]. HKUST-1 prepared at flow rates of 50, 80 and 100 mL/min exhibit Type I isotherms with some Type IV character and H4 hysteresis indicative of inter-particulate mesoporosity [48], [51], also reported previously for HKUST-1 [52]. All materials exhibit Langmuir (SA_{Lang}) and Brunauer–Emmett–Teller surface areas (SA_{BET}) over 1300 m^2/g with no obvious correlation between treatment conditions and surface area (see Table 2).

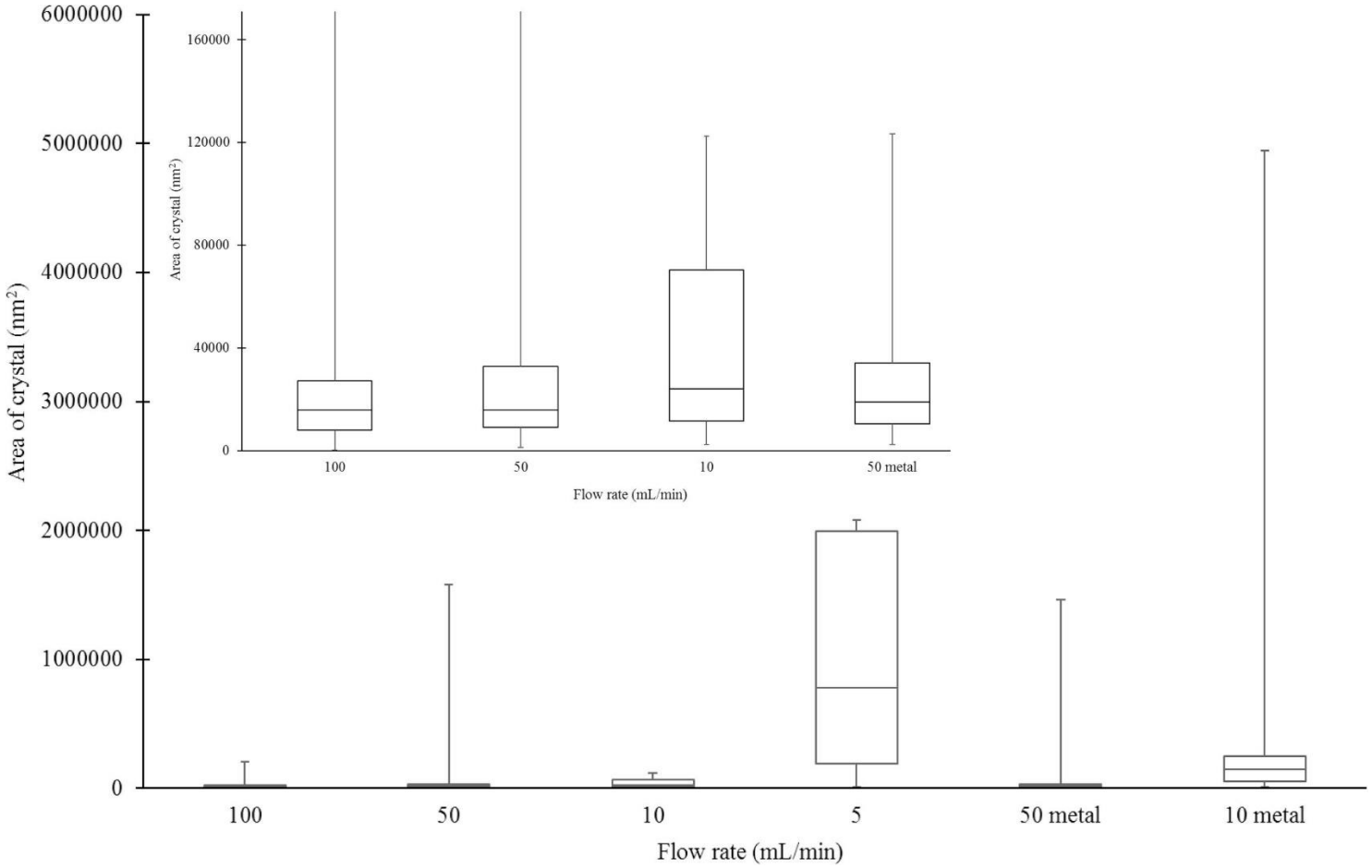


Fig. 5. Box and whisker plot of flow rate *vs.* crystal size for HKUST-1 collected from the MW-CF-OBR rig. Metal denotes the use of metal baffles during MOF production. Data based on SEM analyses (see SI for further details). Inset: zoom of data for flow rates of 100 and 10 mL/min using plastic baffles and 50 mL/min using plastic and metal baffles. Error bars represent the largest and smallest crystal sizes. Boxes represent the interquartile range (outer line) and median (central line) crystal sizes.

180

In our present work, the highest (SA_{BET}) of 2004 ± 0.4 m^2/g was exhibited by HKUST-1 prepared at a flow rate of 30 mL/min which is higher than that reported for HKUST-1 prepared by mechanochemical (1600 m^2/g), electrochemical (1820 m^2/g), solvothermal (1550 m^2/g) and continuous flow (1950 m^2/g) synthesis [6]. A relationship between flow rate and relative microporosity of HKUST-1 was determined by calculating the ratio of the pore volume at low pressure to the pore volume at high relative pressure ($V_{0.1}/V_{Tot}$) [7], [53]. Data in Table 2 (and Fig. S6, SI) show that as the flow rate increases the value of $V_{0.1}/V_{Tot}$ tends away from one, indicating that highly microporous HKUST-1 is produced at flow rates below 50 mL/min and above this intergranular mesoporosity arises. This is consistent with SEM analyses (see SI) and another report where high V_{Tot} and H4 hysteresis were exhibited by expanded aggregated particles of HKUST-1 [54].

In order to compare the surface area of HKUST-1 produced using our MW-CF-OBR rig with that obtained *via* other processes, we have determined the SAPR. The SAPR of HKUST-1 produced using our MW-CF-OBR rig increases with increasing flow rate owing to high SA_{BET} (>1300 m^2/g) as shown in Fig. 6 and Table 2, respectively. While this result is expected, a related microwave-heated continuous flow study by McKinstry *et al.*, [21] reported a decrease in the SA_{Lang} of HKUST-1 from 1930 to 1550 m^2/g with an increase in flow rate from 300 to 550 mL/h [21]. The reduction in surface area observed by McKinstry *et al.* may be a consequence of using a non-optimised system, *i.e.* the energy absorbed per unit mass was not controlled, thus resulting in a difference in temperature between the different flow rates and a reduction in quality of the MOF produced [7].

In this work SAPRs between 3.36×10^7 and 1.12×10^{12} $m^2/m^3/day$ (where a day corresponds to 24 h) were achieved, with the highest SAPR reached at a flow rate of 100 mL/min (see Fig. 6). Our highest SAPR is two orders of magnitude higher than the current top SAPR of 2.40×10^9 $m^2/m^3/day$ owing to the superior porosity exhibited by HKUST-1 produced using our rig (Langmuir surface area of 1772 compared to 600 m^2/g) [21].

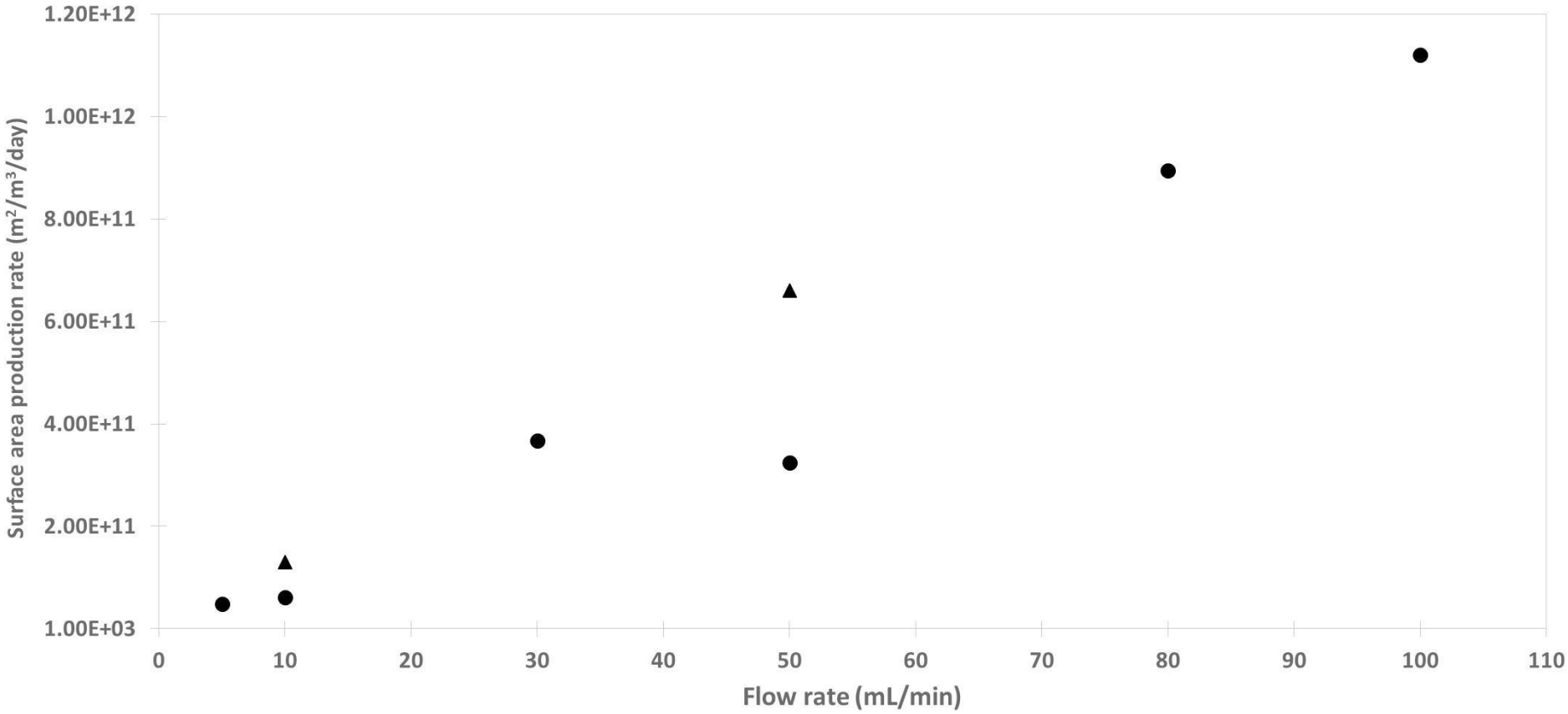


Fig. 6. Plot of flow rate *vs.* surface area production rate for representative samples of HKUST-1 produced using the MW-CF-OBR rig. Circles and triangles represent experiments conducted with a plastic and metal baffle, respectively.

4. Conclusions

We have developed a microwave heated oscillatory baffled reactor (MW-CF-OBR) rig for synthesising HKUST-1 in ethanol under mild conditions (ambient pressure and temperatures below 70 °C). Oscillatory baffled reactors were employed to generate uniform mixing of reactants and suspension of solids, and to facilitate rapid heat transfer to the bulk mixture. Microwave heating enabled a significant reduction in synthesis time with production rates of 97.42 g/h and a space time yield (STY) of 6.32×10^5 kg/m^3/day achieved. This is the highest reported STY and fastest synthesis rate (2.2 s) for any MOF produced to-date using any production method. Process intensification is enabled by both technologies through efficient mixing (uniform suspension of solids and high level of plug flow, OBR technology) and rapid delivery of energy requirements (microwave heating). The rapidity of energy delivery is further enhanced by selective microwave heating of the metal ions in solution [7], [56].

The quality of HKUST-1 materials produced using the MW-CF-OBR rig were assessed by analysing the crystallinity, morphology and porosity. HKUST-1 particle size and morphology were found to be dependent on the flow rate. For example, syntheses conducted at 5 mL/min gave relatively large octahedral and triangular prism shaped crystals (median particle size 0.78 μm^2) whereas flow rates above 50 mL/min gave much smaller irregular shaped crystals (median particle size 0.019 μm^2). A slight reduction in relative crystallinity (although still in line with commercial sources) [46], [47] is exhibited by HKUST-1 produced at flow rates of 100 mL/min compared to lower flow rates, which is probably due shorter reaction times (less time for crystallisation), or crystal breakage due to rapid and harsh mixing. All the HKUST-1 materials produced were highly porous and exhibited Brunauer–Emmett–Teller surface areas (SA_{BET}) over 1300 m^2/g resulting in a surface area production rate (SAPR) of 1.12×10^{12} m^2/m^3/day. This is two orders of magnitude more than the highest reported for HKUST-1 and confirms that the materials produced using the MW-CF-OBR rig are of high quality.

Acknowledgements

AL acknowledges the University of Nottingham for the award of a Nottingham Research Fellowship. We thank the Nanoscale and Microscale Research Centre

(nMRC, University of Nottingham) for access to SEM facilities which are supported by the Engineering and Physical Sciences Research Council (EPSRC) under grant EP/L022494/1. Finally, we thank Christopher G. Morris for training and helpful discussions regarding the PXRD peak fitting.

References

[1] M.T. De Meuse, C.L. Ryan Adv. Polym. Technol., 12 (1993), pp. 197-203

[2] A.L. Antti, P. Perré Wood Sci. Technol., 33 (1999), pp. 123-138

[3] R. Meredith **Engineers' Handbook of Industrial Microwave Heating** The Institution of Engineering and Technology, UK (1998)

[4] H. Wang, A. Mustaffar, A.N. Phan, V. Zivkovic, D. Reay, R. Law, K. Boodhoo Chem. Eng. Process.: Process Intensif., 118 (2017), pp. 78-107

[5] C.O. Kappe, A. Stadler, D. Dallinger **Microwaves in Organic and Medicinal Chemistry** (second ed.), Wiley-VCH, Weinheim, Germany (2005)

[6] M. Rubio-Martinez, C. Avci-Camur, A.W. Thornton, I. Imaz, D. Maspoch, M.R. Hill Chem. Soc. Rev., 46 (2017), pp. 3453-3480

[7] A. Laybourn, J. Katrib, R.S. Ferrari-John, C.G. Morris, S. Yang, O. Udoudo, T.L. Easun, C. Dodds, N.R. Champness, S.W. Kingman, M. Schroder J. Mater. Chem. A, 5 (2017), pp. 7333-7338

[8] J. Klinowski, F.A. Almeida Paz, P. Silva, J. Rocha Dalton Trans., 40 (2011), pp. 321-330

[9] N. Masngut, A.P. Harvey, J. Ikwebe Biofuels, 1 (2010), pp. 605-619

[10] X. Ni, M.R. Mackley Chem. Eng. J., 52 (1993), pp. 107-114

[11] A.P. Harvey, M.R. Mackley, P. Stonestreet Ind. Eng. Chem. Res., 40 (2001), pp. 5371-5377

[12] http://www.nitechsolutions.co.uk/, accessed 21/05/2018.

[13] D.R. Reay, C. Ramshaw, A.P. Harvey**Process Instensification: Engineering for Efficiency, Sustainability and Flexibility** (second ed.), Elsevier, UK (2013)

[14] T. McGlone, N.E.B. Briggs, C.A. Clark, C.J. Brown, J. Sefcik, A.J. Florence Org. Process Res. Dev., 19 (2015), pp. 1186-1202

[15] G. Ferey Chem. Soc. Rev., 37 (2008), pp. 191-214

[16] O.K. Farha, I. Eryazici, N.C. Jeong, B.G. Hauser, C.E. Wilmer, A.A. Sarjeant, R.Q. Snurr, S.T. Nguyen, A.Ö. Yazaydın, J.T. Hupp J. Am. Chem. Soc., 134 (2012), pp. 15016-15021

[17] J.-R. Li, R.J. Kuppler, H.-C. Zhou Chem. Soc. Rev., 38 (2009), pp. 1477-1504

[18] D. Farrusseng, S. Aguado, C. Pinel Angew. Chem. Int. Ed., 48 (2009), pp. 7502-7513

[19] L.E. Kreno, K. Leong, O.K. Farha, M. Allendorf, R.P. Van Duyne, J.T. Hupp Chem. Rev., 112 (2012), pp. 1105-1125

[20] L. Wang, M. Zheng, Z. Xie J. Mater. Chem. B, 6 (2018), pp. 707-717

[21] C. McKinstry, E.J. Cussen, A.J. Fletcher, S.V. Patwardhan, J. Sefcik Chem. Eng. J., 326 (2017), pp. 570-577

[22] D.A. Gómez-Gualdrón, P.Z. Moghadam, J.T. Hupp, O.K. Farha, R.Q. Snurr J. Am. Chem. Soc., 138 (2016), pp. 215-224

[23] D. Cabooter, A. Fanigliulo, G. Bellazzi, B. Allieri, A. Rottigni, G. Desmet J. Chromatogr. A, 1217 (2010), pp. 7074-7081

[24] J. Billen, D. Guillarme, S. Rudaz, J.L. Veuthey, H. Ritchie, B. Grady, G. Desmet J. Chromatogr. A, 1161 (2007), pp. 224-233

[25] K. Horváth, D. Lukács, A. Sepsey, A. Felinger J. Chromatogr. A, 1361 (2014), pp. 203-208

[26] S. Granado, V. Ragel, V. Cabanas, J. San Roman, M. Vallet-Regi J. Mater. Chem., 7 (1997), pp. 1581-1585

[27] G.H. Albuquerque, R.C. Fitzmorris, M. Ahmadi, N. Wannenmacher, P.K. Thallapally, B.P. McGrail, G.S. Herman Cryst. Eng. Comm., 17 (2015), pp. 5502-5510

[28] M. Taddei, D.A. Steitz, J.A. van Bokhoven, M. Ranocchiari Chem. Eur. J., 22 (2016), pp. 3245-3249

[29] Y. Yang, P. Shukla, S. Wang, V. Rudolph, X.-M. Chen, Z. Zhu RSC Adv., 3 (2013), pp. 17065-17072

[30] A. Laybourn, J. Katrib, P.A. Palade, T.L. Easun, N.R. Champness, M. Schroder, S.W. Kingman Phys. Chem. Chem. Phys., 18 (2016), pp. 5419-5431

[31] S.-Y. Chui, S.M.-F. Lo, J.P.H. Charmant, A.G. Orpen, I.D. Williams Science, 283 (1999), pp. 1148-1150

[32] W.B.J. Zimmerman **Multiphysics Modelling with Finite Element Methods** World Scientific, London (2006)

[33] B. Standard, Industrial, scientific and medical (ISM) radio-frequency equipment - Electromagnetic disturbance characteristics - Limits and methods of measurement, BSI, 2007.

[34] C. McKinstry, R.J. Cathcart, E.J. Cussen, A.J. Fletcher, S.V. Patwardhan, J. Sefcik Chem. Eng. J., 285 (2016), pp. 718-725

[35] G.F. Engen IEEE Trans. Microwave Theory Tech. (1997)

[36] E. Grimmond, T. Hadley, A. Monch, I. Harvey, J. Churchill, M. Rubio-Martinez, S. Lim, M. Hill Asia Pacific Confederation of Chemical Engineering Congress 2015: APCChE 2015, incorporating CHEMECA 2015, Engineers Australia, Melbourne (2015), pp. 691-701

[37] P. Schäfer, F. Kapteijn, M.A. van der Veen, K.F. Domke Cryst. Growth Des., 17 (2017), pp. 5603-5607

[38] D. Zacher, J. Liu, K. Huber, R.A. Fischer Chem. Commun. (2009), pp. 1031-1033

[39] M. Shoaee, J.R. Agger, M.W. Anderson, M.P. Attfield, Cryst. Eng. Comm., 10 (2008), pp. 646-648

[40] M. Schlesinger, S. Schulze, M. Hietschold, M. Mehring Microporous Mesoporous Mater., 132 (2010), pp. 121-127

[41] J. Nan, X. Dong, W. Wang, W. Jin, N. Xu Langmuir, 27 (2011), pp. 4309-4312

[42] K.-J. Kim, Y.J. Li, P.B. Kreider, C.-H. Chang, N. Wannenmacher, P.K. Thallapally, H.-G. Ahn Chem. Commun., 49 (2013), pp. 11518-11520

[43] C.-W. Tsai, E.H.G. Langner Microporous Mesoporous Mater., 221 (2016), pp. 8-13

[44] W. Guo, W. Sun, L.-P. Lv, S. Kong, Y. Wang ACS Nano, 11 (2017), pp. 4198-4205

[45] M. Taddei, P.V. Dau, S.M. Cohen, M. Ranocchiari, J.A. van Bokhoven, F. Costantino, S. Sabatini, R. Vivani Dalton Trans., 44 (2015), pp. 14019-14026

[46] https://www.sigmaaldrich.com/catalog/product/aldrich/688614?lang=en&region=GB&gclid=EAIaIQobChMIx7_c6Lmq2QIVrL3tCh1e4gXMEAAYASAAEgKp4PD_BwE, accessed 18/05/18.

[47] http://www.moftechnologies.com/products/, accessed 18/05/18.

[48] K.S.W. Sing Pure Appl. Chem., 54 (1982), pp. 2201-2218

[49] K.-S. Lin, A.K. Adhikari, C.-N. Ku, C.-L. Chiang, H. Kuo Int. J. Hydrogen Energy, 37 (2012), pp. 13865-13871

[50] M. Gimeno-Fabra, A.S. Munn, L.A. Stevens, T.C. Drage, D.M. Grant, R.J. Kashtiban, J. Sloan, E. Lester, R.I. Walton Chem. Commun., 48 (2012), pp. 10642-10644

[51] N.C. Burtch, H. Jasuja, K.S. Walton Chem. Rev., 114 (2014), pp. 10575-10612

[52] L. He, L.F. Dumee, D. Liu, L. Velleman, F. She, C. Banos, J.B. Davies, L. Kong RSC Adv., 5 (2015), pp. 10707-10715

[53] R. Dawson, A. Laybourn, R. Clowes, Y.Z. Khimyak, D.J. Adams, A.I. Cooper Macromolecules, 42 (2009), pp. 8809-8816

[54] G. Majano, J. Pérez-Ramírez Adv. Mater., 25 (2013), pp. 1052-1057

[55] https://www.sigmaaldrich.com/catalog/product/aldrich/688614?lang=en&region=GB&gclid=EAIaIQobChMIx7_c6Lmq2QIVrL3tCh1e4gXMEAAYASAAEgKp4PD_BwE, accessed 22/05/18.

[56] I. Thomas-Hillman, A. Laybourn, C. Dodds, S.W. Kingman J. Mater. Chem. A, 6 (2018), pp. 11564-11581

Supplementary Information

Contents

Further experimental details and data
Powder X-ray diffraction (PXRD) data and split pseudo-Voigt peak fitting
Gas sorption isotherms
Scanning electron microscopy (SEM) images and histogram plots
Thermogravimetric analysis

1. Further experimental details and data

COMSOL Multiphysics simulations

COMSOL Multiphysics is a commercial software dedicated for electromagnetic simulation using the finite element methods. The RF heating module was used to simulate the heating behaviour at 2.45 GHz inside the MW-CF-OBR rig. This has been achieved by calculating the magnitude of the electric field and power density (power absorbed in the reactor) on the meshed geometry. A fine mesh was produced to maintain at least 10 elements per wavelength. **Figure S1** presents a 2D cut of the electric field distribution inside the MW-CF-OBR rig. The simulation shows two hot spots inside the treatment section overlapping in the centre (Figure S1) of the tube to give a homogeneous distribution of power density within ± 6% across the treatment zone (see main text **Figure 3**). This is not surprising as the reactor design is based on a travelling resonant applicator. The principle here is to slow down the propagation of the electromagnetic and thus increase the residence time resulting in better coupling of the energy to the material being treated.

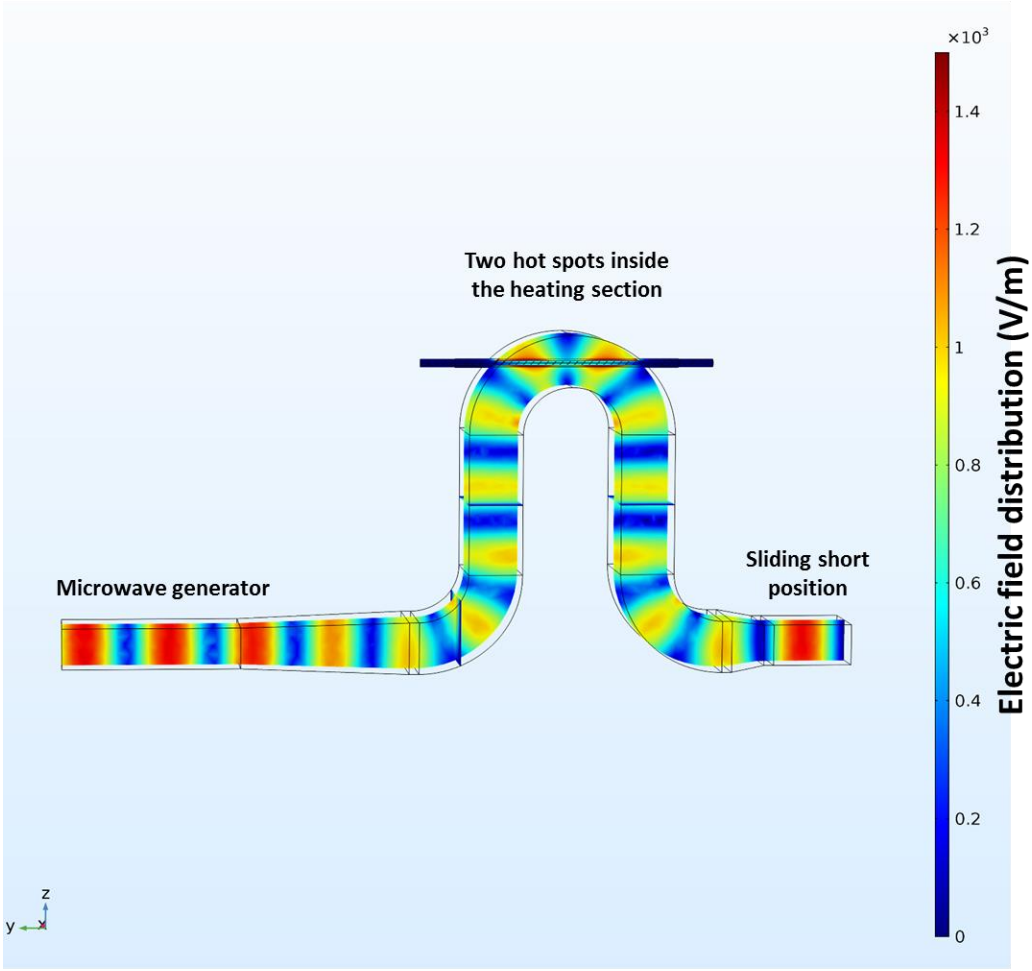


Figure S1: COMSOL Multiphysics simulation of the electric field distribution inside the MW-CF-OBR rig for the entire system (air, OBR, baffle inside OBR, reaction mixture). To assess the uniformity of the electric field inside the reaction mixture we have plotted the electric field distribution inside the mixture as presented in Figure 3, main text. Note: the experimentally determined dielectric properties of the mixture at 2.45 GHz and 65°C are 12.49-j*7.62.

Experimental microwave treatments and oscillation conditions

Continuous synthesis of HKUST-1 was carried out using a mesoscale oscillatory baffled reactor equipped with a homogeneous and controllable microwave applicator. The oscillatory baffled reactor (OBR) consists of a glass tube of 5 mm I.D., 8mm O.D. and 44 mm length, fitted with a helical baffle. Two tube reactors were used in the experiments joined by a PTFE straight connector giving a total length of 88 cm. The helical baffles inserted in the glass tubes were made of PFA, which is microwave

transparent, and stainless steel wire coiled (heats in a microwave field). The PFA helical baffle was supplied by Adtech Polymeric Engineering Ltd. The PFA rod dimensions were 0.8 mm thickness, 7.5 mm pitch, with an O.D. 4.8 mm. The dimensions of stainless steel baffle, supplied by Lion Springs Ltd., were 1 mm rod thickness, 7.5mm pitch and 4.9 mm O.D. The reactor volumes in the microwave cavity were 3.7 and 3.0 mL for PFA and stainless steel, respectively. The metal baffle was completely submerged in the reaction mixture to prevent arcing.

Four confluent pump and valve module syringe pumps (TriContinent Ltd.) were used to provide a superficial flow rate for the feeds solutions and oscillate the fluid inside the system. The oscillatory flow was dispersed using two syringes pumps of 12.5 mL, and the flow rates for the feed solutions were dispersed using two syringe pumps of 5 mL. The frequency was controlled by adjusting the speed of the piston movement. The amplitude (centre to peak) was adjusted by setting the amount of volume dispensed. The parameters were monitored and controlled by a computer, using the SAPPHIRE engineering software.

The fluid mechanics of oscillatory baffled reactors are governed by the dimensional dynamic groups: the Strouhal, St; the oscillatory Reynolds number, Re_o; and the net flow Reynolds number Re_n. The net and oscillation Reynolds numbers (Re_n and Re_o) and Stroughal number were calculated as described in Eq. 1, 2 and 3:

$$Re_n = \frac{\rho u D}{\mu} \quad (1)$$

$$Re_o = \frac{2\pi f_o x_o \rho D}{\mu} \quad (2)$$

$$St = \frac{D}{4\pi x_o} \quad (3)$$

Where ρ: density of the reagent mixture (kg·m^{-3}); u: reactants net flow (axial) velocity (m·s^{-1}); μ: dynamic viscosity of the reactant mixture (Pa·s); D: internal diameter of the baffled tube (m); f_o: oscillatory frequency (Hz); x_o: centre-to-peak amplitude of oscillation (m). The oscillatory Reynolds number describes the intensity of the mixing in the reactor and the Stroughal number is a measure of the effective eddy propagation. If it is too high the eddies will be propagated into the next baffle cavity. Results are given in **Table S1** below.

191

Table S1: Oscillation conditions.

Flow (mL/min)	Frequency (Hz)	Amplitude (Xo)	Xo (m)	superficial velocity (*u*) m/s	velocity ratio= 2*π*f*Xo/*u*	St= D/4πXo	Re_o= 2πfXoρd/μ	Re_n= Dρ*u*/μ	Velocity ratio (Ψ) = Re_o/Re_n
5	7.5	2.5	0.0025	0.00424	27.758	0.159	767	27.65	27.76
10	7.5	2.5	0.0025	0.00849	13.879	0.159	767	55.29	13.88
30	7.5	2.5	0.0025	0.0255	4.626	0.159	767	165.87	4.63
50	7.5	2.5	0.0025	0.0424	2.776	0.159	767	276.45	2.78
80	7.5	2.5	0.0025	0.0679	1.735	0.159	767	442.33	1.73
100	7.5	2.5	0.0025	0.085	1.388	0.159	767	552.91	1.39

Calculations are based on the density and viscosity of ethanol at 60 °C.

The oscillatory frequency (7.5 Hz) and amplitude (2.5 mm) corresponding to oscillatory Reynolds number (Re_o) of 767 provided effective mixing of the reaction solution and quick steady state conversions, so all the experiment were performed under these oscillatory conditions. Without oscillatory flow and using only net flow rates, poor mixing and sedimentation was clearly observed along the reactor, therefore oscillatory flow is necessary to ensure good mixing.

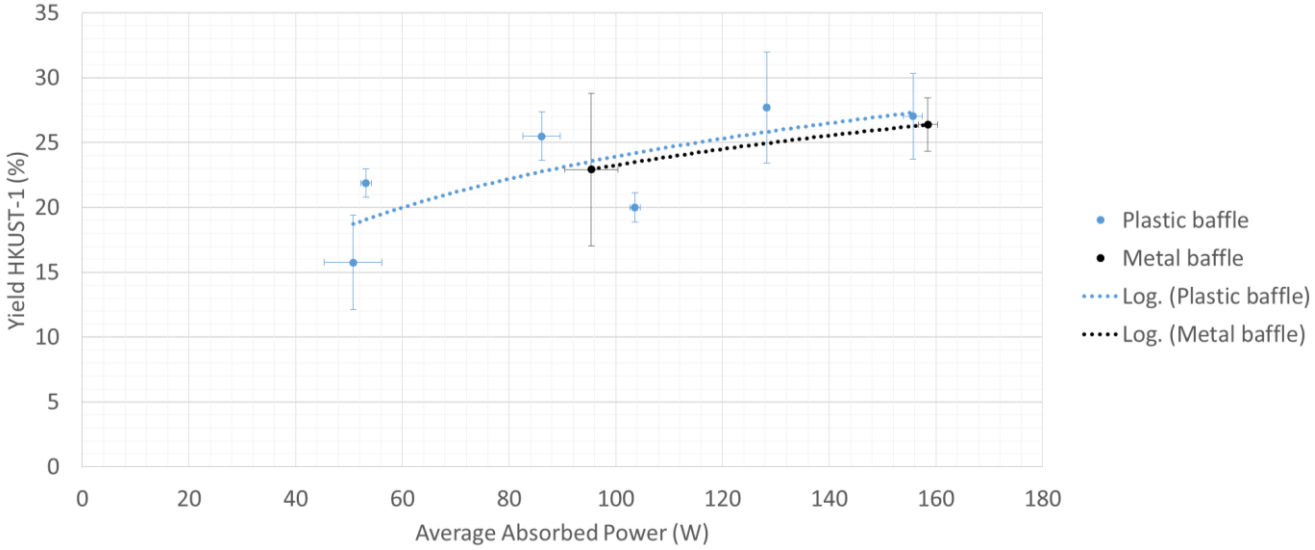


Figure S2: Plot of average absorbed power *vs.* average yield of HKUST-1 obtained from microwave treatments with plastic (blue dots) and metal baffles (black dots). A microwave frequency of 2.45 GHz was used. Error bars are plotted ± one standard deviation.

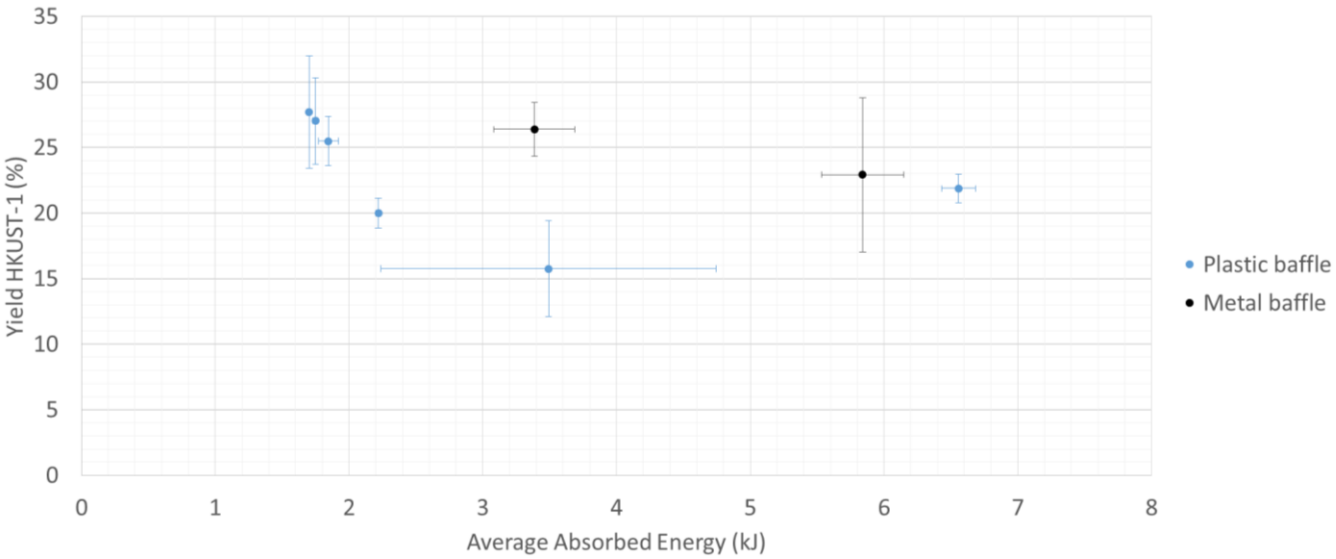


Figure S3: Plot of average absorbed energy *vs.* average yield of HKUST-1 microwave treatments with plastic (blue dots) and metal baffles (black dots). A microwave frequency of 2.45 GHz was used. Error bars are plotted ± one standard deviation.

Table S2: Average data for HKUST-1 produced using the MW-CF-OBR rig.

Flow rate (mL/min)	Average power absorbed energy (W)[a*]	Average absorbed energy (kJ)[c*]	Average absorbed energy per volume of reaction mixture (kJ/mL)[e]	Irradiation time (s)[b]	Yield of HKUST-1 (%)[c]	Median particle size (μm^2)[d]
5	53 ± 1	6.56 ± 0.13	0.52 ± 0.01	44.4	21.89 ± 1.10	0.78
10	51 ± 5	3.49 ± 1.25	0.28 ± 0.13	22.2	15.76 ± 3.67	0.024
10[#]	95 ± 5	5.84 ± 0.31	0.58 ± 0.03	18	22.93 ± 5.88	0.15
30	86 ± 4	1.85 ± 0.07	0.18 ± 0.00	7.4	25.50 ± 1.87	-
50	104 ± 1	2.22 ± 0.02	0.13 ± 0.00	4.4	20.00 ± 1.13	0.016
50[#]	158± 2	3.39 ± 0.30	0.20 ± 0.02	3.6	26.39 ± 2.06	0.019
80	128 ± 0	1.70 ± 0.01	0.12 ± 0.00	2.8	27.69 ± 4.28	-
100	156± 2	1.75 ± 0.02	0.10 ± 0.00	2.2	27.03 ± 3.31	0.016

[a]Values written to the nearest integer. Values are given to 1[b] and 2[c] decimal places. *Each value represents an average of 15 measurements (5 samples from 3 separate experiments). [c]Each value represents an average of 6 measurements (analysis of 2 samples from 3 experiments). Errors are values ± one standard deviation. [#]Metal baffle used during microwave treatments. [d]Data based on SEM analyses (see section 4 in the SI for further details). [e]Values written to two decimal places.

2. Powder X-ray diffraction data

Diffraction patterns were recorded on a PANanalytical diffractometer equipped with a $CuK_{\alpha 1}$ X-ray source and PIXcel DKIW179H1 detector. Samples of HKUST-1 were prepared on 5.1.0 silicon plates and diffraction recorded in the 2θ range of 5-55º operating at 40 kV and 40 mA. Data are given in **Figure S4**. Relative crystallinity was determined using a previously reported method by comparing the reciprocals of full width half maxima for a selected peak.[1-2] In this work the 220 reflection (9.33 °2θ) was selected for peak fitting owing to considerable intensity and resolution. Owing to peak asymmetry, a split pseudo-Voigt peak function was used to fit the peak. Examples of peak fitting are given in **Figure S5**. Data were collected using the same instrumental set-up and masses of HKUST-1 for all measurements to ensure consistency in the contribution of instrumental peak broadening.

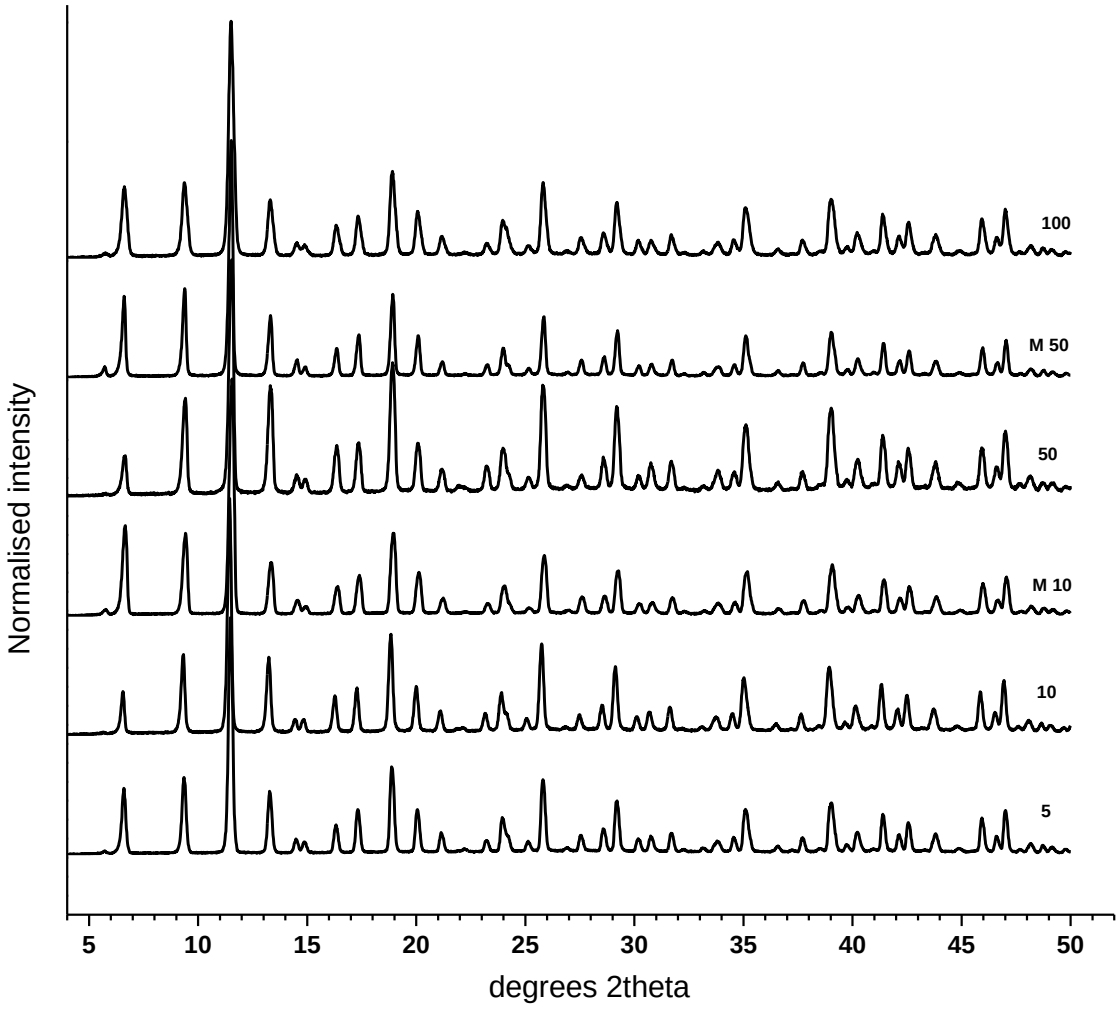


Figure S4: PXRD patterns of HKUST-1 produced at various flow rates (inset in mL/min). ‘M’ denotes the use of a metal baffle.

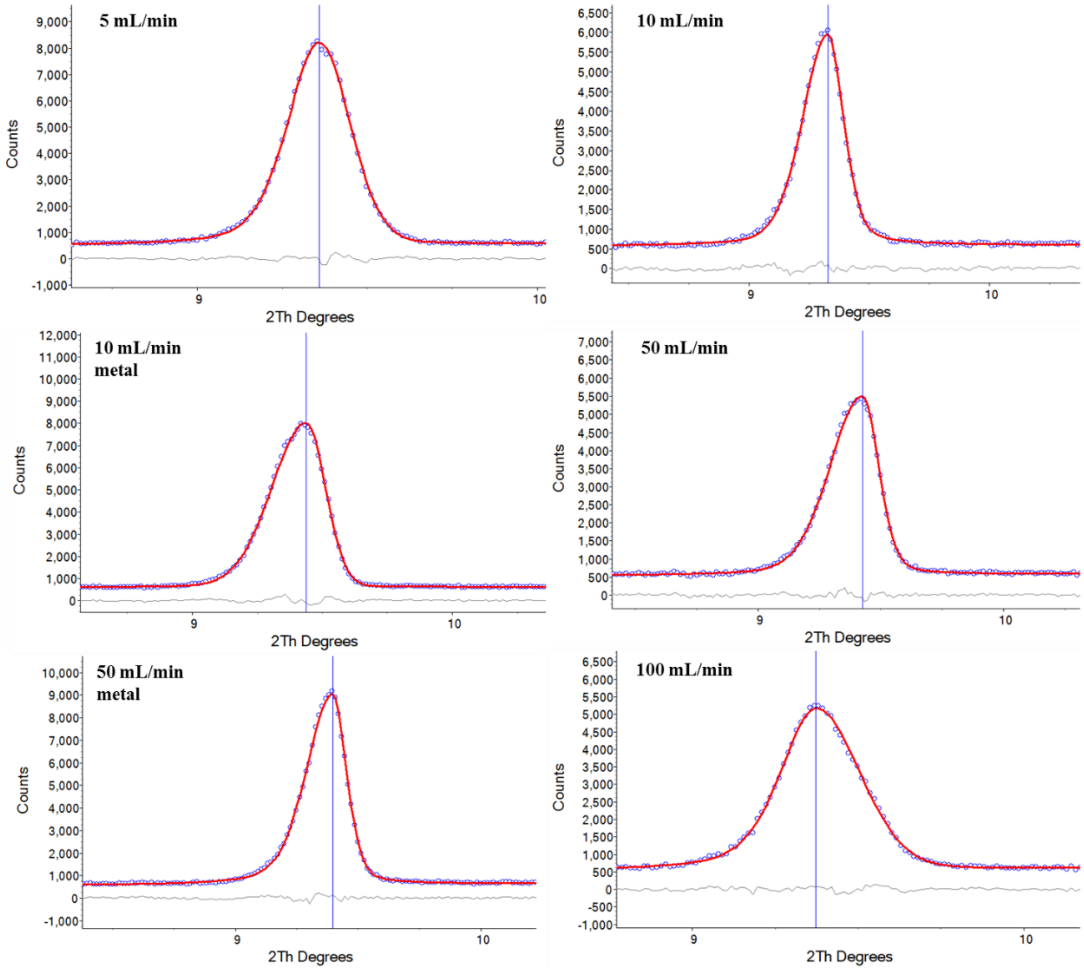


Figure S5: Peak fits of the (2 2 0) reflection of HKUST-1 produced using the MW-CF-OBR rig at various flow rates (labelled inset). Blue hollow circles, red line and grey line correspond to the experimental powder pattern, calculated peak profile and difference, respectively.

3. Gas sorption isotherms

Gas sorption analyses were performed using a Micromeritics 3 Flex volumetric adsorption analyser. Surface areas and pore volumes for HKUST-1 were measured by nitrogen adsorption and desorption at 77.3 K. A total of 95 data points were collected in the range 0.001 – 0.99 P/P_0. Samples were degassed under reduced vacuum (10^{-5} bar) at 120 °C for 16 h before analysis. Isotherms were analysed using Micromeritics MicroActive software and are plotted in **Figure S6** below. Data are also summarised in Table 2 in the main text.

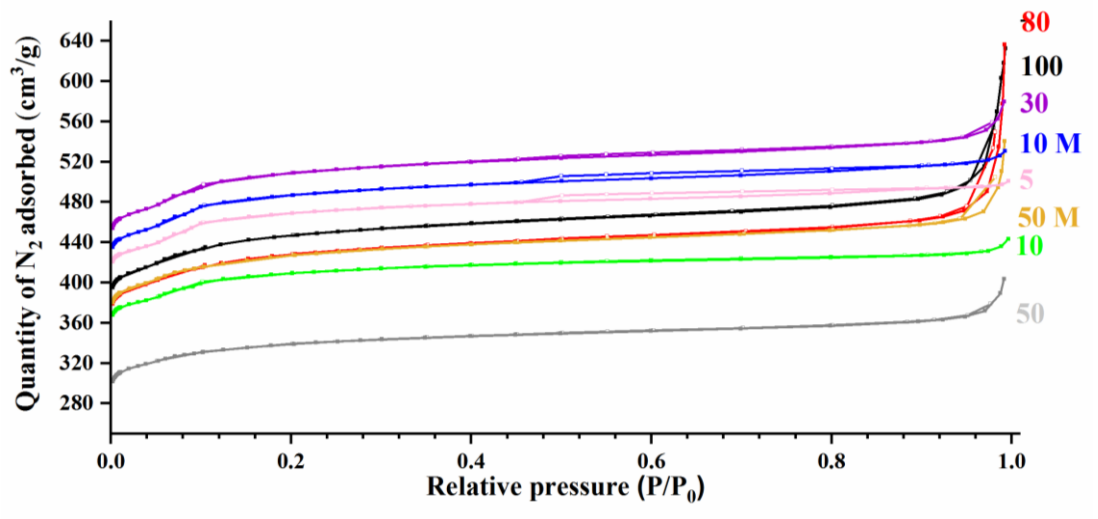


Figure S6: N_2 adsorption-desorption isotherms collected at 77 K for HKUST-1 produced in the MW-CF-OBR rig system at various flow rates (labelled inset in mL/min, 'M' denotes use of metal baffle). Adsorption (filled squares), desorption (hollow squares).

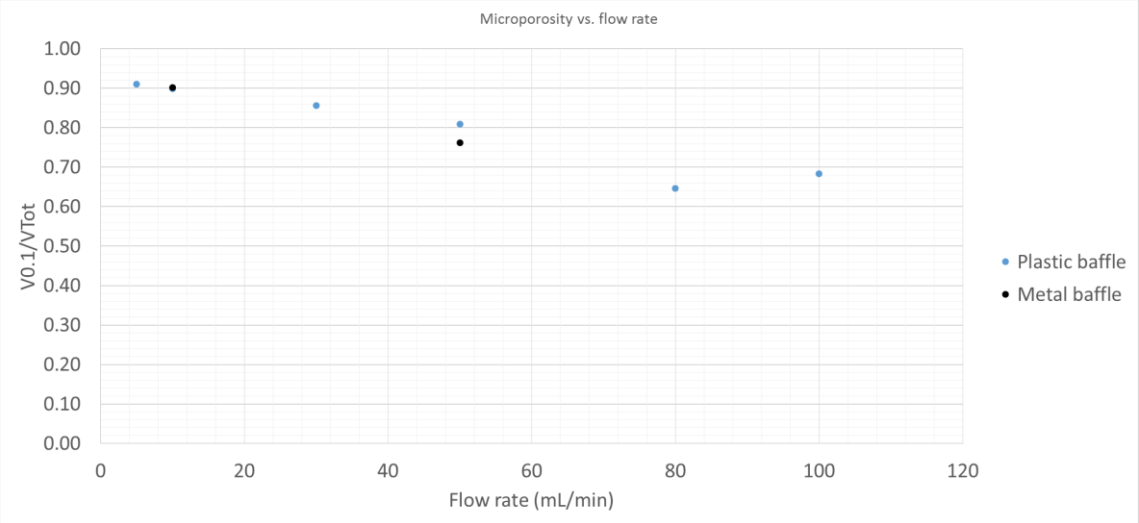


Figure S7: Plot of relative microporosity *vs.* flow rate for HKUST-1 produced using in the MW-CF-OBR rig. $V_{0.1}/V_{Tot}$ was calculated by dividing the pore volume at $P/P_0 = 0.1$ by the total pore volume at $P/P_0 = 0.99$.

4. Scanning electron microscopy (SEM) images and histogram plots

High-resolution SEM images of HKUST-1 were collected using a JEOL 7100F FEG scanning electron microscope equipped with a tungsten filament source, a secondary electron detector and a backscatter electron detector. Samples were prepared on 10 mm aluminium stubs with an adhesive carbon tab, tapping the tab to remove any un-stuck sample. The samples of HKUST-1 were coated with a 3 nm layer of iridium using a Quorum QISOT ES coater. Imaging was conducted at a working distance of 10 mm using the secondary electron detector with an accelerating potential difference of 15 kV. Frame captures of high resolution HKUST-1 morphologies were obtained using Jeol PC-SEM software. A total of 100 crystals of HKUST-1 were sized by calculating the area of one face of the crystal. Crystals were grouped by morphology based on their closest geometric shape equivalent and size in histogram plots (Figures S7-. Exemplar SEM images are given in **Figure S8** below.

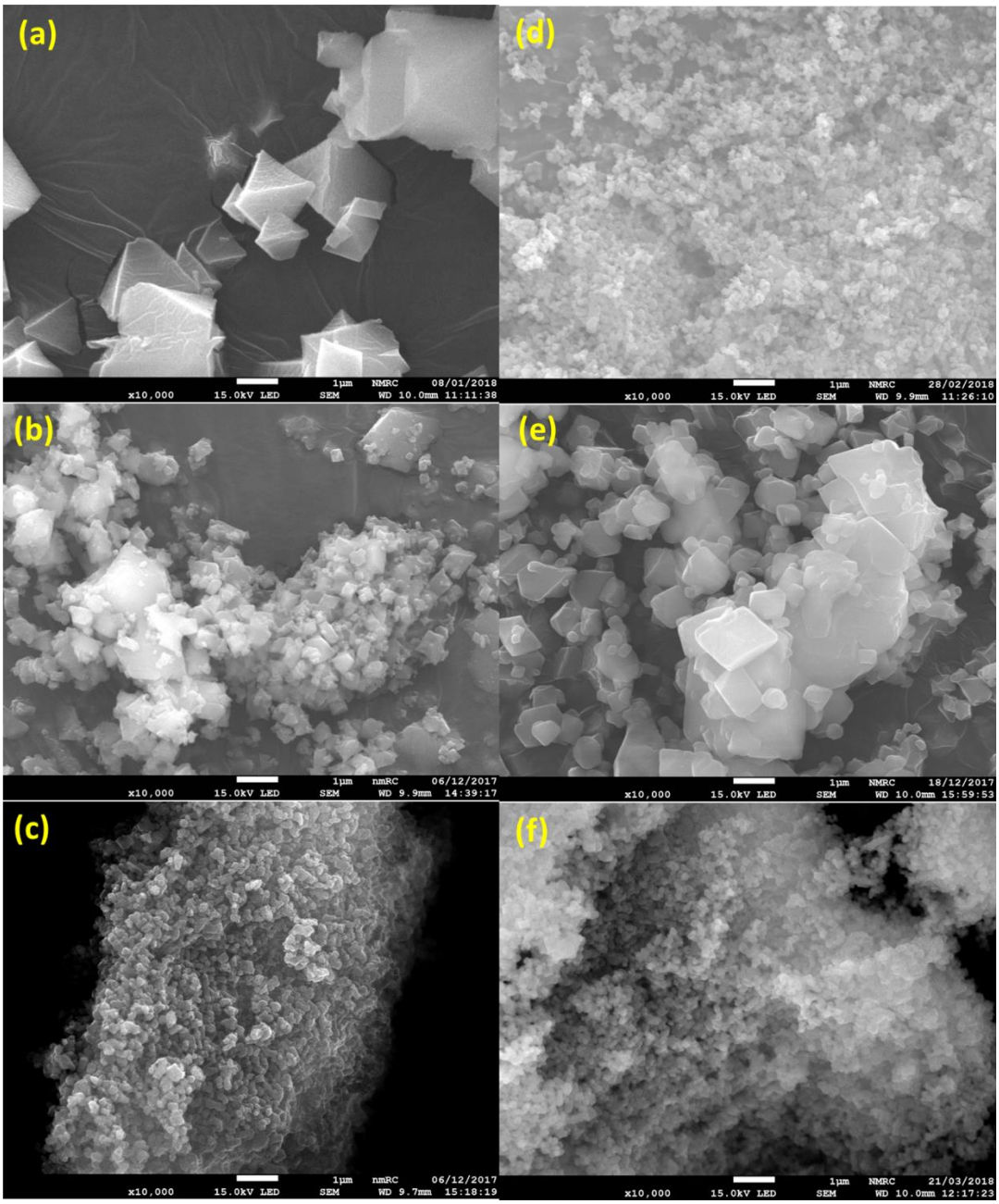


Figure S8: SEM images of HKUST-1 produced using the MW-CF-OBR rig at flow rates of (a) 5, (b) 10, (c) 50 and (d) 100 mL/min using plastic baffles; (e) 10 and (f) 50 mL/min using metal baffles.

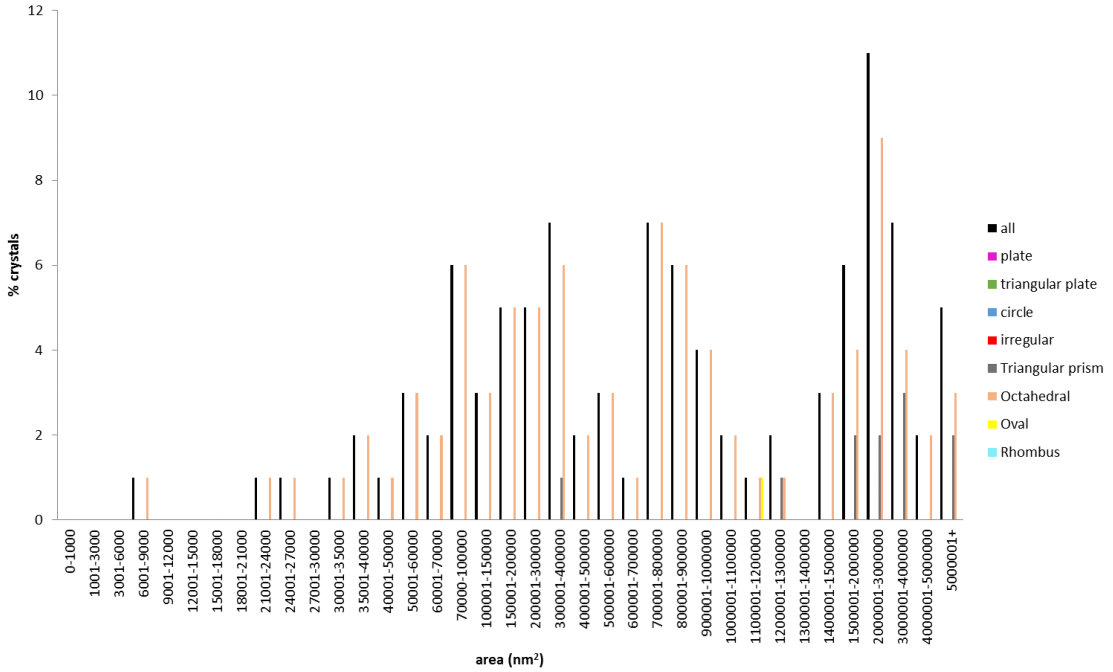


Figure S9: Histogram plot for crystals of HKUST-1 produced in the MW-CF-OBR rig at a flow rate of 5 mL/min using a plastic baffle. Crystals are grouped by size and morphology (key inset).

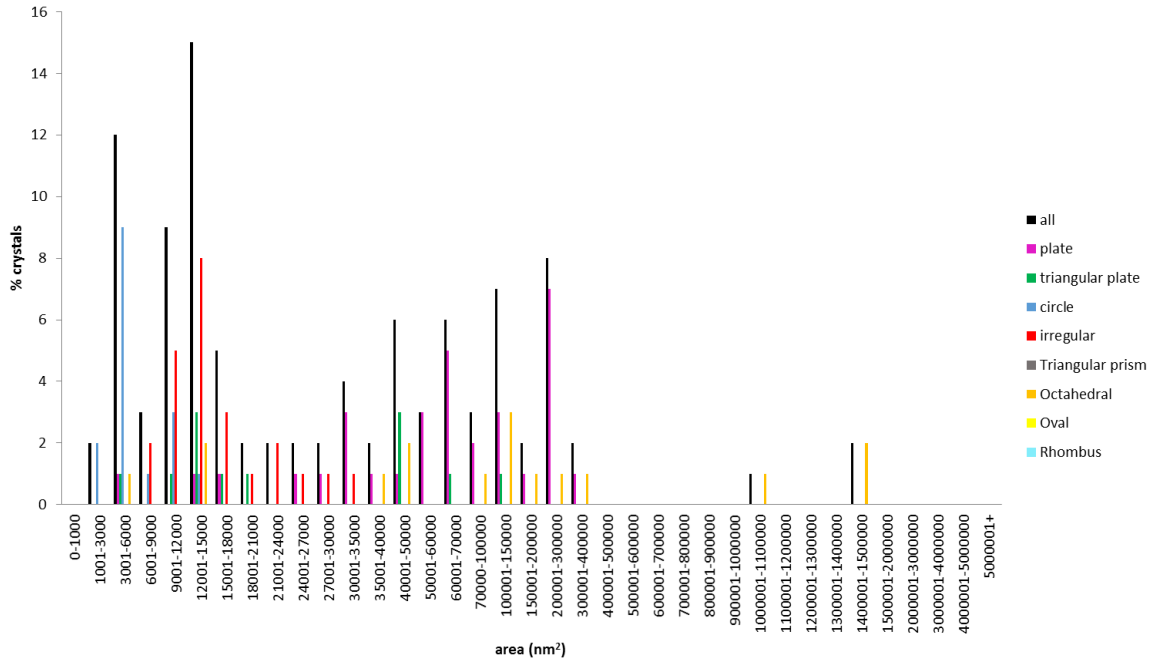


Figure S10: Histogram plot for crystals of HKUST-1 produced in the MW-CF-OBR rig at a flow rate of 10 mL/min using a plastic baffle. Crystals are grouped by size and morphology (key inset).

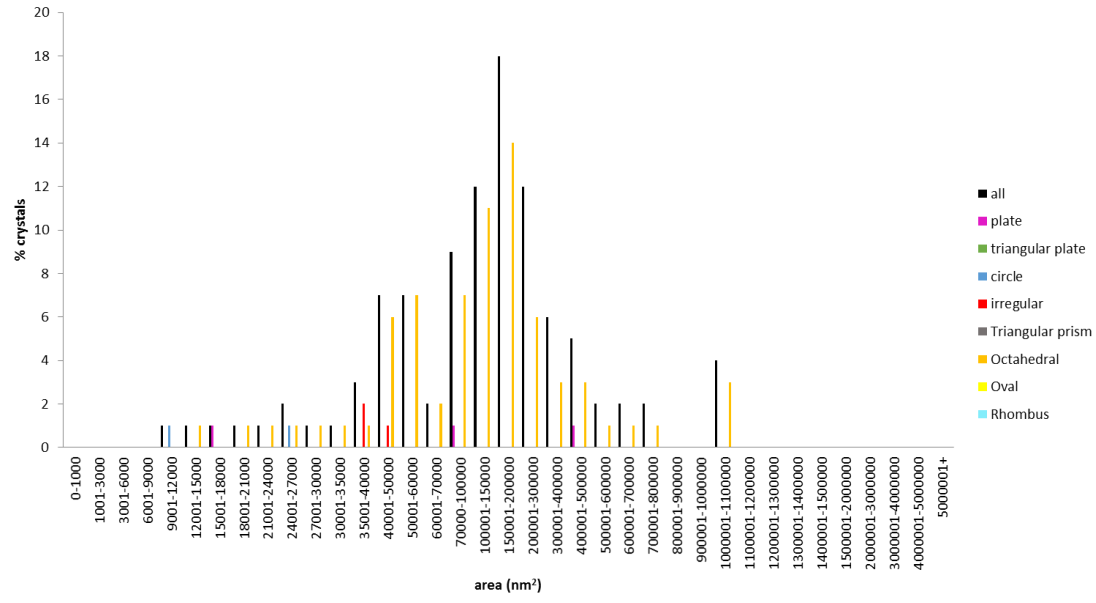


Figure S11: Histogram plot for crystals of HKUST-1 produced in the MW-CF-OBR rig at a flow rate of 10 mL/min using a ***metal*** baffle. Crystals are grouped by size and morphology (key inset).

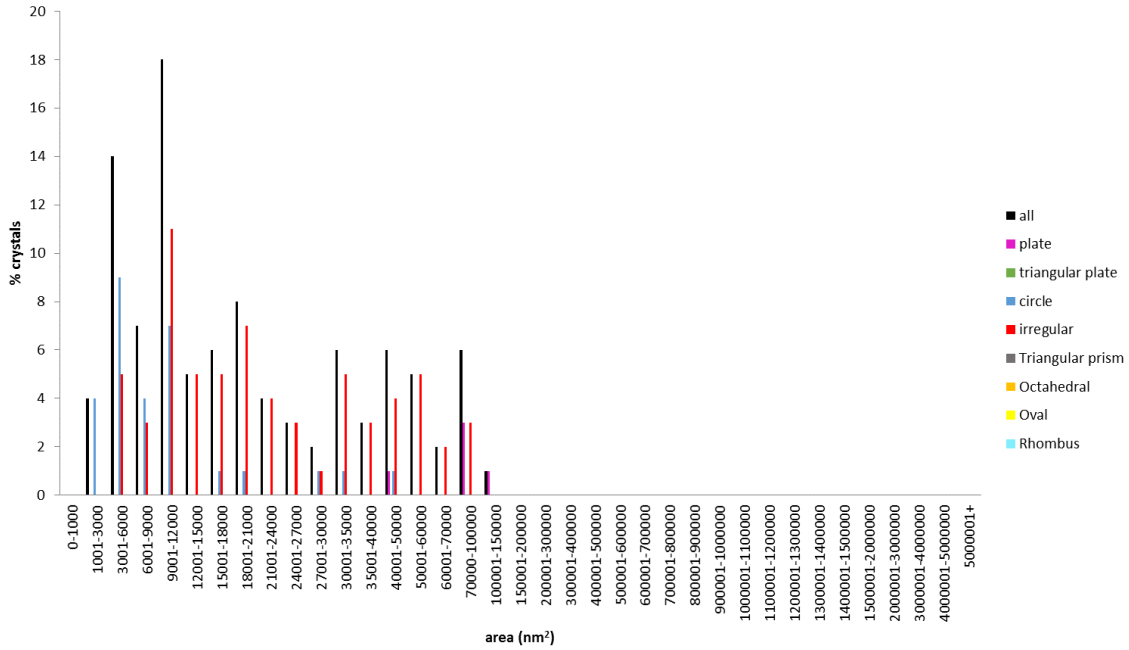


Figure S12: Histogram plot for crystals of HKUST-1 produced in the MW-CF-OBR rig at a flow rate of 50 mL/min using a plastic baffle. Crystals are grouped by size and morphology (key inset).

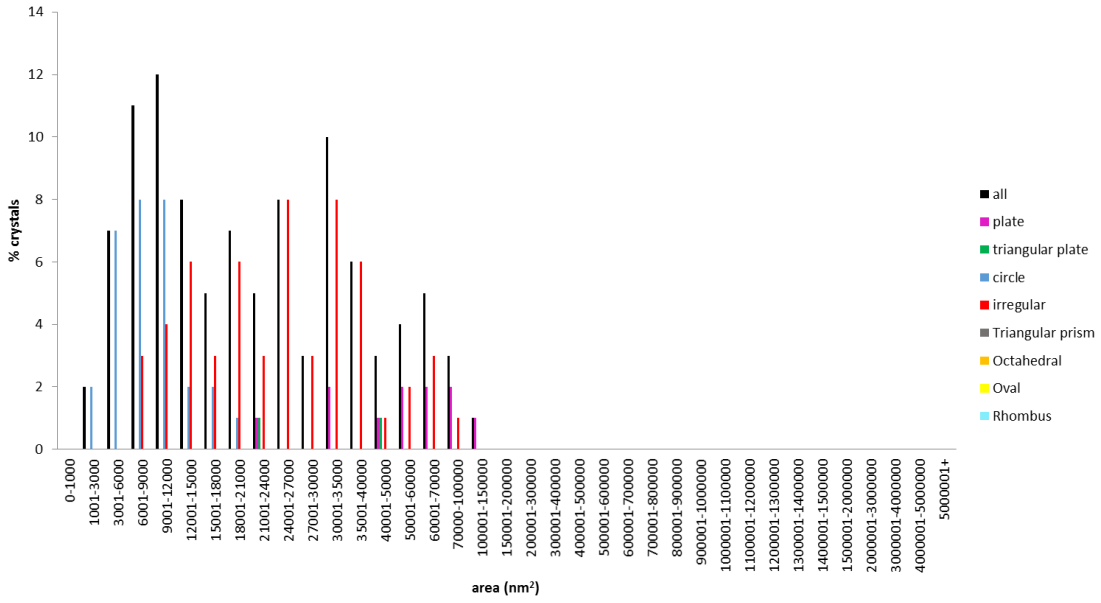


Figure S13: Histogram plot for crystals of HKUST-1 produced in the MW-CF-OBR rig at a flow rate of 50 mL/min using a ***metal*** baffle. Crystals are grouped by size and morphology (key inset).

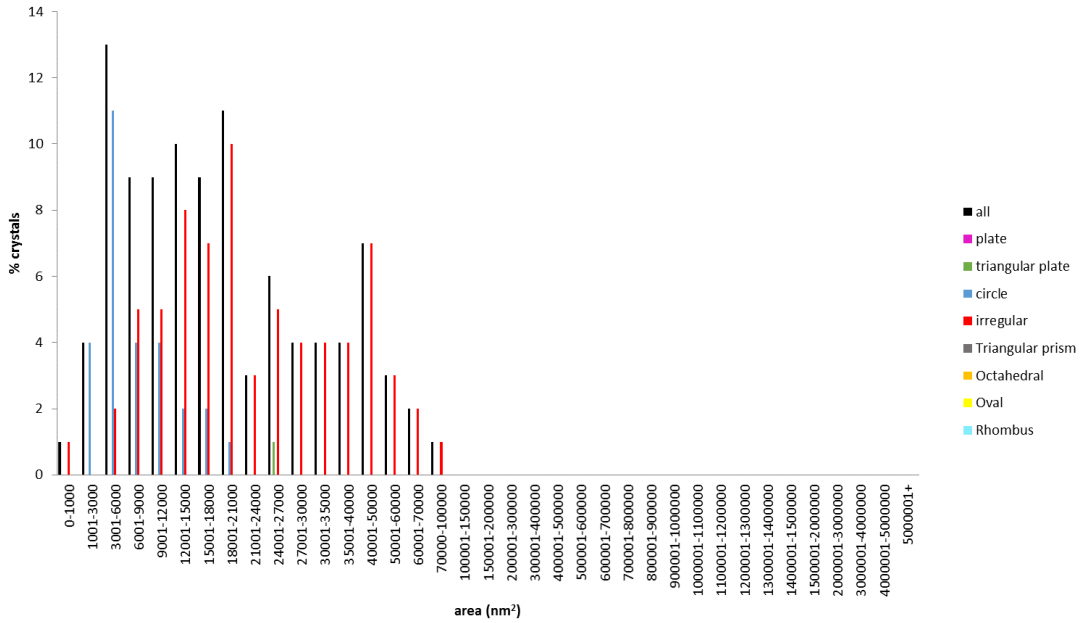


Figure S14: Histogram plot for crystals of HKUST-1 produced in the MW-CF-OBR rig at a flow rate of 100 mL/min using a plastic baffle. Crystals are grouped by size and morphology (key inset).

5. Thermogravimetric analysis (TGA)

TGA were performed using a Q5000IR analyser with an automated vertical overhead thermobalance from TA Instruments. Samples of HKUST-1 were heated at a rate of 5 °C/min under N_2 to a maximum of 600 °C. Representative thermographs for each flow rate are given in **Figure S14** below.

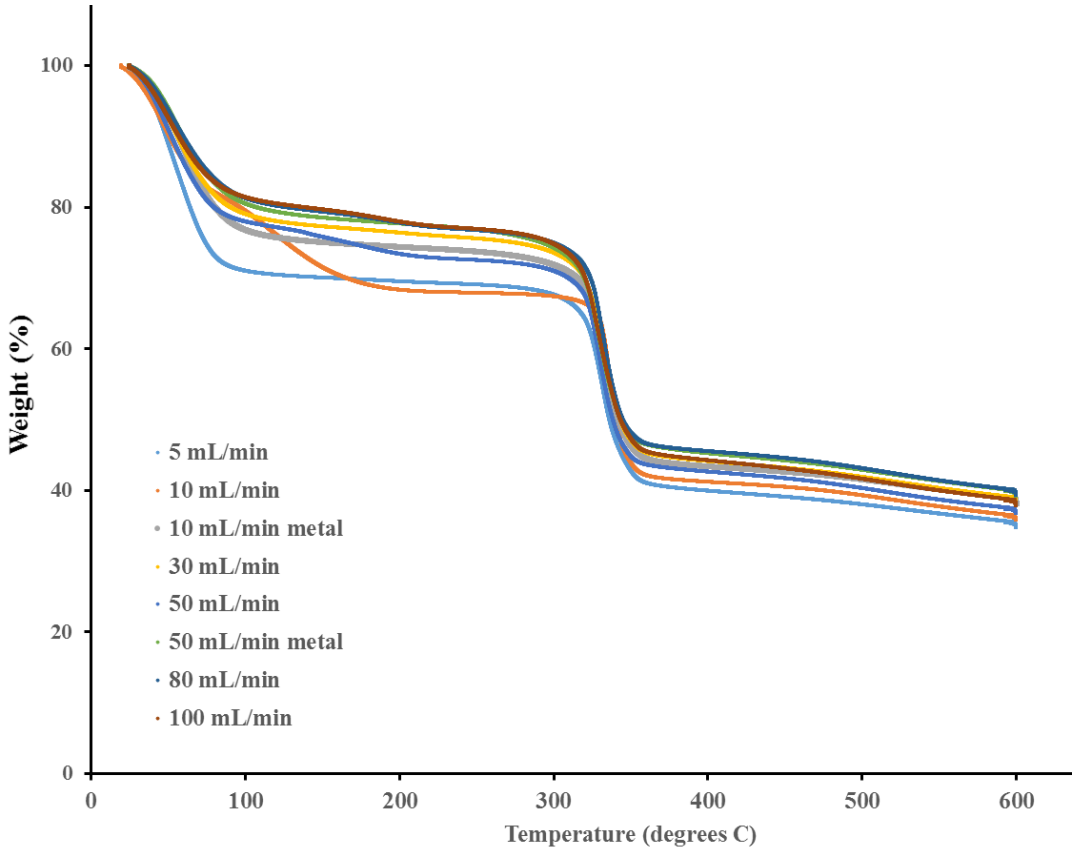


Figure S15: Representative thermographs of HKUST-1 produced using the MW-CF-OBR rig at various flow rates. Legend for the flow rates inset.

6. References

1. Laybourn, A.; Katrib, J.; Ferrari-John, R. S.; Morris, C. G.; Yang, S.; Udoudo, O.; Easun, T. L.; Dodds, C.; Champness, N. R.; Kingman, S. W.; Schroder, M., Metal-organic frameworks in seconds via selective microwave heating. *Journal of Materials Chemistry A* 2017, *5* (16), 7333-7338.

2. Taddei, M.; Dau, P. V.; Cohen, S. M.; Ranocchiari, M.; van Bokhoven, J. A.; Costantino, F.; Sabatini, S.; Vivani, R., Efficient microwave assisted synthesis of metal-organic framework UiO-66: optimization and scale up. *Dalton Transactions* 2015, *44* (31), 14019-14026.